
Dynamical Approach Study of Spurious Steady-State Numerical Solutions of Nonlinear Differential Equations

Part I -The ODE Connection and Its Implications for Algorithm Development in Computational Fluid Dynamics

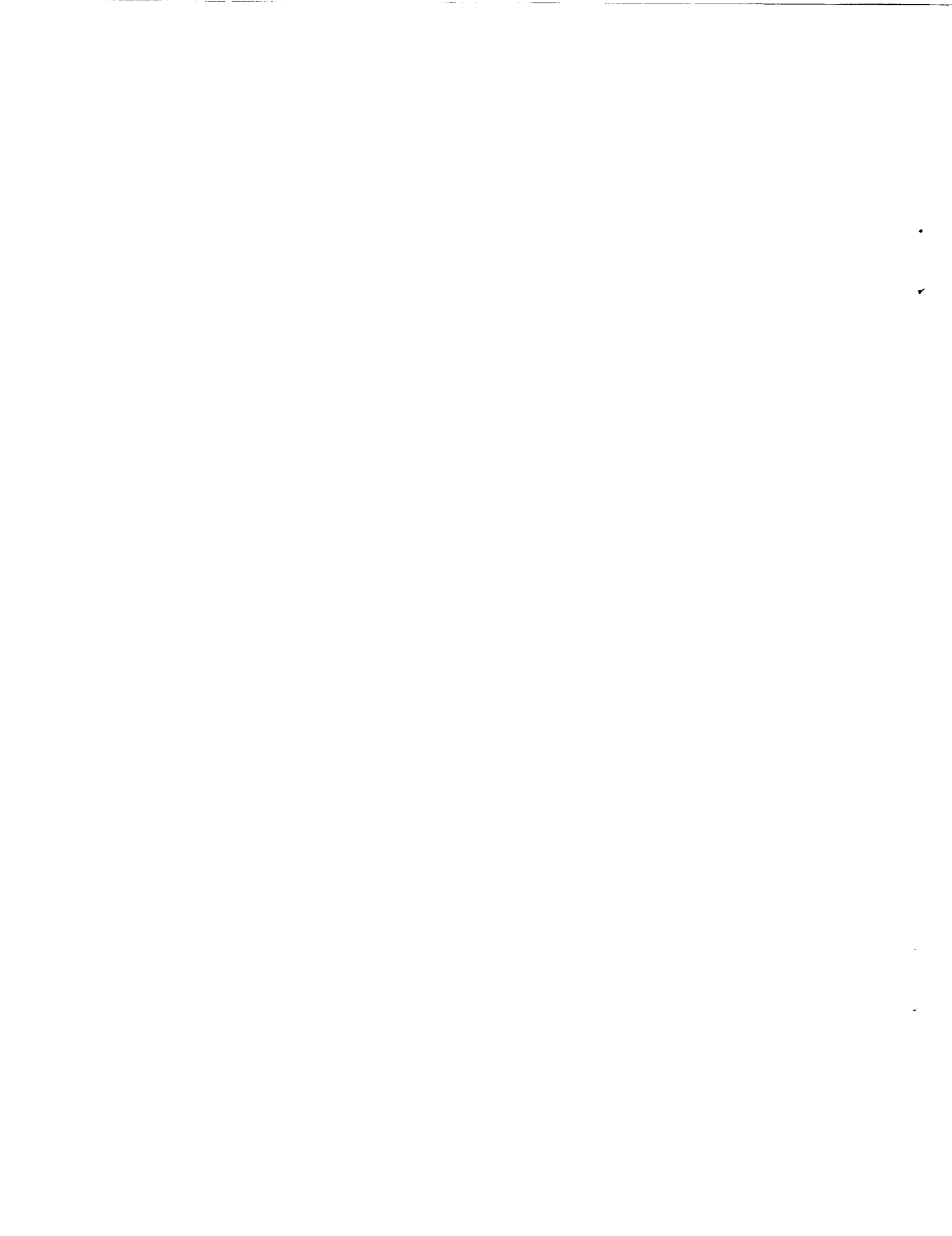
H. C. Yee, Ames Research Center, Moffett Field, California
P. K. Sweby, University of Reading, Whiteknights, Reading, England
D. F. Griffiths, University of Dundee, Dundee, Scotland

April 1990



National Aeronautics and
Space Administration

Ames Research Center
Moffett Field, California 94035-1000



DYNAMICAL APPROACH STUDY OF SPURIOUS STEADY-STATE NUMERICAL SOLUTIONS OF NONLINEAR DIFFERENTIAL EQUATIONS

I. The ODE Connection and Its Implications for Algorithm Development in Computational Fluid Dynamics

H.C. Yee¹

NASA Ames Research Center, Moffett Field, CA 94035, USA

P.K. Sweby²

University of Reading, Whiteknights, Reading RG6 2AX, England

and

D.F. Griffiths³

University of Dundee, Dundee, DD1 4HN, Scotland

ABSTRACT

The goal of this paper is to attempt to give some insight and guidelines on the application of nonlinear dynamic theory to the better understanding of steady-state numerical solutions and nonlinear instability in algorithm development for nonlinear differential equations that display genuinely nonlinear behavior in computational sciences and, in particular, computational fluid dynamics (CFD). This stems from the fact that, although the study of nonlinear dynamics and chaotic dynamics for nonlinear differential equations and for discrete maps have independently flourished rapidly for the last decade, there are very few investigators addressing the issue on the connection between the nonlinear dynamical behavior of the continuous systems and the corresponding discrete map resulting from finite-difference discretizations. This issue is especially vital for computational sciences since nonlinear differential equations in applied sciences can rarely be solved in closed form and it is often necessary to replace them by finite dimensional nonlinear discrete maps. In addition, it is also important to realize that these nonlinear discrete maps can exhibit a much richer range of dynamical behavior than their continuum counterparts.

Furthermore, it is also very important to identify some of the implications of what happens when linear stability breaks down for problems with genuinely nonlinear behavior. Studies indicate that for relatively simple nonlinear ordinary differential equations

¹Research Scientist, Computational Fluid Dynamics Branch.

²Lecturer, Department of Mathematics.

³Senior Lecturer, Department of Mathematical Sciences.

(ODEs) and well-known time-discretization with modest step-sizes some schemes can converge to a spurious (false) steady-state solution in a deceptively "smooth" manner. In some instances, spurious steady states may appear below the linearized stability limit of the schemes, and consequently computation may lead to erroneous results. Our preliminary studies on partial differential equations (PDEs) also show that much of nonlinear dynamic (e.g. chaotic) phenomena have a direct relation for problems containing nonlinear source terms such as the reaction-diffusion, the reaction-convection or the reaction-convection-diffusion equations. Here our object is neither to provide theory nor to illustrate with realistic examples the connection of the dynamical behavior of practical PDEs with their discretized counterparts, but rather to give insight into the nonlinear features unconventional to this type of study and to concentrate on the fundamental ideas. Thus, in order to bring out the special properties, the illustrations center on simple scalar differential equation (DE) examples in which the exact solutions of the DEs are known.

I. INTRODUCTION

While the applied computational fluid dynamicists are busy developing numerical solver computer codes, grid generation codes, three-dimensional graphical stereo displays, and stretching the limits of the faster supercomputers in the world to numerically simulate the various 3-D complex aerodynamic configurations [1], there is a group of applied mathematicians, physicists, chemists, biologists, applied mechanics, and meteorologists who are involved in a new science called “chaotic dynamics” (or nonlinear dynamics). The science of chaotic dynamics has cut across many traditional scientific disciplines for the last decade since chaotic dynamics is a science of the everyday world. It offers a way of seeing order and pattern where formerly only the random, the erratic, and the unpredictable were present. It explains much of the genuinely nonlinear phenomena that were once unexplainable. See references [2-10] for an introduction to this subject.

Nonlinear Dynamics & Chaotic Dynamics: Before the birth of chaotic dynamical theory, traditional study of nonlinear dynamics belonged to the applied mechanics disciplines of mechanical engineering. Modern nonlinear dynamics (since the late seventies) includes chaotic dynamics. Thus, unless otherwise stated, the term nonlinear dynamics and chaotic dynamics are used interchangeably. That is, nonlinear dynamics includes chaotic dynamics and vice versa.

Loosely speaking, the study of asymptotic behavior (steady-state solutions) of nonlinear differential equations (DEs) and nonlinear discrete maps (difference equations) and how the asymptotes change as parameters of the system are varied is most often referred to as nonlinear dynamic analysis and chaotic dynamic theory. Topics in this area include bifurcation theory, period doubling cascades resulting in chaos, etc. Stable chaotic solutions (chaotic attractors) may be defined loosely and simply as stable asymptotes that have infinite period and yet are still bounded. It is emphasized here that unless otherwise stated, all DEs and discrete maps are nonlinear and consist of system parameters, and the terms discrete maps and difference equations are used interchangeably.

Types of Dynamical Systems: Consider an ordinary differential equation (ODE) and a partial differential equation (PDE) of the forms

$$\frac{du}{dt} = \alpha S(u), \quad (1.1)$$

$$\frac{\partial u}{\partial t} + \frac{\partial f(u)}{\partial x} = \epsilon \frac{\partial^2 u}{\partial x^2} + \alpha S(u), \quad (1.2)$$

where α and ϵ are parameters and S is a nonlinear function in u and is independent of α (and ϵ). The function $f(u)$ can be linear or nonlinear in u . An ODE of this form in which t does not appear explicitly in S is called an autonomous dynamical

system. One can also consider a function S which is nonlinear in u and depends on t . ODEs of this type are called nonautonomous dynamical systems and they are more difficult to analyze; see references [5,8] for a discussion. The analysis would be more complicated if $S = S(u, \alpha)$ is nonlinear in both u and α . In this case, the DE is not only nonlinear in the dependent variable u (and independent variable t), but also nonlinear in the parameter space α . One can also consider systems that depend on more than one parameter and/or systems of equations of the above type.

Next consider nonlinear discrete maps (nonlinear difference equations) of the forms

$$u^{n+1} = u^n + D(u^n, u^{n-1}, r), \quad (1.3)$$

and

$$u_j^{n+1} = u_j^n + G(u_j^n, u_{j\pm 1}^n, r). \quad (1.4)$$

Here r is a parameter, and D is nonlinear in u^n and u^{n-1} and linear or nonlinear in the parameter space r . The situation is similar for the function G . One can also consider discrete systems that depend on more than one parameter. A typical example is a discrete map arising from a finite-difference approximation of DEs such as (1.1) or (1.2). For the ODE, the resulting discrete maps might be nonlinear in α as well as the time step Δt , depending on the ODE solvers. For the PDE, again depending on the differencing scheme, the resulting discretized counterparts can be nonlinear in α , Δt , the grid spacing Δx and the numerical dissipation parameters even though the DEs consist of only one parameter or none.

One can also consider discrete maps (scalar or system) of the forms

$$u^{n+1} = u^n + D(u^{n+k}, \dots, u^n, \dots, u^{n-l}, r_1, r_2, \dots, r_m), \quad (1.5)$$

where k, l, m are positive integers and r_1, r_2, \dots, r_m are parameters, and

$$u_j^{n+1} = u_j^n + G(u_{j\pm 1}^{n+k}, \dots, u_{j\pm 1}^n, \dots, u_{j\pm 1}^{n-l}, u_j^{n+k}, \dots, u_j^n, \dots, u_j^{n-l}, r_1, r_2, \dots, r_m). \quad (1.6)$$

Again, (1.6) can depend on more than the three indices $j, j \pm 1$. Systems (1.4) and (1.6) are sometimes referred to as a partial-difference equation. The dynamical behavior of (1.4) and (1.6) can be many orders of magnitude more difficult than (1.3) and (1.5). Any of the systems (1.1)-(1.6) are examples of dynamical systems.

Important Consideration: It is emphasized here that discrete maps, regardless of their origin, are dynamical systems on their own right. It is also important to distinguish the following five types of discrete maps:

1. Discrete maps arise naturally in physical sciences. They commonly arise through the inability to measure populations at all points in space and time [5,10,11] in population dynamics. They can also arise through the study of periodic excitation of dynamical systems [12,13] in applied mechanics.

2. Discrete maps arise from Poincaré sections in ODEs [2].
3. Discrete maps arise from discrete approximations of ODEs.
4. Discrete maps (partial-difference equations) arise from temporal and spatial finite difference approximations of PDEs.
5. Discrete models arise from the “Inverse Problems of Nonlinear Dynamics” in time series analysis of observable data or experiments [9].

Discrete maps of types 1 and 5 sometimes might not have any relationship with a specific continuum DE. As a matter of fact, there might be no concrete associated governing equations (continuum or otherwise) to start with for type 5 except the surrogated discrete map arising from the time series analysis. Type 2 arises naturally from the study of dynamical behavior of nonlinear ODEs. However, types 3 and 4 have an intimate link (but with a different tie than type 2) between the original governing continuum DEs and their discretized counterparts. Furthermore, it is important to distinguish the complexity involved in the analysis of types 3 and 4. Type 4 involves spatial as well as temporal dynamical behavior.

Note that for discrete maps of types 3 and 4, even though the DEs might be linear in the parameter space, depending on the numerical methods, the discretized counterparts might be linear or nonlinear in that parameter space. In addition, extra parameters which may be linear or nonlinear can also be introduced by the scheme as noted in the paragraph after equation (1.4). An important concept is that even though the DE does not depend on any parameter, its discretized counterpart does depend on at least one parameter. As can be seen in the subsequent sections, the nature of the dynamical behavior of these discrete maps is strongly influenced by properties of the numerical method and the types and forms of nonlinearity on the DEs. Furthermore, when dealing with nonlinear conservation laws of PDEs, the dynamical behavior of the discretized counterparts is also strongly influenced by elements such as conservation and nonlinearity of the schemes, and treatment of the source terms [14-18]. These issues are very crucial for the existence of spurious steady-state numerical solutions which will be explained in a later section. Here the term nonlinear scheme refers to a case where the resulting discrete maps are nonlinear when applied to scalar constant coefficient linear DEs.

Objectives: Our ultimate objective is to conduct long term basic research on the interdisciplinary field of integrating the theory of nonlinear dynamics with computational sciences and, in particular, with computational fluid dynamics (CFD). This new approach to CFD is extremely difficult and complex to analyze. A summary of the difficulty involved was discussed in Yee [14] and will be elaborated in sections IV and V. Our immediate goal is to study the behavior of spurious steady-state numerical solutions for nonlinear DEs and the dynamical behavior of this type of numerical solutions. Even within this frame work, the subject is still very young, board, difficult and unfamiliar to computational scientists as well as researchers working in nonlinear dynamics and

nonlinear physics.

The intent of this paper is to give a flavor of the subject, to familiarize the reader in computational sciences with this new and exciting area, and most of all, to explain through simple illustrations why it is so important for computational scientists to learn about the subject. Some challenging topics for future research are also proposed.

Because of the complexity involved, there is a vast difference in the degree of difficulty on the study of the subject between the discretized counterparts of nonlinear ODEs and the discretized counterparts of nonlinear PDEs. In order to achieve our final goal of studying the dynamical behavior of numerical methods for nonlinear PDEs that arise from, e.g., computational fluid dynamics (CFD), we have to first fully understand this subject on the time discretization and later link this knowledge to the study of both the temporal and spatial nonlinear dynamical behavior of finite-difference methods for nonlinear PDEs of the nonhomogeneous hyperbolic and parabolic types.

Therefore, the content of this paper will concentrate on the dynamical behavior of time discretization for ODEs or systems of ODEs obtained from time-splitting [19] or method of lines [20] for PDEs, and emphasis will be placed on its implication for algorithm development in CFD and computational sciences in general. Hopefully this will be part I of a series of many future research papers to come under the same topic. Our companion paper [21] studies the dynamical behavior of the class of explicit Runge-Kutta methods in detail. The intent of this paper is to not only serve as a study of the state-of-the-art of nonlinear dynamical behavior of ODE solvers, but also more importantly to serve as an introduction and to present new results to motivate this vast, new yet unconventional concept. Thus the mission of this paper is not to provide the answer or theory or to illustrate the connection of dynamical behavior of practical PDEs to their discretized counterparts, but rather to gain insight into the nonlinear features unconventional to this type of study and concentrate on the fundamentals. In order to bring out the new features, the illustrations concentrate on the simple scalar DEs examples in which the exact solutions of the DEs are known.

Outline: The outline of the paper is as follows: First, a brief background, motivation and basic ideas will be given. Then some typical characteristics of dynamical systems with genuinely nonlinear behavior will be discussed. Next, the dynamical behavior of discrete maps arising from time discretization of ODEs will be studied and the main results and their implications for computational sciences will be described. Studies on discrete maps arising from finite-difference approximations of PDEs will not be elaborated. Rather, the level of complexity involved and state-of-the-art study on this subject will be briefly described. The paper will conclude with a few recommendations. Remarks will be given on the popular misconception of residual test for convergence in steady-state solution via the “time-dependent” approach and the popular misconception of the use of the “Inverse Problems of Nonlinear Dynamics” to analyze the dynamical behavior of time series data from a computer code in an attempt to learn about the true physical solution behavior of the governing PDEs. This application of time series analysis can be misleading and a wrong conclusion can be reached if the practitioner does not know by other means

other than the numerical solutions the exact solution behavior of the PDEs .

II. MOTIVATION & RELEVANCE

As discussed in the introduction, dynamical systems occur in the form of DEs and discrete maps. In order to motivate why the study of numerical analysis will not be complete without the utilization of the nonlinear dynamic approach, and to convey to practitioners in computational sciences the importance of distinguishing the difference between weakly nonlinear problems and genuinely nonlinear problems, this section is devoted to a discussion of the typical behavior of dynamical systems with genuinely nonlinear behavior and the basic characteristic difference in dynamical behavior between DEs and discrete maps in general. This discussion leads to the key elements of this paper, namely: (1) to establish the connection between the DEs and their discretized counterparts and (2) to convey to computational scientists how one should change the traditional way of thinking and practices when dealing with genuinely nonlinear problems.

2.1. Typical Characteristics of Dynamical Systems with Genuinely Nonlinear Behavior

The terms “nonlinear behavior” and “genuinely nonlinear behavior” are used quite often in the literature and there seems to be no unified exact definition or meaning [9]. Here these terms are used for nonlinear dynamical systems that exhibit mainly the following characteristics.

(1) The study of nonlinear dynamics most often emphasizes the importance of obtaining a global qualitative understanding of the character of the system’s dynamics since local analysis is not sufficient to give the global behavior of genuinely nonlinear dynamical systems. As a matter fact, this is one of the major reasons why sometimes it required orders of magnitude more work than solving their linear counterparts.

(2) Unlike linear or weakly nonlinear problems, the solutions of genuinely nonlinear DEs and discrete maps are strongly dependent on initial data, boundary conditions and system parameters.

(3) Only genuinely nonlinear dynamical systems can have chaotic behavior and one of the striking characteristics of chaotic behavior is sensitivity of the solution to initial data. This characteristic is independent of whether the dynamical system is a continuum or a discrete map.

From here on, the terms “dynamical systems with genuinely nonlinear behavior” and “genuinely nonlinear dynamical systems” are used interchangeably. For convenience, the word “genuinely” is omitted in most parts of the paper.

2.2. Typical Difference in Dynamical Behavior of ODEs and Discrete Maps

The study of discrete maps is the discrete analog to the study of ODEs, as the study of recursion formulas is a discrete analog to the study of series expansions of functions. Much of the theory of ODEs can carry over to discrete maps with some slight modifications. However, there are new phenomena occurring in discrete maps which are absent in differential systems [22,23,12,13].

With respect to the topographical behavior, there are new kinds of behavior of trajectories in the neighborhood of equilibrium points of discrete maps. The behavior of separatrices associated with a saddle type of equilibrium point for a nonlinear difference system is far more complicated than the behavior of separatrices for a differential system. See Yee, Hsu and Hsu et al. [12,13,24,25] for details and examples.

With respect to similar equation types, the minimum number of first-order nonlinear autonomous ODEs is three for the existence of chaotic phenomena. However, a simple scalar first-order difference equation [26-30] like the logistic map

$$v^{n+1} = \mu v^n \left(1 - \frac{v^n}{4}\right), \quad \mu \text{ a parameter}, \quad (2.1)$$

or its piecewise linear approximation [31]

$$\begin{aligned} v^{n+1} &= \mu v^n, & v^n &\leq 1 \\ &= \mu, & 1 &\leq v^n \leq 3 \\ &= \mu(4 - v^n) & 3 &\leq v^n. \end{aligned} \quad (2.2)$$

possesses very rich dynamical behavior such as period-doubling cascades resulting in chaos. Equation (2.2) has the same behavior as (2.1) except that simple closed form asymptotic solutions of all periods can be obtained. These characteristic trade differences between ODEs and discrete maps are very general. The discrete maps can arise from any of the five types as discussed in the introduction. It is in this spirit that we say that discrete maps can exhibit a much richer range of dynamical behavior than DEs. The next two sections focus on the typical difference and connection between the dynamical behavior of ODEs and their discretized counterparts.

2.3. Background and Motivation

Spurious asymptotic numerical solutions such as chaos were observed by Ushike [32] and Brezzi et al. [33] on the leapfrog method for the logistic ODE

$$\frac{du}{dt} = \alpha u(1 - u). \quad (2.3)$$

In reference [34], Schreiber and Keller discussed the existence of spurious asymptotic numerical solutions for a driven cavity problem. Some related studies are reported in [35].

Spurious solutions of Burgers' equation and channel flows have been studied and computed in [36-38]. Many other investigators in the computational sciences (e.g. [39-43]) have observed some kind of strange or chaotic behavior introduced by the numerical methods but were not able to explain systematically the source, the cause of their results, or most of all the implication and impact in practical applications in computational sciences. Due to the popularity of searching for chaotic phenomena, it is very trendy to relate inaccuracy in numerical methods with the onset of chaos. It is emphasized here that inaccuracy in long time integration of discrete maps resulting from finite discretization of nonlinear DEs comes in other forms prior to the onset of chaotic phenomena. Stable and unstable spurious steady states and spurious periodic numerical solutions set in before chaotic behavior occurs. These spurious asymptotes of finite period are just as inaccurate as chaotic phenomena as far as numerical integration is concerned. In other words, the prelude to chaotic behavior is the key element that we want to stress (i.e., before the the onset of chaos or a divergent solution) since the result of operating the time step beyond the linearized stability limit is not always a divergent solution in genuinely nonlinear behavior; spurious steady-state solutions can occur. As can be seen at a later section, this behavior is more difficult to detect than chaotic phenomena in practical computations.

Recently, it has been realized by numerical analysts that numerical methods for ODEs and PDEs can be considered as dynamical systems. Several papers [44,45] on numerical methods as dynamical systems have appeared in recent years. These investigators studied the dynamical behavior of the different ODE solvers per se without relating its close tie with the ODEs themselves. Although the study of chaotic dynamics for nonlinear differential equations and for discrete maps have independently flourished rapidly for the last decade, there are very few investigators addressing the issue of the connection between the nonlinear dynamical behavior of the continuous systems and the corresponding discrete map resulting from finite difference discretizations. This issue is especially vital for computational sciences since nonlinear differential equations in applied sciences can rarely be solved in closed form and it is often necessary to replace them by finite dimensional nonlinear discrete maps. Most often, typical applied scientists rely on numerical methods to give insight into the solution behavior of nonlinear DEs. It is not always clear how well a numerical solution can mimic the true physics of problems that possess genuinely nonlinear types of behavior.

Why is there such a need to study the connection between the continuum and its discretized counterparts for CFD applications? This stems from the fact that current supercomputer power can perform numerical simulations on virtually any simple 3-D aerodynamic configuration and, due to the limited available experimental data, the applied engineers are relying on or trusting the numerical simulations whole heartedly to help design our next generation aircraft and spacecraft. However, many of these

applied scientists are still using linear analysis as their guide to study highly nonlinear equations, and most often they are not aware of the limitations and pitfalls of many of the numerical procedures. Furthermore, most of the numerical algorithms in use operate under the accuracy and stability limit guidelines of the linearized model equation. It is only appropriate to analyze nonlinear problems with the nonlinear approach; i.e., by the nonlinear dynamic approach.

The unique dynamical property of the separate dependence of solutions on initial data for the individual nonlinear DE and its discretized counterpart is especially important for employing a “time-dependent” approach to the steady state with given initial data in hypersonic CFD. In many CFD computations, the steady-state equations are PDEs of the mixed type and a time-dependent approach to the steady state can avoid the complication of dealing with elliptic-parabolic or elliptic-hyperbolic types of PDEs. However, this time-dependent approach has created a new dimension of uncertainty. This uncertainty stems from the fact that in practical computations, the initial data are not known and a freestream condition or an intelligent guess for the initial conditions is used. In particular the controversy of the “existence of multiple steady-state solutions” through numerical experiments will not be exactly resolved until there is a better understanding of the separate dependence on initial data for both the PDEs and the discretized equations.

2.4. Connection Between the Dynamical Behavior of the Continuum and Its Discretized Counterpart

Aside from truncation error and machine round-off error, a more fundamental distinction between the continuum and its discretized counterparts is new behavior in the form of spurious stable and unstable asymptotes created by the numerical methods. This is due to the fact that nonlinear discrete maps can exhibit a much richer range of dynamical behavior than their continuum counterparts as discussed in section 2.2. Some instructive examples will be given in section III. These new phenomena were partially explored by the University of Dundee group [46-54], Sanz Serna [55], Iserles [56,57] and Stuart [58-62]. Their main emphasis was on phenomena beyond the linearized stability limit. The main contribution of our current study is (1) the occurrence of spurious steady-state numerical solutions below the linearized stability limit of the scheme for genuinely nonlinear problems, (2) the strong dependence of numerical solutions on the initial data, as well as other system parameters of the DEs such as boundary conditions and numerical dissipations terms, and (3) the implications for practical computations in hypersonic CFD.

Before discussing the numerical examples, the next two subsections will give an overall summary of our current findings (integrating with other relevant recent results). The discussion is divided into steady-state solutions and asymptotes of any period, and transient solutions.

2.4.1. Steady-state Solutions and Asymptotes of Period Higher Than One:

Table 2.1 shows the possible stable asymptotic solution behavior between DEs (ODEs or PDEs) and their discretized counterparts. Some of the phenomena will be supported by simple examples in section III. The main connection between the DEs and their discretized counterparts is that steady-state solutions of the continuum are solutions of the discretized counterparts but not the reverse. Their main difference is that new phenomena are introduced by the numerical methods in the form of spurious stable and unstable asymptotic solutions of any period. In the past, the phenomena of spurious asymptotes were observed largely beyond the linearized stability of the schemes. Some numerical analysts and applied computational scientists were not alarmed and were skeptical about these phenomena since, theoretically, one is always guided by the linearized stability limit of the scheme. However, this reasoning is only valid if one is solving a scalar nonlinear ODE and the initial data are known. Another important concept is that the result of operating with time steps beyond the linearized stability limit is not always a divergent solution; spurious steady-state solutions and spurious asymptotes of higher period can occur.

Our current study also indicated that depending on the form of the nonlinear DEs, all ODE solvers can introduce spurious asymptotic solutions of some period or all periods. However, the most striking result is that for certain schemes and depending on the form of the nonlinear DEs, spurious steady states can occur below the linearized stability limit. See section III and our companion paper [21] for more details.

Another important factor is that associated with the same (common) steady-state solution, the basin of attraction (domain of attraction) of the continuum might be vastly different from the discretized counterparts. This is due entirely to the separate dependence and sensitivity on initial and boundary conditions for the individual system. The situation is compounded by the existence of spurious steady states and asymptotes of period higher than one and possibly chaotic attractors.

Here the basin of attraction of a dynamical system is the domain for which the set of initial conditions time asymptotically approaches a specific asymptote. Figures 2.1 and 2.2 show the basins of attraction of two popular ODE dynamical systems. Figure 2.1 shows the multiple stable steady states and their basins of attraction for the damped pendulum equation

$$\frac{du}{dt} = v, \tag{2.4a}$$

$$\frac{dv}{dt} = -\epsilon v - \sin(u) \tag{2.4b}$$

for $\epsilon = 0.4$. Figure 2.2 shows the multiple steady states and their basins of attraction for the simple predator-prey equation

$$\frac{du}{dt} = -3u + 4u^2 - uv/2 - u^3, \tag{2.5a}$$

$$\frac{dv}{dt} = -2.1v + uv. \quad (2.5b)$$

where u is the population of the prey and v is the population of the predator. These figures are taken from Parker and Chua [8] and were generated by the use of a variable time step Runge-Kutta-Fehlberg method with built in accuracy check (if the numerical solutions are approximating the true solution of the ODE). See reference [8] for details. These figures, although generated numerically, with the built in accuracy check the fixed points and basins of attraction coincide with the ODEs. The stable fixed points of the damped pendulum equation are $2n\pi$, $n = 0, 1, \dots$. The unstable fixed points (saddles) are $(2n + 1)\pi$. The separatrices of the saddle points divide the phase plane into the different basins of attraction for the corresponding stable fixed points. The fixed points of the predator and prey equation are slightly less regular than the damped pendulum equation. Figure 2.2 shows two saddle points at $u = 1, v = 0$ and $u = 3, v = 0$, one stable focal point at $u = 2.1, v = 2$ and one stable nodal point at $u = 0, v = 0$. Again the separatrices of the saddle points divide the phase plane into the basins of attraction for the corresponding stable fixed points.

Intuitively, in the presence of spurious asymptotes, the basin of the true steady states (steady states of the DEs) can be separated by the basins of attraction of the spurious asymptotes and interwoven by unstable asymptotes, whether due to the physics (i.e., present in both the DEs and the discretized counterparts) or spurious in nature (i.e., introduced by the numerical methods).

For PDEs, another added dimension is that even with the same time discretization but different spatial discretizations or vice versa, the basins of attraction can also be extremely different. However, mapping out the basins of attraction for any nonlinear continuum dynamical system other than the very simple scalar equations relies on numerical methods. The type of nonlinear behavior and the dependence and sensitivity to initial conditions for both the PDEs and their discretized counterparts make the understanding of the true physics extremely difficult when numerical methods are the sole source. Under this situation, how can one delineate the numerical solutions that approximate the true physics from the numerical solutions that are spurious in nature? Hopefully, with our simple illustrations in section III, we can demonstrate the importance of the current subject and, most of all, stress the importance of knowing the general dynamical behavior of asymptotes of the schemes for genuinely nonlinear scalar DEs before applying these schemes in practical calculations.

2.4.2. Transient or Time-Accurate Solutions:

It is a common misconception that inaccuracy in long time behavior poses no consequences on transient or time-accurate solutions. This is not the case when one is dealing with genuinely nonlinear DEs. For genuinely nonlinear problems, due to the possible existence of spurious solutions, larger numerical errors can be introduced by the nu-

merical methods than one can expect from local linearized analysis or weakly nonlinear behavior. The situation will get more intensified if the initial data of the DE is in the basin of attraction of a chaotic transient [63-65] of the discretized counterpart. This is due to the fact that existence of spurious asymptotes transact wrong behavior in finite time. In fact, it is possible the whole solution trajectory is likely to be erroneous.

We'd like to end this section with a direct quote from Sanz-Serna and Vadillo's paper [55]. This quote indicates the danger of relying on linearized stability and convergence theory in analyzing nonlinear dynamical problems. Reference [55] is one of the few papers trying to convey to numerical analysts the flavor of the powerful "nonlinear dynamic approach". Hopefully, with the current discussion, we can convey to computational fluid dynamicists the flavor of the importance of the "nonlinear dynamic approach" in CFD analysis.

"Assume that the convergence of a numerical method has been established; it is still possible that for a given choice of Δt , or even for any such a choice, the qualitative behaviour of the numerical sequence $u^0, u^1, \dots, u^n, \dots$ be completely different from that of the theoretical sequence $u(t_0), u(t_1), \dots, u(t_n), \dots$. This discrepancy which refers to n tending to ∞ , Δt fixed cannot be ruled out by the convergence requirement, as this involves a different limit process (namely Δt tending to 0).

. The fact that analyses based on linearization cannot accurately predict the qualitative behaviour of u^n for fixed Δt should not be surprising: there is a host of nonlinear phenomena (chaos, bifurcations, limit cycles ...) which cannot possibly be mimicked by a linear model."

III. THE ODE CONNECTION

In this section, we review some of the fundamentals and available theory and discuss our major results. The discussion will have some overlap with our companion paper [21].

3.1. Preliminaries

Consider an autonomous nonlinear ODE of the form

$$\frac{du}{dt} = \alpha S(u), \quad (3.1)$$

where α is a parameter and $S(u)$ is nonlinear in u . For simplicity of discussion, we consider only autonomous ODEs where α is linear in (3.1); i.e., α does not appear explicitly in S .

A fixed point u^* of an autonomous system (3.1) is a constant solution of (3.1); that is

$$S(u^*) = 0. \quad (3.2)$$

Note that the terms “equilibrium points”, “critical points”, “stationary points”, “asymptotic solutions” (exclude periodic solutions for the current definition), “steady-state solutions” and “fixed points” are sometimes used with slightly different meanings in the literature, e.g., in bifurcation theory. For the current discussion and for the majority of nonlinear dynamic literature, these terms are used interchangeably. We might want to mention that certain researchers reserve the term “fixed point” for discrete maps only.

Consider a nonlinear discrete map from finite discretization of (3.1)

$$u^{n+1} = u^n + D(u^n, r), \quad (3.3)$$

where $r = \alpha \Delta t$ and $D(u^n, r)$ is linear or nonlinear in r depending on the ODE solvers. Here the analysis is similar if D is a nonlinear function of u^{n+p} , $p = 0, 1, \dots, m$. Examples to illustrate the dependence on the numerical schemes for cases where D is linear or nonlinear in the parameter space will be given in the subsequent section.

A fixed point u^* of (3.3) (or fixed point of period 1) is defined by $u^{n+1} = u^n$, or

$$u^* = u^* + D(u^*, r) \quad (3.4a)$$

or

$$D(u^*, r) = 0. \quad (3.4b)$$

One can also define a fixed point of period p , where p is a positive integer by requiring that $u^{n+p} = u^n$ or

$$u^* = E^p(u^*, r) \quad \text{but} \quad u^* \neq E^k(u^*, r) \quad \text{for} \quad 0 < k < p. \quad (3.5)$$

Here, $E^p(u^*, r)$ means that we apply the difference operator E p times, where $E(u^n, r) = u^n + D(u^n, r)$. For example, a fixed point of period 2 means $u^{n+2} = u^n$ or

$$u^* = E(E(u^*, r)). \quad (3.6)$$

In this context, when dealing with discrete systems, the term “fixed point” without indicating the period means “fixed point of period 1” or the steady-state solution of (3.3).

In order to illustrate the basic idea, the simplest form of the Riccati ODE, i.e., the logistic ODE (2.3) with

$$S(u) = u(1 - u) \quad (3.7)$$

is considered. For this ODE, the exact solution is

$$u(t) = \frac{u^0}{u^0 + (1 - u^0)e^{-\alpha t}}, \quad (3.8)$$

where u^0 is the initial condition. The fixed points of the logistic equation are roots of $u^*(1 - u^*) = 0$; it has two fixed points $u^* = 1$ and $u^* = 0$.

To study the stability of these fixed points, we perturb the fixed point with a disturbance ξ , and obtain the perturbed equation

$$\frac{d\xi}{dt} = \alpha S(u^* + \xi). \quad (3.9)$$

Next, $S(u^* + \xi)$ can be expanded in a Taylor series around u^* , so that

$$\frac{d\xi}{dt} = \alpha \left[S(u^*) + S_u(u^*)\xi + \frac{1}{2}S_{uu}(u^*)\xi^2 + \dots \right], \quad (3.10)$$

where $S_u(u^*) = \left. \frac{dS}{du} \right|_{u^*}$. Stability can be detected by examining a small neighborhood of the fixed point provided if for given α , u^* is not a hyperbolic point [3,7,9] (i.e., if the real part of $\alpha S_u(u^*) \neq 0$). Under this condition ξ can be assumed small, its successive powers ξ^2, ξ^3, \dots can normally be neglected and the following linear perturbed equation is obtained

$$\frac{d\xi}{dt} = \alpha S_u(u^*)\xi. \quad (3.11)$$

The fixed point u^* is asymptotically stable if $\alpha S_u(u^*) < 0$ whereas u^* is unstable if $\alpha S_u(u^*) > 0$. If $\alpha S_u(u^*) = 0$, a higher order perturbation is necessary.

If we perturb the logistic equation around the fixed point with $\alpha > 0$, one can find that $u^* = 1$ is stable and $u^* = 0$ is unstable. It is well known that the general asymptotic solution behavior of the logistic ODE is that for any $u^0 > 0$, the solution will eventually tend to $u^* = 1$. Figure 3.1 shows the solution behavior of the logistic ODE.

Now, let us look at three of the well known ODE solvers. These are explicit Euler (Euler, forward Euler), leapfrog and Adam-Bashforth. For the ODE (3.1) with $S(u) = u(1-u)$, the dynamical behavior of their corresponding discrete maps is well established. The explicit Euler is given by

$$u^{n+1} = u^n + rS(u^n), \quad (3.12)$$

and it is after a linear transformation, the well known logistic map [26-30]. The leapfrog scheme can be written as

$$u^{n+1} = u^{n-1} + 2rS(u^n), \quad (3.13)$$

and it is a form of the Hénon map [32]. The Adam-Bashforth method given by

$$u^{n+1} = u^n + \frac{r}{2} \left[3S(u^n) - S(u^{n-1}) \right], \quad (3.14)$$

is again a variant of the Hénon map and has been discussed by Prüffer [44] in detail.

We can determine fixed points of the discrete maps (3.12)-(3.14) and their stability properties in a similar manner as for the ODE. It turns out that all three of the discrete maps have the same fixed points as the ODE (3.1) — a desired property which is important for obtaining asymptotes of nonlinear DE numerically. Here we use asymptotes to mean fixed points of any period.

The corresponding linear perturbed equation for the discrete map (3.3), found by substituting $u^n = u^* + \xi^n$ in (3.3) and ignoring terms higher than ξ^n is

$$\xi^{n+1} = \xi^n [1 + \Delta t D_u(u^*, \Delta t)]. \quad (3.15)$$

Here the parameter α of the ODE has been absorbed in the parameter Δt due to the assumption that α does not appear explicitly in $S(u)$. For stability we require

$$|1 + \Delta t D_u(u^*, \Delta t)| < 1. \quad (3.16)$$

Again, for $|1 + \Delta t D_u(u^*, \Delta t)| = 1$, higher order perturbation is necessary. For a fixed point of period p the corresponding linear perturbed equation and stability criterion are

$$\xi^{n+p} = \xi^n E_u^p(u^*, \Delta t). \quad (3.17)$$

and

$$|E_u^p(u^*, \Delta t)| < 1, \quad (3.18a)$$

with

$$E_u^p(u^n, \Delta t) = \frac{d}{du} E(u^{n+p-1}, \Delta t) \dots \frac{d}{du} E(u^n, \Delta t) \quad (3.18b)$$

For $S(u) = u(1 - u)$, the stability of the stable fixed points of period 1 and 2 for discrete maps (3.12)-(3.14) with $r = \alpha\Delta t$ are

Explicit Euler:

$$\begin{array}{ll} u^* = 1 & \text{stable if } 0 < r < 2 \\ \text{period 2} & \text{stable if } 2 < r < \sqrt{6}. \end{array}$$

Leapfrog:

$$\begin{array}{ll} u^* = 1 & \text{unstable for all } r \geq 0 \\ \text{chaotic solution exist for all } r & \text{no matter how small} \end{array}$$

Adam-Bashforth:

$$\begin{array}{ll} u^* = 1 & \text{stable if } 0 < r < 1 \\ \text{period 2} & \text{stable if } 1 < r < \sqrt{2}. \end{array}$$

Figure 3.2 shows the stable fixed point diagram of period 1, 2, 4, 8 by solving numerically the roots of (3.12) for $S(u) = u(1 - u)$. The r axis is divided into 1,000 equal intervals. The numeric labelling of the branches denotes their period. The subscript E on the period 1 branch indicates the stable fixed point of the DE.

Two of these three examples serve to illustrate that the result of operating with a time step beyond the linearized stability limit of the stable fixed points of the nonlinear ODEs is not always a divergent solution; spurious asymptotes of higher period can occur. This is in contrast to the ODE solution, where only a single stable asymptotic value $u^* = 1$ exists for any $\alpha > 0$ and any initial data $u^0 > 0$. It is emphasized here that these spurious asymptotes, regardless of the period, stable or unstable, are solutions in their own right of the discrete maps resulting from a finite discretization of the ODE.

3.2. Spurious Steady-State Numerical Solutions

For the previous three ODE solvers, we purposely picked the type of schemes that do not exhibit spurious fixed points [56] but allow spurious fixed point of period higher than 1. In this section, we discuss the existence of spurious steady-state numerical solutions. Again, it is emphasized here that these spurious steady states, stable or unstable, are solutions in their own right of the resulting discrete maps. Consider two second-order Runge-Kutta schemes, namely, the modified Euler (R-K 2) and the improved Euler (R-K 2), the fourth-order Runge-Kutta method (R-K 4), and the second and third-order predictor-corrector method [66-68] of the forms

Modified Euler (R-K 2) method:

$$u^{n+1} = u^n + rS\left(u^n + \frac{1}{2}rS^n\right) \quad S^n = S(u^n) \quad (3.18)$$

Improved Euler (R-K 2) method:

$$u^{n+1} = u^n + \frac{r}{2} \left\{ S[u^n + S(u^n + rS^n)] \right\} \quad (3.19)$$

R-K 4 method:

$$\begin{aligned} u^{n+1} &= u^n + \frac{r}{6} (k_1 + 2k_2 + 2k_3 + k_4) \\ k_1 &= S^n \\ k_2 &= S\left(u^n + \frac{1}{2}rk_1\right) \\ k_3 &= S\left(u^n + \frac{1}{2}rk_2\right) \\ k_4 &= S\left(u^n + \frac{1}{2}rk_3\right) \end{aligned} \quad (3.21)$$

Predictor-corrector method of order m:

$$\begin{aligned} u^{(0)} &= u^n + rS^n \\ u^{(k+1)} &= u^n + \frac{r}{2} \left[S^n + S^{(k)} \right], \quad k = 0, 1, \dots, m-1 \\ u^{n+1} &= u^n + \frac{r}{2} \left[S^n + S^{(m-1)} \right]. \end{aligned} \quad (3.22)$$

Using the same procedures, one can obtain the fixed points for each of the above schemes (3.18) - (3.22). Figures 3.3 - 3.7 show the stable fixed point diagrams of period 1,2,4 and 8 for these five schemes for $S(u) = u(1 - u)$. Some of the fixed points of lower period were obtained by closed form analytic solution and/or by a symbolic manipulator such as MAPLE [69] to check against the computed fixed point. The majority are computed numerically [2,8]. The stability of these fixed points was examined by checking the discretized form of the appropriate stability conditions. Again the axis is divided into 1,000 equal intervals. The numeric labelling of the branches denotes their period, although some labels for period 4 and 8 are omitted due to the size of the labelling areas. The subscript E on the main period one branch indicates the stable fixed point of the DE while the subscript S indicates the spurious fixed points introduced by the numerical scheme. Spurious fixed points of period higher than one are obvious and are not labeled

except for special cases. Note that these diagrams, which appear in most parts as solid lines are actually points, which are only apparent in areas with high gradients.

To contrast the results, similar stable fixed point diagrams are also computed for $S(u) = u(1 - u)(b - u)$, $0 < b < 1$. See figures 3.8 - 3.14. The stable fixed point for the ODE in this case is $u^* = b$ and the unstable ones are $u^* = 0$ and $u^* = 1$. For any $0 < u^0 < 1$ and any $\alpha > 0$, the solution will asymptotically approach the only stable asymptote of the ODE $u^* = b$.

Note that contrary to the DE, the maximum number of stable and unstable fixed points (real and complex) for each scheme varied between 4 to 16 for $S(u) = u(1 - u)$ and 9 to 81 for $S(u) = u(1 - u)(b - u)$, depending on the numerical methods and the r value. The domains of all of the fixed point diagrams are chosen so that they cover the most interesting part of the scheme and ODE combinations. Notice that asymptotes might occur in other parts of the domain as well.

Aside from the striking difference in topography in the stable fixed point diagrams of the various methods and ODE combinations, all of these diagrams have one similar feature; i.e., they all exhibit spurious stable fixed points, as well as spurious stable fixed points of period higher than one. Although in the majority of cases, these occur for values of r above the linearized stability limit, this not always the case, as in the modified Euler scheme applied to the logistic ODE and $du/dt = \alpha u(1 - u)(b - u)$, $0 < b < .5$, and the R-K 4 applied to the logistic DE. For these two methods and ODE combinations, stable spurious fixed points occur below the linearized stability limit. In some of the instances, these spurious fixed points are outside the interval of the stable and unstable fixed points of the ODEs. Others not only lie below the linearized stability limit but also in the region between the fixed points of the DEs and so could be very easily achieved in practice.

One might argue that for the ODEs that we are considering, it is trivial to check whether an asymptote is spurious or not. For example, if \bar{u} is a spurious asymptote of period one, then $S(\bar{u}) \neq 0$. The main purpose of the current illustration is to set the baseline dynamical behavior of the scheme so that one can use it wisely in other more complicated settings such as when nonlinear PDEs are encountered in which the exact solutions are not known. Under this situation, spurious asymptotes could be computed and mistaken for the correct steady-state solutions.

Note that for the modified Euler method, spurious fixed points of higher periods and chaotic attractors as well as spurious steady states occur below the linearized stability limit. Let Ω be the basin of attraction of the fixed point of the ODE and let r^* be the corresponding linearized stability limit value of the scheme. Then there exists a portion of the basin Ω denoted by Ω^c in which $\Omega^c \subset \Omega$ and an interval of r with $0 < r < r^*$ which actually belongs to the basin of attraction of the chaotic attractor of the discretized counterparts. There also exist some other $\Omega^p \subset \Omega$ and an interval of r with $0 < r < r^*$ and $p \geq 1$ an integer, which actually belongs to the basin of attraction of a stable asymptote of period p of the corresponding discrete map. This leads to the

issue of the dependence of solutions on initial data which will be a subject of the next subsection.

3.3. Strong Dependence of Solutions on Initial Data

For simple nonlinear ODEs that we are considering, the fixed point diagram is extremely useful for the understanding of the dynamics of the DEs and their discretized counterparts. However, when fixed points of higher periods and/or complex nonlinear equations are sought, searching for the roots and testing for stability of highly complicated nonlinear algebraic equations can be expensive and might lead to inaccuracy.

Equally useful for understanding the dynamics are the bifurcation diagram and basin of attraction of fixed points for both the DEs and the difference schemes. The bifurcation diagram for the one-dimensional discrete maps displays the iterated solution u^n vs. r after iterating the discrete map for a given number of iterations with a chosen initial condition (or multiple initial conditions) for each of the r parameter values.

Bifurcation is broadly used to describe significant qualitative changes that occur in the orbit structure of a dynamical system as the system parameters are varied. In general, bifurcation theory can be divided into two general classes, namely, local and global. Local bifurcation theory is concerned with the bifurcation of fixed points of nonlinear equations and discrete maps. Global bifurcation studies phenomena away from the fixed points. It studies the interaction between different types of fixed points. One might define a bifurcation point as being any dynamical system which is structurally unstable [3,8,9]. A fixed point is structurally stable if nearby solutions have qualitatively the same dynamics. The linearized stability limit of a fixed point of a scheme is the same as the bifurcation point in the corresponding bifurcation diagram of the resulting discrete map.

For the numerical computations of the bifurcation diagrams with a given interval of r and a chosen initial condition (or multiple initial conditions), the r axis is divided into 500 equal spaces. In each of the computations, the discrete maps were iterated with 600 preiterations and the next 200 iterations were plotted for each of the 500 r values. The domains of the r and u^n axes are chosen to coincide with the stable fixed point diagrams shown previously. For our current interest, it is not necessary to distinguish the difference between a stable fixed point of period 200 and a chaotic attractor.

Figure 3.15 shows the bifurcation diagram of the Euler scheme applied to the logistic DE with an initial condition $u^0 > 0$. It is of interest to know that in this case the bifurcation diagram looks practically the same for any $u^0 > 0$. This is due to the fact that no spurious fixed points or spurious asymptotes of low periods exist for $r < 2.627$. Comparing the bifurcation diagram with figure 3.2, one can see that if we computed all of the fixed points of period up to 200 for figure 3.2, the resulting fixed point diagram would look the same as the corresponding bifurcation diagram (assuming 800 iterations

of the logistic map are sufficient to obtain the converged stable asymptotes of period upto 200 and a proper set of initial data are chosen to cover the basins of all of the periods in question). The numeric labelling of the branches in the bifurcation diagram denote their period, with only the essential ones labelled for identification purposes.

In order to interpret the bifurcation diagram for other ODE and scheme combinations, some knowledge of the fixed point diagram is necessary, at least for the lower order periods. Otherwise, one cannot identify the exact periodicity of the asymptotes easily. As can be seen later, a "full" bifurcation diagram cannot be obtained efficiently without the aid of the stable and unstable fixed point diagram for schemes that exhibit spurious fixed points of any period, especially lower periods. In most cases, the unstable asymptotes divide the domain into the proper basins of attraction for the stable asymptotes (spurious or otherwise), and at least one initial data point is used from each of the basins of attraction before a full bifurcation diagram can be obtained.

In all of the fixed point diagrams 3.3 - 3.14, the bifurcation phenomena can be divided into three kinds. For the first kind, the paths (spurious or otherwise) resemble period doubling bifurcations (flip bifurcation) [2-5] similar to the logistic map. See figures 3.2, 3.6 and 3.8 for examples. The second kind occurs, most often, at the main branch 1_E , with the spurious paths branching from the correct fixed point as it reaches the linearized stability limit, and quite often even bifurcating more than once (pitchfork bifurcation or supercritical bifurcation [70,7]), as r increases still further before the onset of period doubling bifurcations. See figures 3.4, 3.7, 3.9 - 3.11 and 3.13 for examples. The third kind again occurs most often at the main branch 1_E . The spurious paths near the linearized stability limit of 1_E would experience a transcritical bifurcation [3,7,9,70]. See figures 3.3, 3.5, 3.7 and 3.14 for examples. Notice that the occurrence of transcritical and supercritical bifurcations are not limited to the main branch 1_E . See figures 3.11 - 3.14 for examples. The other commonly occurring bifurcation phenomenon is the subcritical bifurcation which was not observed in our two chosen $S(u)$ functions. With a slight change in the form of our cubic function $S(u)$, a subcritical bifurcation can be achieved [70,3,7,9]. The consequence of the latter three bifurcation behaviors is that bifurcation diagrams calculated from a single initial condition u^0 will appear to have missing sections of spurious branches, or even seem to jump between branches. This is entirely due to the existence of spurious asymptotes of some period or more than one period, and its dependence on the initial data. This occurs even for the Euler scheme as depicted in figure 3.8. See section 3.4 for further discussion of these four types of bifurcation phenomena.

Figures 3.16 - 3.18 show the bifurcation diagram by the modified Euler method for the logistic ODE with three different starting initial conditions. In contrast to the explicit Euler method, none of these diagrams look alike. One can see the influence and the strong dependence of the asymptotic solutions on the initial data. Figure 3.19 shows the corresponding "full" bifurcation diagram, their earlier stages resembling the fixed point diagram 3.3. Figures 3.20 - 3.22 illustrate similar bifurcation behavior for the corresponding R-K 4 method. Figure 3.12 serves as an example to illustrate that the effect of overplotting a number of initial data, but not the appropriate ones, would not

be sufficient to cover all of the essential spurious branches. Figures 3.23 - 3.25 show a similar illustration for $S(u) = u(1 - u)(b - u)$, $0 < b \leq .5$ by the improved Euler, R-K 4 and the modified Euler method. The strong dependence of solutions on initial data is evident from the various examples in which this type of behavior is very common for genuinely nonlinear problems.

In order to compute a “full” bifurcation diagram, we must overplot a number of diagrams obtained by the guide of the stable and unstable fixed point diagram as an appropriate set of starting initial data. In the case where the fixed point diagrams are extremely difficult to compute, a brute force method of simply dividing the domain of interest of the u^n axis into equal increments and using these u^n values as initial data is employed. The “full” bifurcation diagram is obtained by simply overplotting all of these individual diagrams on one.

For completeness, figures 3.26 - 3.38 show the “full” bifurcation diagrams for the corresponding fixed point diagrams shown previously. Figures 3.36 and 3.37 show a blow up section of figures 3.34 and 3.35. Notice that the exact values of the initial data are immaterial as long as these values cover all of the basins of attraction of the essential lower order periods (i.e., at least one initial data point is used from each of the basins). Here, we use the term “full” bifurcation diagram to mean just that. No attempt has been made to compute the true full bifurcation diagram since this is very costly and involves a complete picture of the basins of attraction for the domain of interest in question.

3.4. Classification of ODE solvers (According to the Existence of Spurious Fixed Points)

In reference [56], Iserles studied the stability of ODE solvers for nonlinear autonomous ODE via the dynamical approach. He proved that linear multistep methods (LMM) [66-68] that give bounded values at infinity always produce correct asymptotic behavior, but it is not the case with Runge-Kutta methods and some predictor-corrector methods. He demonstrated that the Runge-Kutta and predictor-corrector methods may lead to false asymptotes. However, he did not discuss the possibility of these spurious asymptotes existing below the linearized stability limit.

For implicit LMM, he assumed the resulting nonlinear algebraic equations are solved exactly. He also showed the influence of nonlinear algebraic solvers on the size of stability regions for implicit LMM. His conclusion was that the standard nonlinear algebraic solver — the modified Newton-Raphson method

$$u_{n+1}^{(k+1)} = u_{n+1}^{(k)} - \frac{u_{n+1}^{(k)} - u_n - \frac{\tau}{2} [S(u_n) + S(u_n^{(k)})]}{1 - \frac{\tau}{2} S_u(u_n)}, \quad (3.23)$$

can drastically degrade the region of stability limit as compared to the Newton-Raphson method

$$u_{n+1}^{(k+1)} = u_{n+1}^{(k)} - \frac{u_{n+1}^{(k)} - u_n - \frac{\tau}{2} [S(u_n) + S(u_n^{(k)})]}{1 - \frac{\tau}{2} S_u(u_n^{(k)})}. \quad (3.24)$$

On the other hand, the direct iteration method

$$u_{n+1}^{(k+1)} = u_n + \frac{\tau}{2} [S(u_n) + S(u_{n+1}^{(k)})] \quad (3.25)$$

converges only if the step size is of the same order of magnitude as that required for an explicit method. Thus the advantage of using an implicit method to enhance stability is lost. Here for clarity of notation, when iteration procedures are involved, u_n is used in place of u^n of the previous section.

The implications of behavior detailed in Iserles' work [56] range far beyond pure ODE. For most CFD application, the use of implicit time discretization to "time" march the solution to steady state is very common. The resulting nonlinear algebraic systems are solved by either noniterative linearization [71,14] or by some kind of iterative or relaxation procedures. Very often, applied computational fluid dynamicists experience a non-convergent solution where the residual will decrease only so far before reaching a plateau with a time step larger than the explicit method. Therefore the behavior observed in Iserles' work could explain the degradation in the stability of the implicit scheme in practice. Indeed, even though the mechanisms involved are far more complicated than those studied here, elements such as spatial discretization dynamical behavior and nonlinear coupling effect for systems, could well be an explanation.

More recently, Iserles and Sanz-Serna [57] established conditions for using a variable step size analysis to avoid spurious fixed points in a class of Runge-Kutta methods.

Looking at the problem from another perspective, it is very useful to find the cause of the existence of spurious asymptotes by looking at the form and properties of the resulting discrete maps, regardless of the methods. We have the following two observations.

(1) Assume that the only parameter that was introduced by a numerical method is Δt . Then from Iserles results and our current investigation, one obvious necessary condition for the existence of spurious steady states of ODE solvers for (3.1) is the introduction of nonlinearity in the parameter space Δt . This is evident from our examples and general analysis. For example, if Δt (or τ) is linear in (3.3), then (3.3) can be written as

$$u^{n+1} = u^n + crS(u^n), \quad c \text{ a constant of the scheme.} \quad (3.26)$$

Therefore any fixed point of (3.3) is a fixed point of (3.1). Without loss of generality, a similar proof applies to the resulting difference operator D from a p time level scheme.

(2) The second observation is that one can classify the types of spurious steady state in the form of bifurcation theory near a bifurcation point or a bifurcation limit

point. Figures 3.39 and 3.40 show the definition of the various types of branching points and the stability of solution in the neighborhood of branch points. In other words, the classification is according to the onset of spurious asymptotes of subcritical, supercritical or transcritical bifurcations. See figure 3.41 for the definition of the three types of phenomena.

Assume an ODE solver introduces nonlinearity in the parameter space Δt for (3.1). Then a necessary and sufficient condition for the occurrence of spurious steady states below the linearized stability limit on the main branch 1_E (stable fixed points of the DE) is that a transcritical or subcritical bifurcation of the types shown in figures 3.42 and 3.43 exist at the bifurcation point or near a bifurcation limit point. It is emphasized here that the existence of spurious fixed points of higher period can be independent of the existence of spurious steady states (fixed points of period 1).

A detailed analytical analysis on the existence of transcritical, subcritical and supercritical bifurcations for the class of Runge-Kutta methods can be found in our companion paper [21]. Figures 3.44 - 3.54 illustrate the onset of different types of spurious steady states by showing the stable and unstable fixed points of periods 1 and 2, and the types of bifurcation phenomena for the modified Euler, Improved Euler and R-K 4 and the predictor-corrector schemes of order 2 and 3 for $S(u) = u(1 - u)$ and $S(u) = u(1 - u)(b - u)$, $0 < b \leq .5$. In order to illustrate the different behavior in an uncluster fashion, not all of the periods 1, 2 and branching points are labeled. It is interesting to see the manner in which the onset of the different types of bifurcations occur, in particular, the birth of the different types of bifurcations away from the 1_E branches.

3.5. Basins of Attraction

Due to the separate dependence and sensitivity on initial data for the individual DEs and the discretized counterparts, in conjunction with the existence of spurious steady states and asymptotes of higher periods, even associated with the same (common) steady-state solution, the basin of attraction of the continuum might be vastly different from the discretized counterparts.

Take for example, $S(u) = u(1 - u)$. The only stable fixed point of the logistic ODE is $u = 1$. The entire domain of the real u^n -axis is divided into two basins of attraction for the ODE independent of any positive α . Now if one numerically integrates the ODE by the modified Euler method, extra stable and unstable fixed points can be introduced by the scheme depending on the value of r . That is for certain ranges of the r values, the u^n -axis is divided into four basins of attraction. But of course for other ranges of r , higher period spurious numerical solutions exist, more basins of attraction are created within the same u^n -axis range, etc. Stable and unstable fixed point diagrams such as figures 3.44 - 3.54 are very useful in the division of the u^n -axis into different basins of lower periods.

3.6. Systems of ODEs

As can be seen from the previous sections, the rich and complicated dynamical behavior of discrete maps resulting from finite discretization of simple nonlinear scalar autonomous ODEs is very enlightening, educational and useful in giving some indications of the strange behavior encountered in practice. One would naturally ask how highly coupled nonlinear first-order autonomous systems complicate the issue. After all, these types of systems occur naturally in physical science and engineering fields. Examples are

- (1) second or higher order nonlinear scalar autonomous or nonautonomous ODEs arising from mechanical systems,
- (2) meteorology,
- (3) chemical reaction equations arising from chemistry,
- (4) system of ODEs arising from the method of lines approach in reaction-diffusion, reaction-convection and reaction-convection-diffusion equations.

Future work will be directed towards investigation into the nonlinear dynamical effect of using ODE solvers for nonlinear system of ODEs. Here, we do not attempt to give a detailed discussion on this subject, but rather indicate some of the implications from our experience as well as what is available in the literature.

First, the coupling of first-order nonlinear systems arising from a higher-order scalar nonlinear ODE is very different from the truly nonlinear coupling on systems of first-order ODEs. This difference carries over to their discretized counterparts. Second, due to the nonlinear coupling effect, whatever is observed in the nonlinear scalar case will definitely exist in the coupled system case in a more complex manner. Even with the help of the center manifold theorem [2-5], nonlinear systems of higher than three first-order ODEs are still extremely difficult to analyze. One major factor in analyzing the associated discrete maps from finite discretization of the continuum is that when three or more time levels of ODE solvers are used, even though the continuum is a first-order scalar autonomous ODE, the resulting discrete maps are $(p - 1)$ th-order, where p is the time level. One can extrapolate the complexity involved if nonlinear coupled systems of higher-order ODEs were discretized by p -time levels of ODEs solvers. Some aspects and implications of numerical integration of second- and third-order ODEs are discussed in references [39,40,72]. Some of our preliminary numerical experiments agree with the above general conclusion.

3.7. Suitability to the Type of Computational Environment

The main approach that we use in this paper is to establish the necessary mathematical reasoning and then to support this reasoning with extensive numerical experiments.

Our current study on one-dimensional scalar nonlinear dynamical equations which consist of a single parameter indicates that the understanding of the nonlinear effects encountered when applying finite-difference schemes to nonlinear differential equations is greatly aided by the analysis of bifurcation diagrams which record the values of successive iterations for a range of parameters. Equally useful are diagrams showing the basins of attraction of equilibria, both those of the differential equations and the spurious attractors generated by the difference scheme. The generation of such diagrams, however, is computationally expensive, especially for the basins of attraction where each point on the diagram represents a different choice of parameters for which many iterations of the scheme must be performed to determine its significance.

In all the bifurcation diagrams, the computations were performed on the VMS VAX in double precision. Take for example, figure 3.34. Each dot on the plot represents a solution obtained by integrating the discretized equation 800 times with each of the 20 prescribed initial data and each of the 500 equally spaced values of $r = \alpha\Delta t$. In other words, we are integrating the same equation for 10,000 different values of r and initial data combinations, and also iterating the same equation for each of these combinations with 800 iterations. The task can therefore be greatly enhanced by parallel computation, since essentially the same process needs to be applied to each point in a fine two- or three-dimensional array, each element representing a pixel on a high resolution screen or plotter. It is therefore a task highly suited to machines, such as the Connection machine, which have large numbers of processors enabling the entire region or subregions of the problem to be analysed in one pass rather than in a sequential point-by-point approach. The intensity of (repetitive) computing involved is too great to gain major benefit from machines such as the CRAY.

For multidimensional systems consisting of several parameters, we envision that the intensity of repetitive computing to obtain a bifurcation diagram or a basin of attraction cannot be realized if it is not performed on a massively parallel computer such as the Connection machine.

IV. LEVEL OF COMPLEXITY FOR PDEs

In order to systematically approach the subject of studying spurious steady-state numerical solutions of nonlinear nonhomogeneous hyperbolic and parabolic PDEs via the nonlinear dynamic approach, we propose to pursue the subject in three stages. First, we will attempt to obtain a full understanding of the subject for time discretization of ODEs. The investigation can give insight into numerical methods employing the Strang type of operator splittings or methods of lines approach for nonhomogeneous hyperbolic and parabolic PDEs. The second stage will involve the study of the discrete travelling wave solutions of the reaction-convection and reaction-convection-diffusion equations. The third stage will involve the study of the complete temporal-spatial discretizations of the reaction-convection and reaction-convection-diffusion equations. The last stage of the proposed plan is extremely difficult to analyze. Some aspects of full discretizations and discrete travelling wave solutions were investigated by [46-54, 58-62,73,74,10].

The question now is in what specific area will this approach advance the state-of-the-art in CFD. Our preliminary study indicated that many existing results for nonlinear dynamical systems such as chaos, bifurcations, and limit cycles (closed periodic orbits [5]) have a direct application to problems containing nonlinear source terms such as the reaction-diffusion, reaction-convection or the reaction-convection-diffusion equations. Also they have a direct application to most of the nonlinear shock-capturing methods such as the total variation diminishing (TVD) schemes [14,75-78]. With the advent of increasing demand for numerical accuracy, stability, efficiency, and uniqueness of numerical solutions in modeling such equations, an interdisciplinary approach for the analysis of these systems and schemes is needed. Besides it is a common practice in CFD to employ a time-dependent approach to achieve steady state. The separate dependence of solutions on initial data and system parameters for the individual PDE and its finite-difference equations is the crucial element in determining how well a numerical solution can mimic the true physics of the problem.

The following is an attempt to give a flavor of the subject and at the same time provide a justification for the importance of this subject area in CFD algorithm development for our next generation aerodynamics needs.

4.1. Model Equations

One of the recent areas of emphasis in CFD has been the development of appropriate finite-difference methods for nonequilibrium gas dynamics in the hypersonic range [14,78-81]. A nonlinear scalar reaction-diffusion model equation would be of the form

$$\frac{\partial u}{\partial t} = \varepsilon \frac{\partial^2 u}{\partial x^2} + \alpha S(u), \quad \varepsilon, \alpha \text{ system parameters}, \quad (4.1)$$

a nonlinear scalar reaction-convection model equation would be of the form

$$\frac{\partial u}{\partial t} + \frac{\partial f(u)}{\partial x} = \alpha S(u), \quad (4.2)$$

and a nonlinear scalar reaction-convection-diffusion model equation would be of the form

$$\frac{\partial u}{\partial t} + \frac{\partial f(u)}{\partial x} = \varepsilon \frac{\partial^2 u}{\partial x^2} + \alpha S(u). \quad (4.3)$$

Here $f(u)$ a linear or nonlinear function of u . The nonlinear source term (or the reaction term) $S(u)$ can be very stiff. Note that phenomena such as chaos, bifurcations and limit cycles only relate to source terms $S(u)$ which are nonlinear in u . Equation (4.3) can be viewed as a model equation in combustion or as one of the species continuity equations in nonequilibrium flows (except in this case, the source term is coupled with other species mass fractions).

The above model equations are good starting points in the investigation of correlation between the theory of chaotic dynamical systems and uniqueness, stability, accuracy and convergence rate of finite-difference methods for CFD.

4.2. Level of Complexity

The main interest is to investigate what types of new phenomena arise from the numerical methods that are not present in the original nonlinear PDE, as a function of the stiff coefficient α , the diffusion coefficient ε , and the time step Δt with a fixed (or variable) grid spacing Δx . The time step can vary greatly depending on whether the time discretization is explicit or implicit. More precisely, one wants to weed out all undesirable phenomena due to the numerical method (e.g., additional equilibrium points introduced by the time as well as spatial discretizations, degradation of the domain of attraction, etc.) and to identify whether the numerical method really describes the true solution of the PDE under prescribed initial and boundary conditions with α , ε , the time step Δt and the grid spacing Δx being parameters. The study can be divided into steady and unsteady behavior with or without *shock waves*.

The major stumbling block is that combustion-related and high speed hypersonic flow problems usually contain multiple equilibrium states and shock waves that are inherent in the governing equations. Furthermore, spurious equilibrium states can be introduced by the time differencing and/or the spatial differencing. In many instances the stable and unstable equilibrium states, whether due to the physics or spurious in nature, are interwoven over the domain of interest and are usually very sensitive to the initial conditions and the time steps (even when the chosen time step is within the linearized stability limit as indicated in our study) as well as variation of parameters such as angle of attack, Reynolds number and coefficients of physical and numerical dissipations and physical and numerical boundary conditions.

The sensitivity of numerical solutions to coefficients of physical and numerical dissipations is evident from the study of Mitchell and Bruch on the reaction-diffusion equation. Their main result is that diffusion, which is usually perceived as having a stabilizing effect, is able to produce chaotic as well as divergent numerical solutions. Another interesting result due to Mitchell and Bruch was the production of chaos by decreasing the space increment or increasing the time increment. They showed that the addition of diffusion poses severe problems unless waves of constant speed c are assumed, in which case it reverts to an ODE with $x + ct$ as the independent variable. The sensitivity of numerical solutions to numerical boundary condition procedures was discussed in [82,83].

On the subject of sensitivity and dependence of solutions on initial data, the basin of attraction might be very different between the PDE and the discretized counterpart. The basin of attraction might contract or be very different from the basin of attraction for the original PDEs depending on the numerical methods. In many instances, even with the same spatial discretization but different time discretizations, the basins of attraction can also be extremely different. One can extrapolate the complexity involved when the influence of the various temporal as well as spatial discretizations are sought on the basins of attractivity.

Table 4.1 summarizes the level of complexity for a systematic approach to these types of PDE. The check mark on each type of PDE and approach indicate the ones where some work has been done on this subject. The majority are credited to the University of Dundee group [46-54] and some related theory by A. Stuart [58-62].

4.3. Involvement in the Study of Full Discretization of PDE

Consider a three-level explicit time differencing and a three-point spatial differencing of the reaction-convection-diffusion equation (4.3) of the form

$$u_j^{n+1} = u_j^n + H(u_{j-1}^n, u_j^n, u_{j+1}^n, u_{j-1}^{n-1}, u_j^{n-1}, u_{j+1}^{n-1}, \alpha, \epsilon \Delta t, \Delta x), \quad (4.4)$$

where u_j^n is the numerical solution at $t = n\Delta t$ and $x = j\Delta x$. Then the study of the asymptotes of (4.4) amounts to the study of fixed point behavior of period p in time and period q in space, denoted by (p, q) , where p and q are integers. Here the fixed point of the partial-difference equation (4.4) is defined in a slightly more complicated way than for the ODE.

For example, a fixed point of period (1,1) is defined as $u_{j+1}^{n+1} = u_j^n$ and a fixed point of period (2,1) is defined as $u_{j+1}^{n+2} = u_j^n$. However, a fixed point of period (1,2) is defined as $u_{j+2}^{n+1} = u_j^n$. Thus, in general a fixed point of period (p,q) is defined as $u_{j+q}^{n+p} = u_j^n$. One can see that for $p, q > 3$, solving the resulting nonlinear algebraic equation is very involved, especially when physical boundary conditions and physical dissipation terms as well as numerical boundary conditions [82,83,34] and numerical dissipation [47] are

additional dimensions of consideration. Current available work involved the studies beyond the linearized stability limit of the schemes, and assumed the nonexistence of spurious fixed points of period (1,1). See references [46-54] for details.

4.4. Influence in Dynamical Behavior by Property of the PDEs and Schemes, and Treatment of the Source Terms

Although the general study of the dynamical behavior of partial-difference equations for the conservation law [84,85] of (4.3) is an enormous task, if we can isolate certain restricted subsets of the PDEs and schemes in hand which are immune to the type of phenomena discussed in section III for time discretization as well as spatial discretization, then we can concentrate on the rest of the unknowns.

As can be seen in section III, the nature of the dynamical behavior of the discretized counterparts is strongly influenced by properties of the numerical method and the types and form of nonlinear DEs. Here we want to study the influence on the dynamical behavior of elements such as conservation and nonlinearity of the schemes, and treatment of the source terms [14-17,78-81] when nonlinear conservation laws of PDEs are sought.

First, take the convection equation (4.2) with $S(u) = 0$ and consider a conservative explicit scheme [76,14] which is consistent with the conservation law of the form

$$u_j^{n+1} = u_j^n - \lambda \left[h_{j+\frac{1}{2}}^n - h_{j-\frac{1}{2}}^n \right], \quad (4.5)$$

where $\lambda = \Delta t / \Delta x$ and $h_{j\pm\frac{1}{2}}^n$ are the numerical flux functions. For a two-time level and five-point spatial scheme, $h_{j\pm\frac{1}{2}}^n = h(u_j^n, u_{j\pm 1}^n, u_{j\pm 2}^n)$.

We also can consider a two-parameter family of scheme

$$\begin{aligned} u_j^{n+1} + \frac{\lambda\theta}{1+\omega} \left[h_{j+\frac{1}{2}}^{n+1} - h_{j-\frac{1}{2}}^{n+1} \right] &= u_j^n - \frac{\lambda(1-\theta)}{1+\omega} \left[h_{j+\frac{1}{2}}^n - h_{j-\frac{1}{2}}^n \right] \\ &+ \frac{\omega}{1+\omega} (u_j^n - u_j^{n-1}). \end{aligned} \quad (4.6)$$

where $0 \leq \theta \leq 1$. When $\theta = 0$, the scheme is explicit and when $\theta = \omega + 1/2$, the scheme is temporally second-order accurate. One can obtain (4.5) from (4.6) by setting $\theta = 0$ and $\omega = 0$. The time differencing belongs to the class of LMM. Under the assumption that this scheme is conservative and consistent with the conservation law, discrete map (4.6) will have no spurious steady-state numerical solution since consistency means

$$h(u^*, u^*, u^*) = f(u^*). \quad (4.7)$$

Thus any steady-state solutions of (4.6) are steady-state solutions of the original PDE.

Now the situation is different when $S(u) \neq 0$. Under this situation, even if the same time and spatial discretization are employed, one still has to evaluate \bar{S} properly. Here \bar{S} is the function S evaluated at some proper average state \bar{u} [14-17] for the full discretization that is consistent with the scheme [18], and achieves conservation at jumps. For a discussion on this subject, see references [78, 15-17] for details. The other crucial aspect is that when $S(u) \neq 0$, a full investigation on the dynamical behavior of the temporal and spatial discretization is necessary. The knowledge gained from the finite-difference methods analysis for $S(u) = 0$ does not carry over to the $S(u) \neq 0$ case.

4.5. Discrete travelling Waves

Analysis of the dynamical behavior of the full discretization of nonlinear nonhomogeneous PDEs of the hyperbolic and parabolic types is very involved. In this section, we look at a more restricted class of solutions — the discrete travelling wave solutions.

Consider a reaction-diffusion equation

$$\frac{\partial u}{\partial t} = \frac{\partial^2 u}{\partial x^2} + \tilde{S}(u). \quad (4.8)$$

Solution $u(x, t)$ depend on the space variable x and on the time t . Every zero of $\tilde{S}(u)$ constitutes an equilibrium of the PDE. Then a travelling wave solution is a profile $U(x)$ that travels along the x -axis with propagation speed $\bar{\lambda}$. Neither the shape of the wave nor the speed of propagation changes. To find travelling waves, we seek solutions

$$u(x, t) = U(x - \bar{\lambda}t), \quad (4.9)$$

resulting in an ODE

$$U'' + \bar{\lambda}U' + \tilde{S}(U) = 0. \quad (4.10)$$

By solving this ODE, one can calculate asymptotic states for the PDE. Let U_1 and U_2 be roots of $\tilde{S}(u)$ and hence equilibrium solutions for both the PDE and ODE. The asymptotic behavior of solution U for $x \rightarrow \pm\infty$ determines the type of travelling wave. Every solution with

$$U(\infty) = u_1 \quad (4.11a)$$

$$U(-\infty) = u_2, \quad (4.11b)$$

with $u_1 \neq u_2$, is a front wave of the ODE. This corresponds to a heteroclinic orbit [3] of the ODE, connecting the two stationary points u_1 and u_2 . Here for a second-order autonomous ODE (4.10), when distinct saddles are connected, one encounters a heteroclinic orbit; also a heteroclinic orbit may also join a saddle to a node or vice versa. Another type of special orbit is a homoclinic orbit. A homoclinic orbit connects a saddle point to itself and such orbits have an infinite period. Several heteroclinic orbits

may form a closed path called a homoclinic cycle. Both the heteroclinic and homoclinic orbits are of great interest in applications because they form the profiles of travelling wave solutions of many reaction-diffusion problems. See references [3,10,73,74] for a discussion.

Similarly, one can study discrete travelling wave solutions for the finite discretization of (4.8). See references [73,74] for a discussion. Understanding of the discrete traveling wave solutions of the corresponding PDEs only gives insight into a very small subset of the dynamics of the PDEs. In most cases, it provides no information at all for the fully discretized equation.

V. IMPLICATIONS & RECOMMENDATIONS

Due to the complexity of the large increase in system dimension and the involvement of multiple floating parameters for finite difference methods in PDEs, we are not certain that a similar systematic general result can be arrived at for more complex nonlinear systems. The main indication at this point is from our time discretization study.

5.1. Results Drawn from the ODE Connection Study

Our study illustrates a few very important implications which are very fundamental in explaining what happens when linear stability breaks down for truly nonlinear problems; i.e., equations that display genuinely nonlinear types of behavior. The important points are as follows:

(1) There is sensitivity to initial data and strong dependence on discretization parameters such as the time step and the grid spacing Δx . Dependence of solutions on initial condition is important for employing a time-dependent approach to the steady-state with a given initial condition and boundary conditions in hypersonic or combustion flows, especially when initial data of the governing PDE are not known.

(2) Associated with the same (common) steady-state solution the basin of attraction of the DEs might be vastly different from the discretized counterparts. This is mainly due to the dependence and sensitivity on initial conditions and boundary conditions for the individual systems. In the absence of the influence of the initial and boundary conditions, the difference in the basins of attraction between the continuum and its discretized counterparts occurs even when an implicit LMM type of method is used unless the resulting nonlinear algebraic equations are solved exactly.

(3) Nonunique steady-state solutions can be introduced by the spatial discretization even though the original PDEs might possess only an unique steady-state solution and a LMM type of time discretization is used so that no spurious steady-state exists in time. The tie between temporal and spatial dynamical behavior is more severe when one is dealing with the nonseparable temporal and spatial finite-difference discretization such as the Lax-Wendroff type, where the time and spatial difference cannot be separated from each other. The situation would be more complicated if the governing nonlinear PDE possesses more than one steady-state solution as well as the spurious ones that are purely due to the numerical method.

(4) For certain time discretizations, spurious steady-state solutions may occur below the linearized stability limit of the scheme.

(5) The result of operating with a time step beyond the linearized stability limit is not always a divergent solution; spurious steady-state solutions can occur.

(6) There is a misconception that computational instability or inaccuracy can often be cured simply by making Δt smaller. Other elements such as (1) - (5) above as well as the variation of the grid spacings, numerical dissipation terms and system parameters other than the time steps can interfere with the dynamical behavior.

(7) When linearized stability limits are used as a guide for a time step constraint for highly coupled nonlinear system problems, this time step might exceed the actual linearized stability limit of the coupled equations. Therefore all of the situations in (1) - (6) can occur. In particular, when one tries to stretch the maximum limit of the linearized allowable time step for highly coupled systems, most likely all of the different type of spurious branches of supercritical, subcritical and transcritical bifurcations can be achieved in practice depending on the initial conditions. That is why the occurrence of spurious steady-state solutions beyond the linearized stability limit is not just secondary but might be as important as the occurrence of spurious steady states below the linearized stability limit.

5.2. Recommendations

It is of utmost importance to know the nonlinear dynamical behavior of the various schemes before their actual use for practical applications. Otherwise, it might be very difficult to assess the accuracy (spurious or otherwise) of the solution when the numerical method is the sole source of the understanding of the physical solutions. When in doubt, it is always safer to use schemes that do not produce spurious steady-state solutions for the nonlinear scalar case. Some examples of methods of this type in time discretization can be listed:

(1) LMM [56] ODE solvers such as the explicit, implicit Euler, three-point backward differentiation, etc. can be used.

(2) One can use the “Regular” Runge-Kutta methods [57].

(3) Solving the nonlinear algebraic systems arising from implicit LMM method exactly would avoid spurious steady state numerical solutions. Otherwise, the type of iteration method in solving nonlinear algebraic systems can degrade the basin of attractivity of implicit LMM [57].

The insight gained from time discretization will only give an indication in separable schemes or method of lines approaches. Also, the commonly used residual test [86-88] in the time-dependent approach to the steady state might be misleading. This is the direct consequence of what was indicated in section 5.1. The popular misconception of using the inverse problem of nonlinear dynamics to analyze a time series data from a finite difference method computer code in an attempt to learn about the true physical solution behavior of the continuum governing PDEs without knowing by other means the exact solution behavior of the PDEs other than the numerical solutions can also be misleading. These will be discussed in the next two sections.

5.3. Residual Test

Consider a quasilinear PDE of the form

$$\frac{\partial u}{\partial t} = G(u, u_x, u_{xx}, \alpha, \epsilon), \quad (5.1)$$

where G is nonlinear in u , u_x and u_{xx} and α and ϵ are system parameters. For simplicity, consider a two time level and a $(p + q)$ point grid stencil of the form

$$u_j^{n+1} = u_j^n - H(u_{j+q}^n, \dots, u_j^n, \dots, u_{j-p}^n, \alpha, \epsilon, \Delta t, \Delta x) \quad (5.2)$$

for the PDE (5.1). Let U^* , a vector representing $(u_{j+q}^*, \dots, u_j^*, \dots, u_{j-p}^*)$ be a steady-state numerical solution of (5.2). It is a common practice in CFD to use a time dependent approach such as (5.2) to solve the steady-state equation $G(u, u_x, u_{xx}, \alpha, \epsilon) = 0$. The iteration is stopped when the residual H or some L_2 norm of the dependent variable u between two successive iterates is less than a pre-selected level.

Aside from the various standard numerical error such as truncation error, machine round-off error, etc. [89], there is a more fundamental question on the validity of the residual test and/or L_2 norm test. If the scheme happens to produce spurious steady-state numerical solutions, these spurious solutions would still satisfy the residual and L_2 norm tests in a deceptively smooth manner. Moreover, aside from the spurious solutions issue, depending on the combination of time as well as spatial discretizations, it is not easy to check whether $G(u^*, u_x^*, u_{xx}^*, \alpha, \epsilon) \rightarrow 0$ even though $H(U^*, \alpha, \epsilon, \Delta t, \Delta x) \rightarrow 0$. This is contrary to the ODE case, where if u^* is spurious in (1.1) then $S(u^*) \neq 0$. Among other factors, this is one of the contributing factors in the increase in magnitude of difficulty for analyzing the dynamical behavior of numerical methods for hyperbolic and parabolic PDEs.

One might argue that one can judge the accuracy of the scheme by comparing the numerical solutions with more than one numerical methods and by doing a sequence of grid refinement and time step reductions. The latter approach might not be feasible at an acceptable cost. The former might not be foolproof if one does not know the dynamical behavior of the finite difference schemes being used. One important contributing factor on the use of the Lax-Wendroff types of schemes [90,91] is that these schemes are more accurate and sometimes more stable when operated on or near the linearized stability limit.

5.4. The Inverse Problems of Nonlinear Dynamics

The use of the inverse problem of nonlinear dynamics to analyze the dynamical behavior of time series data arising from experimental or observable data has received much attention in nonlinear physics as well as in many of the engineering disciplines. The approach is very useful for gaining some insights into the nonlinear dynamical behavior

in problems where experimental or observable data are the main source of information. Often the associated governing equations (continuum or otherwise) do not exist to start with. There has been an explosion of theory, numerical procedures and computer software addressing this rapidly growing direction [92-95]. There also has been much recent interest in forecasting algorithms that attempt to analyze a time series by fitting nonlinear models. The attractive feature of this approach is that when used correctly on the correct problems one can reduce the complexity of the problem from un-manageable higher dimensions to a very low dimension. It is therefore a natural tendency for practitioners in computational sciences to apply this approach to analyze the dynamical behavior of time series data from a finite difference method computer code in an attempt to learn about the true physical solution behavior of the governing PDEs. This application of time series analysis can be misleading and can lead to a wrong conclusion if the practitioner does not know by other means the exact solution behavior of the PDEs other than from the numerical solutions. Examples of the use of this type of approach in CFD computations have been presented in references [96-98]. It can be seen from our study that the conclusions drawn from this type of time series analysis provide very little information, but rather can actually mislead one as to the true physics of the problem.

VI. CONCLUDING REMARKS

Spurious stable as well as unstable steady-state numerical solutions, spurious asymptotic numerical solutions of higher period, and even stable chaotic behavior can occur when finite-difference methods are used to solve nonlinear DEs numerically. The occurrence of spurious asymptotes is independent of whether the DE possesses a unique steady state or has additional periodic solutions and/or exhibits chaotic phenomena. The form of the nonlinear DEs and the type of numerical schemes are the determining factor. In addition, the occurrence of spurious steady states is not restricted to the time steps that are beyond the linearized stability limit of the scheme. In many instances, it can occur below the linearized stability limit. Therefore, it is essential for practitioners in computational sciences to be knowledgeable about the dynamical behavior of finite-difference methods for nonlinear scalar DEs before the actual application of these methods to practical computations. It is also important to change the traditional way of thinking and practices when dealing with genuinely nonlinear problems.

In the past, spurious asymptotes were observed in numerical computations but tended to be ignored because they all were assumed to lie beyond the linearized stability limits of the time step parameter Δt . As can be seen from our study, bifurcations to and from spurious asymptotic solutions and transitions to computational instability not only are highly scheme dependent and problem dependent, but also initial data and boundary condition dependent, and not limited to time steps that are beyond the linearized stability limit.

The symbiotic relation among all of these various factors makes this topic fascinating

and yet extremely complex. The main fundamental conclusion is that, in the absence of truncation and machine round-off errors, there are qualitative features of the nonlinear DE which cannot be adequately represented by the finite-difference methods and vice versa. The major feature is that convergence in practical calculations involved fixed Δt as $n \rightarrow \infty$ rather than $\Delta t \rightarrow 0$ as $n \rightarrow \infty$. It should be emphasized that the resulting discrete maps from finite discretizations can exhibit a much richer range of dynamical behavior than their continuum counterparts. A typical feature is the existence of spurious numerical asymptotes that can interfere with stability, accuracy and basins of attraction of the true physics of the continuum.

References

- [1] NASA Computational Fluid Dynamics Conference, NASA Conference Publication 10038, Vol. 1 and 2, March 7-9, 1989.
- [2] R.L. Devaney, *An Introduction to Chaotic Dynamical Systems*, Addison Wesley, New York, 1987.
- [3] R. Seydel, *From Equilibrium to Chaos*, Elsevier, New York, 1988.
- [4] J. Guckenheimer and P. Holmes, *Nonlinear Oscillations, Dynamical Systems, and Bifurcations of Vector Fields*, Springer-Verlag, New York, 1983.
- [5] J.M.T. Thompson and H.B. Stewart, *Nonlinear Dynamics and Chaos*, John Wiley, New York, 1986.
- [6] C.S. Hsu, *Cell-to-Cell Mapping*, Springer-Verlag, New York, 1987.
- [7] M. Kubíček and M. Marek, *Computational Methods in Bifurcation Theory and Dissipative Structures*, Springer-Verlag, New York, 1983.
- [8] T.S. Parker and L.O. Chua, *Practical Numerical Algorithms for Chaotic Systems*, Springer-Verlag, New York, 1989.
- [9] E. A. Jackson, *Perspectives of Nonlinear Dynamics*, Cambridge, Cambridge, 1989.
- [10] E. Beltrami, *Mathematics for Dynamic Modeling*, Academic Press, Orlando, 1987.
- [11] R.M. May, "Biological Populations Obeying Difference Equations: Stable Points, Periodic Orbits and Chaos," *J. Theoret. Biol.*, Vol. 51, 1975, pp. 511-524.
- [12] H.C. Yee, "A Study of Two-Dimensional Nonlinear Difference Systems and Their Applications," Ph.D. Dissertation, University of Calif, Berkeley, Calif., USA, 1975.
- [13] C.S. Hsu, "On Nonlinear Parametric Excitation Problems," *Advances in Applied Mechanics*, Vol. 17, 1977, pp. 245-301, Academic Press, New York.
- [14] H.C. Yee, "A Class of High-Resolution Explicit and Implicit Shock-Capturing Methods," NASA TM-101088, Feb. 1989.
- [15] P.K. Sweby, " "TVD" Schemes for Inhomogeneous Conservation Laws," *Proc. Nonlinear Hyperbolic Equations*, Eds. J. Ballmann & R. Jeltsch, Notes on Numerical Fluid Mechanics, 24, 1989, pp. 599-607.
- [16] P.K. Sweby, "Source Terms and Conservation Laws: A Preliminary Discussion," Numerical Analysis Report 6/89, Department of Mathematics, University of Reading, England.
- [17] B. Engquist and B. Sjögreen, "Numerical Approximation of Hyperbolic Conservation Laws with Stiff Terms," CAM Report 89-07, Department of Mathematics,

UCLA, Calif. USA, March 1989.

- [18] K.W. Wallace, "Spurious Period Doubling Bifurcations in a Discretized Reaction-Advection Model," M.S. Thesis, Faculty of Science, University of Dundee, Scotland, Sept. 1989.
- [19] G. Strang, "On the Construction and Comparison of Difference Schemes," *SIAM J. Num. Anal.* Vol. 5, 1968, pp. 506-517.
- [20] R.D. Richtmyer and K.W. Morton, *Difference Methods for Initial-Value Problems*, Interscience-Wiley, New York, 1967.
- [21] P.K. Sweby, H.C. Yee and D.F. Griffiths, "On Spurious Steady-State Solutions of Explicit Runge-Kutta Schemes," NASA TM, March 1990.
- [22] A.M. Panov, "Behavior of the Trajectories of a System of Finite Difference Equations in the Neighbourhood of a Singular Point," *Uch. Zap. Ural. Gos. Univ. vyp.* Vol. 19, 1956, pp. 89-99.
- [23] O. Perron, "Über Stabilität und Asymptotisches Überhalten der Lösungen eines Systems endlicher Differenzgleichungen," *J. Reine Angew. Math.* Vol. 161, 1929, pp. 41-64.
- [24] C.S. Hsu, H.C. Yee and W.H. Cheng, "Determination of Global Regions of Asymptotic Stability for Difference Dynamical Systems," *J. Appl. Mech.*, Vol. 44, pp., 1977, pp. 147-153.
- [25] C.S. Hsu, H.C. Yee and W.H. Cheng, "Steady-State Response of a Nonlinear System Under Impulsive Periodic Parametric Excitation," *J. Sound Vib.*, Vol. 50, 1977, pp. 95-116.
- [26] R.M. May, "Simple Mathematical Models with Very Complicated Dynamics," *Nature*, Vol. 261, 1976, pp. 459-467.
- [27] R.M. May, "Biological Populations with Nonoverlapping Generations: Stable Points, Stable Cycles, and Chaos," *Science*, Vol. 186, No. 15, 1974, pp. 645-647.
- [28] T.Y. Li and J.A. Yorke, "Period Three Implies Chaos," *Am. Math. Monthly*, Vol. 82, 1975, pp. 985-992.
- [29] E.N. Lorenz, "The Problem of Deducing the Climate from the Governing Equations," *Tellus*, Vol. 16, 1964, pp. 1-11.
- [30] M.J. Feigenbaum, "Quantitative Universality for a Class of Nonlinear Transformations," *J. Stat. Phys.*, Vol. 19, 1978, pp. 25-52.
- [31] C.S. Hsu and H.C. Yee, "Behavior of Dynamical Systems Governed by a Simple Nonlinear Difference Equation," *J. Appl. Mech.*, Vol. 44, 1975, pp. 870-876.
- [32] S. Ushiki, "Central Difference Scheme and Chaos," *Physica 4D*, 1982, pp. 407-424.
- [33] F. Brezzi, S. Ushiki and H. Fujii, "Real and Ghost Bifurcation Dynamics in Dif-

- ference Schemes for Ordinary Differential Equations," *Numerical Methods for Bifurcation Problems*, T. Kupper, H.D. Mittleman and H. Weber eds., Birkhauser-Verlag, Boston, 1984.
- [34] R. Schreiber and H.B. Keller, "Spurious Solution in Driven Cavity Calculations," *J. Comput. Phys.*, Vol. 49, No. 1, 1983.
- [35] W.J. Beyn and E.J. Doedel, "Stability and Multiplicity of Solutions to Discretizations of Nonlinear Ordinary Differential Equations," *SIAM J. Sci. Statist. Comput.*, Vol. 2, 1981, pp. 107-120.
- [36] R.B. Kellogg, G.R. Shubin, and A.B. Stephens, *SIAM J. Numer. Anal.* Vol. 17, No. 6, 1980, pp. 733-739.
- [37] A.B. Stephens and G.R. Shubin, *SIAM J. Sci. Statist. Comput.*, Vol. 2, 1981, pp. 404-415.
- [38] G.R. Shubin, A.B. Stephens and H.M. Glaz, "Steady Shock Tracking and Newton's Method Applied to One-Dimensional Duct Flow," *J. Comput. Phys.*, Vol. 39, 1981, pp. 364-374.
- [39] P.G. Reinhall, T.K. Caughey and D.W. Storti, "Order and Chaos in a Discrete Duffing Oscillator: Implications on Numerical Integration," *Trans. of the ASME, J. Appl. Mech.*, 89-APM-6, 1989.
- [40] E.N. Lorenz, "Computational Chaos - A Prelude to Computational Instability," *Physica D*, Vol. 35, 1989, pp. 299-317.
- [41] A.J. Lichtenberg and M.A. Lieberman, *Regular and Stochastic Motion*, Appl. Math. Sci. Bd. 38, 1983, Springer-Verlag, New York.
- [42] R.H. Miller, "A Horror Story about Integration Methods," to appear.
- [43] W.A. Mulder and B. van Leer, "Implicit Upwind Methods for the Euler Equations," AIAA-83-1930, July 1983.
- [44] M. Prüffer, "Turbulence in Multistep Methods for Initial Value Problems," *SIAM J. Appl. Math.* Vol. 45, 1985, pp. 32-69.
- [45] W.-J. Beyn, "On the Numerical Approximation of Phase Portraits Near Stationary Points," *SIAM J. Numer. Anal.*, Vol. 24, No. 5, 1987, pp. 1095-1113.
- [46] A.R. Mitchell and D.F. Griffiths, "Beyond the Linearized Stability Limit in Non Linear Problems," Report NA/88 July 1985, Department of Mathematical Sciences, University of Dundee, Scotland U.K.
- [47] A.R. Mitchell and J.C. Bruch, Jr., "A Numerical Study of Chaos in a Reaction-Diffusion Equation," *Numerical Methods for PDEs*, Vol. 1, 1985, pp. 13-23.
- [48] A.R. Mitchell, P. John-Charles and B.D. Sleeman, "Long Time Calculations and Non Linear Maps," Numerical Analysis Report 93, May 1986, Department of Mathematical Sciences, University of Dundee, Scotland.

- [49] V.S. Manoranjan, A.R. Mitchell, and B.D. Sleeman, "Bifurcation Studies in Reaction-Diffusion," *J. Comput. App. Math.*, Vol. 11, 1984, pp. 27-37.
- [50] B.D. Sleeman, D.F. Griffiths, A.R. Mitchell and P.D. Smith, "Stable Periodic Solutions in Nonlinear Difference Equations," *SIAM J. Sci. Stat. Comput.*, Vol. 9, No. 3, May 1988, pp. 543-557.
- [51] D.F. Griffiths and A.R. Mitchell, "Stable Periodic Solutions of a Nonlinear Partial Difference Equation in Reaction Diffusion," Report NA/113, Jan. 1988, Dept. Math. and Compt. Science, University of Dundee, Scotland.
- [52] A.R. Mitchell, G. Stein and M. Maritz, "Periodic Structure Beyond a Hopf Bifurcation," *Comm. Appl. Num. Meth.*, Vol. 4, 1988, pp. 263-272.
- [53] D.F. Griffiths and A.R. Mitchell, "Stable Periodic Bifurcations of an Explicit Discretization of a Nonlinear Partial Differential Equation in Reaction diffusion," *Inst. Math. Applics., J. Num. Analy.*, Vol. 8, 1988, pp. 435-454.
- [54] A.R. Mitchell and S.W. Schoombie, "Nonlinear Diffusion and Stable Period 2 Solutions of a Discrete Reaction-Diffusion Model," *J. Comp. Appl. Math.*, Vol 25, 1989, pp. 363-372.
- [55] J.M. Sanz-Serna and F. Vaddillo, "Nonlinear Instability, the Dynamic Approach," in *Proceedings Dundee, 1985*, G.A. Watson and D.F. Griffiths, eds., Pitman, London.
- [56] A. Iserles, "Nonlinear Stability and Asymptotics of O.D.E. Solvers," *International Conference on Numerical Mathematics, Singapore*, R.P. Agarwal, ed., Birkhauser, Basel, 1989.
- [57] A. Iserles and J.M. Sanz-Serna, "Equilibria of Runge-Kutta Methods," *Numerical Analysis Reports, DAMTP 1989/NA4*, May 1989, Univeristy of Cambridge, England.
- [58] A.M. Stuart, "Linear Instability Implies Spurious Periodic Solutions," submitted to *IMA J. Num. Anal.*, 1988.
- [59] A. Stuart, "The Global Attractor Under Discretisation," to appear, *Proc. NATO Conference on Continuation & Bifurcation*, 1989.
- [60] A. Stuart and A. Peplow, "The Dynamics of the Theta Method," to appear, *SIAM J. Sci. Stat. Comput.*
- [61] A. Stuart, "Nonlinear Instability in Dissipative Finite Difference Schemes," *SIAM Review*, Vol. 31, No. 2, 1989, pp. 191-220.
- [62] A. Stuart, "Linear Instability Implied Spurious Periodic Solutions," to appear, *IMA J. Numer. Anal.*
- [63] C. Grebogi E. Ott and J. Yorke, "Chaos, Strange Attractors, and Fractal Basin Boundaries in Nonlinear Dynamics," *Science*, Vol. 238, 1987, pp. 585-718.
- [64] S.W. McDonald, C. Grebogi E. Ott and J. Yorke, "Fractal Basin Boundaries,"

- Physica 17D, 1985, pp. 125-153.
- [65] C. Grebogi E. Ott and J. Yorke, "Crises, Sudden Changes in Chaotic Attractors, and Transient Chaos," *Physics* 7D, 1983, pp. 181-200.
 - [66] J.D. Lambert, *Computational Methods in Ordinary Differential Equations*, John Wiley, New York, 1973.
 - [67] C.W. Gear, *Numerical Initial Value Problems in Ordinary Differential Equations* (Prentice-Hall, 1971).
 - [68] J.C. Butcher, *The Numerical Analysis of Ordinary Differential Equations*, John Wiley, New York, 1987.
 - [69] MAPLE, algebraic manipulation package, University of Waterloo, Canada, 1988
 - [70] D. Whitley, "Discrete Dynamical Systems in Dimensions One and Two," *Bull. London Math Soc.* Vol. 15, 1983, pp. 177-217.
 - [71] R.M. Beam and R.F. Warming, "Implicit Numerical Methods for the Compressible Navier-Stokes and Euler Equations," *Lecture Notes for Computational Fluid Dynamics*, von Karman Institute for Fluid Dynamics, March 29 - April 2, 1982, Rohde-Saint-Genèse, Belgium.
 - [72] J. Maynard Smith, *Mathematical Ideas in Biology*, Cambridge University Press, Cambridge, 1968.
 - [73] H. Ikeda, M. Mimura and Y. Nishiura, "Global Bifurcation Phenomena of Travelling Wave Solutions for Some Bistable Reaction-Diffusion Systems," *Nonlinear Analysis, Theory, Methods and Applications*, Vol. 13, No. 5, 1989, pp. 507-526.
 - [74] T. Hagstrom and H.B. Keller, "The Numerical Calculation of travelling Wave Solutions of Nonlinear Parabolic Equations," *SIAM J. Sci. Stat. Comput.*, Vol. 7, No. 3, 1986.
 - [75] A. Harten and S. Osher, "Uniformly High-Order Accurate Nonoscillatory Schemes I," *SIAM J. Num. Analy.* Vol. 24, No. 2, 1987, pp. 279-309.
 - [76] A. Harten, "On a Class of High Resolution Total-Variation-Stable Finite-Difference Schemes," *SIAM J. Num. Anal.*, Vol. 21, 1984, pp. 1-23.
 - [77] P.L. Roe, "Some Contributions to the Modelling of Discontinuous Flows," *Lectures in Applied Mathematics*, Vol. 22 (Amer. Math. Soc., Providence, R.I., 1985).
 - [78] R.J. LeVeque and H.C. Yee, "A study of Numerical Methods for Hyperbolic Conservation Laws with Stiff Source Terms," NASA TM-100075, March 1988, *J. Comput. Phys.*, Vol. 86, No. 1, Jan. 1990.
 - [79] M. Pandolfi, M. Germano and N. Botta, "Non-Equilibrium Reacting Hypersonic Flow About Blunt Bodies: Numerical Prediction, AIAA-88-0514, Jan. 1988.
 - [80] P. Colella, A. Majda, and V. Roytburd, "Theoretical and Numerical Structure for Reacting Shock Waves," *SIAM J. Sci. Stat. Comput.* Vol. 7, 1986, pp.

1059-1080.

- [81] T.R. Young and J.P. Boris, "A Numerical Technique for Solving Stiff Ordinary Differential Equations Associated with the Chemical Kinetics of Reactive-Flow Problems," *J. Phys. Chem.* Vol. 81, 1977, pp. 2424-2427.
- [82] H.C. Yee, "Numerical Approximation of Boundary Conditions with Applications to Inviscid Equations of Gas Dynamics," NASA TM-81265, 1981.
- [83] H.C. Yee, R.M. Beam and R.F. Warming, "Boundary Approximations for Implicit Schemes for One-Dimensional Inviscid Equations of Gasdynamics," *AIAA J.*, Vol. 20, No. 9, 1982, pp. 1203-1211.
- [84] P.D. Lax and B. Wendroff, "Systems of Conservation Laws," *Commun. Pure Appl. Math.*, Vol. 13, 1960, pp. 217-237.
- [85] R.J. LeVeque, "Hyperbolic Conservation Laws and Numerical Methods," *Lecture Series on Computational Fluid Dynamics*, von Karman Institute for Fluid Dynamics, Rhode-St-Genèse, Belgium, March 5-9, 1990.
- [86] A. Jameson, W. Schmidt and E. Turkel, "Numerical Solutions of the Euler Equations by Finite Volume Methods Using Runge-Kutta Time-Stepping Schemes," AIAA-81-1259, 1981.
- [87] J.D. Anderson, Jr, "Introduction to Computational Fluid Dynamics," von Karman Institute for Fluid Dynamics, 1985 lecture series, Rhode-Saint-Genèse, Belgium.
- [88] G.A. Sod, *Numerical Methods in Fluid Dynamics*, Cambridge University Press, Cambridge, 1985.
- [89] J.H. Ferziger, "Estimation and Reduction of Numerical Error," *Forum on Methods of Estimating Uncertainty Limits in Fluid Flow Computations*, ASME Winter Annual Meeting, San Francisco, Dec. 1989.
- [90] P.D. Lax and B. Wendroff, "Difference Schemes for Hyperbolic Equations with High Order of Accuracy," *Commun. Pure Appl. Math.*, Vol. 17, 1964, pp. 381-398.
- [91] R.W. MacCormack, "The Effect of Viscosity in Hypervelocity Impact Cratering," AIAA-69-354, Cincinnati, Ohio, 1969.
- [92] N.H. Packard, J.P. Crutchfield, J.D. Farmer and R.S. Shaw, "Geometry from a Time Series," *Physical Review Letters*, Vol. 45, No. 9, 1980, pp. 712-716.
- [93] J.P. Eckmann and D. Ruelle, "Ergodic Theory of Chaos and Strange Attractors," *Rev. Mod. Phys.*, Vol. 57, No. 3, Part I, 1985, pp. 617-656.
- [94] H. Froehling, J.P. Crutchfield, D. Farmer, N.H. Packard and R. Shaw, "On Determining the Dimension of Chaotic Flows," *Physica 3D*, 1981, pp. 605-617.
- [95] E.J. Kostelich and J.A. Yorke, "The Analysis of Experimental Data Using Time-Delay Embedding Methods," *Institute for Physical Science and Technology Technical Report*, University of Maryland, College Park, Maryland, USA.

- [96] T.H. Pulliam, "Low Reynolds Number Numerical Solutions of Chaotic Flows," AIAA-89-1023, Jan. 9-12, 1989.
- [97] T.H. Pulliam, "Numerical Simulation of Chaotic Flows: Measures of Chaos," Forum on Chaotic Dynamics in Fluid Dynamics, ASME Fluids Engineering Spring Conference, La Jolla, Calif. July 1989.
- [98] A. Fortin, M. Fortin and J.J. Gervais, "A numerical Simulational Flow," J. Comput. Phys., 70, 1987, pp. 295-310.

Figure Captions

- Table 2.1 Possible stable asymptotic solution behavior for DEs and their discretized counterparts.
- Fig. 2.1 Phase portrait and basins of attraction of the damped pendulum equation (this figure is taken from reference [8]).
- Fig. 2.2 Phase portrait and basins of attraction of the predator-prey equation (this figure is taken from reference [8]).
- Fig. 3.1 Asymptotic solution behavior of the logistic ODE $du/dt = \alpha u(1 - u)$ for $\alpha > 0$.
- Fig. 3.2 Stable fixed points of periods 1,2,4,8 of the explicit Euler scheme for the logistic ODE $du/dt = \alpha u(1 - u)$.
- Fig. 3.3 Stable fixed points of periods 1,2,4,8 of the modified Euler (R-K 2) scheme for the logistic ODE $du/dt = \alpha u(1 - u)$.
- Fig. 3.4 Stable fixed points of periods 1,2,4,8 of the improved Euler (R-K 2) scheme for the logistic ODE $du/dt = \alpha u(1 - u)$.
- Fig. 3.5 Stable fixed points of periods 1,2,4,8 of the Runge-Kutta 4th-order (R-K 4) scheme for the logistic ODE $du/dt = \alpha u(1 - u)$.
- Fig. 3.6 Stable fixed points of periods 1,2,4,8 of the predictor-corrector scheme of order 2 for the logistic ODE $du/dt = \alpha u(1 - u)$.
- Fig. 3.7 Stable fixed points of periods 1,2,4,8 of the predictor-corrector scheme of order 3 for the logistic ODE $du/dt = \alpha u(1 - u)$.
- Fig. 3.8 Stable fixed points of periods 1,2,4,8 of the explicit Euler scheme for the ODE $du/dt = \alpha u(1 - u)(0.5 - u)$.
- Fig. 3.9 Stable fixed points of periods 1,2,4,8 of the modified Euler (R-K 2) scheme for the ODE $du/dt = \alpha u(1 - u)(0.5 - u)$.
- Fig. 3.10 Stable fixed points of periods 1,2,4,8 of the improved Euler (R-K 2) scheme for the ODE $du/dt = \alpha u(1 - u)(0.5 - u)$.
- Fig. 3.11 Stable fixed points of periods 1,2,4,8 of the Runge-Kutta 4th-order (R-K 4) scheme for the ODE $du/dt = \alpha u(1 - u)(0.5 - u)$.

- Fig. 3.12 Stable fixed points of periods 1,2,4,8 of the predictor-corrector scheme of order 2 for the ODE $du/dt = \alpha u(1 - u)(0.5 - u)$.
- Fig. 3.13 Stable fixed points of periods 1,2,4,8 of the predictor-corrector scheme of order 3 for the ODE $du/dt = \alpha u(1 - u)(0.5 - u)$.
- Fig. 3.14 Stable fixed points of periods 1,2,4,8 of the modified Euler (R-K 2) scheme for the ODE $du/dt = \alpha u(1 - u)(b - u)$, $b = 0.1, 0.2, 0.3, 0.4$.
- Fig. 3.15 Bifurcation diagram of the explicit Euler scheme for the logistic ODE $du/dt = \alpha u(1 - u)$.
- Fig. 3.16 Bifurcation diagram of the modified Euler (R-K 2) scheme for the logistic ODE $du/dt = \alpha u(1 - u)$ with $u^0 = 2.7$.
- Fig. 3.17 Bifurcation diagram of the modified Euler (R-K 2) scheme for the logistic ODE $du/dt = \alpha u(1 - u)$ with $u^0 = 1.5$.
- Fig. 3.18 Bifurcation diagram of the modified Euler (R-K 2) scheme for the logistic ODE $du/dt = \alpha u(1 - u)$ with $u^0 = 0.25$.
- Fig. 3.19 “Full” bifurcation diagram of the modified Euler (R-K 2) scheme for the logistic ODE $du/dt = \alpha u(1 - u)$.
- Fig. 3.20 Bifurcation diagram of the Runge-Kutta 4th-order (R-K 4) scheme for the logistic ODE $du/dt = \alpha u(1 - u)$ with $u^0 = 0.5$.
- Fig. 3.21 Bifurcation diagram of the Runge-Kutta 4th-order (R-K 4) scheme for the logistic ODE $du/dt = \alpha u(1 - u)$ with multiple initial data.
- Fig. 3.22 “Full” bifurcation diagram of the Runge-Kutta 4th-order (R-K 4) scheme for the logistic ODE $du/dt = \alpha u(1 - u)$.
- Fig. 3.23 Bifurcation diagrams of the improved Euler (R-K 2) scheme for the ODE $du/dt = \alpha u(1 - u)(0.5 - u)$ for four different sets of initial input data.
- Fig. 3.24 Bifurcation diagrams of the Runge-Kutta 4th-order (R-K 4) scheme for the ODE $du/dt = \alpha u(1 - u)(0.5 - u)$ for four different sets of initial input data.
- Fig. 3.25 Bifurcation diagrams of the modified Euler (R-K 2) scheme for the ODE $du/dt = \alpha u(1 - u)(0.4 - u)$ for four different sets of initial input data.
- Fig. 3.26 “Full” bifurcation diagram of the improved Euler (R-K 2) scheme for the logistic ODE $du/dt = \alpha u(1 - u)$.

- Fig. 3.27 “Full” bifurcation diagram of the Adam-Bashforth scheme for the logistic ODE $du/dt = \alpha u(1 - u)$.
- Fig. 3.28 “Full” bifurcation diagram of the predictor-corrector scheme of order 2 for the logistic ODE $du/dt = \alpha u(1 - u)$.
- Fig. 3.29 “Full” bifurcation diagram of the predictor-corrector scheme of order 3 for the logistic ODE $du/dt = \alpha u(1 - u)$.
- Fig. 3.30 “Full” bifurcation diagrams of the modified Euler (R-K 2) scheme for the ODE $du/dt = \alpha u(1 - u)(b - u)$, $b = 0.1, 0.2, 0.3, 0.4$.
- Fig. 3.31 “Full” bifurcation diagrams of the explicit Euler scheme for the ODE $du/dt = \alpha u(1 - u)(0.5 - u)$.
- Fig. 3.32 “Full” bifurcation diagram of the modified Euler (R-K 2) scheme for the ODE $du/dt = \alpha u(1 - u)(0.5 - u)$.
- Fig. 3.33 “Full” bifurcation diagram of the Adam-Bashforth scheme for the ODE $du/dt = \alpha u(1 - u)(0.5 - u)$.
- Fig. 3.34 “Full” bifurcation diagram of the improved Euler (R-K 2) scheme for the ODE $du/dt = \alpha u(1 - u)(0.5 - u)$.
- Fig. 3.35 “Full” bifurcation diagram of the Runge-Kutta 4th-order (R-K 4) scheme for the ODE $du/dt = \alpha u(1 - u)(0.5 - u)$.
- Fig. 3.36 “Full” bifurcation diagram of the improved Euler (R-K 2) scheme for the ODE $du/dt = \alpha u(1 - u)(0.5 - u)$ (enlarged).
- Fig. 3.37 “Full” bifurcation diagram of the Runge-Kutta 4th-order (R-K 4) scheme for the ODE $du/dt = \alpha u(1 - u)(0.5 - u)$ (enlarged).
- Fig. 3.38 “Full” bifurcation diagram of the predictor-corrector scheme of order 2 for the ODE $du/dt = \alpha u(1 - u)(0.5 - u)$.
- Fig. 3.39 Types of branching points.
- Fig. 3.40 Stability of solutions in the neighborhood of branch points, one-dimensional case. — stable, - - - unstable a,b,c,d: limit (regular turning) point; e,f,g,h: bifurcation (double) points; i,j,k,l: bifurcation-limit (singular turning) points; m,n,o,p,q: additional possible cases when the dimension of u is greater than one (this figure is taken from reference [7]).

- Fig. 3.41 Stability of steady-state solutions arising through three types of bifurcation phenomena (— stable, - - - unstable).
- Fig. 3.42 Spurious fixed points arising from transcritical bifurcations.
- Fig. 3.43 Spurious fixed points arising from subcritical bifurcation.
- Fig. 3.44 Stable and unstable fixed points of periods 1,2 of the modified Euler (R-K 2) scheme for the logistic ODE $du/dt = \alpha u(1 - u)$.
- Fig. 3.45 Stable and unstable fixed points of periods 1,2 of the improved Euler (R-K 2) scheme for the logistic ODE $du/dt = \alpha u(1 - u)$.
- Fig. 3.46 Stable and unstable fixed points of periods 1,2 of the Runge-Kutta 4th-order (R-K 4) scheme for the logistic ODE $du/dt = \alpha u(1 - u)$.
- Fig. 3.47 Stable and unstable fixed points of periods 1,2 of the predictor-corrector scheme of order 2 for the logistic ODE $du/dt = \alpha u(1 - u)$.
- Fig. 3.48 Stable and unstable fixed points of periods 1,2 of the predictor-corrector scheme of order 3 for the logistic ODE $du/dt = \alpha u(1 - u)$.
- Fig. 3.49 Stable and unstable fixed points of periods 1,2 of the modified Euler (R-K 2) scheme for the ODE $du/dt = \alpha u(1 - u)(0.5 - u)$.
- Fig. 3.50 Stable and unstable fixed points of periods 1,2 of the improved Euler (R-K 2) scheme for the ODE $du/dt = \alpha u(1 - u)(0.5 - u)$.
- Fig. 3.51 Stable and unstable fixed points of periods 1,2 of the Runge-Kutta 4th-order (R-K 4) scheme for the ODE $du/dt = \alpha u(1 - u)(0.5 - u)$.
- Fig. 3.52 Stable and unstable fixed points of periods 1,2 of the predictor-corrector scheme of order 2 for the ODE $du/dt = \alpha u(1 - u)(0.5 - u)$.
- Fig. 3.53 Stable and unstable fixed points of periods 1,2 of the predictor-corrector scheme of order 3 for the ODE $du/dt = \alpha u(1 - u)(0.5 - u)$.
- Fig. 3.54 Stable and unstable fixed points of periods 1,2 of the modified Euler (R-K 2) scheme for the ODE $du/dt = \alpha u(1 - u)(0.2 - u)$.
- Table 4.1 Systematic approach – level of complexity.

SOLUTION TYPE	ODEs OR PDEs	DISCRETIZED COUNTERPARTS
# OF ASYMPTOTES OR STEADY-STATE SOLUTIONS	SINGLE	SINGLE
	SINGLE	MULTIPLE
	MULTIPLE	SAME # OF MULTIPLE
	MULTIPLE	ADDITIONAL # OF MULTIPLE
PERIODIC SOLUTIONS	NO	YES
	YES	YES (+ EXTRA)
CHAOS	NO	YES
	YES	YES (+ EXTRA)

Table 2.1 Possible stable asymptotic solution behavior for DEs and their discretized counterparts.

I. <u>ODE CONNECTION:</u> GAIN INSIGHT INTO TIME DISCRETIZATION OF PDEs SCALAR SYSTEM — TIME SPLITTING OR METHOD OF LINES	
II. <u>DISCRETE TRAVELLING WAVE:</u>	$\frac{\partial u}{\partial t} + c \frac{\partial u}{\partial X} = \epsilon \frac{\partial^2 u}{\partial X^2} + \alpha S(u)$
SCALAR:	$\left\{ \begin{array}{l} \text{REACTION-DIFFUSION} \checkmark \\ \text{REACTION-CONVECTION} \\ \text{REACTION-CONVECTION-DIFFUSION} \end{array} \right.$
III. <u>FULL DISCRETIZATION (TEMPORAL AND SPATIAL):</u>	
SCALAR: (S≠0)	$\left(\begin{array}{l} \text{—————} \checkmark \\ \text{—————} \checkmark \\ \text{—————} \checkmark \end{array} \right) \quad \underline{\text{LINEAR}} \text{ SCHEME FOR SPATIAL DISCRETIZATION}$
SCALAR: (S=0)	$\left(\begin{array}{l} \text{—————} \\ \text{—————} \\ \text{—————} \end{array} \right) \quad \underline{\text{NONLINEAR}} \text{ SCHEME FOR SPATIAL DISCRETIZATION}$
SCALAR: (S≠0)	$\left(\begin{array}{l} \text{—————} \\ \text{—————} \\ \text{—————} \end{array} \right) \quad \underline{\text{NONLINEAR}} \text{ SCHEME FOR SPATIAL DISCRETIZATION}$

Table 4.1 Systematic approach – level of complexity.

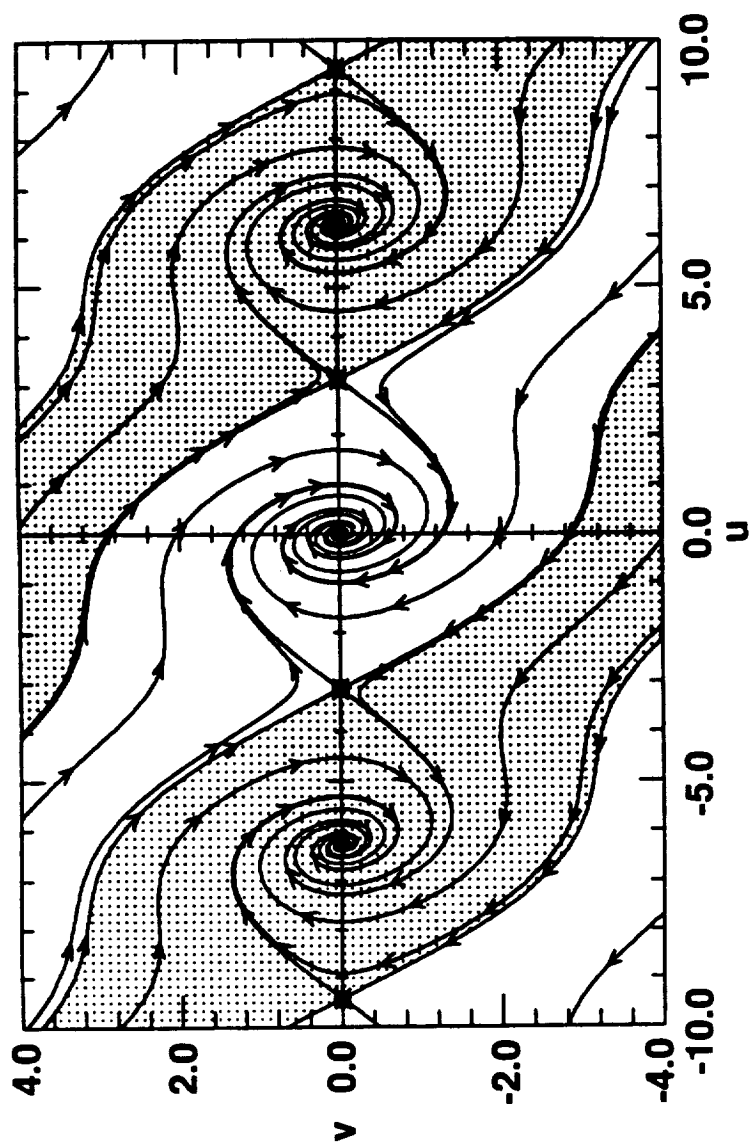


Fig. 2.1 Phase portrait and basins of attraction of the damped pendulum equation
(this figure is taken from reference [8]).

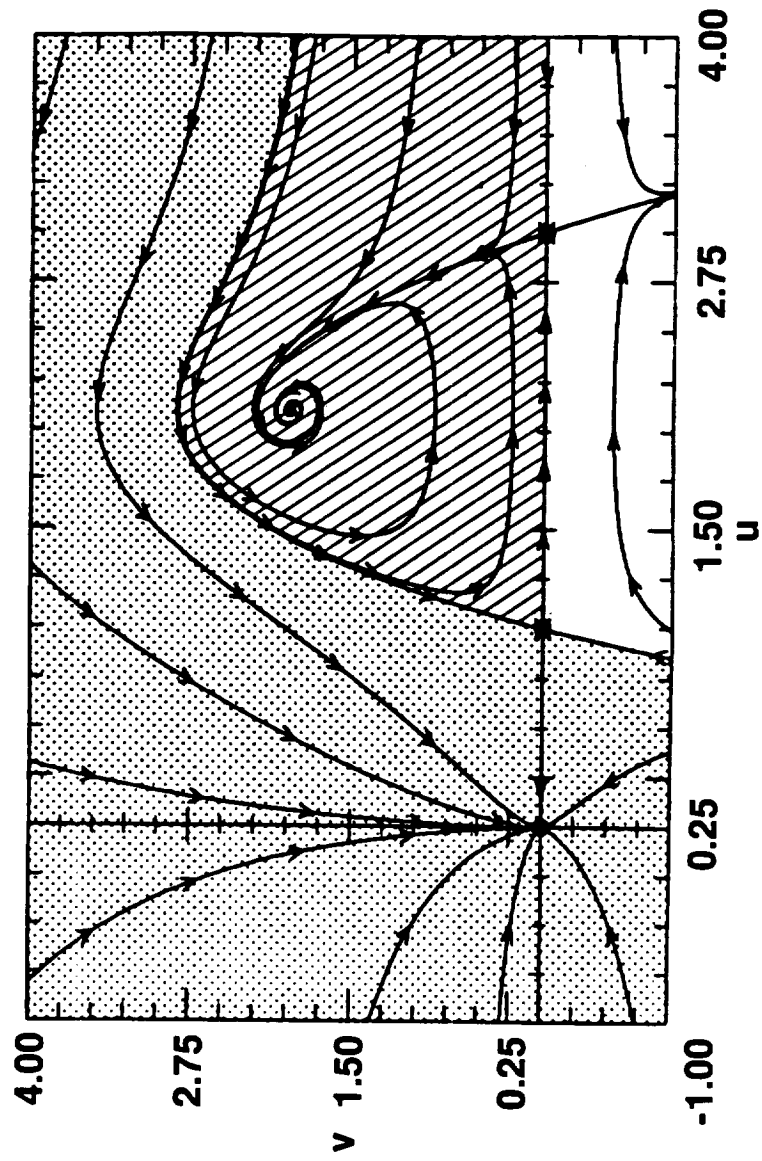


Fig. 2.2 Phase portrait and basins of attraction of the predator-prey equation (this figure is taken from reference [8]).

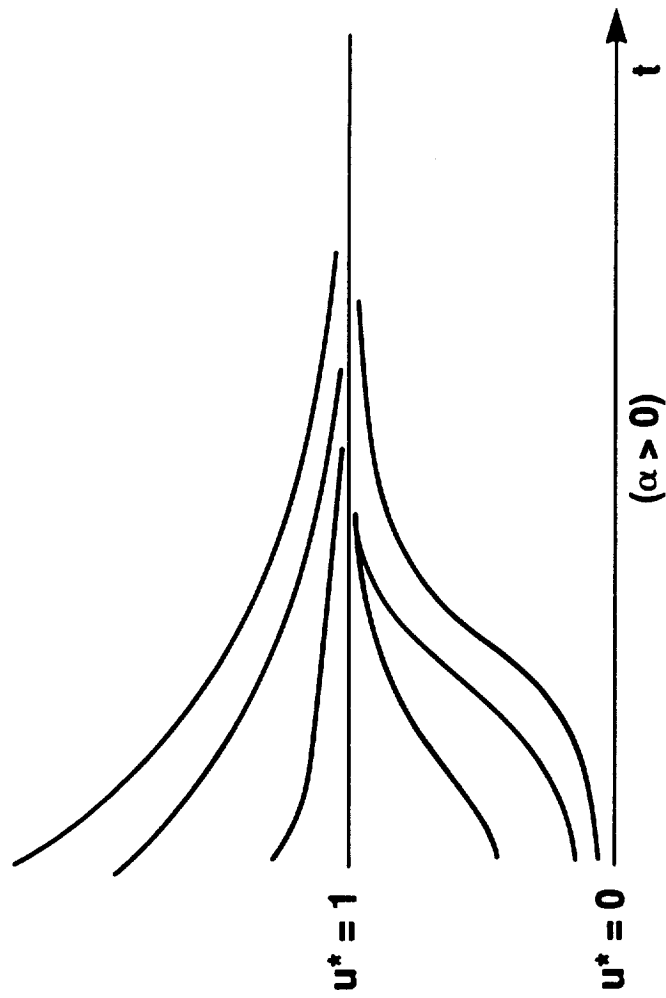


Fig. 3.1 Asymptotic solution behavior of the logistic ODE $du/dt = \alpha u(1 - u)$ for $\alpha > 0$.

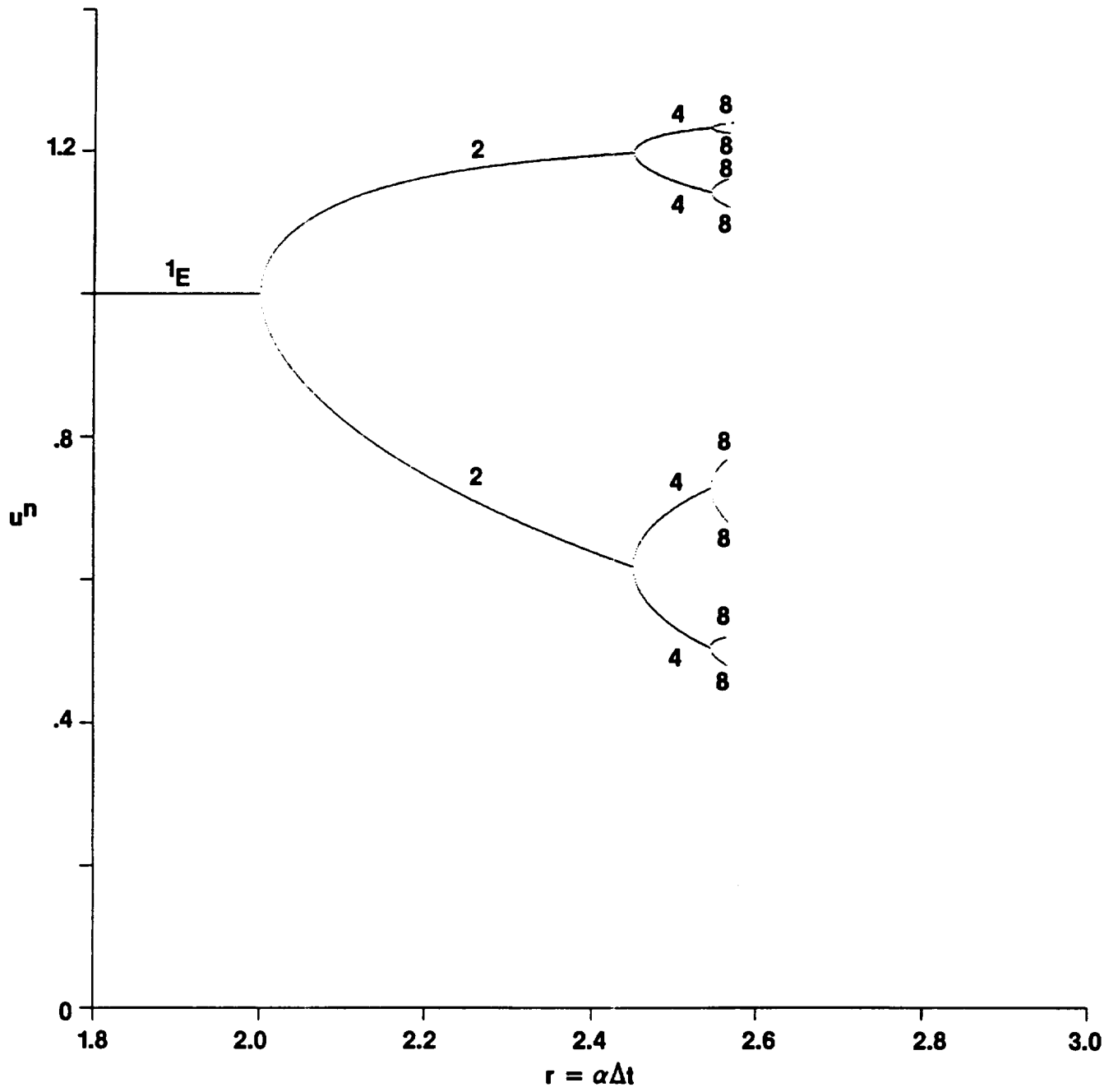


Fig. 3.2 Stable fixed points of periods 1,2,4,8 of the explicit Euler scheme for the logistic ODE $du/dt = \alpha u(1 - u)$.

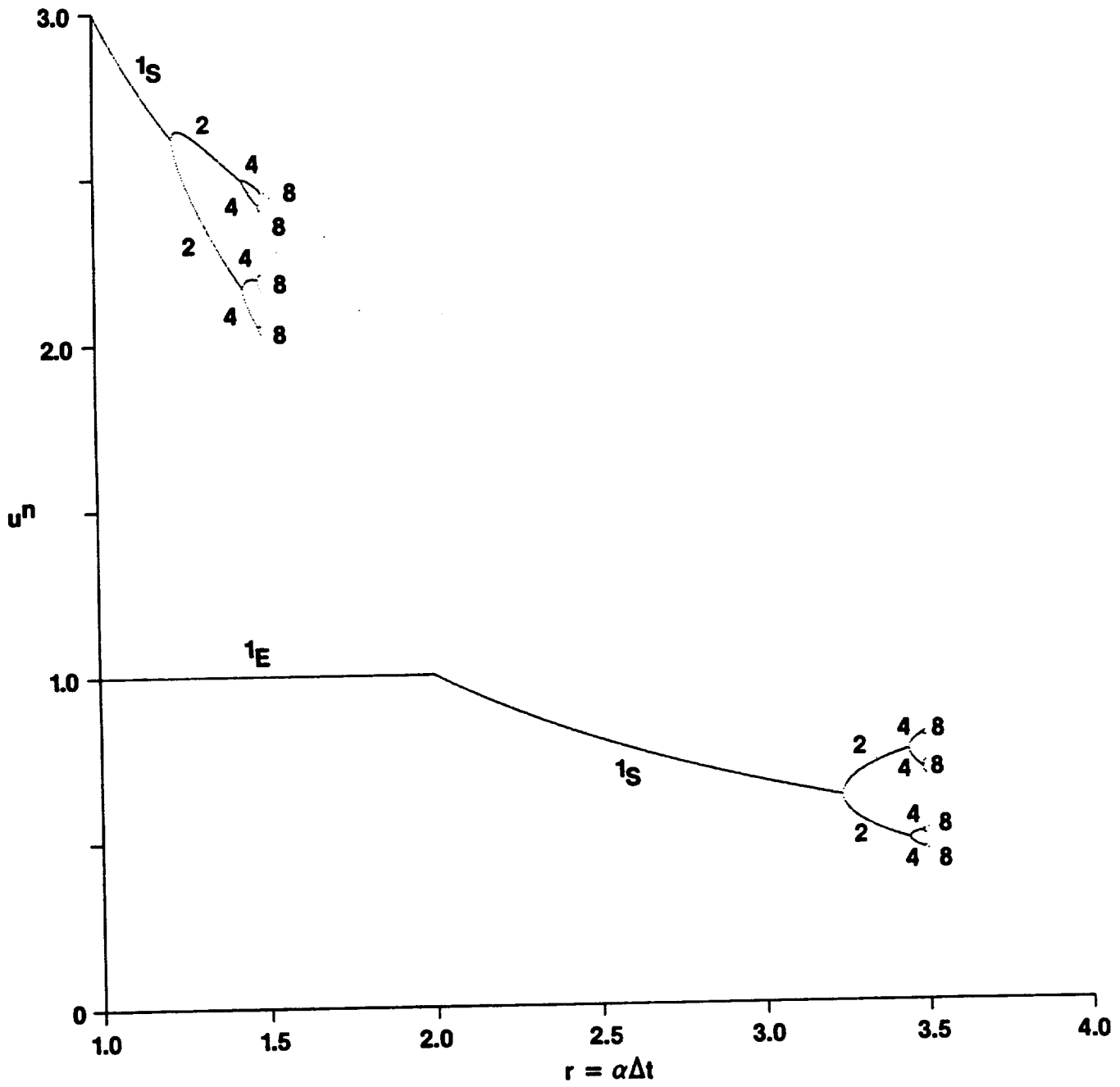


Fig. 3.3 Stable fixed points of periods 1,2,4,8 of the modified Euler (R-K 2) scheme for the logistic ODE $du/dt = \alpha u(1 - u)$.

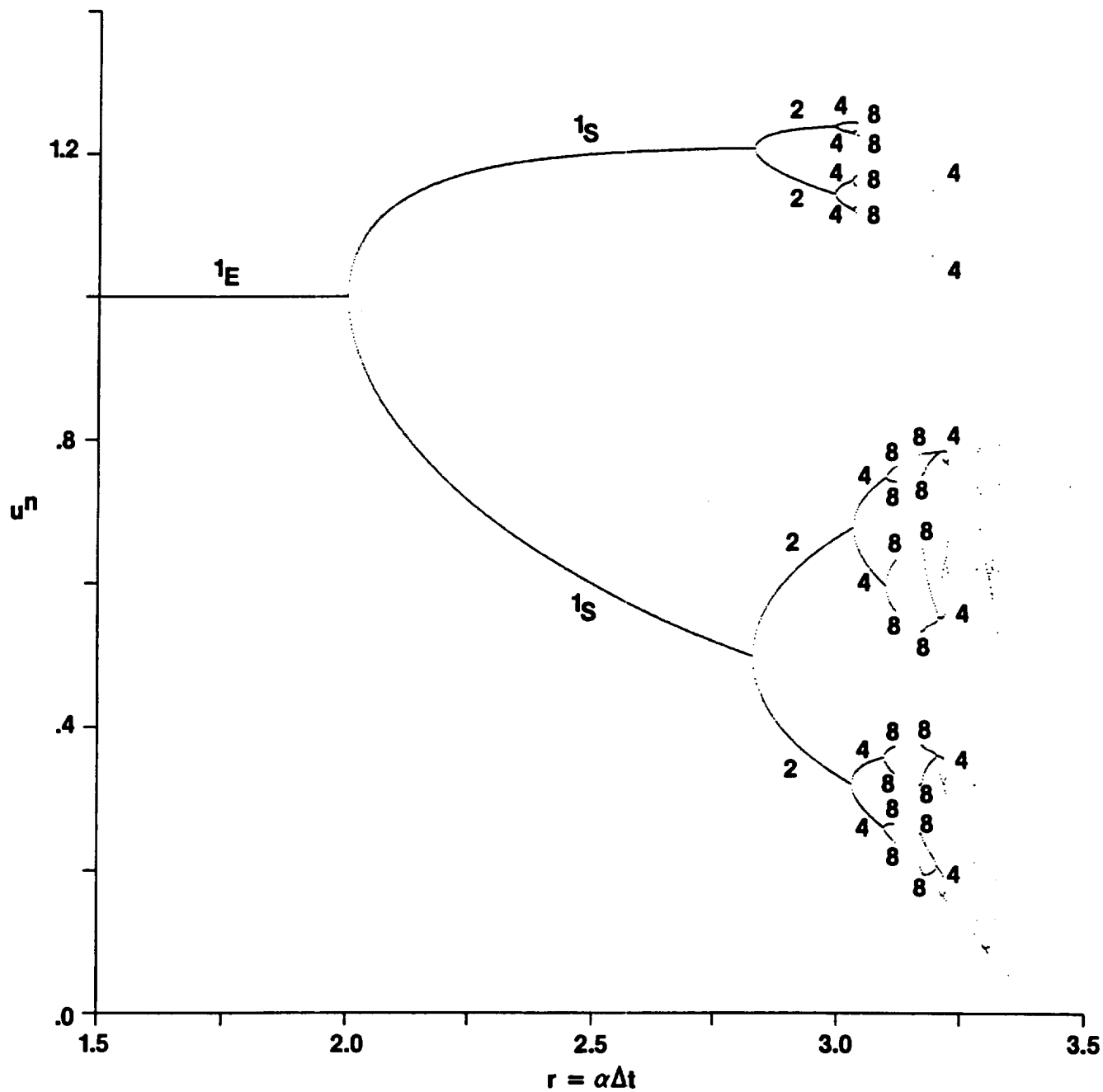


Fig. 3.4 Stable fixed points of periods 1,2,4,8 of the improved Euler (R-K 2) scheme for the logistic ODE $du/dt = \alpha u(1 - u)$.

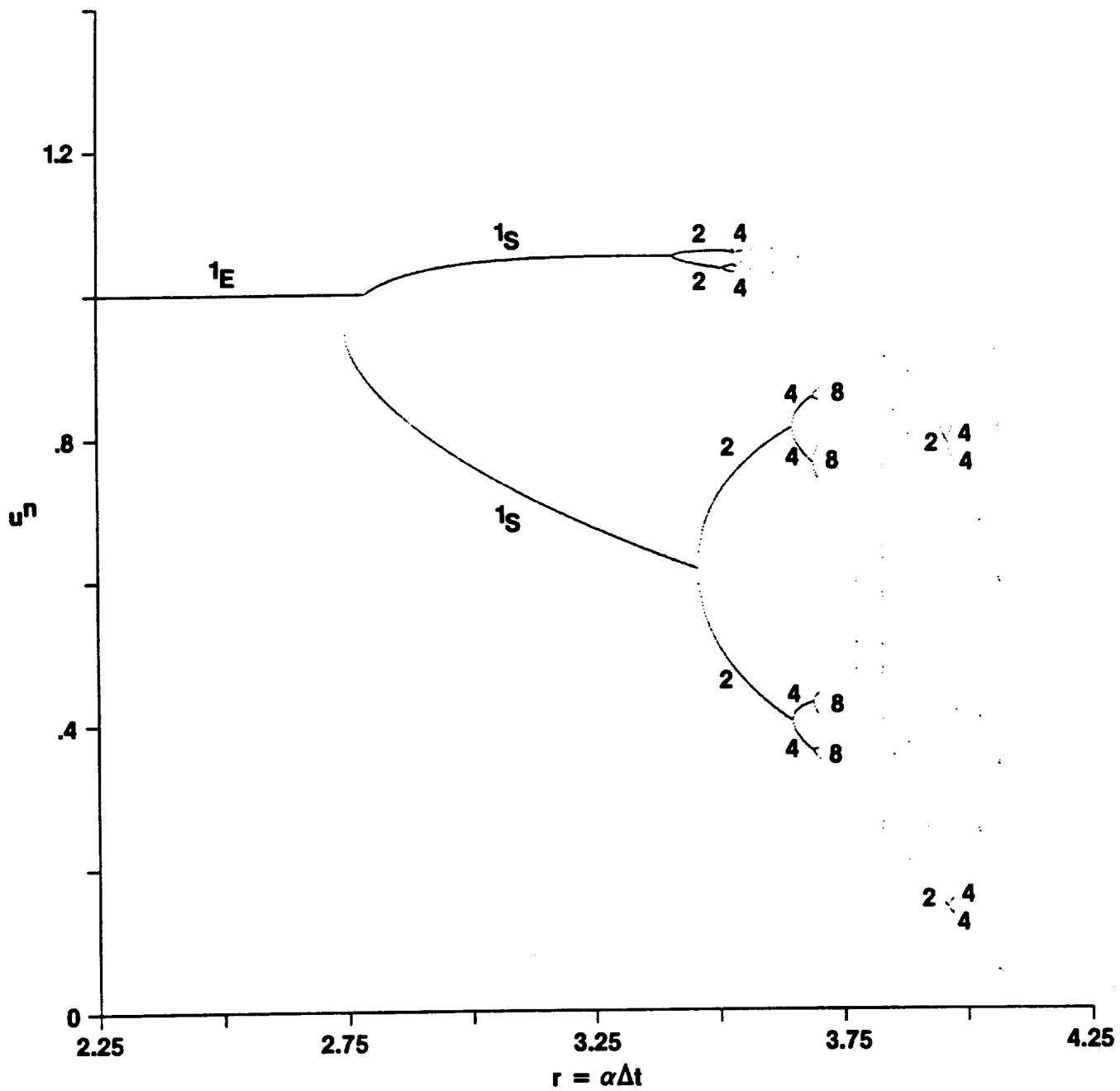


Fig. 3.5 Stable fixed points of periods 1,2,4,8 of the Runge-Kutta 4th-order (R-K 4) scheme for the logistic ODE $du/dt = \alpha u(1 - u)$.

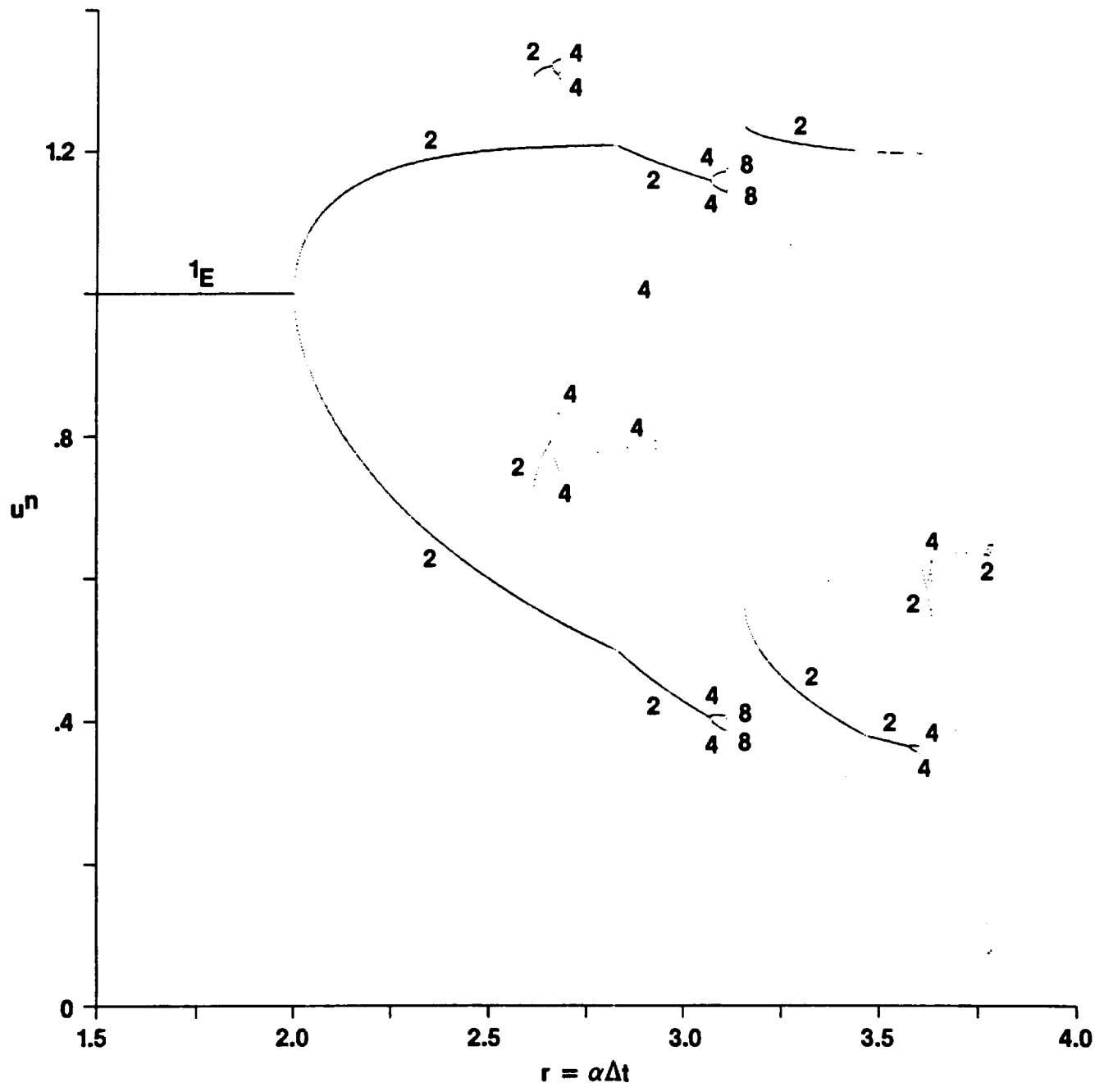


Fig. 3.6 Stable fixed points of periods 1,2,4,8 of the predictor-corrector scheme of order 2 for the logistic ODE $du/dt = \alpha u(1 - u)$.

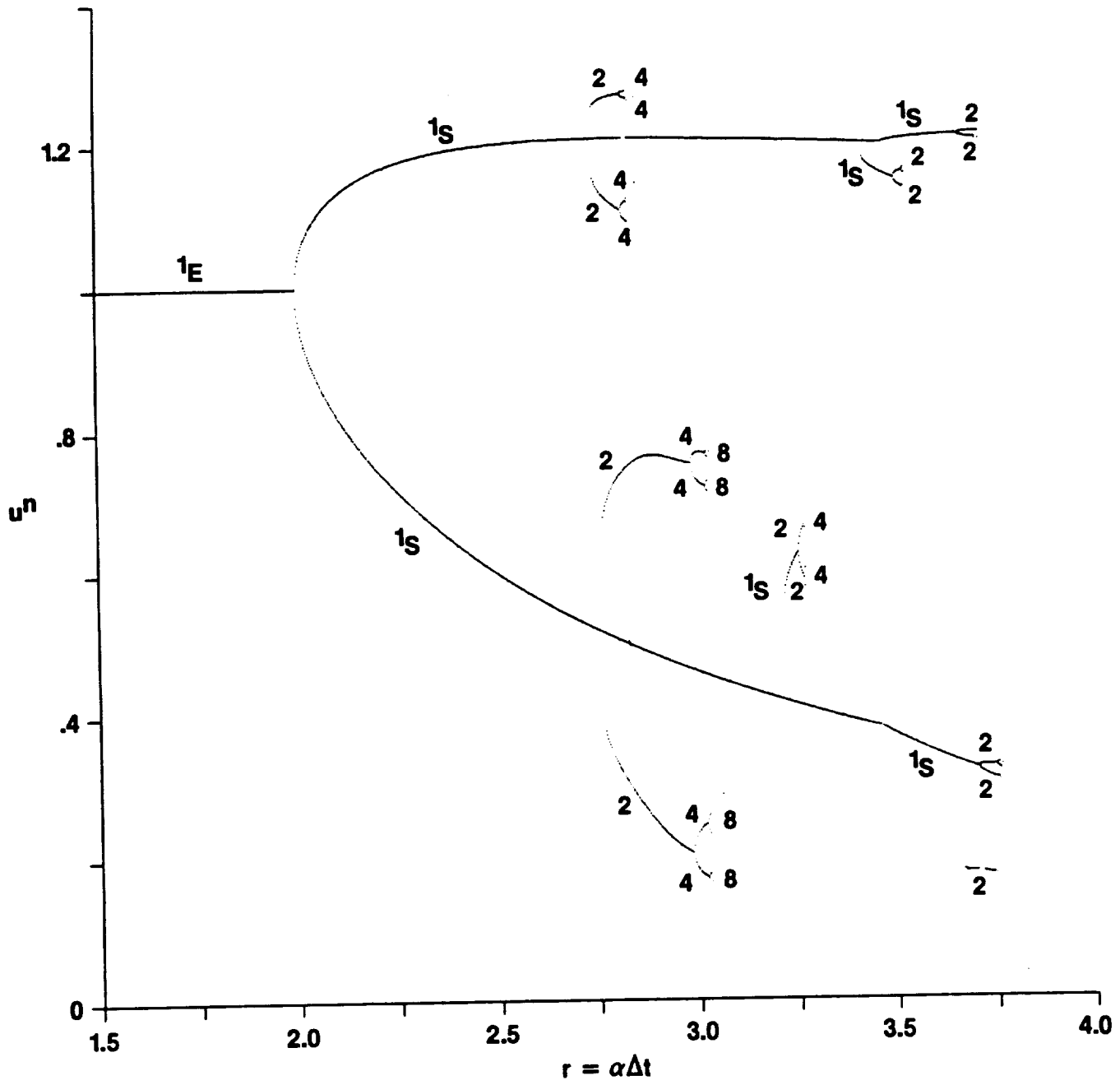


Fig. 3.7 Stable fixed points of periods 1,2,4,8 of the predictor-corrector scheme of order 3 for the logistic ODE $du/dt = \alpha u(1 - u)$.

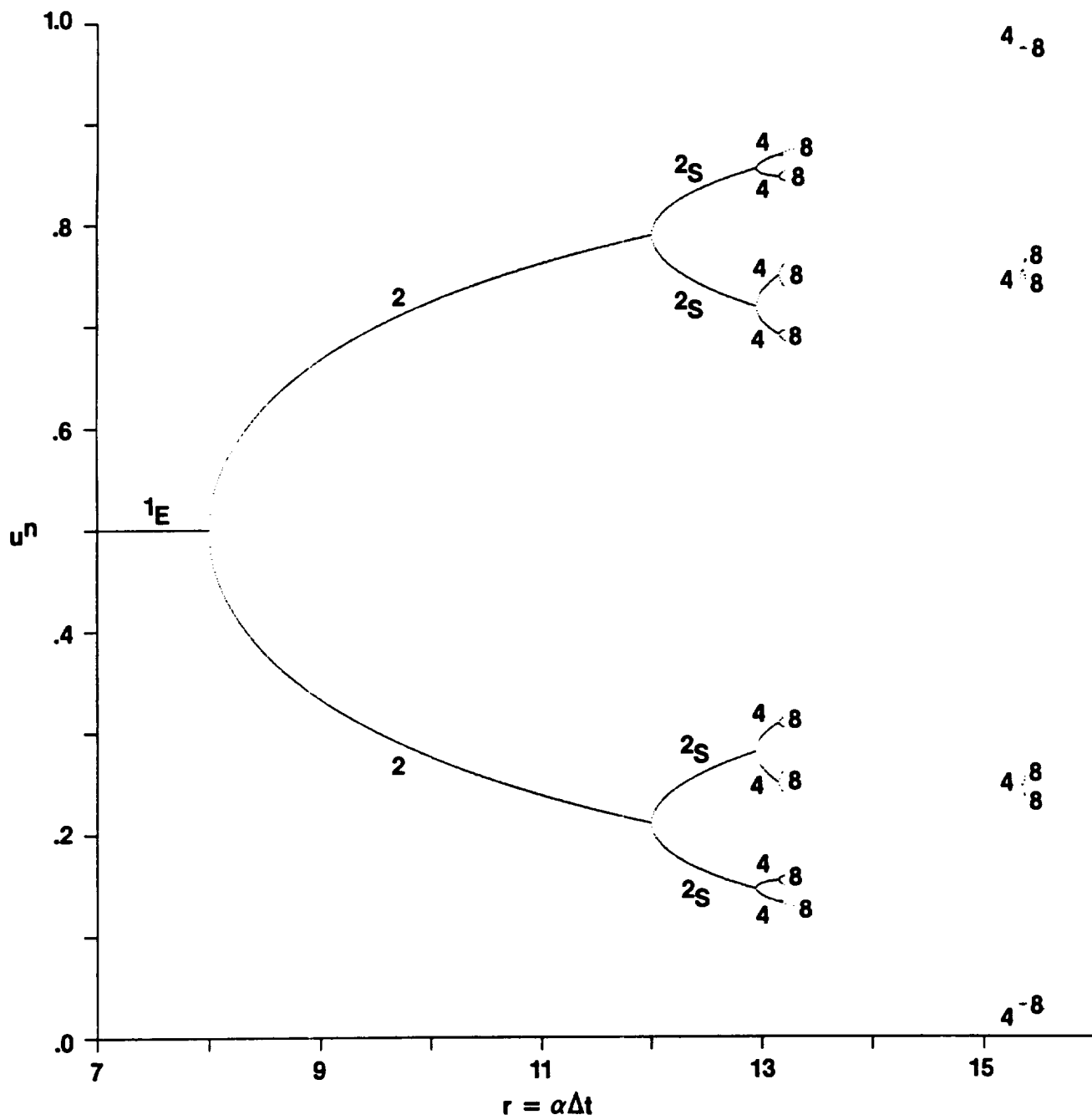


Fig. 3.8 Stable fixed points of periods 1,2,4,8 of the explicit Euler scheme for the ODE $du/dt = \alpha u(1 - u)(0.5 - u)$.

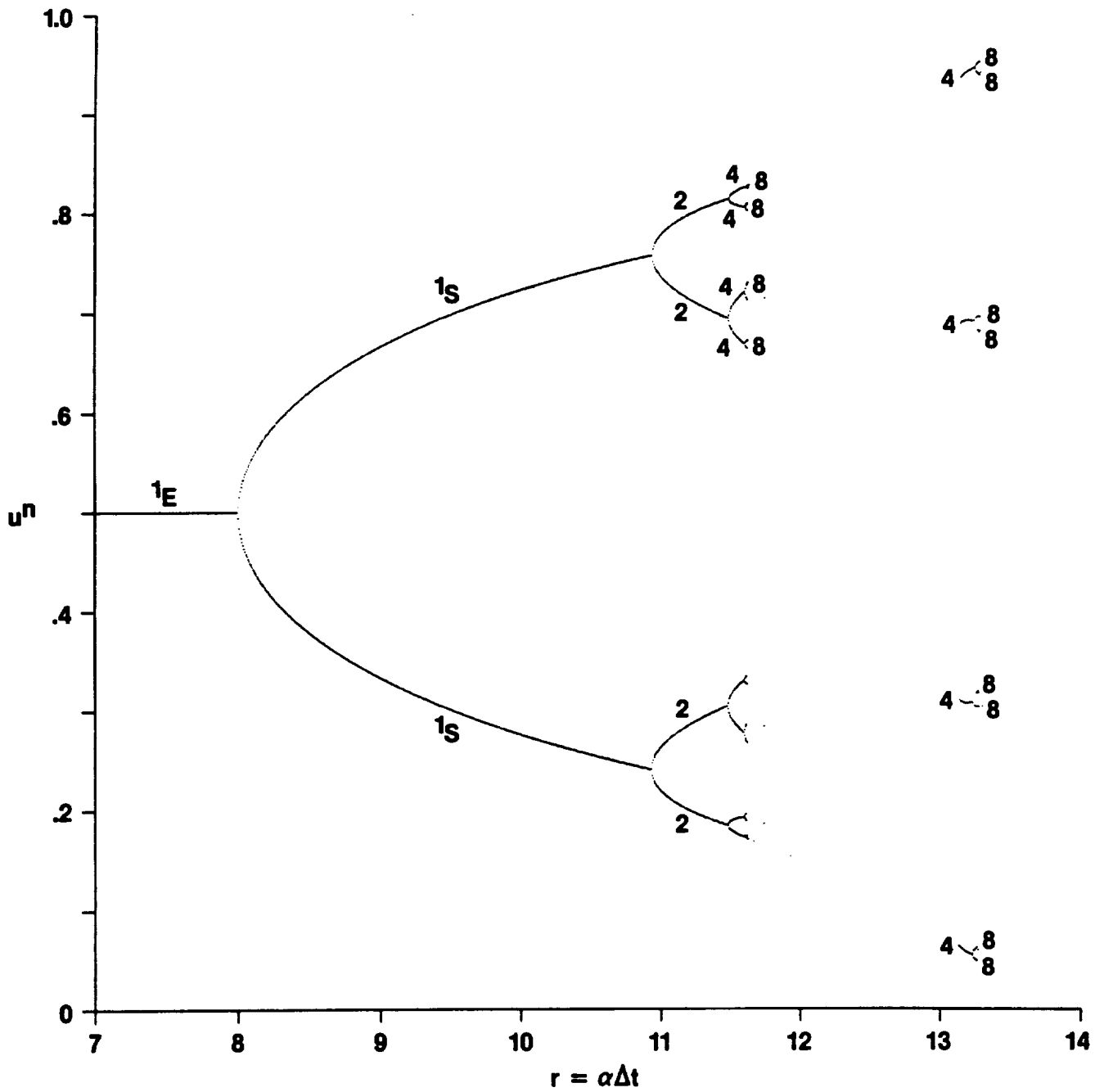


Fig. 3.9 Stable fixed points of periods 1,2,4,8 of the modified Euler (R-K 2) scheme for the ODE $du/dt = \alpha u(1 - u)(0.5 - u)$.

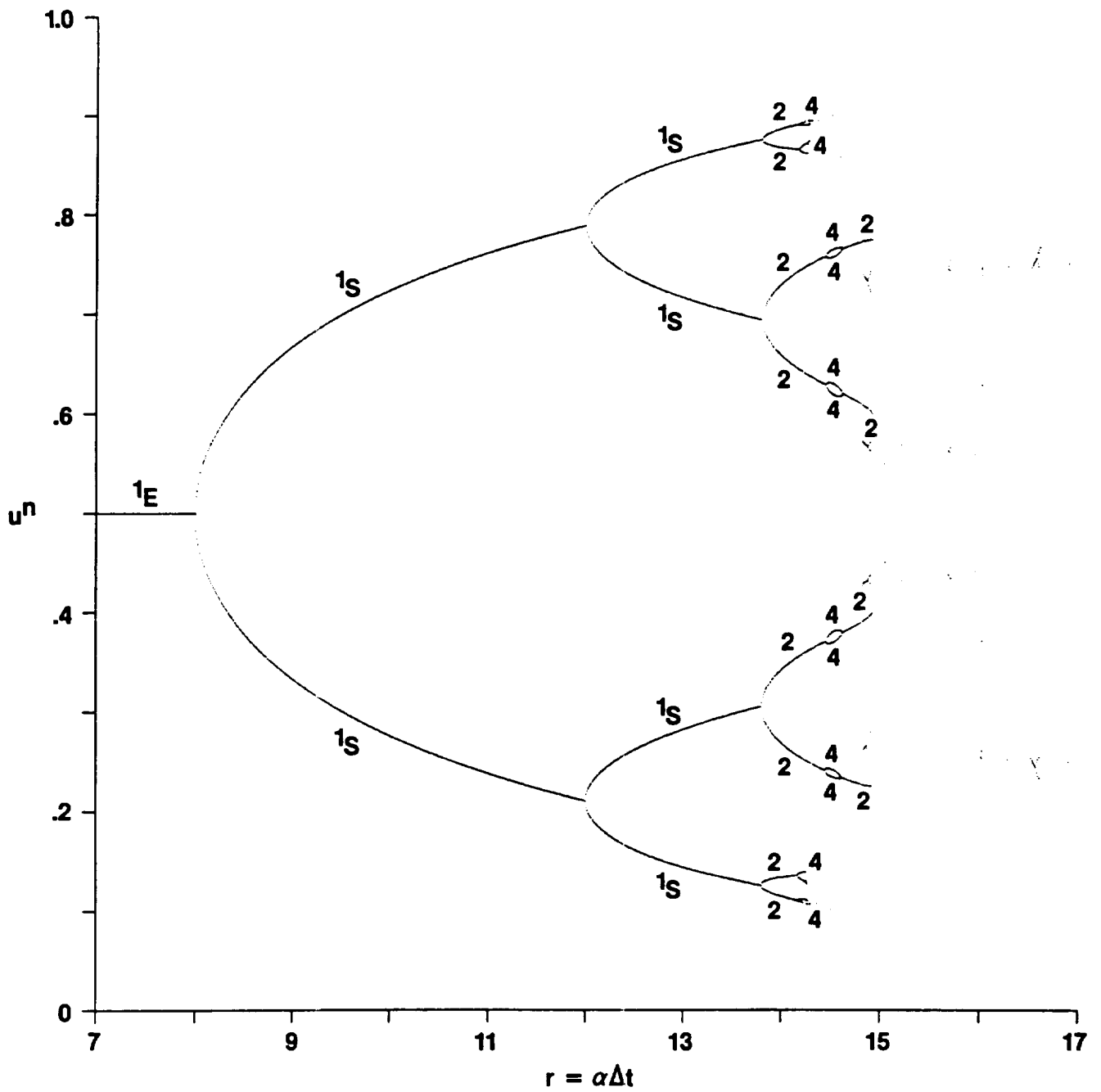


Fig. 3.10 Stable fixed points of periods 1,2,4,8 of the improved Euler (R-K 2) scheme for the ODE $du/dt = \alpha u(1 - u)(0.5 - u)$.

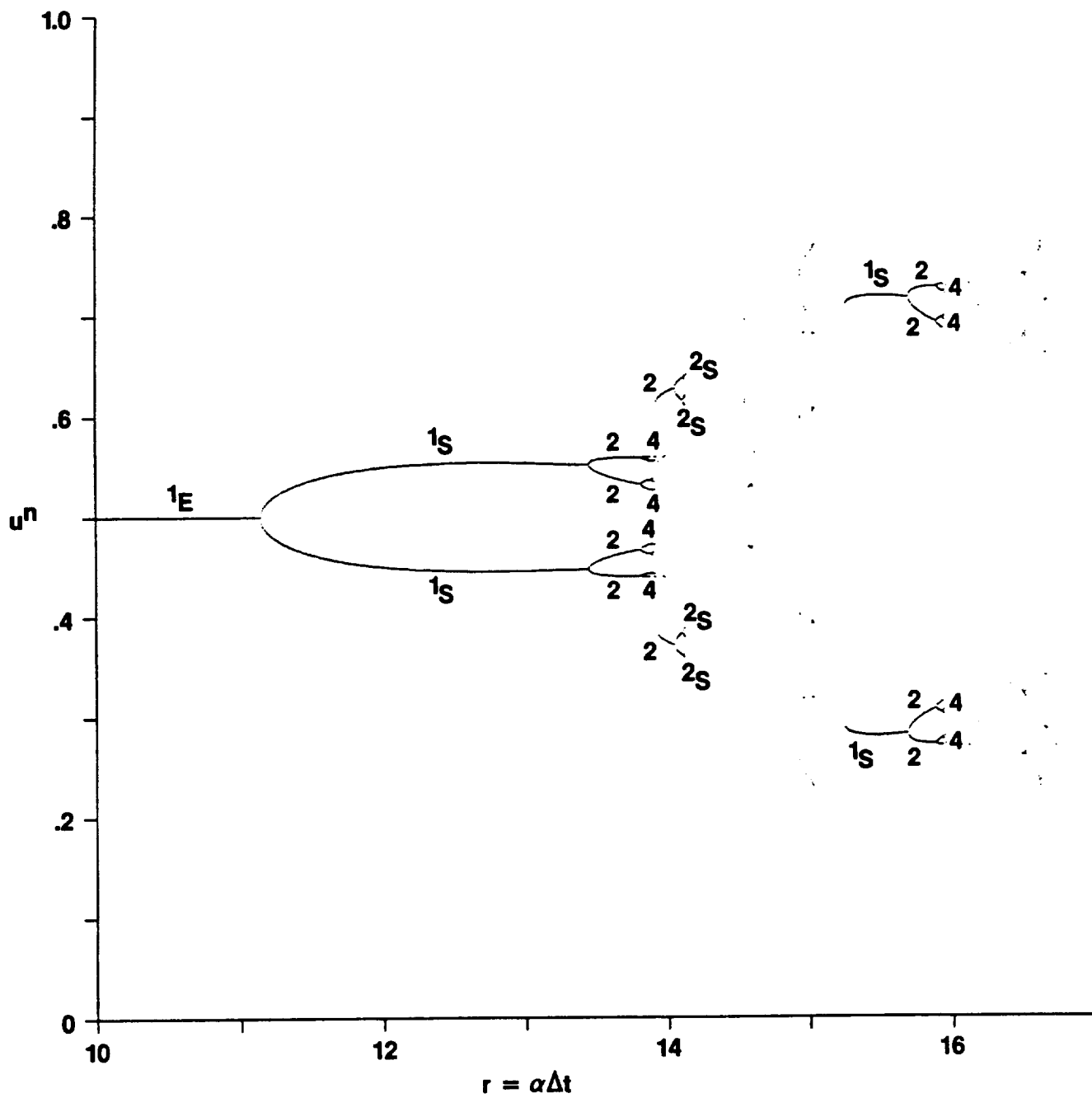


Fig. 3.11 Stable fixed points of periods 1,2,4,8 of the Runge-Kutta 4th-order (R-K 4) scheme for the ODE $du/dt = \alpha u(1-u)(0.5-u)$.

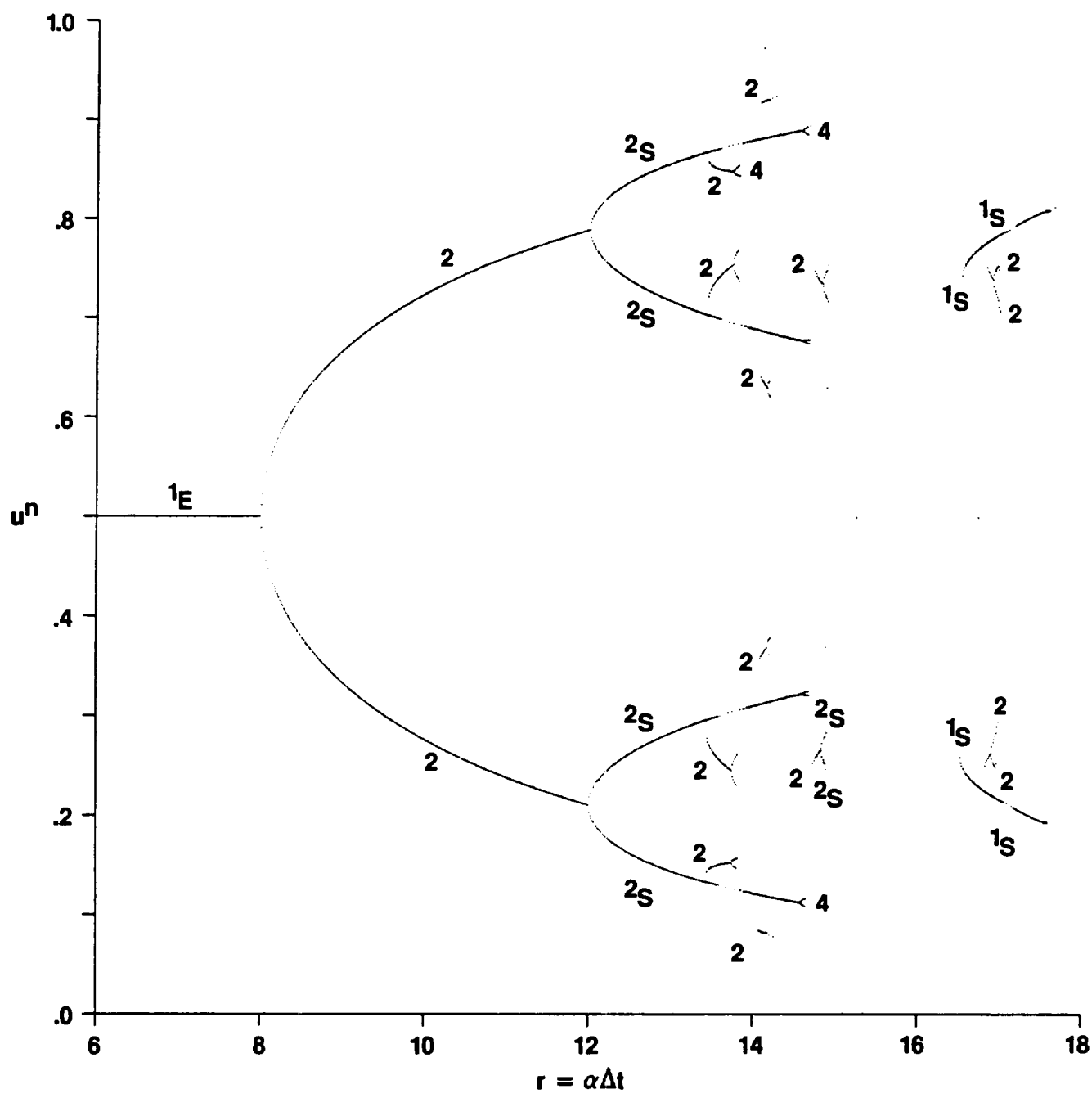


Fig. 3.12 Stable fixed points of periods 1,2,4,8 of the predictor-corrector scheme of order 2 for the ODE $du/dt = \alpha u(1 - u)(0.5 - u)$.

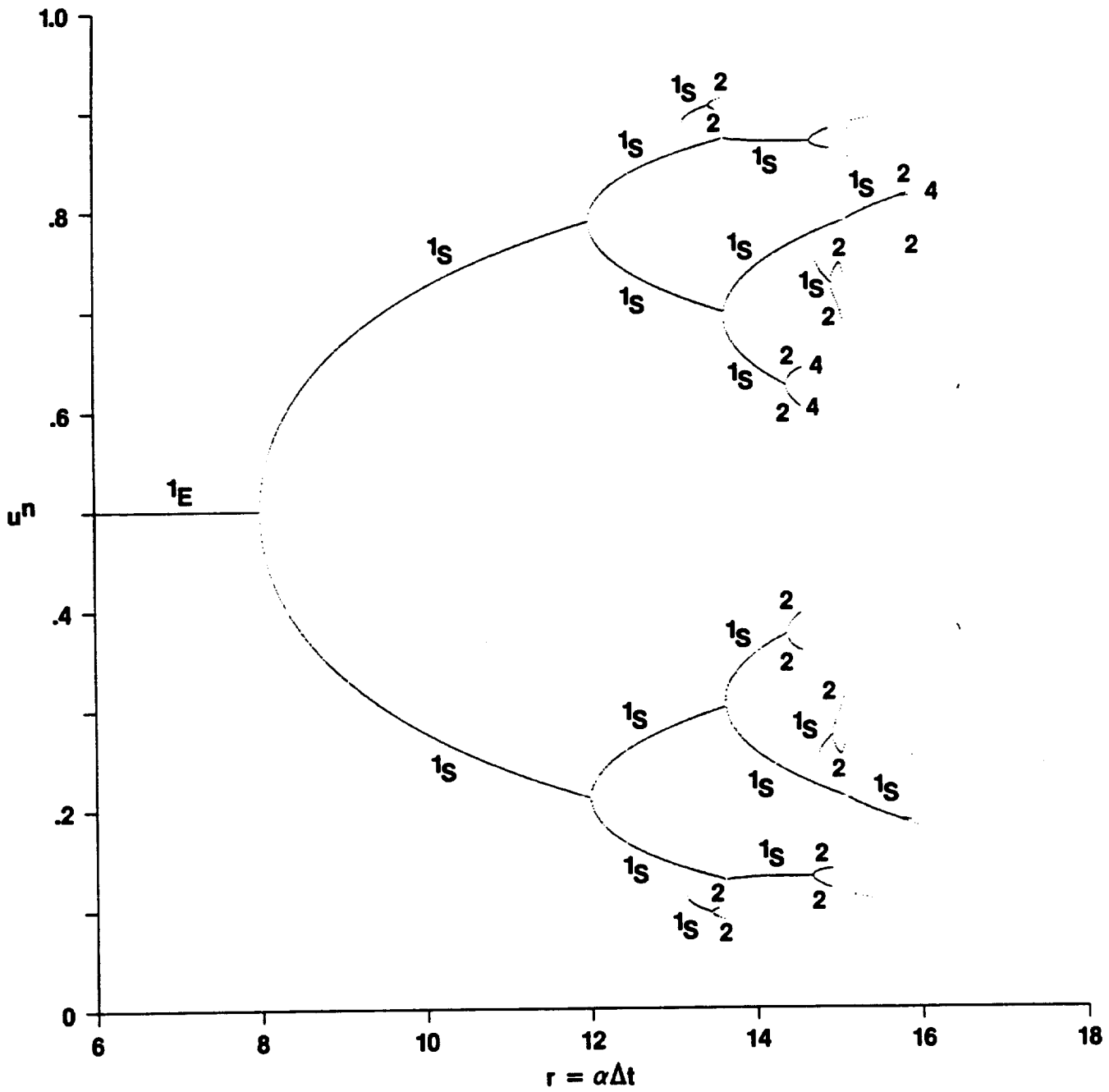


Fig. 3.13 Stable fixed points of periods 1,2,4,8 of the predictor-corrector scheme of order 3 for the ODE $du/dt = \alpha u(1 - u)(0.5 - u)$.

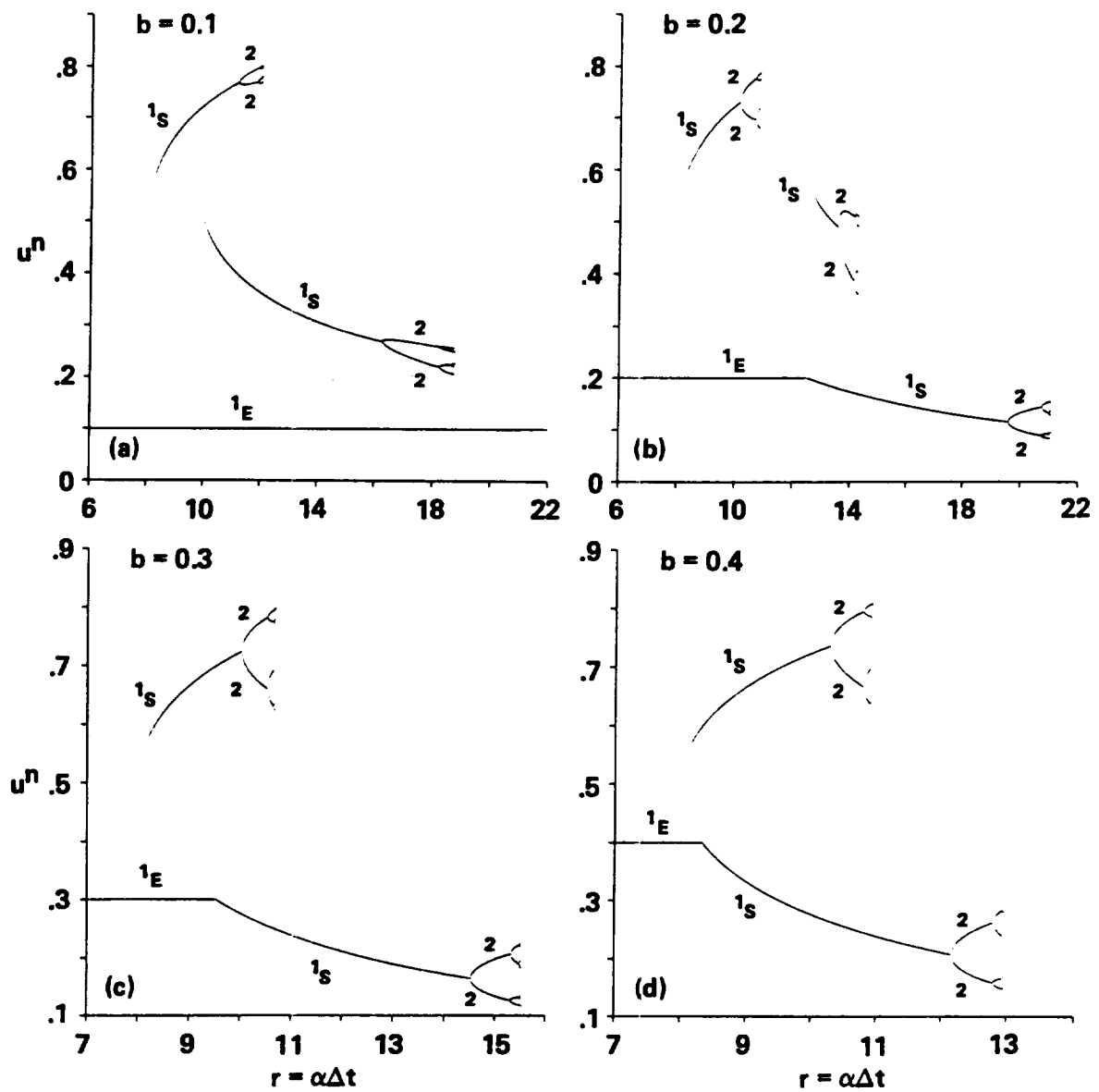


Fig. 3.14 Stable fixed points of periods 1,2,4,8 of the modified Euler (R-K 2) scheme for the ODE $du/dt = \alpha u(1-u)(b-u)$, $b = 0.1, 0.2, 0.3, 0.4$.

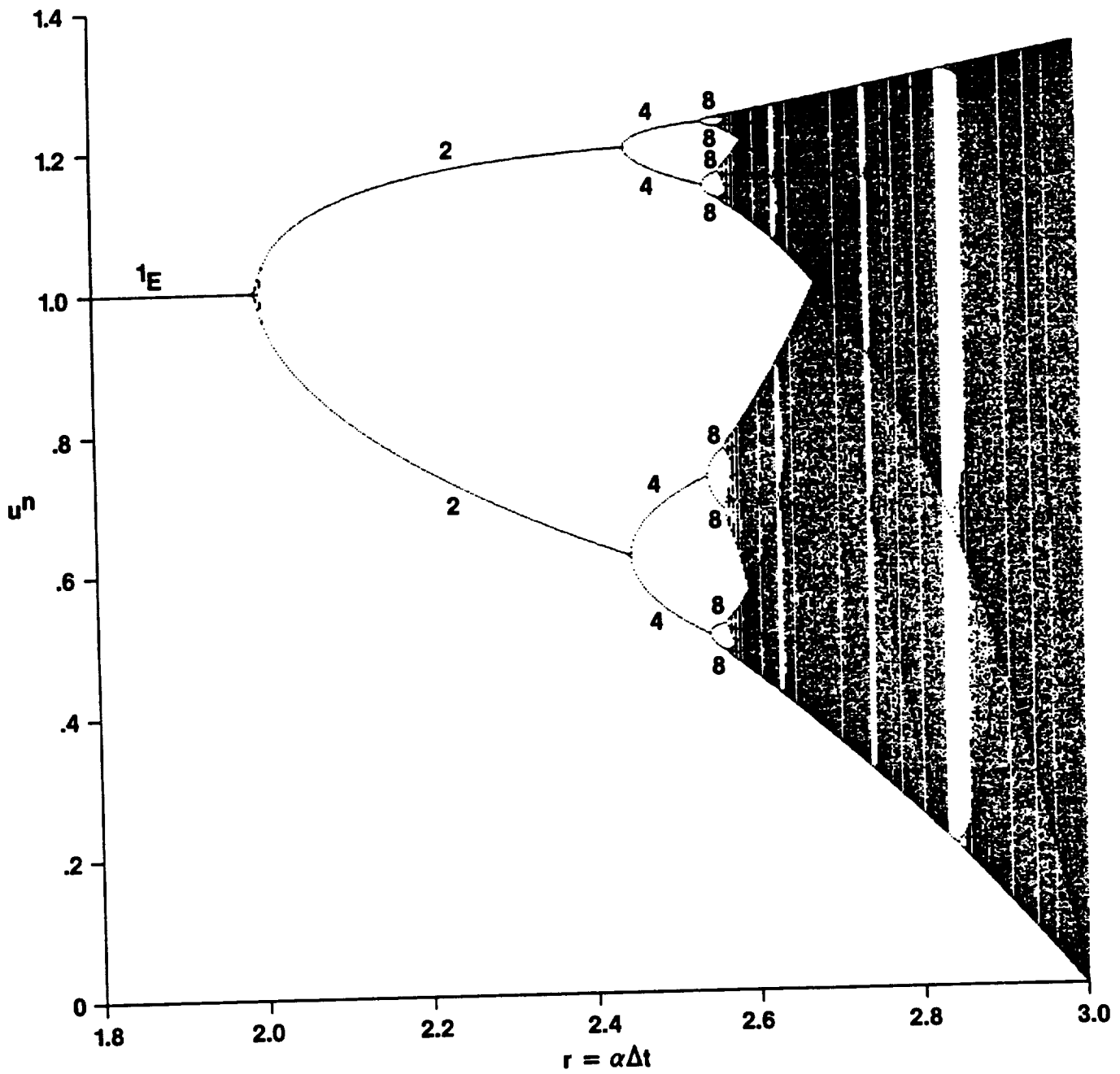


Fig. 3.15 Bifurcation diagram of the explicit Euler scheme for the logistic ODE $du/dt = \alpha u(1 - u)$.

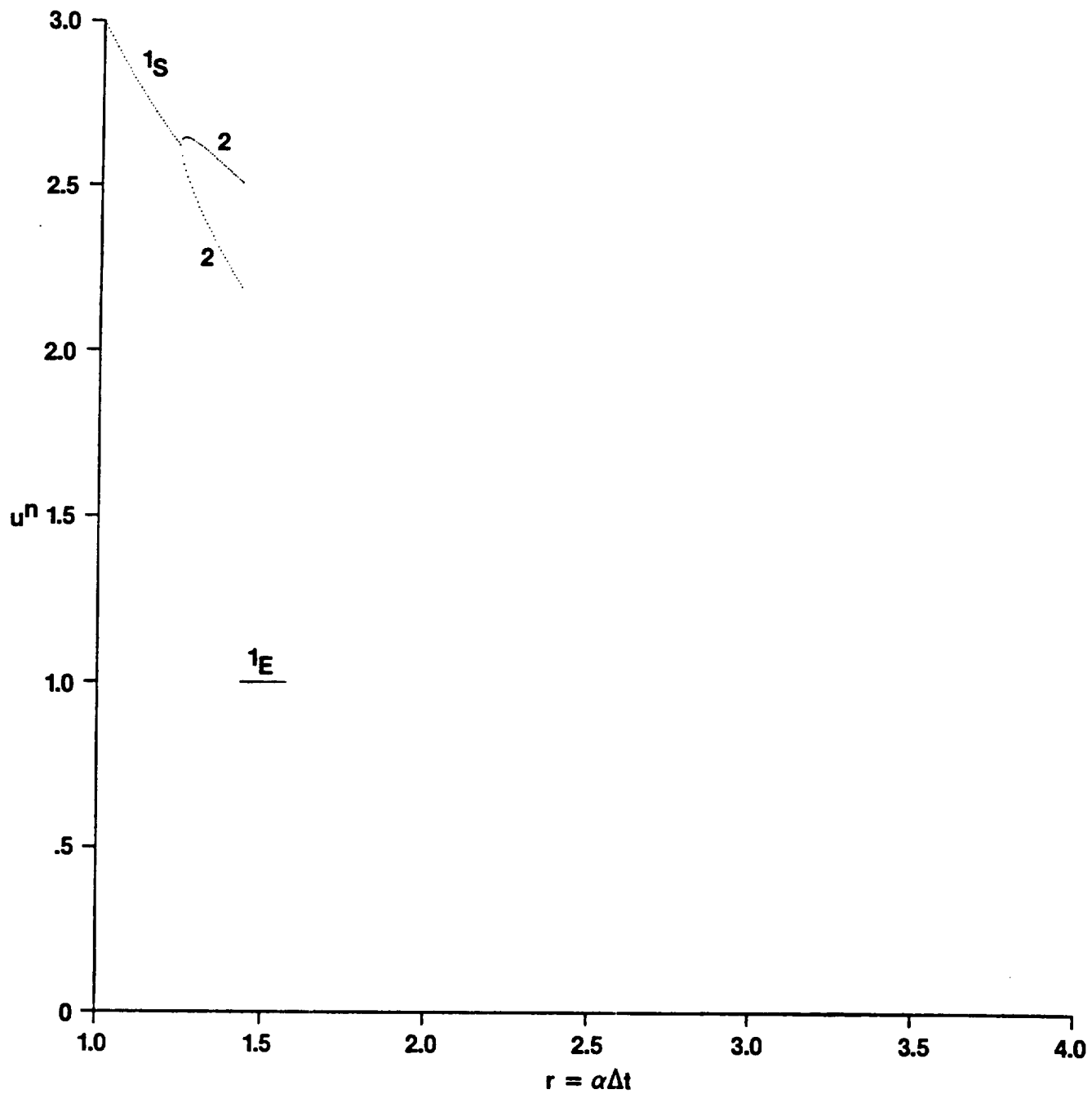


Fig. 3.16 Bifurcation diagram of the modified Euler (R-K 2) scheme for the logistic ODE $du/dt = \alpha u(1 - u)$ with $u^0 = 2.7$.

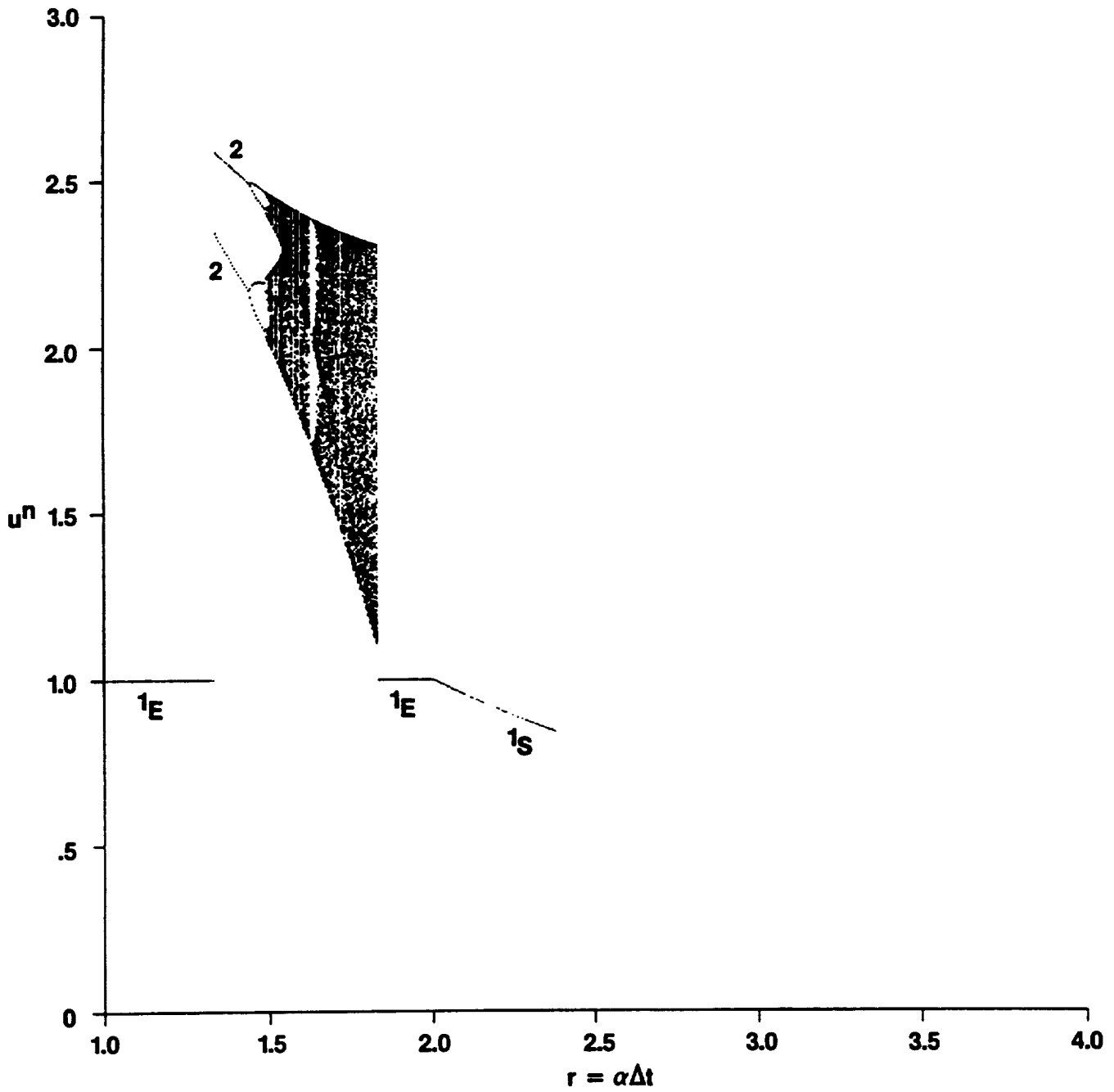


Fig. 3.17 Bifurcation diagram of the modified Euler (R-K 2) scheme for the logistic ODE $du/dt = \alpha u(1 - u)$ with $u^0 = 1.5$.

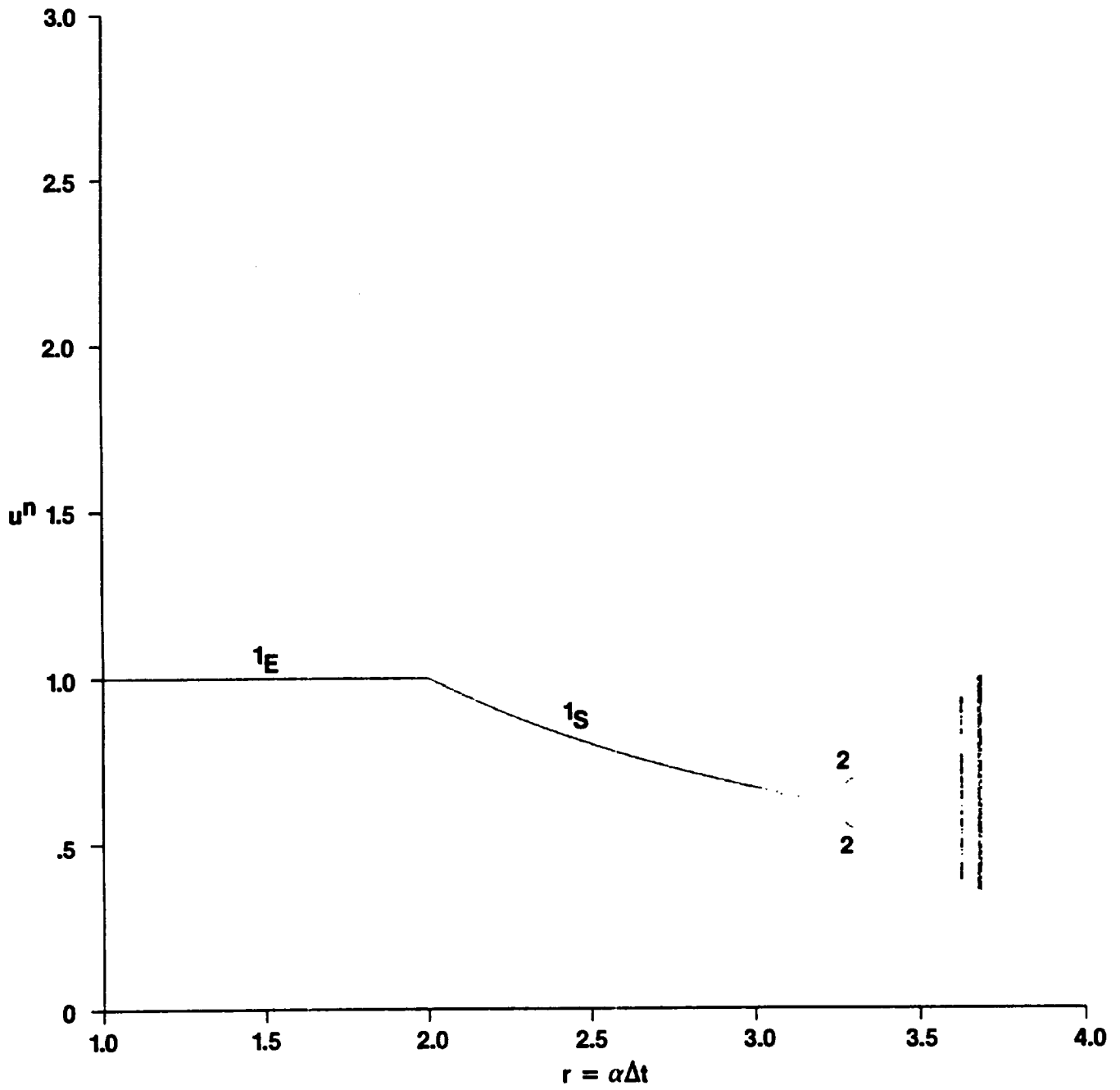


Fig. 3.18 Bifurcation diagram of the modified Euler (R-K 2) scheme for the logistic ODE $du/dt = \alpha u(1 - u)$ with $u^0 = 0.25$.

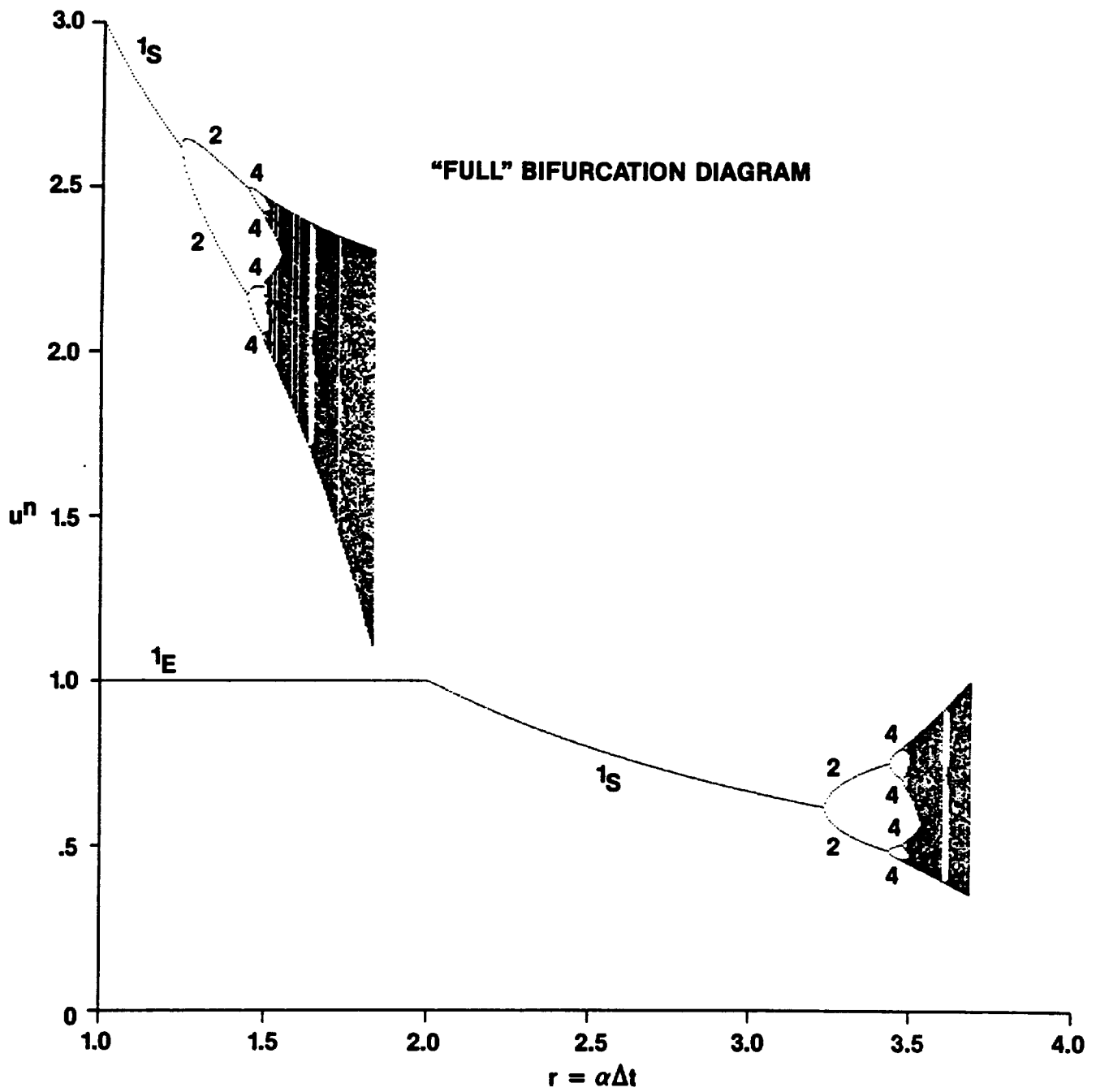


Fig. 3.19 "Full" bifurcation diagram of the modified Euler (R-K 2) scheme for the logistic ODE $du/dt = \alpha u(1 - u)$.

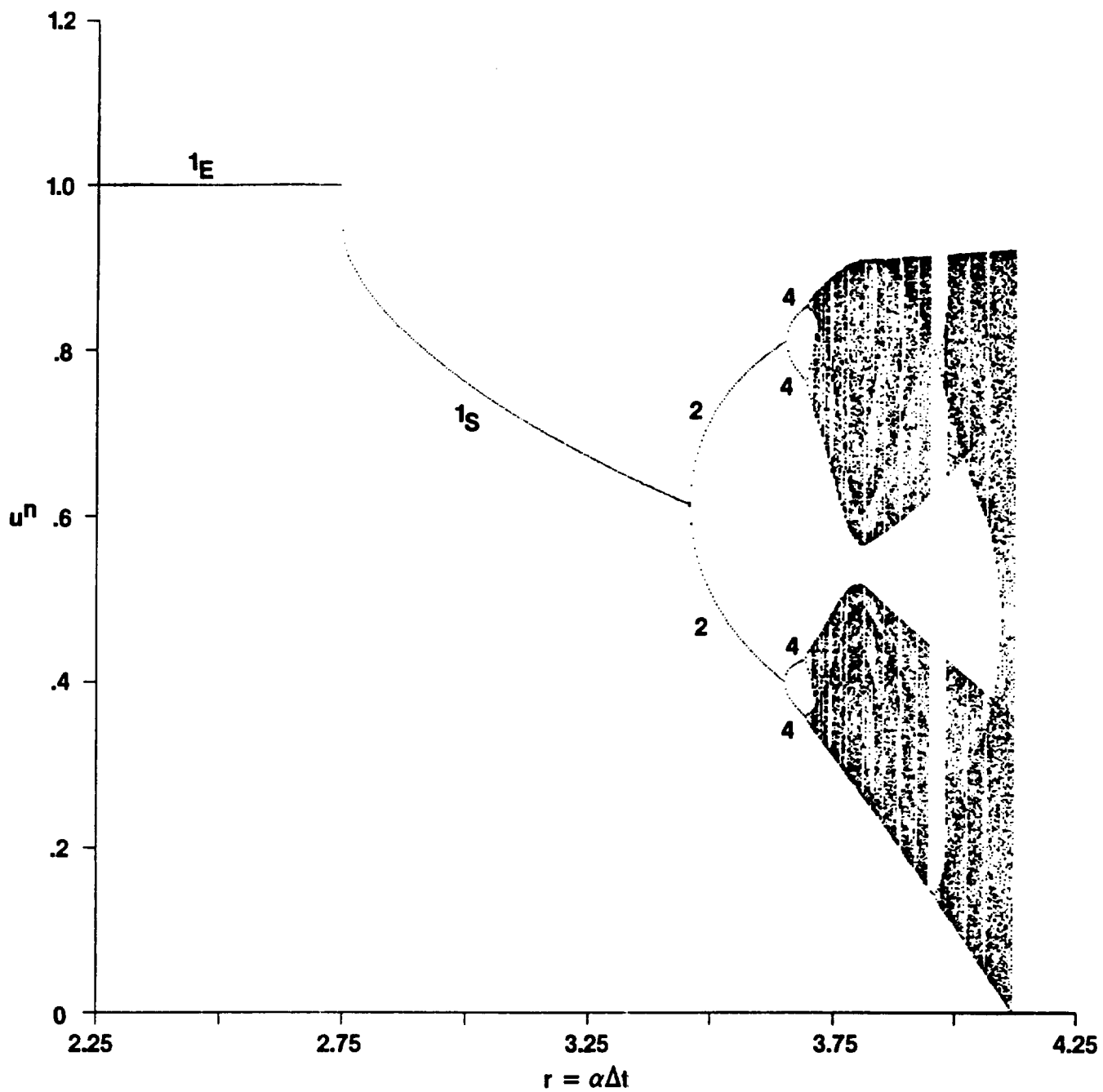


Fig. 3.20 Bifurcation diagram of the Runge-Kutta 4th-order (R-K 4) scheme for the logistic ODE $du/dt = \alpha u(1 - u)$ with $u^0 = 0.5$.

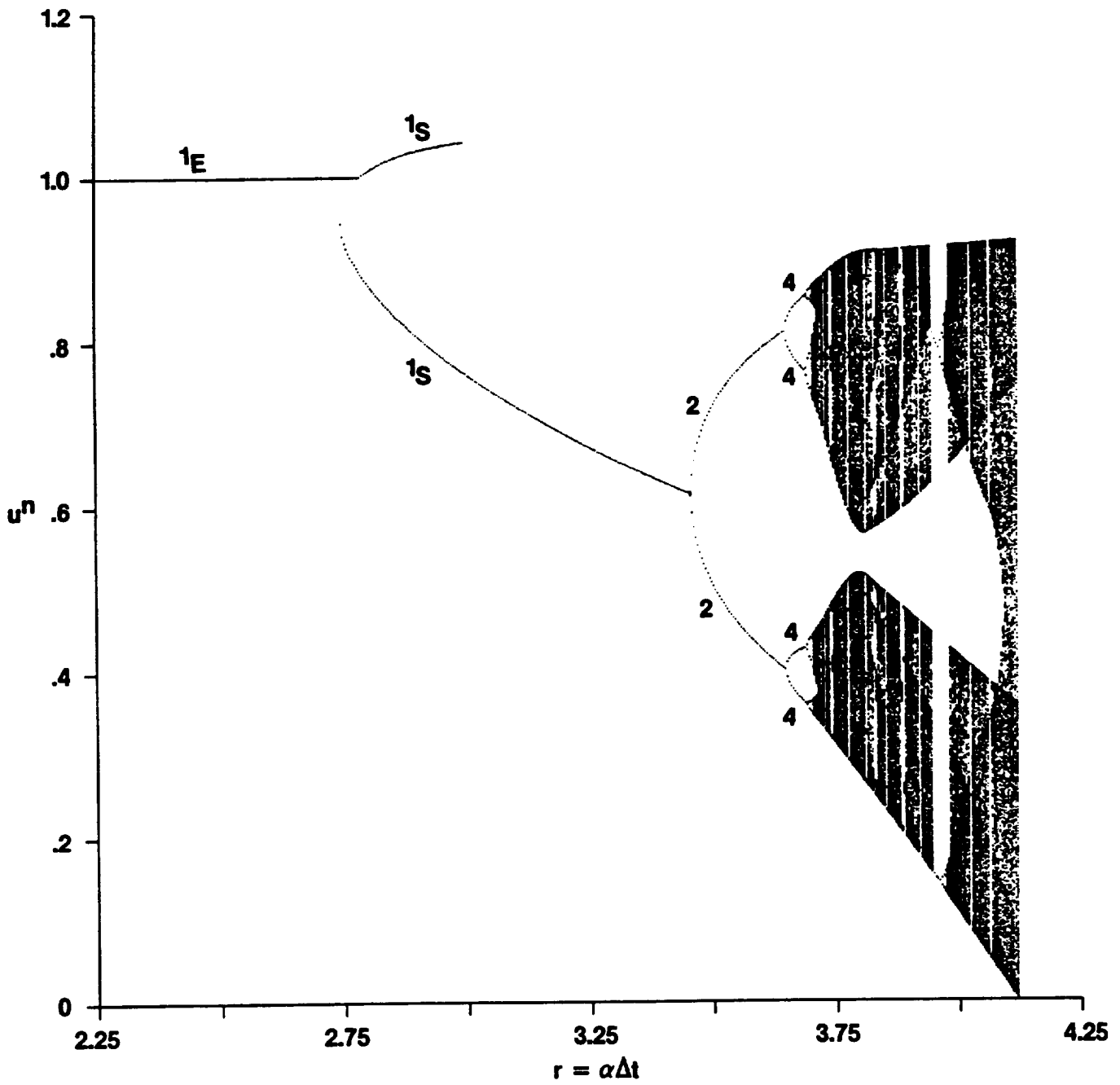


Fig. 3.21 Bifurcation diagram of the Runge-Kutta 4th-order (R-K 4) scheme for the logistic ODE $du/dt = \alpha u(1 - u)$ with multiple initial data.

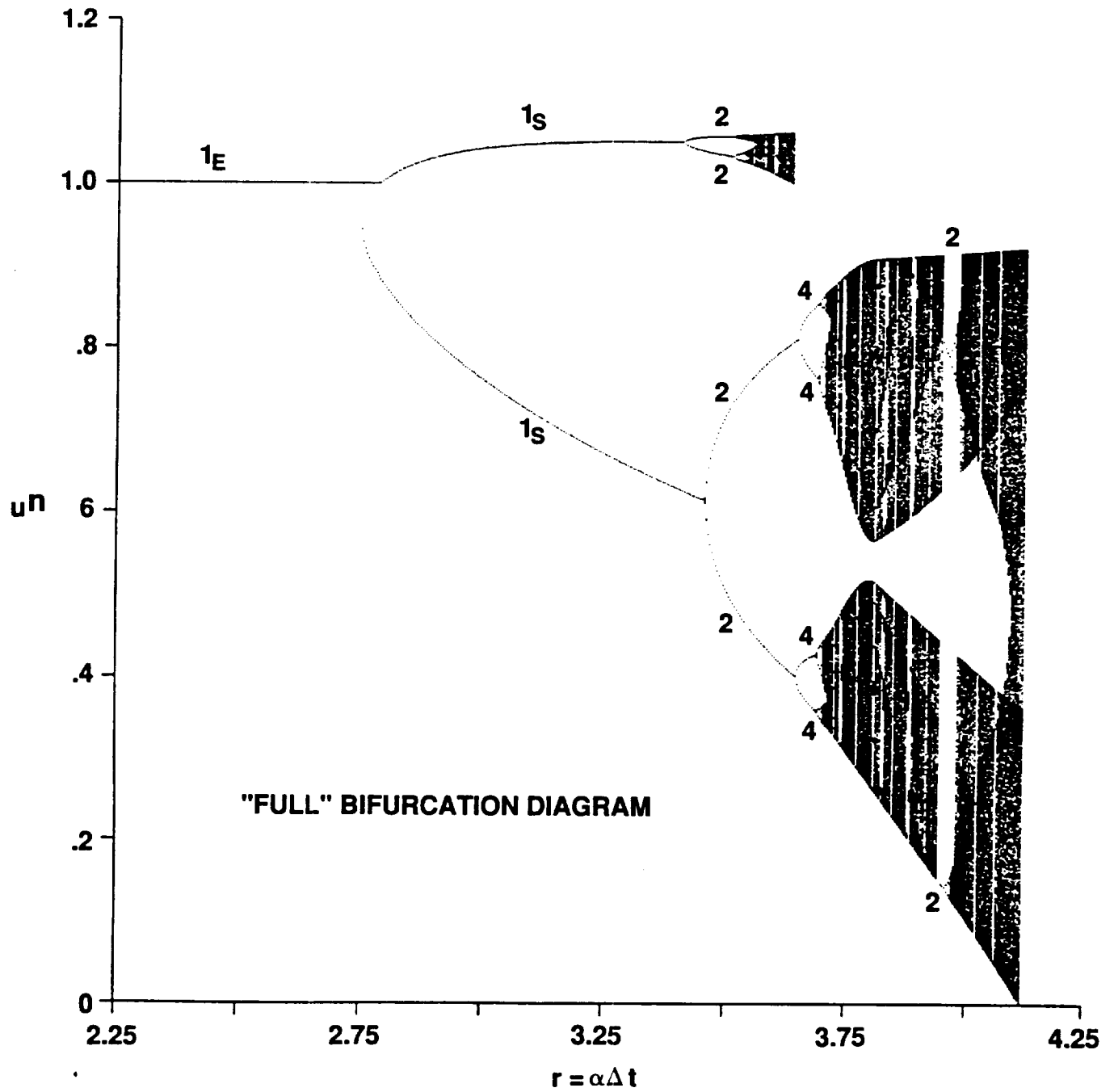


Fig. 3.22 "Full" bifurcation diagram of the Runge-Kutta 4th-order (R-K 4) scheme for the logistic ODE $du/dt = \alpha u(1 - u)$.

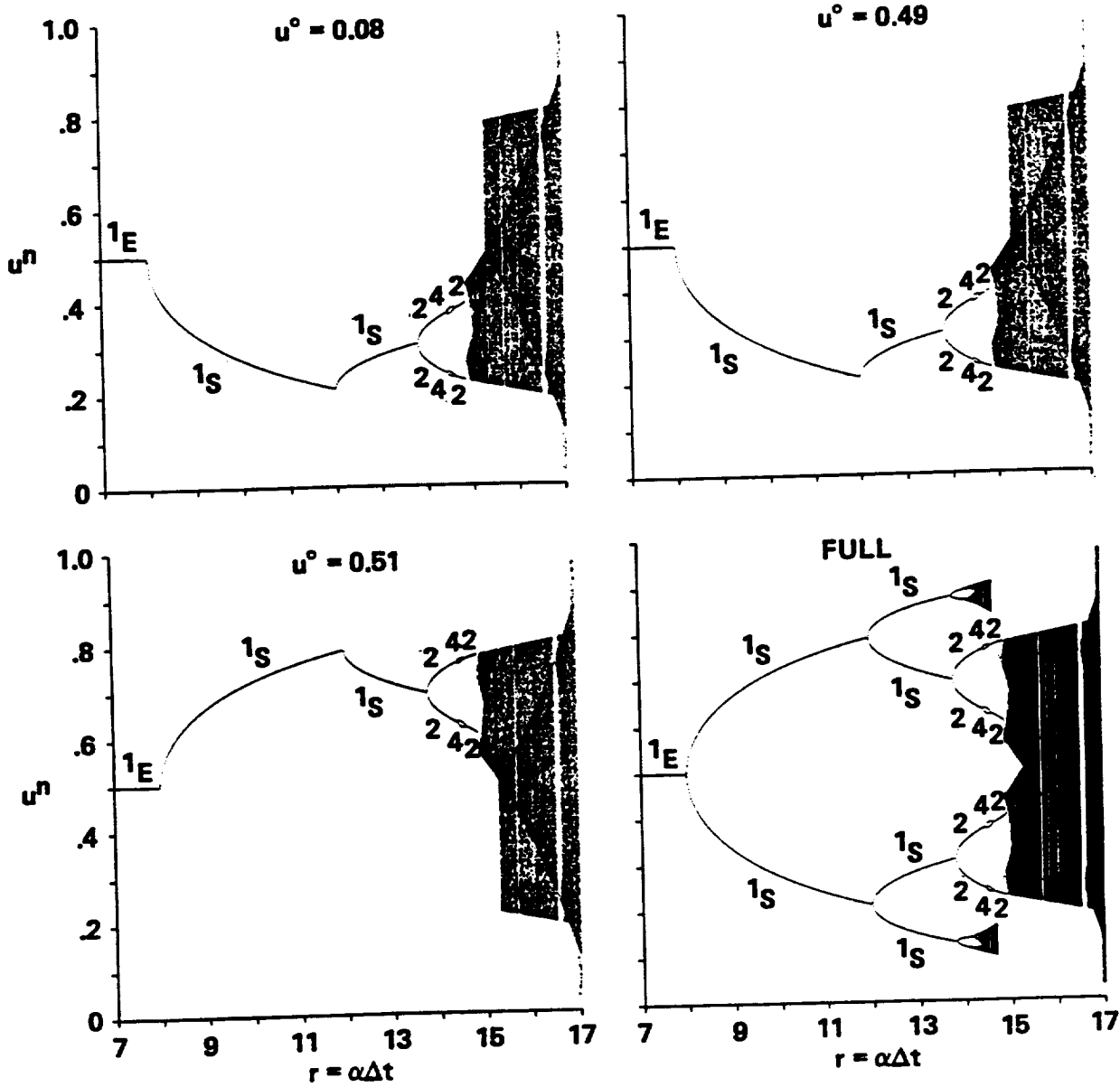


Fig. 3.23 Bifurcation diagrams of the improved Euler (R-K 2) scheme for the ODE $du/dt = \alpha u(1 - u)(0.5 - u)$ for four different sets of initial input data.

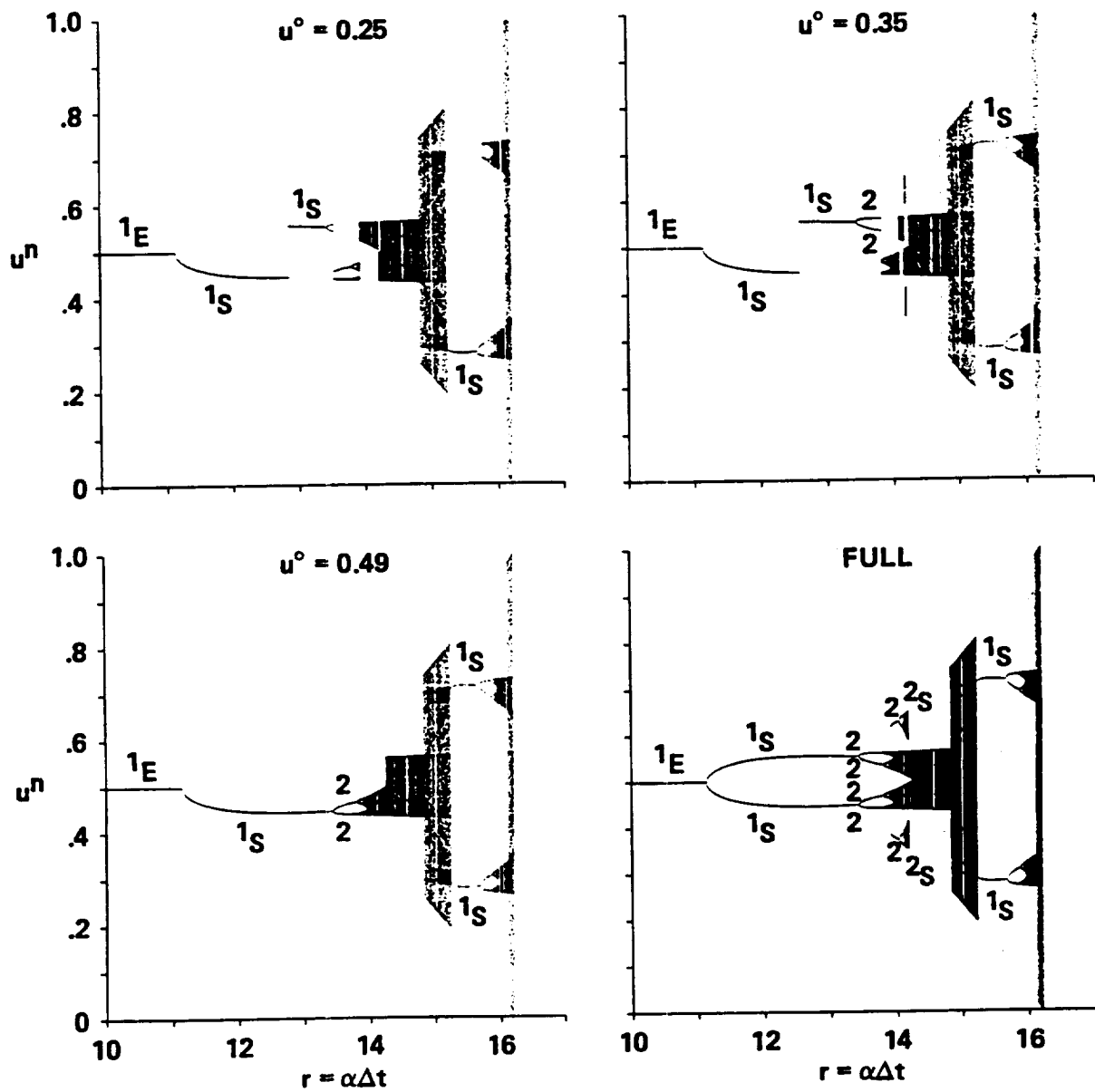


Fig. 3.24 Bifurcation diagrams of the Runge-Kutta 4th-order (R-K 4) scheme for the ODE $du/dt = \alpha u(1-u)(0.5-u)$ for four different sets of initial input data.

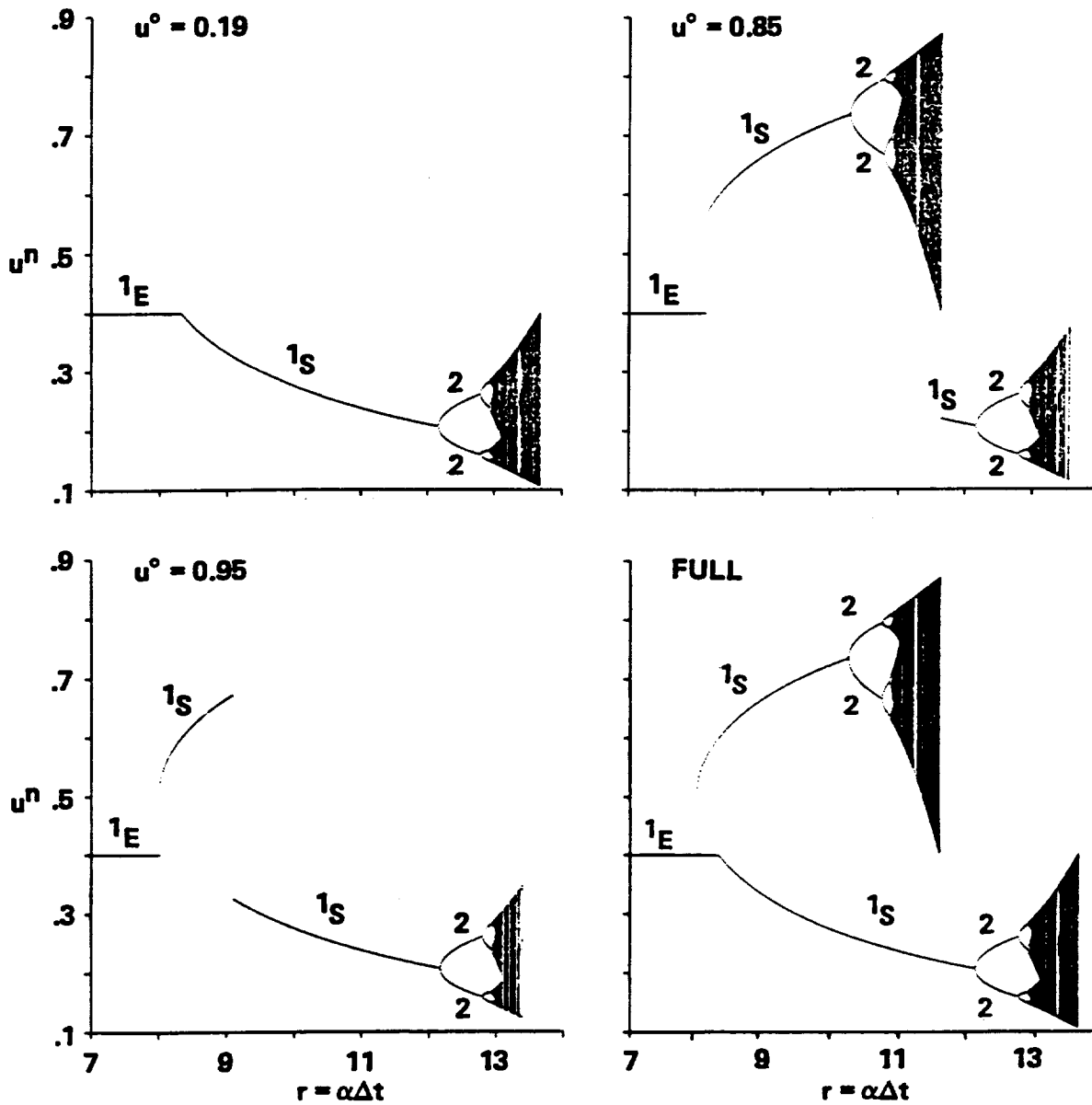


Fig. 3.25 Bifurcation diagrams of the modified Euler (R-K 2) scheme for the ODE $du/dt = \alpha u(1 - u)(0.4 - u)$ for four different sets of initial input data.

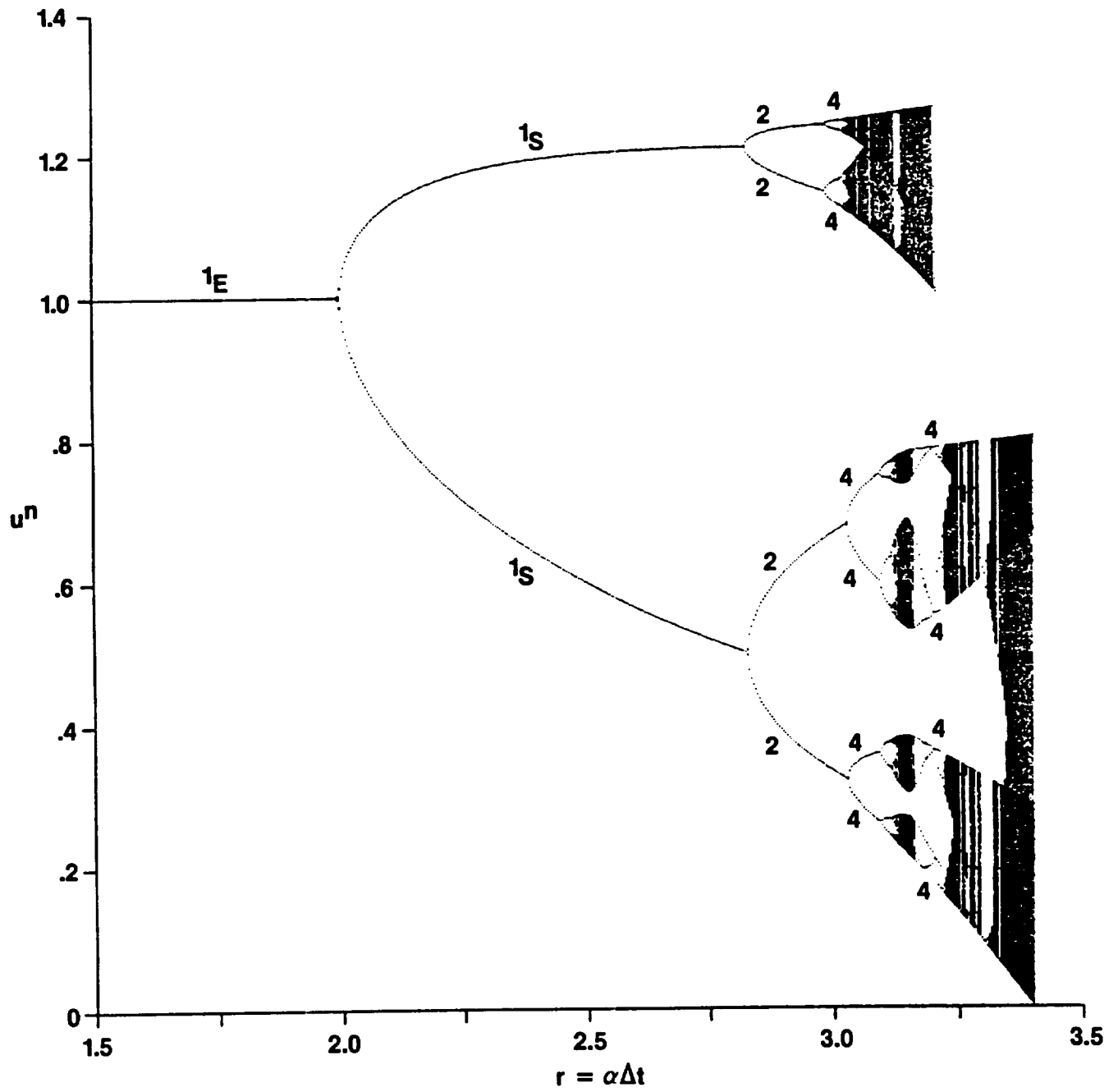


Fig. 3.26 "Full" bifurcation diagram of the improved Euler (R-K 2) scheme for the logistic ODE $du/dt = \alpha u(1 - u)$.

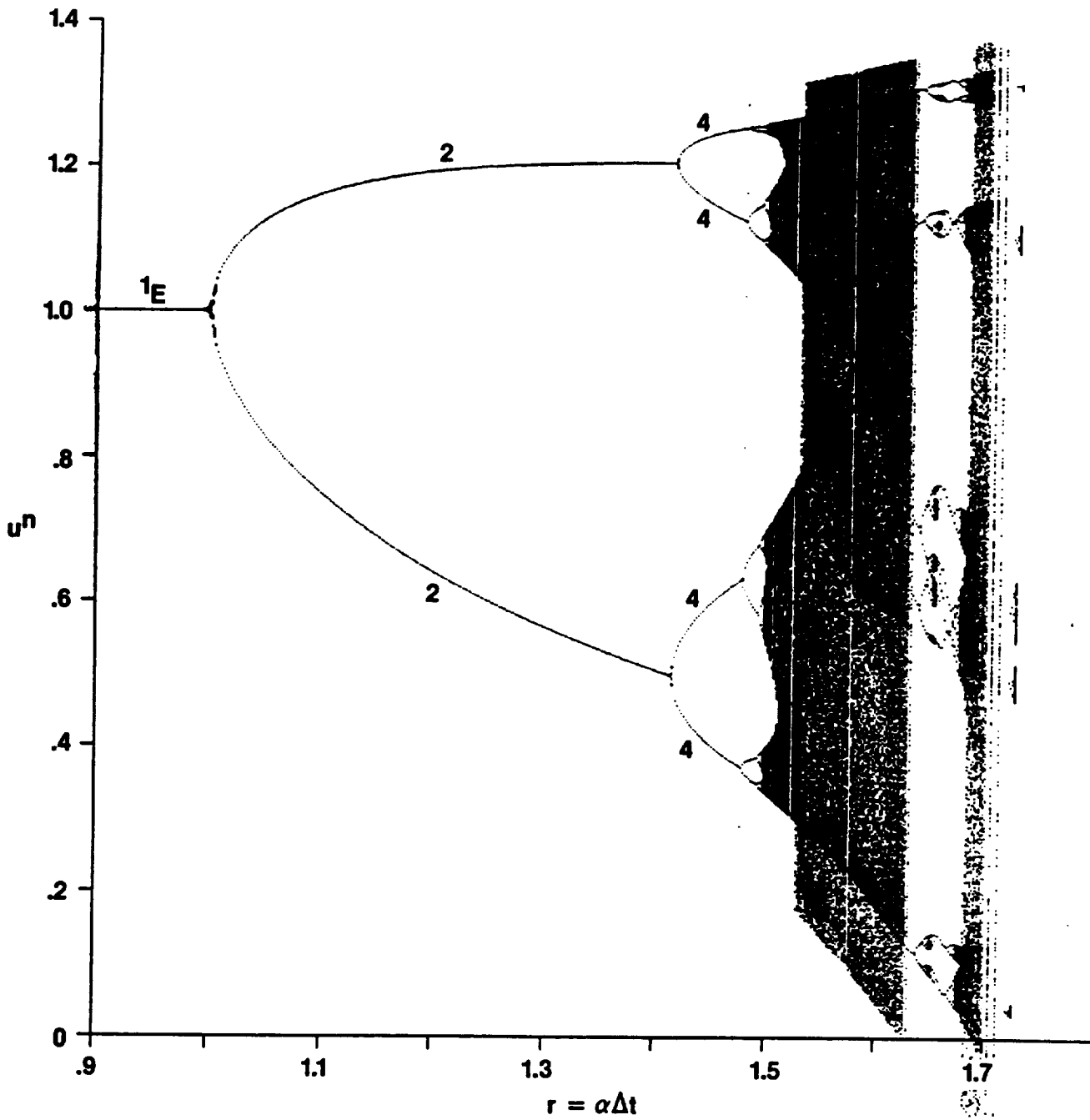


Fig. 3.27 "Full" bifurcation diagram of the Adam-Bashforth scheme for the logistic ODE $du/dt = \alpha u(1 - u)$.

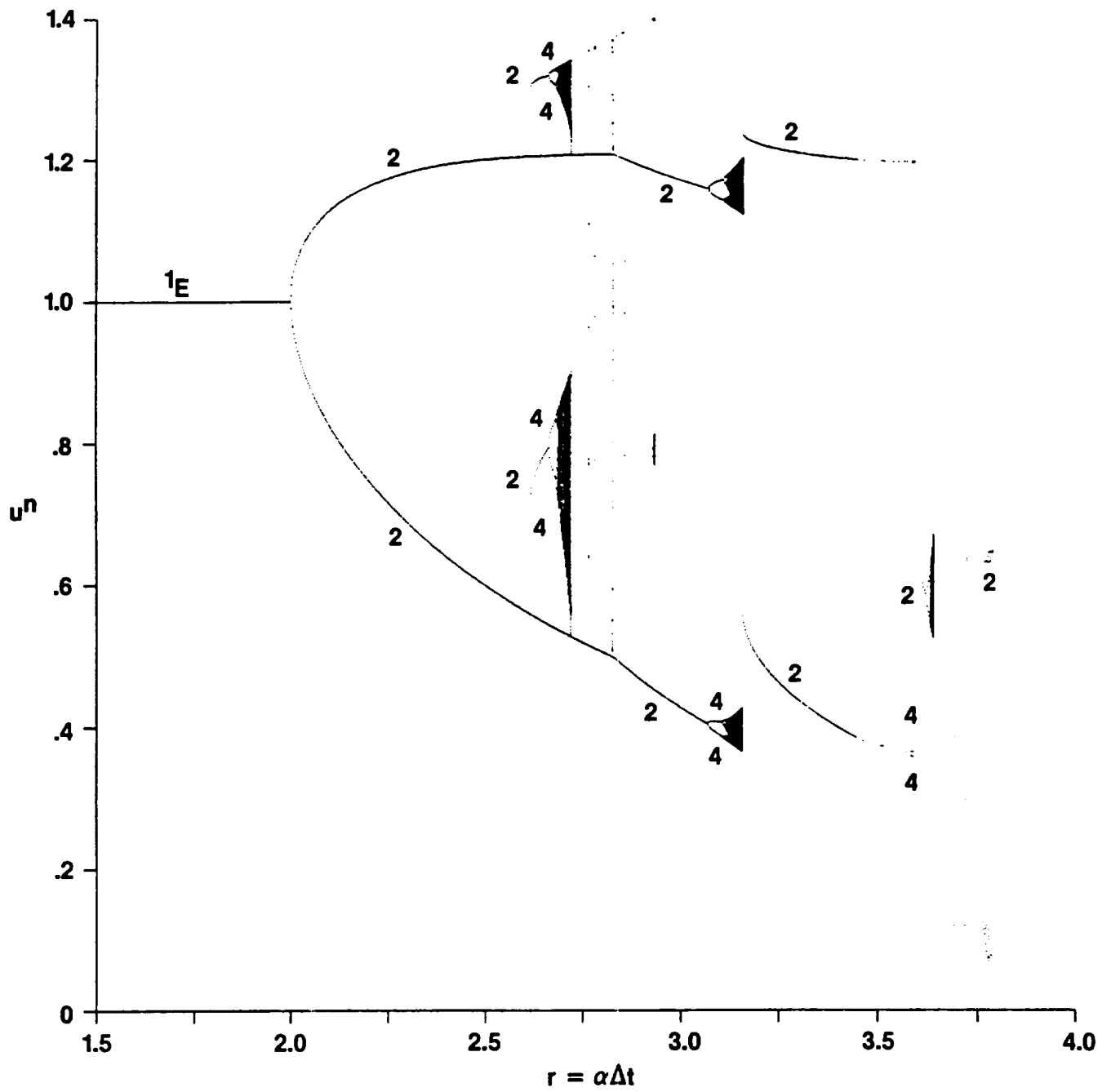


Fig. 3.28 "Full" bifurcation diagram of the predictor-corrector scheme of order 2 for the logistic ODE $du/dt = \alpha u(1 - u)$.

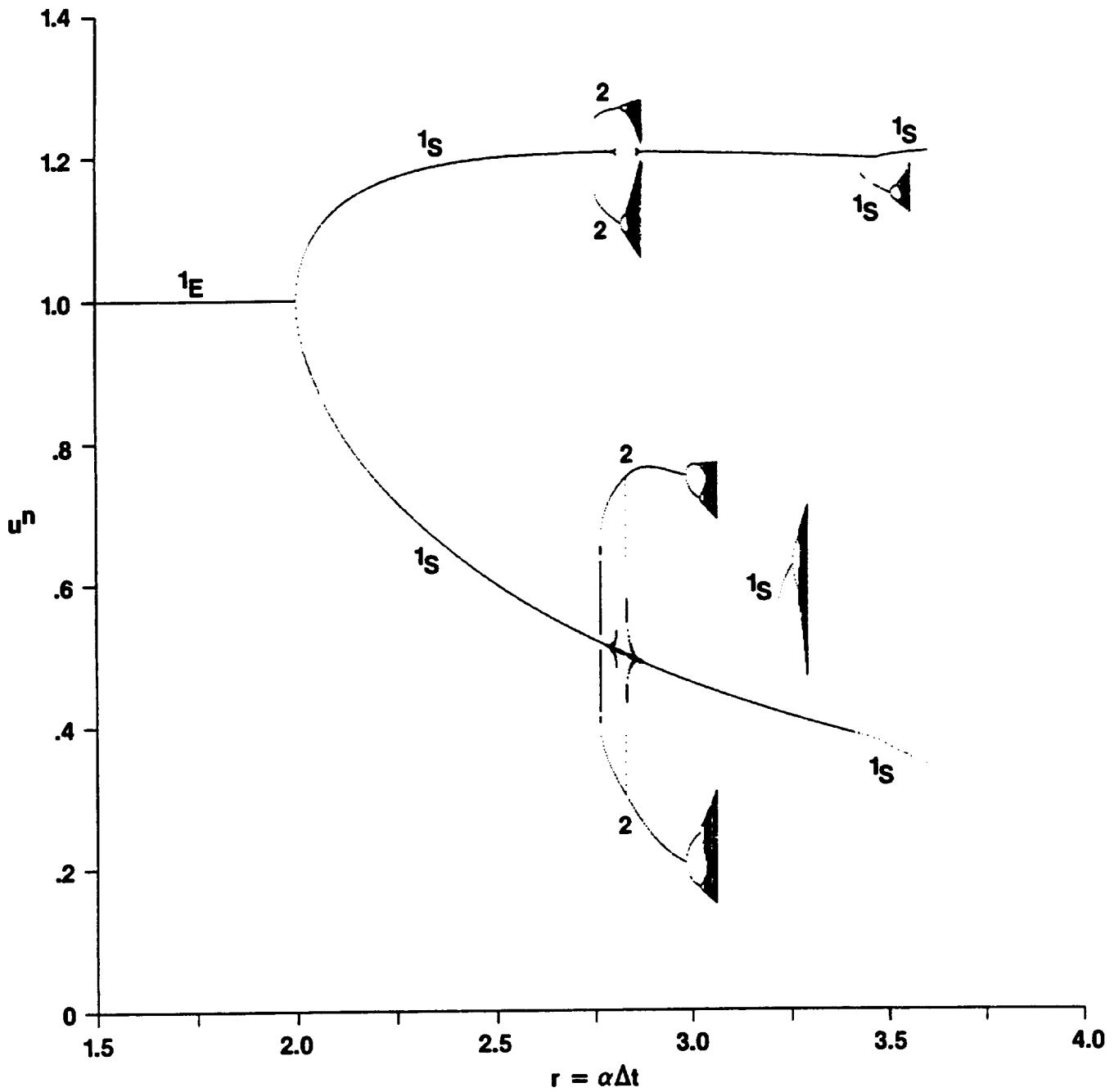


Fig. 3.29 "Full" bifurcation diagram of the predictor-corrector scheme of order 3 for the logistic ODE $du/dt = \alpha u(1 - u)$.

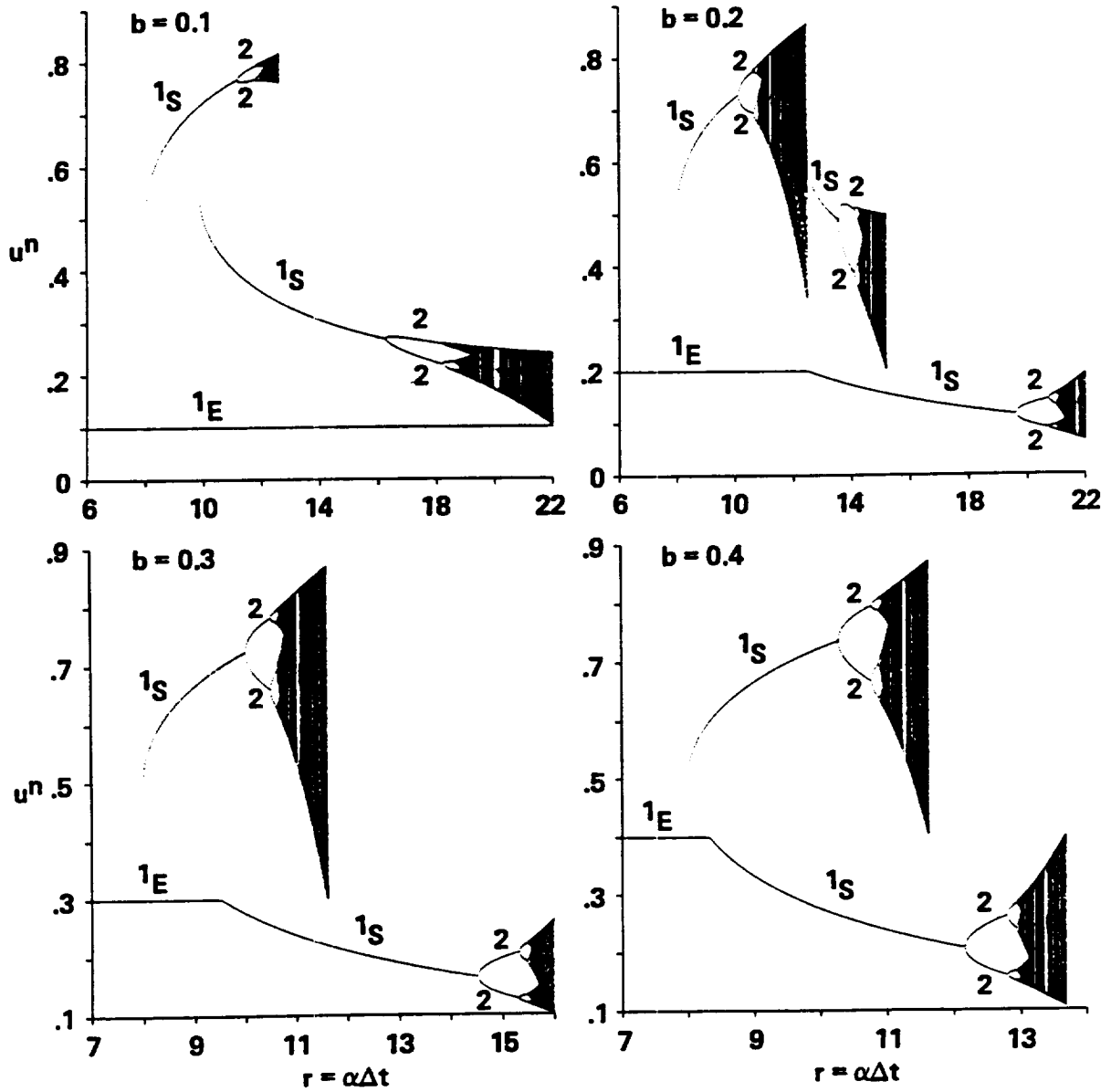


Fig. 3.30 "Full" bifurcation diagrams of the modified Euler (R-K 2) scheme for the ODE $du/dt = \alpha u(1-u)(b-u)$, $b = 0.1, 0.2, 0.3, 0.4$.

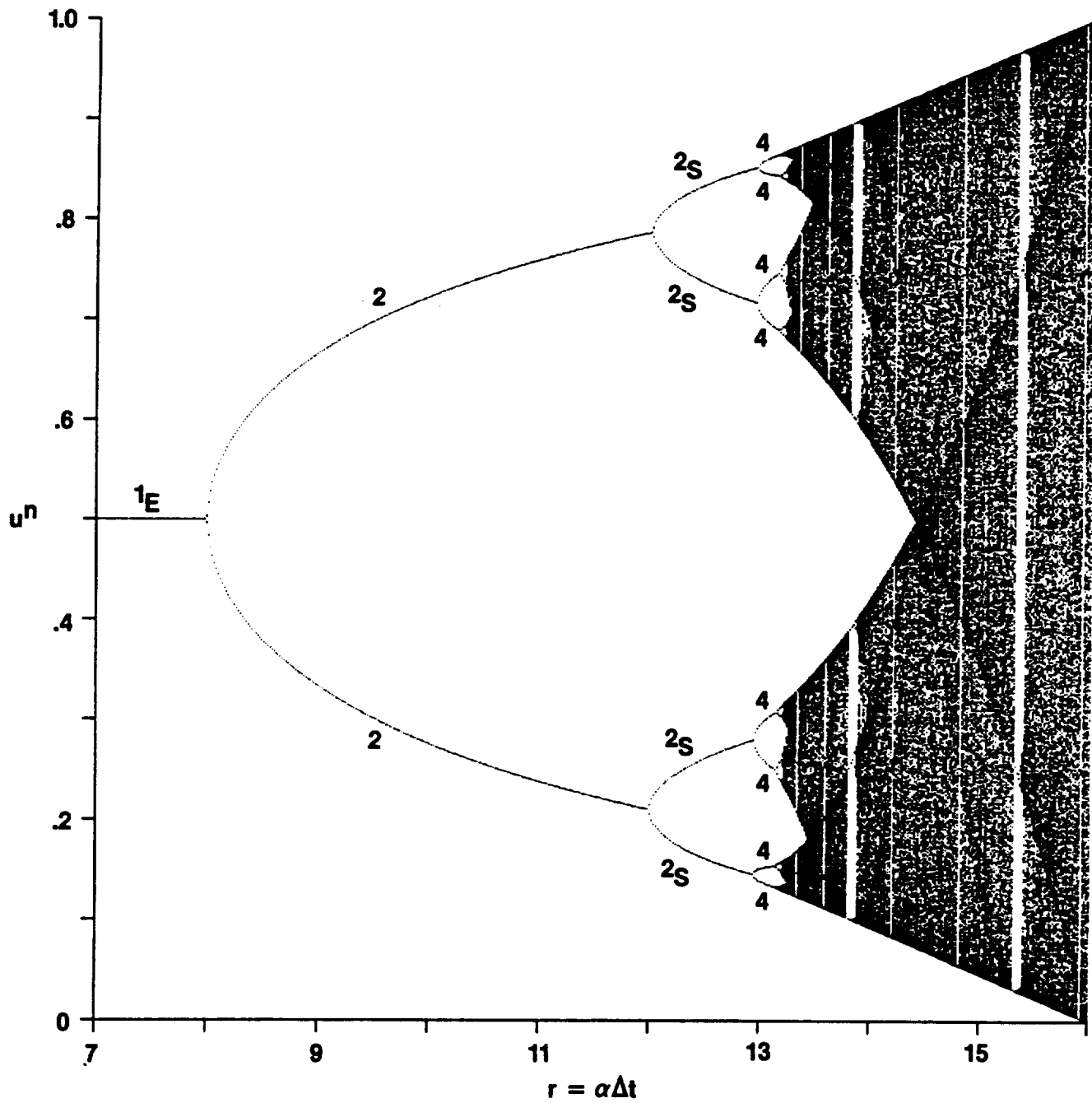


Fig. 3.31 "Full" bifurcation diagrams of the explicit Euler scheme for the ODE $du/dt = \alpha u(1-u)(0.5-u)$.

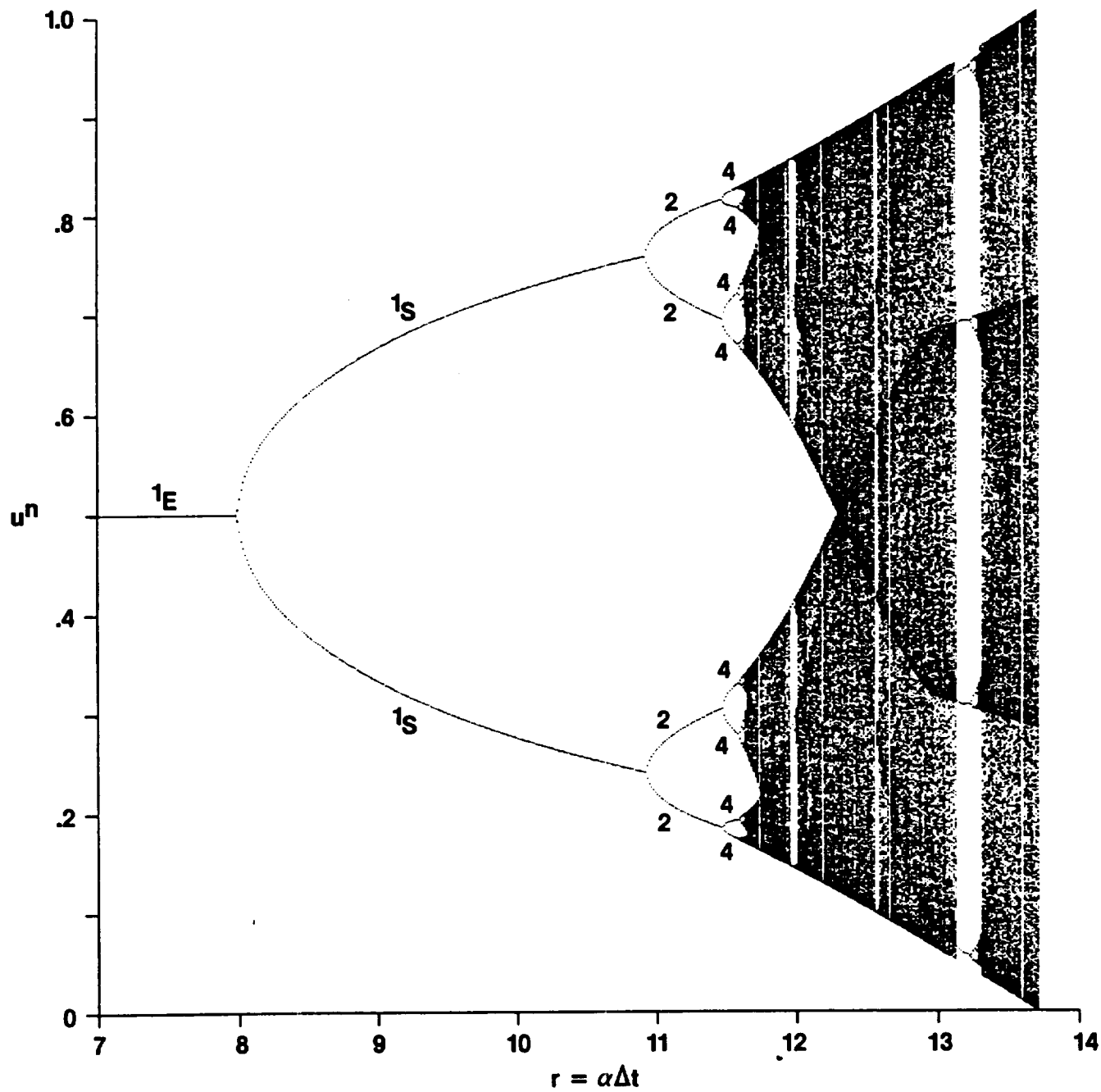


Fig. 3.32 "Full" bifurcation diagram of the modified Euler (R-K 2) scheme for the ODE $du/dt = \alpha u(1-u)(0.5-u)$.

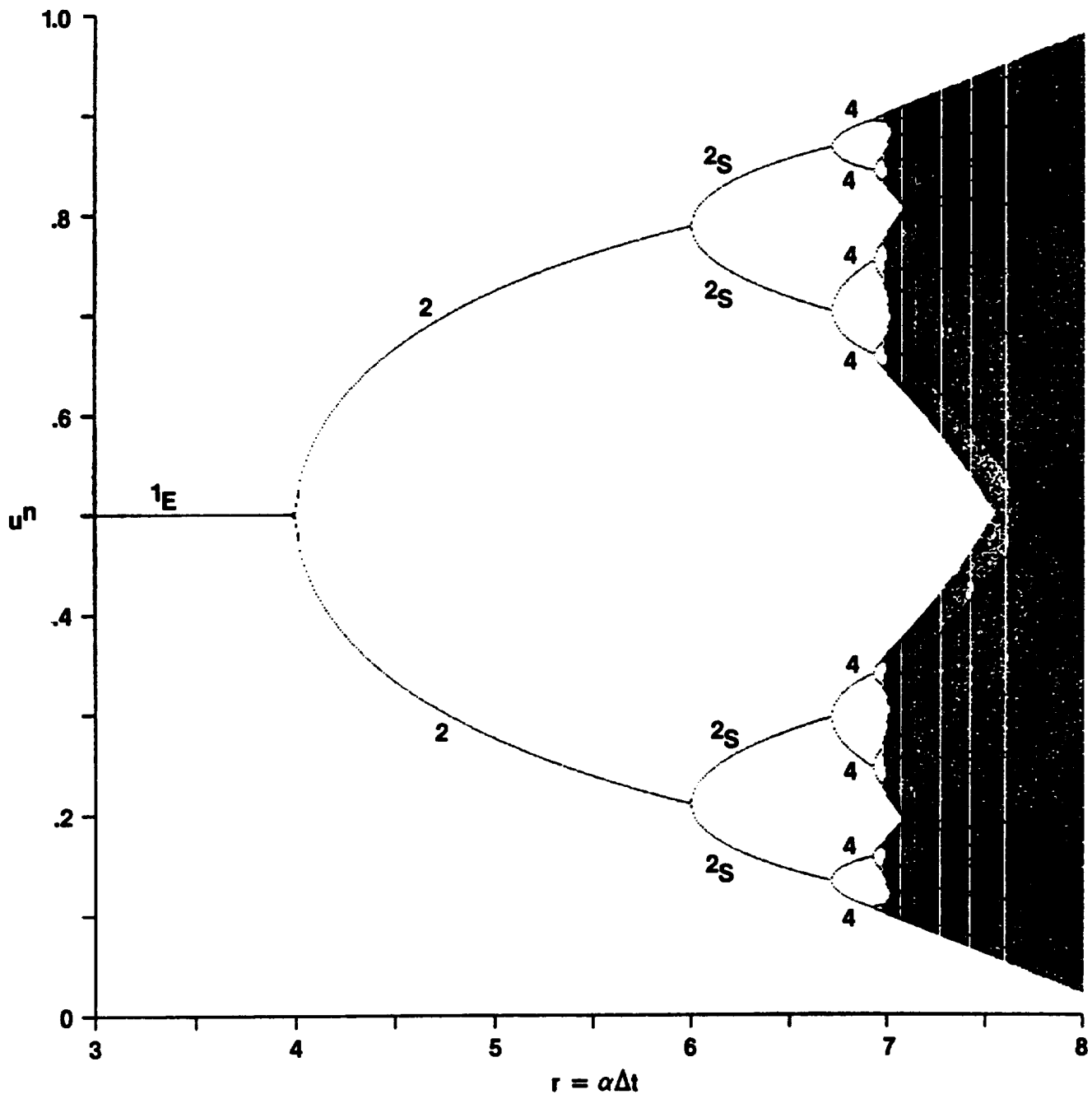


Fig. 3.33 "Full" bifurcation diagram of the Adam-Bashforth scheme for the ODE $du/dt = \alpha u(1-u)(0.5-u)$.

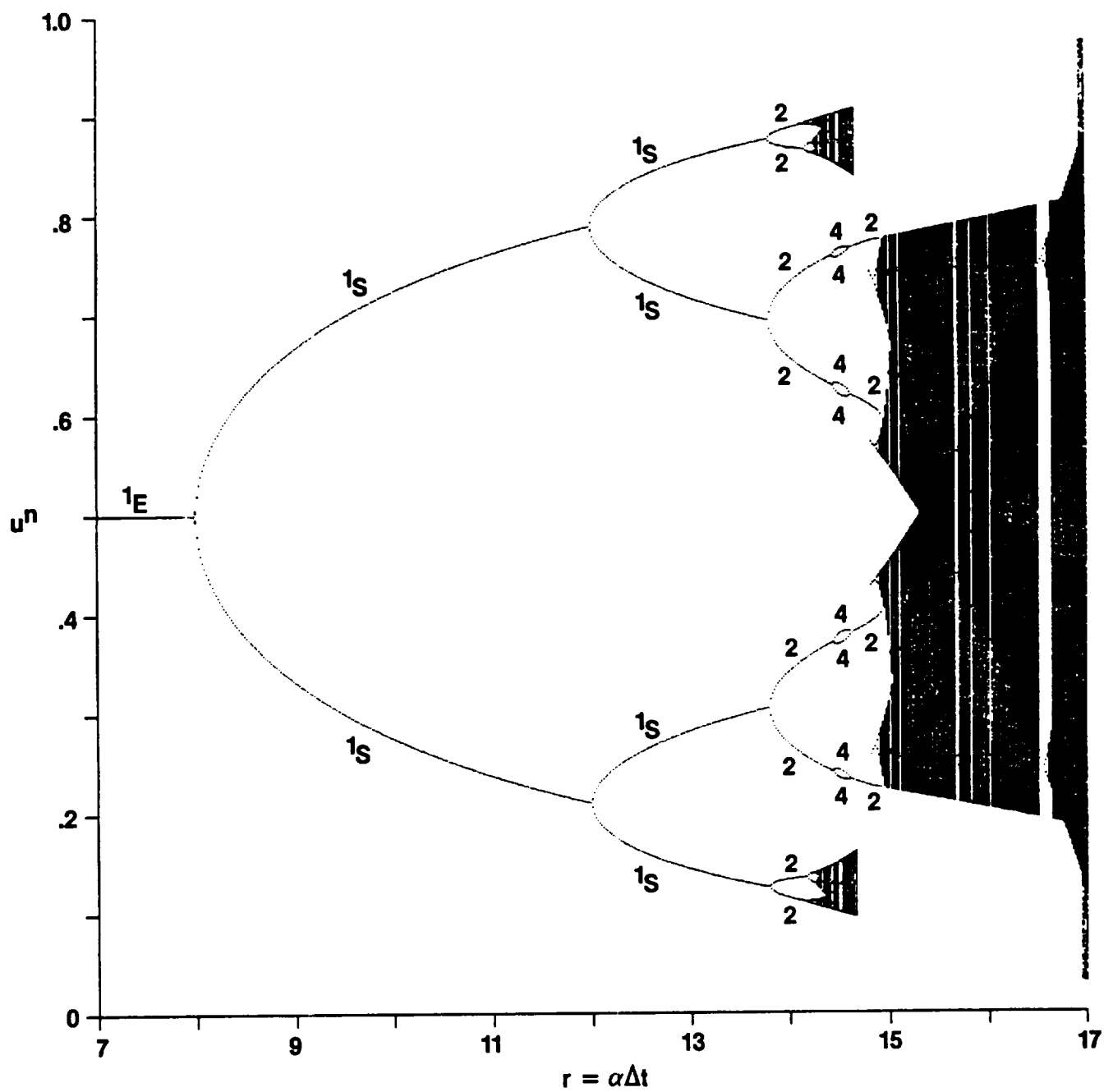


Fig. 3.34 "Full" bifurcation diagram of the improved Euler (R-K 2) scheme for the ODE $du/dt = \alpha u(1-u)(0.5-u)$.

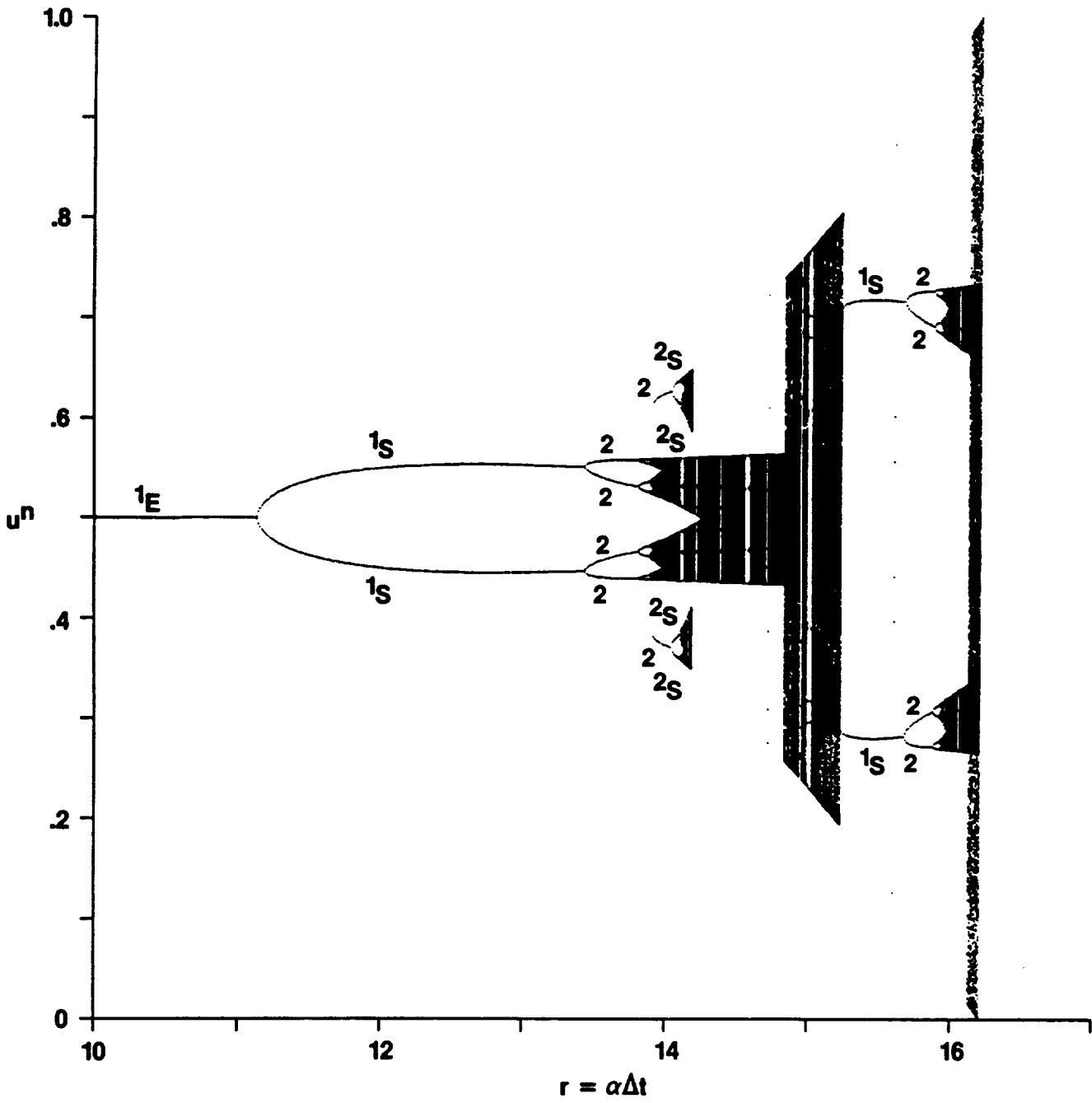


Fig. 3.35 "Full" bifurcation diagram of the Runge-Kutta 4th-order (R-K 4) scheme for the ODE $du/dt = \alpha u(1-u)(0.5-u)$.

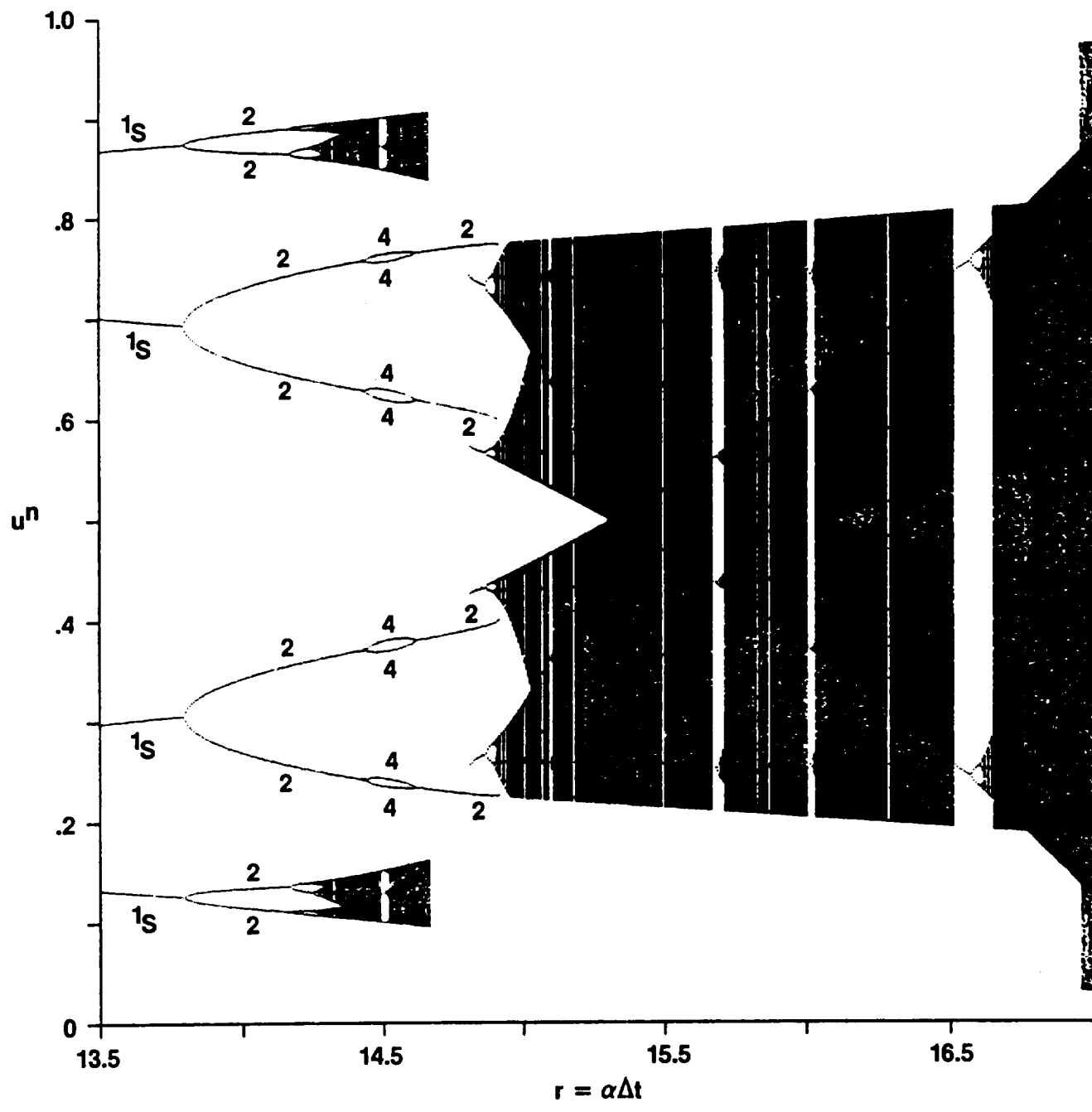


Fig. 3.36 "Full" bifurcation diagram of the improved Euler (R-K 2) scheme for the ODE $du/dt = \alpha u(1 - u)(0.5 - u)$ (enlarged).

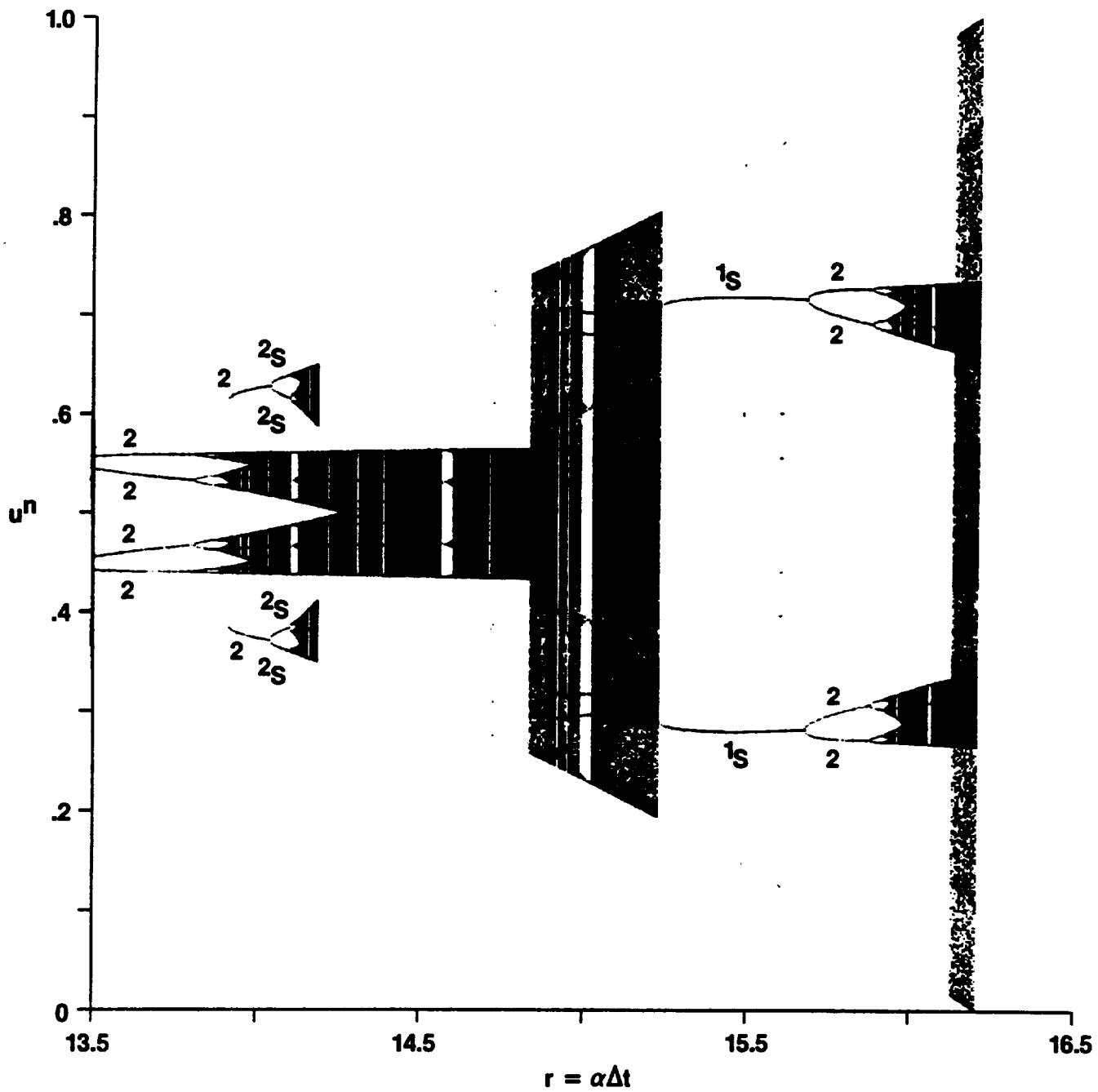


Fig. 3.37 "Full" bifurcation diagram of the Runge-Kutta 4th-order (R-K 4) scheme for the ODE $du/dt = \alpha u(1-u)(0.5-u)$ (enlarged).

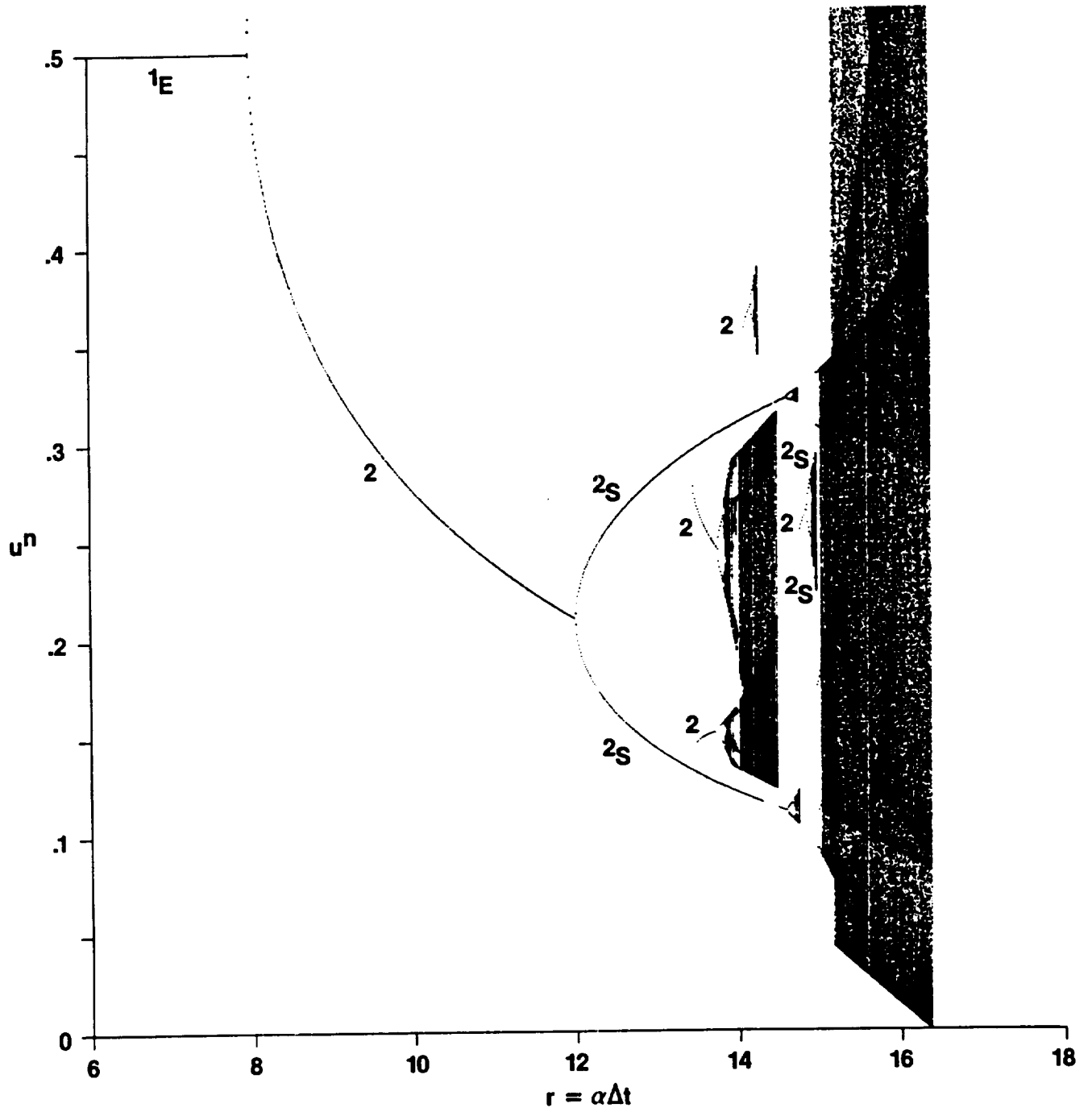


Fig. 3.38 "Full" bifurcation diagram of the predictor-corrector scheme of order 2 for the ODE $du/dt = \alpha u(1 - u)(0.5 - u)$.

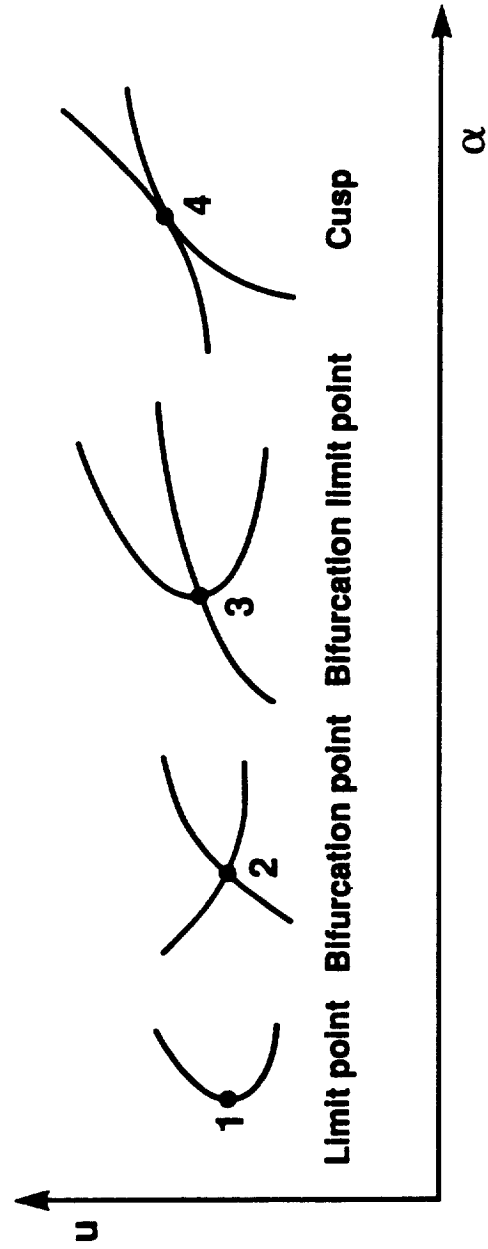


Fig. 3.39 Types of branching points.

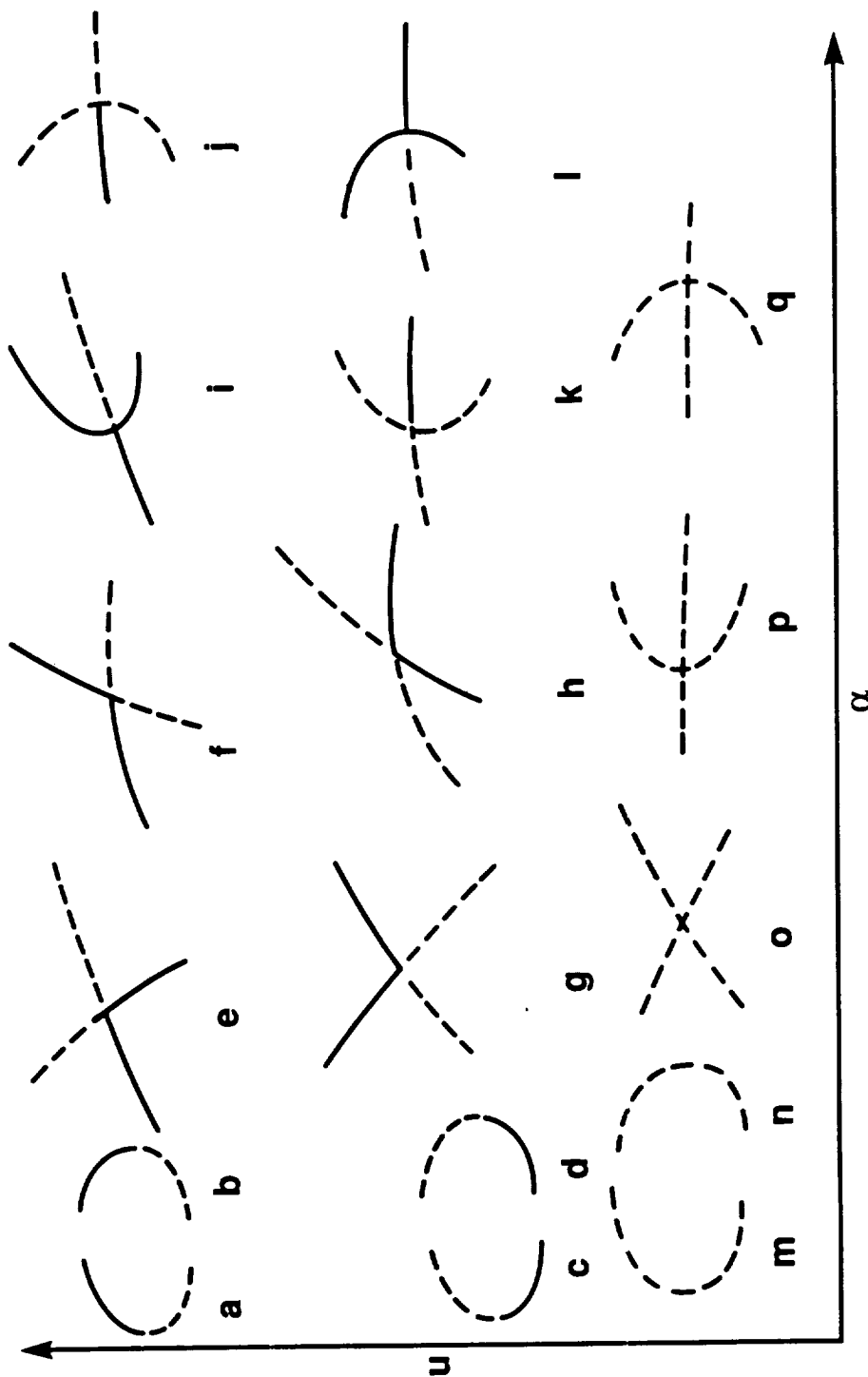


Fig. 3.40 Stability of solutions in the neighborhood of branch points, one-dimensional case. — stable, - - - unstable a,b,c,d: limit (regular turning) point; e,f,g,h: bifurcation (double) points; i,j,k,l: bifurcation-limit (singular turning) points; m,n,o,p,q: additional possible cases when the dimension of u is greater than one (this figure is taken from reference [7]).

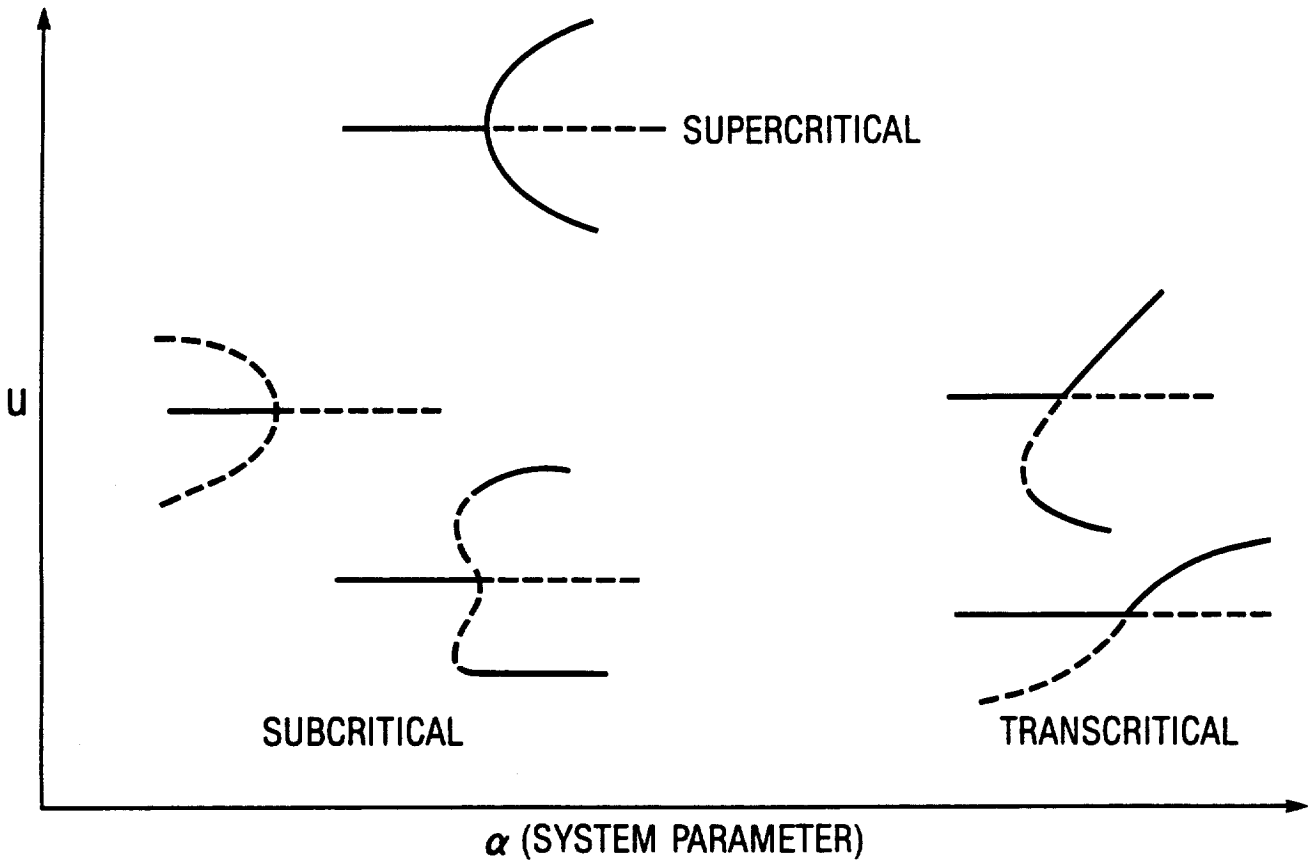


Fig. 3.41 Stability of steady-state solutions arising through three types of bifurcation phenomena (— stable, - - - unstable).

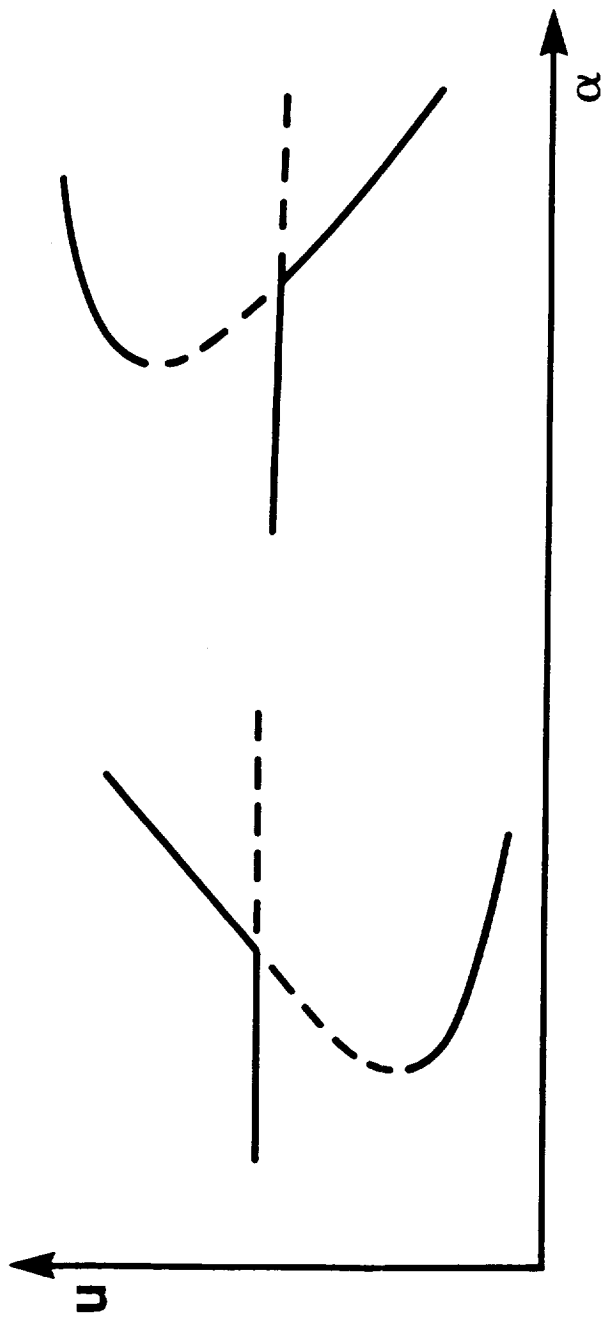


Fig. 3.42 Spurious fixed points arising from transcritical bifurcations.

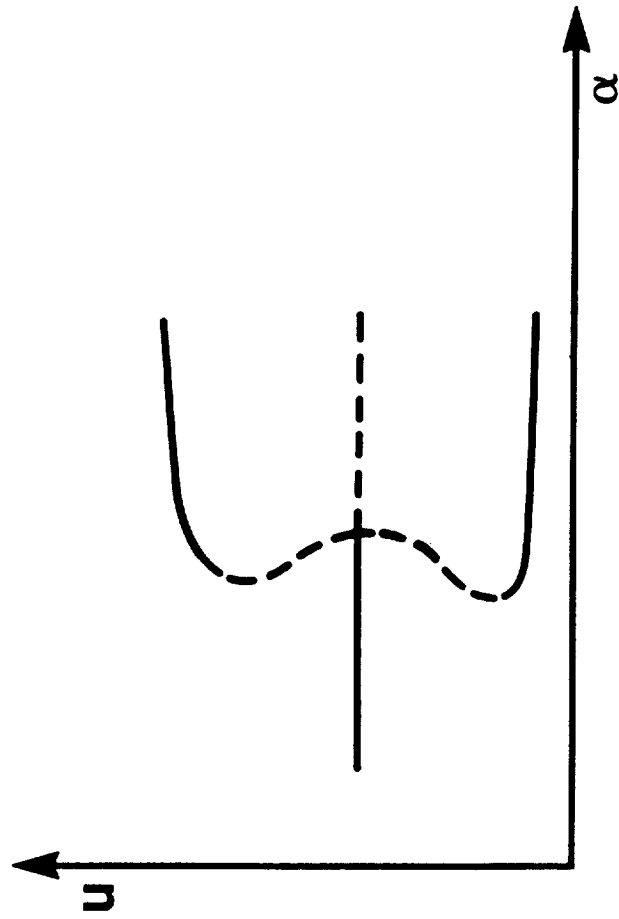


Fig. 3.43 Spurious fixed points arising from subcritical bifurcation.

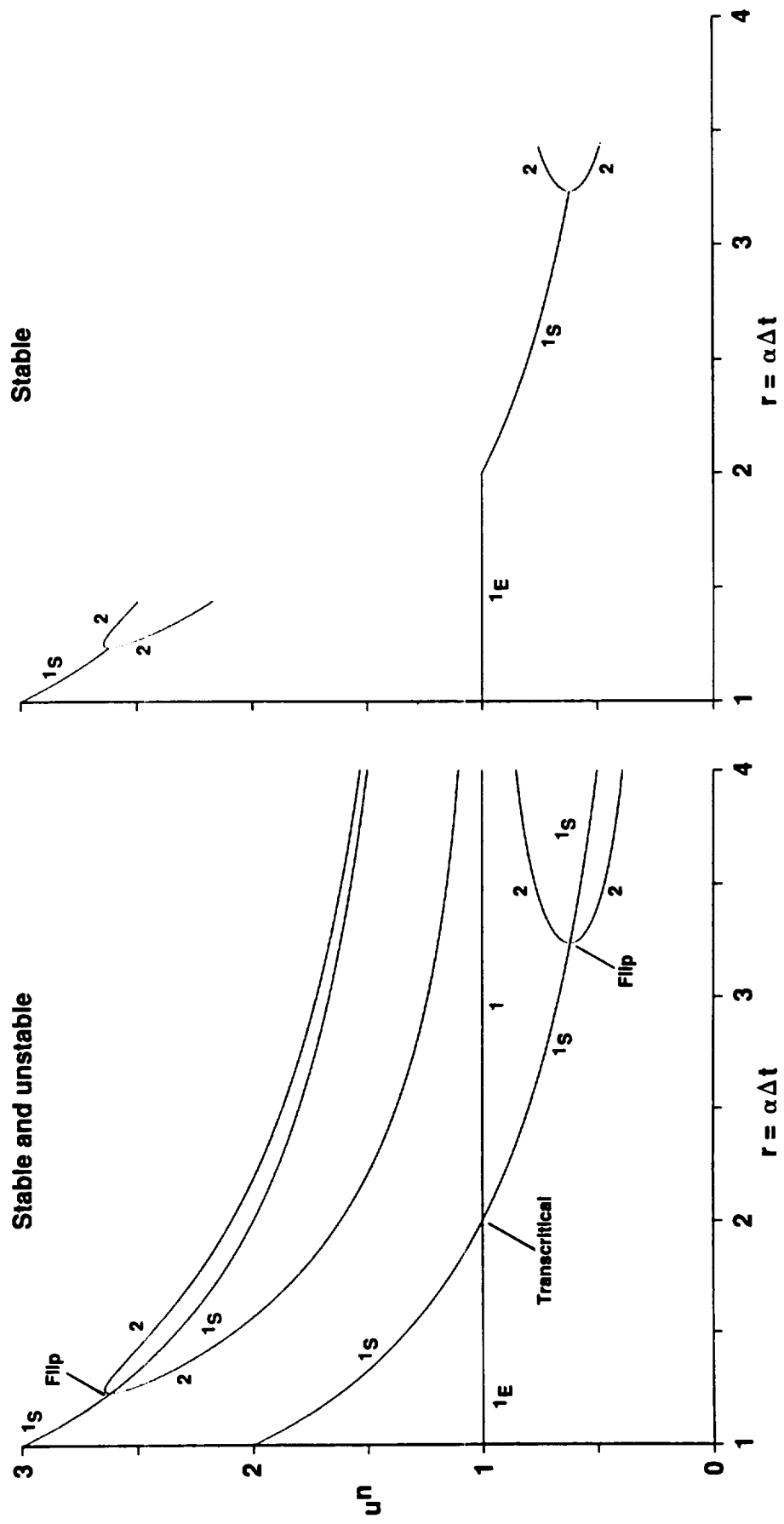


Fig. 3.44 Stable and unstable fixed points of periods 1,2 of the modified Euler (R-K) scheme for the logistic ODE $du/dt = \alpha u(1 - u)$.

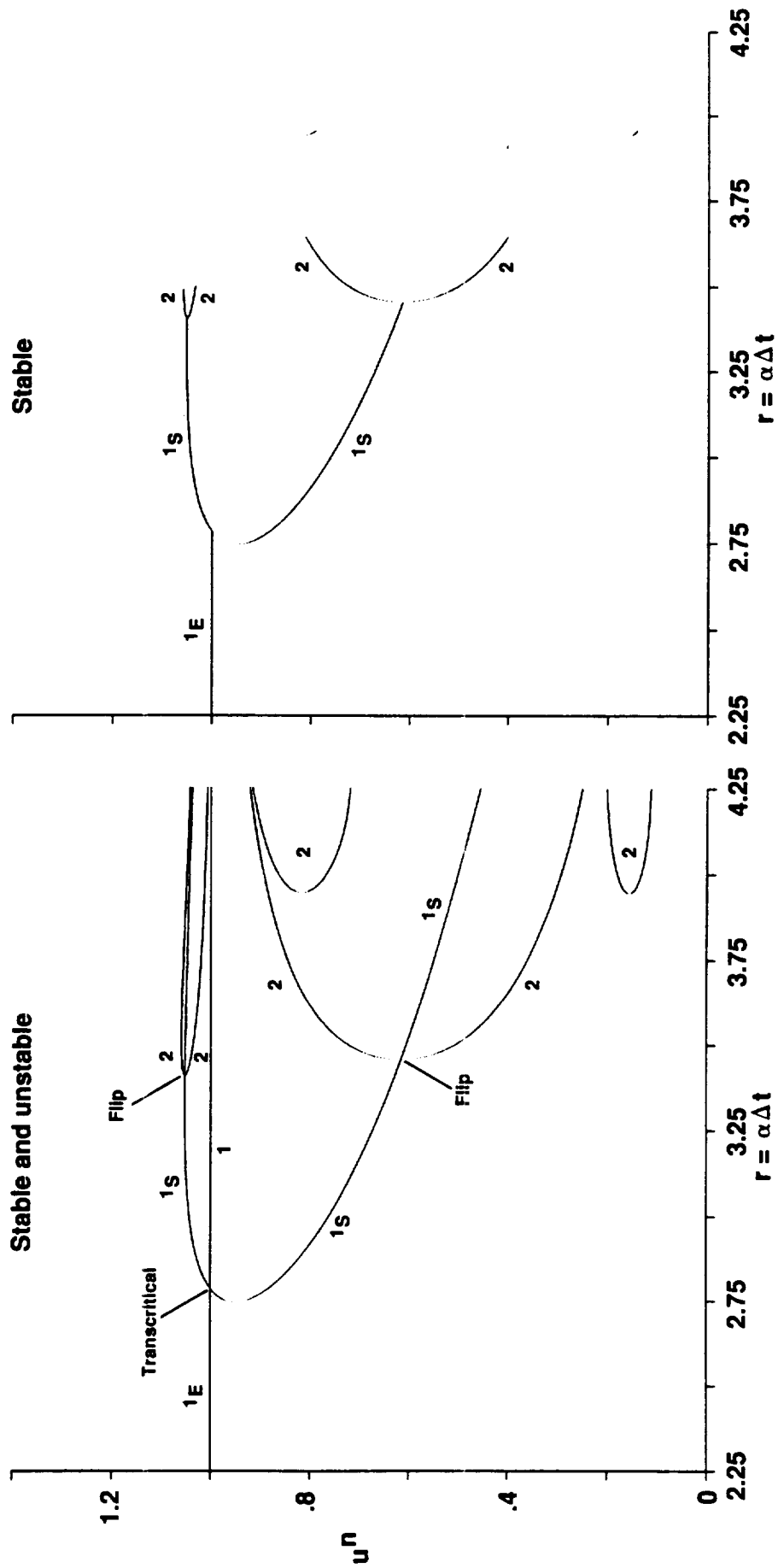


Fig. 3.46 Stable and unstable fixed points of periods 1,2 of the Runge-Kutta 4th-order (R-K 4) scheme for the logistic ODE $du/dt = \alpha u(1 - u)$.

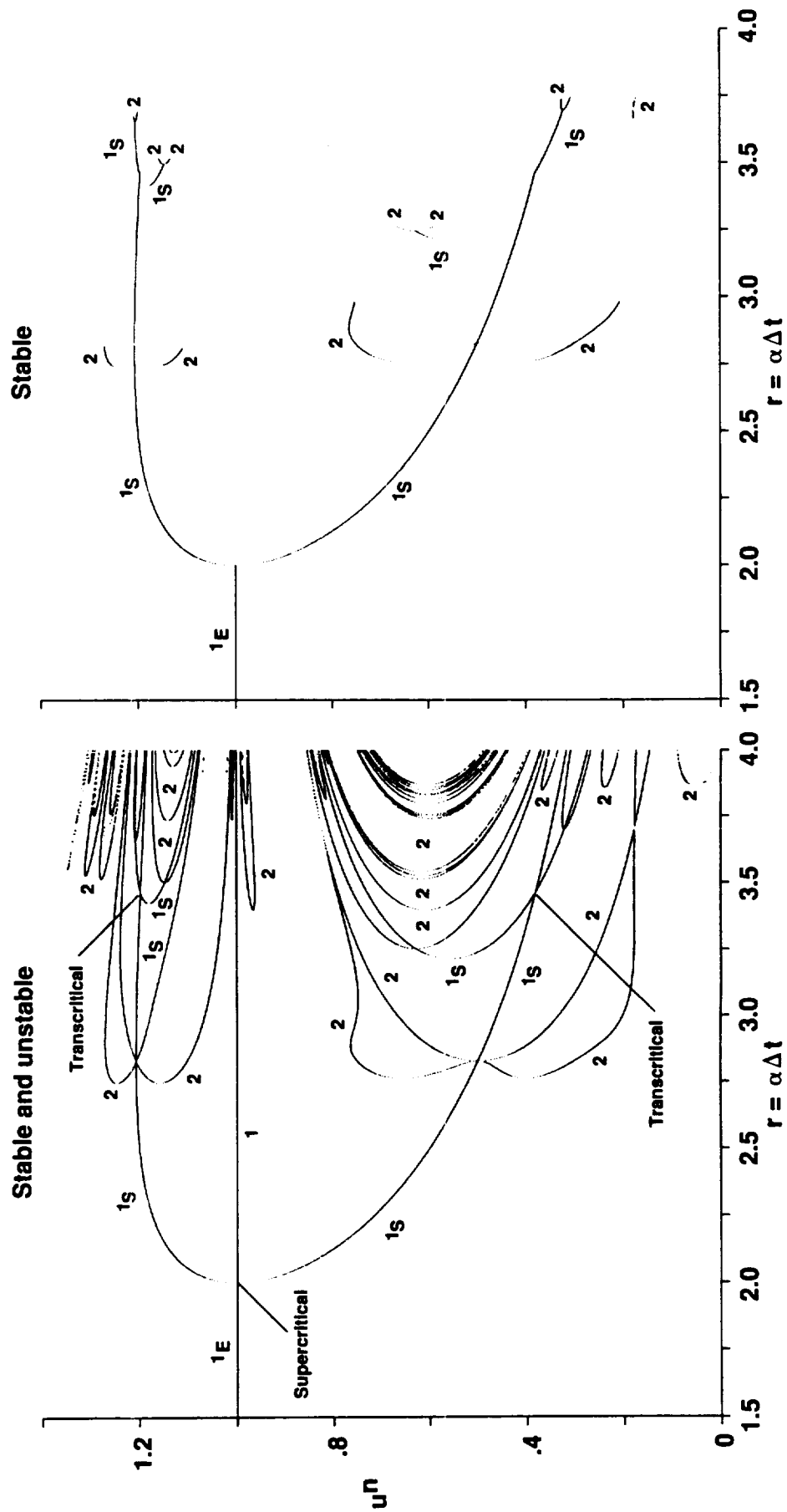


Fig. 3.48 Stable and unstable fixed points of periods 1,2 of the predictor-corrector scheme of order 3 for the logistic ODE $du/dt = \alpha u(1 - u)$.

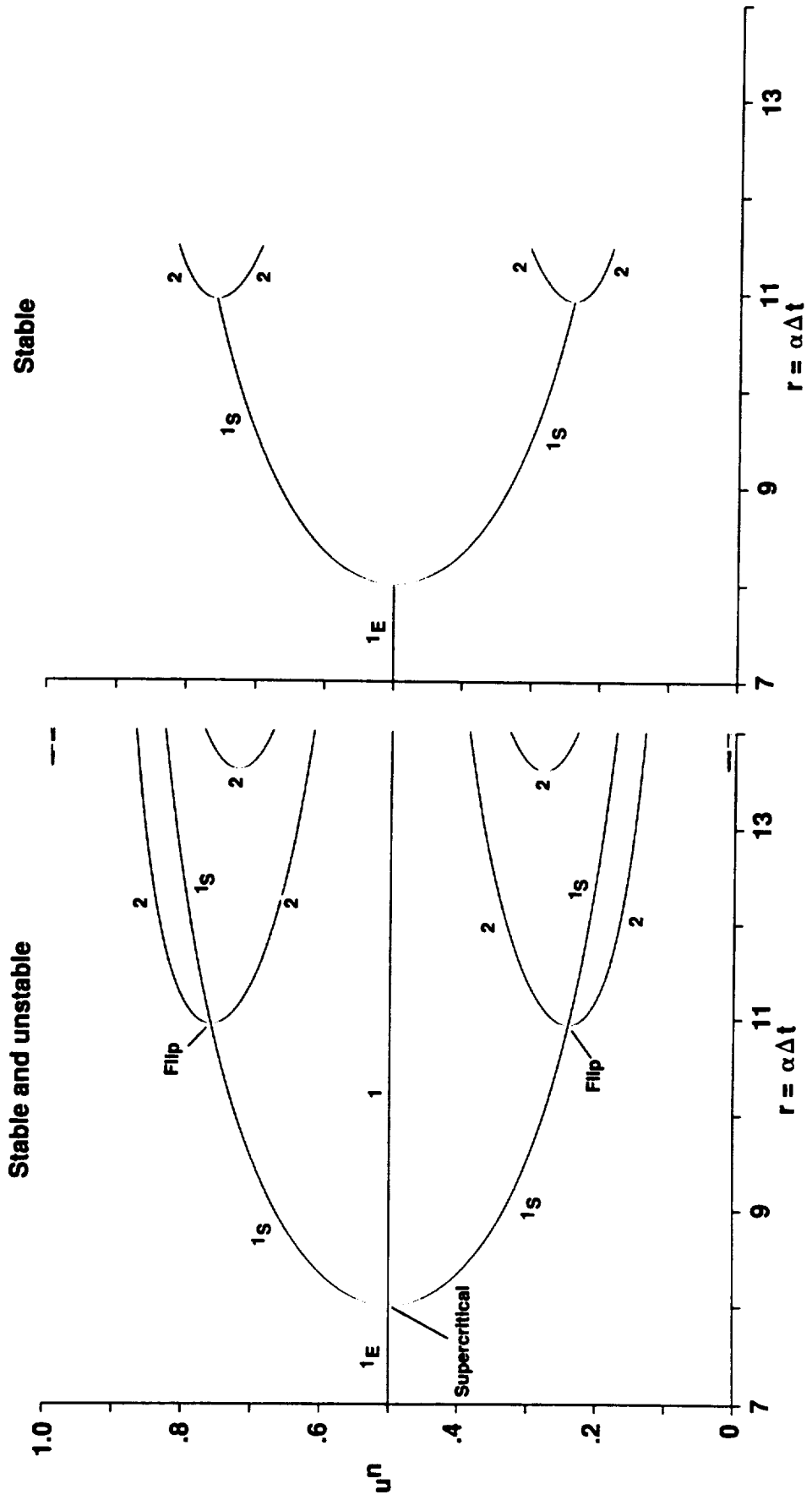


Fig. 3.49 Stable and unstable fixed points of periods 1,2 of the modified Euler (R-K 2) scheme for the ODE $du/dt = \alpha u(1 - u)(0.5 - u)$.

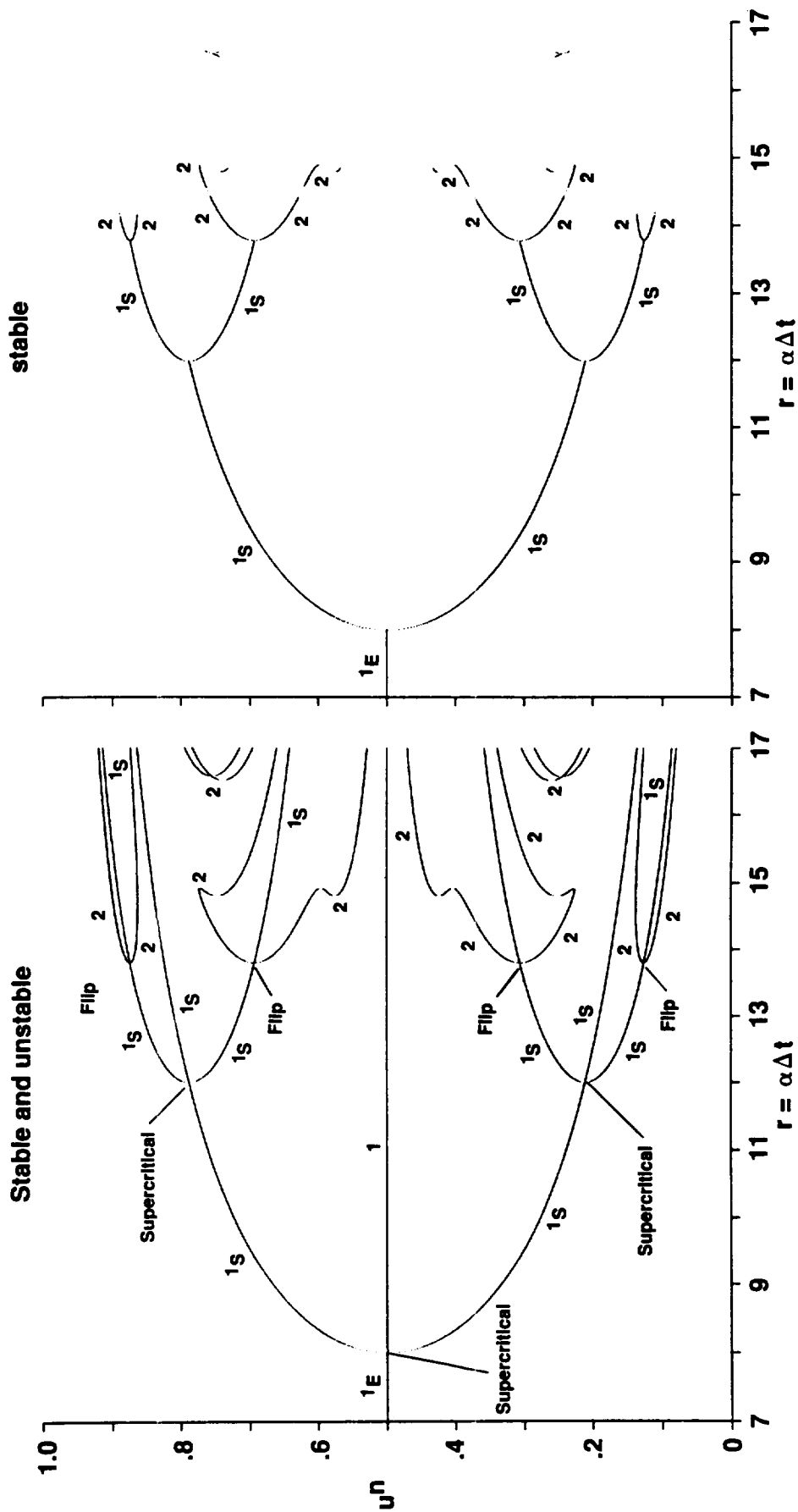


Fig. 3.50 Stable and unstable fixed points of periods 1,2 of the improved Euler (R-K) scheme for the ODE $du/dt = \alpha u(1-u)(0.5-u)$.

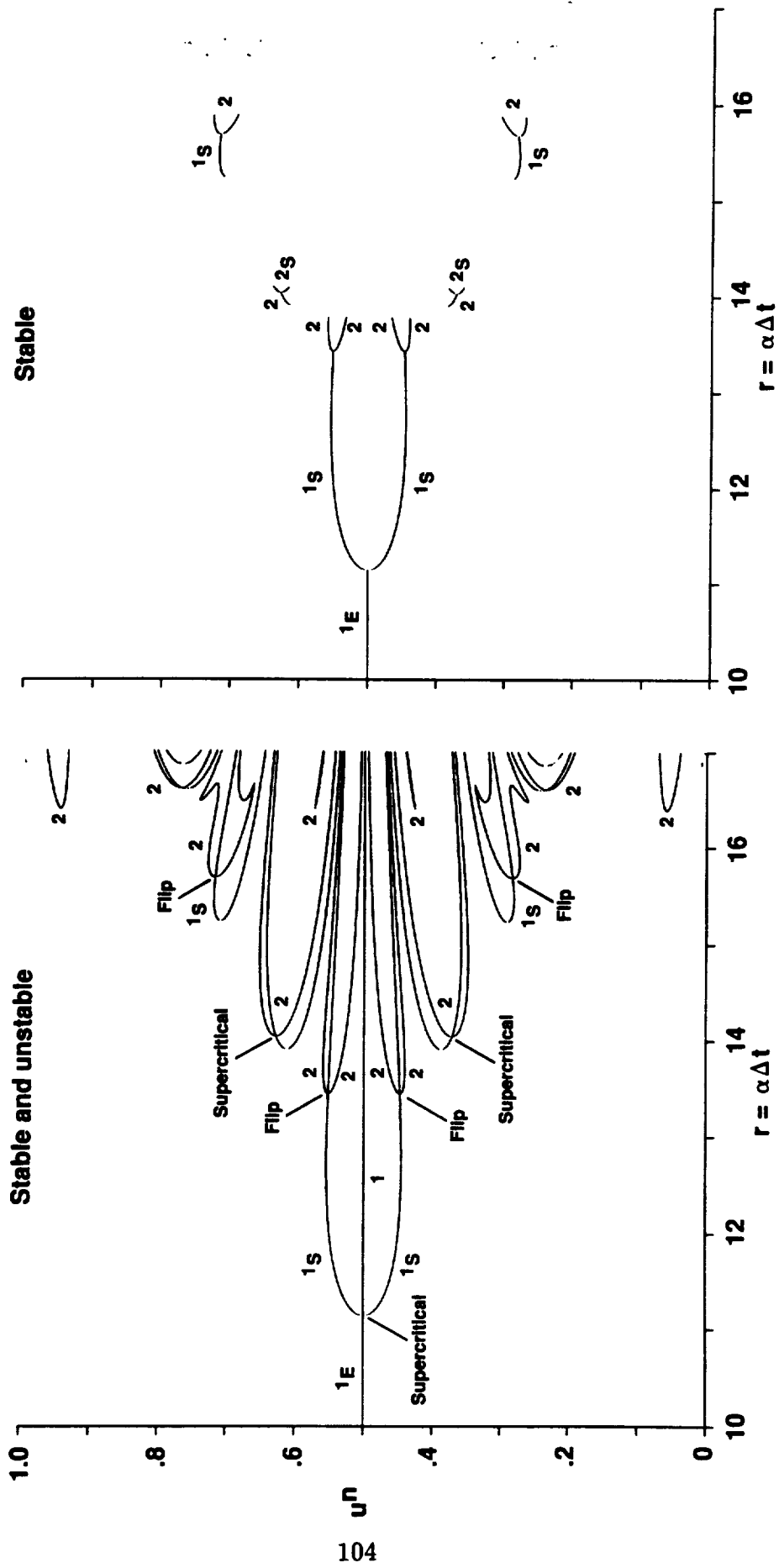


Fig. 3.51 Stable and unstable fixed points of periods 1,2 of the Runge-Kutta 4th-order (R-K 4) scheme for the ODE $du/dt = \alpha u(1-u)(0.5-u)$.

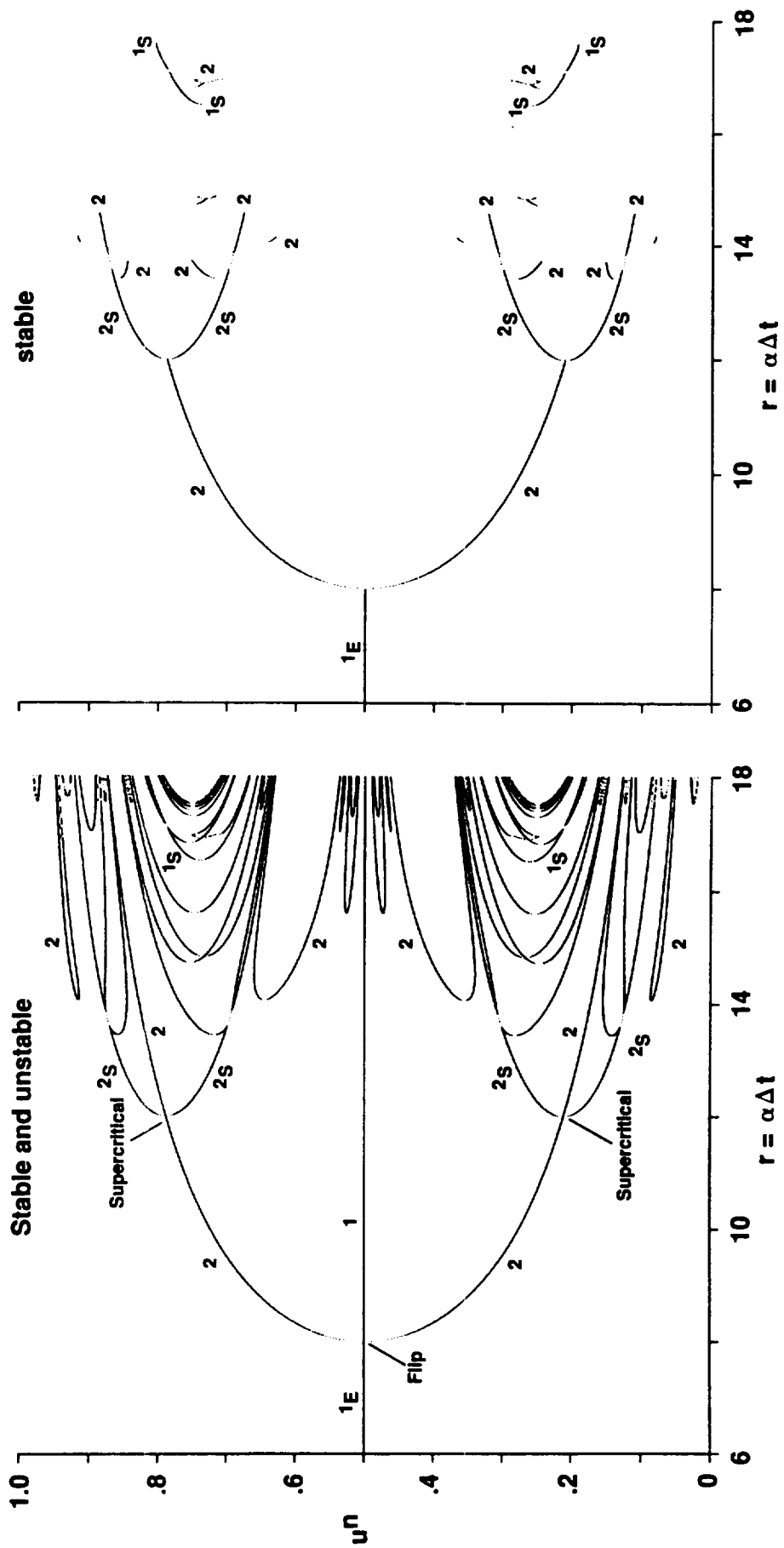


Fig. 3.52 Stable and unstable fixed points of periods 1,2 of the predictor-corrector scheme of order 2 for the ODE $du/dt = \alpha u(1-u)(0.5-u)$.

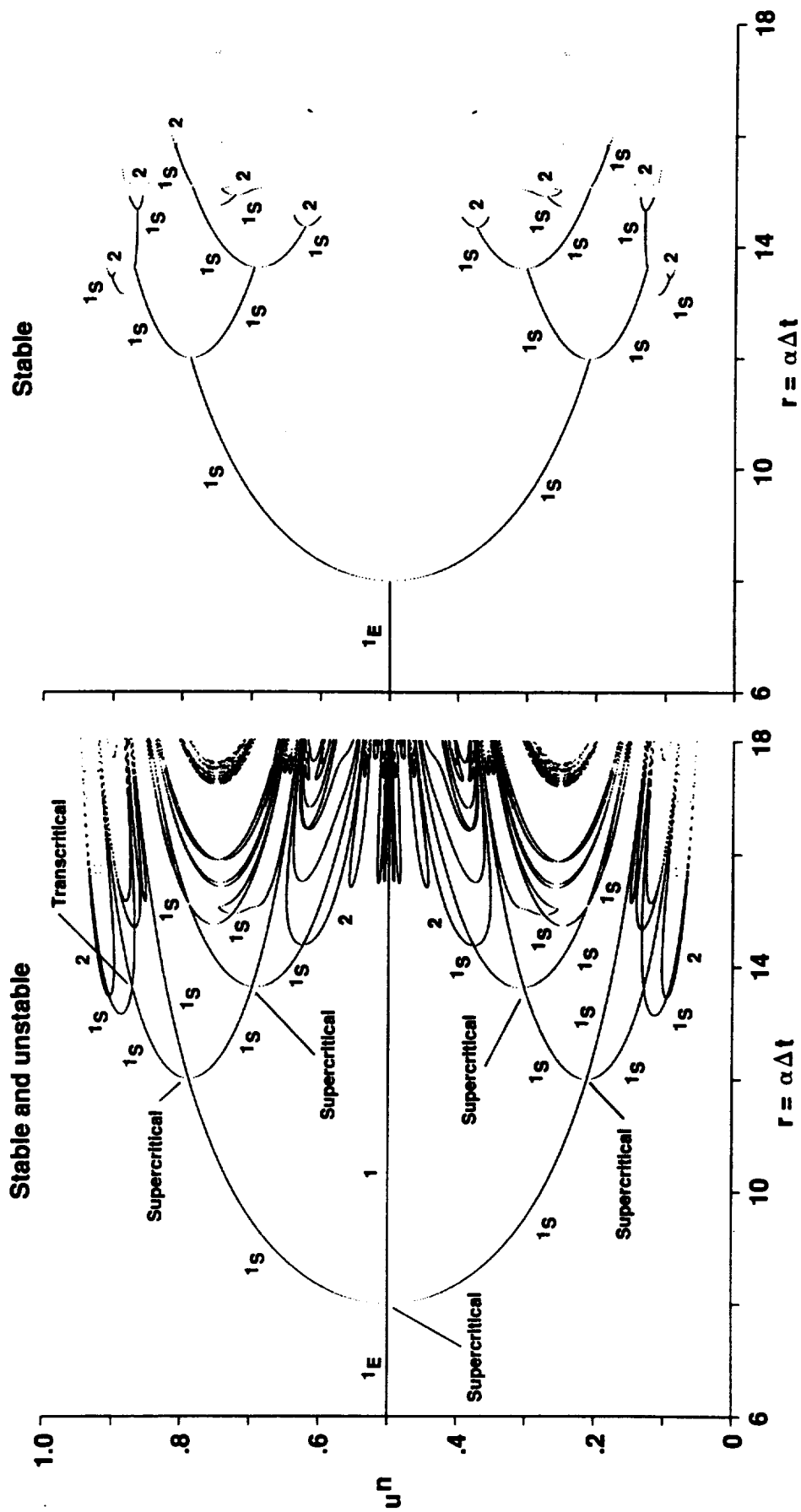


Fig. 3.53 Stable and unstable fixed points of periods 1,2 of the predictor-corrector scheme of order 3 for the ODE $du/dt = \alpha u(1-u)(0.5-u)$.

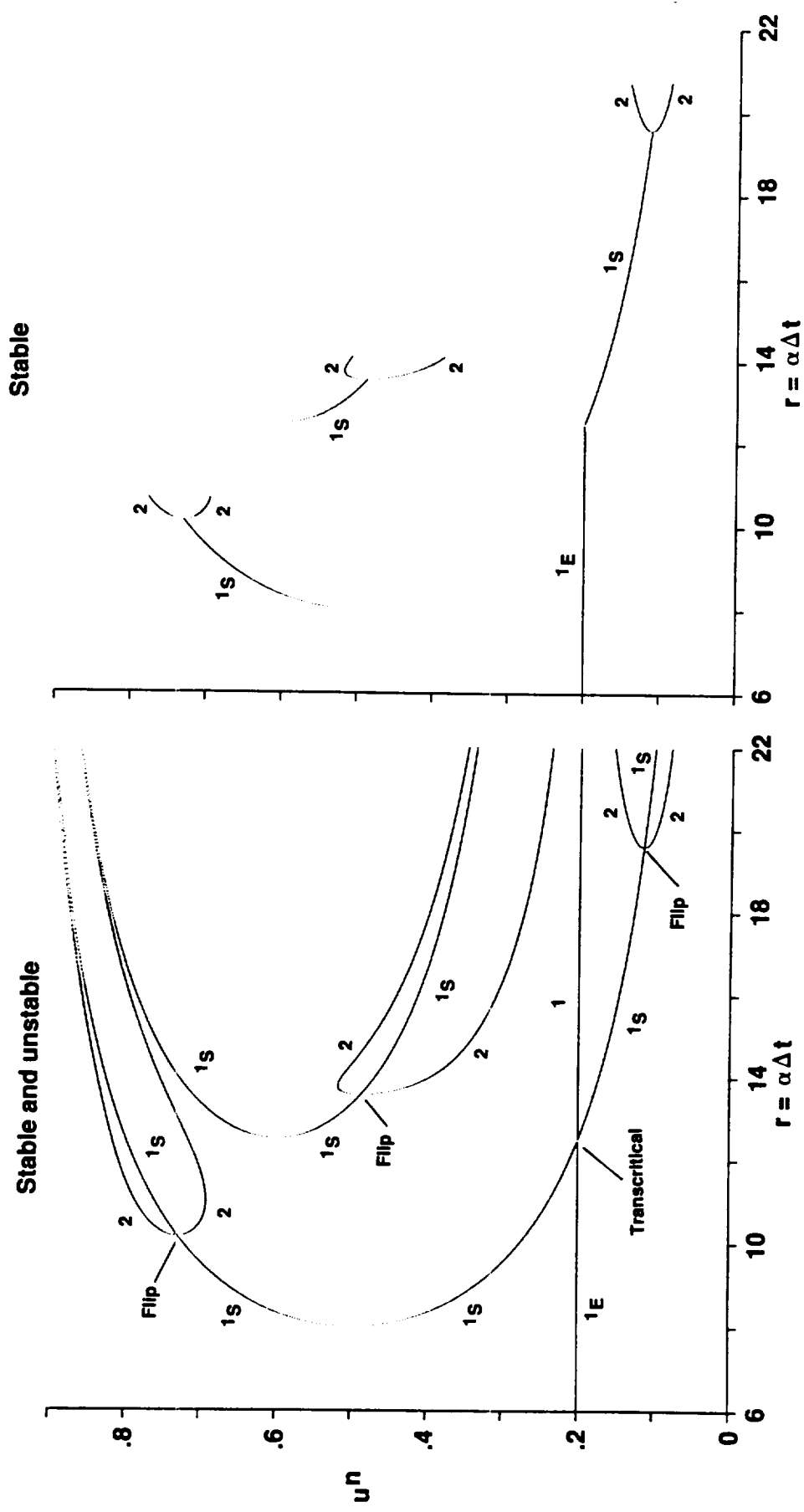


Fig. 3.54 Stable and unstable fixed points of periods 1,2 of the modified Euler (R-K) scheme for the ODE $du/dt = \alpha u(1-u)(0.2-u)$.



Report Documentation Page

1. Report No. NASA TM-102820		2. Government Accession No.		3. Recipient's Catalog No.	
4. Title and Subtitle Dynamical Approach Study of Spurious Steady-State Numerical Solutions of Nonlinear Differential Equations Part 1 – The ODE Connection and Its Implications for Algorithm Development in Computational Fluid Dynamics				5. Report Date April 1990	
				6. Performing Organization Code	
7. Author(s) H. C. Yee, P. K. Sweby (University of Reading, Whiteknights, and), and D. F. Griffiths (University of Dundee, and)				8. Performing Organization Report No. A-90149	
				10. Work Unit No. 505-60	
9. Organization Name and Address Ames Research Center Moffett Field, CA 94035-1000				11. Contract or Grant No.	
				13. Type of Report and Period Covered Technical Memorandum	
10. Agency Name and Address National Aeronautics and Space Administration Washington, DC 20546-0001				14. Sponsoring Agency Code	
				Notes Presented at 12th International Conference on Numerical Methods in Fluid Dynamics, Oxford, England, July 9-13, 1990.	
<p>stable as well as unstable steady-state numerical solutions, spurious asymptotic numerical solutions of higher order. In addition, stable chaotic behavior can occur when finite-difference methods are used to solve nonlinear differential equations numerically. The occurrence of spurious asymptotes is independent of whether the DE possesses a unique steady state, additional periodic solutions and/or exhibits chaotic phenomena. The form of the nonlinear DEs and the type of numerical schemes are the determining factor. In addition, the occurrence of spurious steady states is not restricted to the time step beyond the linearized stability limit of the scheme. In many instances, it can occur below the linearized stability limit. Therefore, it is essential for practitioners in computational sciences to be knowledgeable about the dynamical behavior of numerical difference methods for nonlinear scalar DEs before the actual application of these methods to practical computations. It is important to change the traditional way of thinking and practices when dealing with genuinely nonlinear problems. In our study, spurious asymptotes were observed in numerical computations but tended to be ignored because they all were beyond the linearized stability limits of the time step parameter Δt. As can be seen from our study, bifurcations to spurious asymptotic solutions and transitions to computational instability not only are highly scheme dependent but also initial data and boundary condition dependent, and not limited to time steps that are beyond the linearized stability limit.</p>					
17. Keywords (if any) suggested by Author(s) Nonlinear dynamics, Chaotic dynamics, Dynamics of nonlinear systems, Numerics, Computational fluid dynamics, Hypersonic reacting flows, Nonlinear ordinary differential equations, Nonlinear dynamical systems				18. Distribution Statement Unclassified-Unlimited Subject Category – 64	
19. Security Classif. (of this report) Unclassified		20. Security Classif. (of this page) Unclassified		21. No. of Pages 110	22. Price A06



DYNAMICAL APPROACH STUDY OF SPURIOUS STEADY-STATE NUMERICAL SOLUTIONS OF NONLINEAR DIFFERENTIAL EQUATIONS II. GLOBAL ASYMPTOTIC BEHAVIOR OF TIME DISCRETIZATIONS*

H. C. YEE

*Fluid Dynamics Division, NASA Ames Research Center,
Moffett Field, CA, 94035, USA*

P. K. SWEBY[†]

*Department of Mathematics, University of Reading,
Whiteknights, Reading RG6 2AX, England*

(Received 19 August 1993; in final form 10 February 1994)

SUMMARY

The global asymptotic nonlinear behavior of 11 explicit and implicit time discretizations for four 2×2 systems of first-order autonomous nonlinear ordinary differential equations (ODEs) is analyzed. The objectives are to gain a basic understanding of the difference in the dynamics of numerics between the scalars and systems of nonlinear autonomous ODEs and to set a baseline global asymptotic solution behavior of these schemes for practical computations in computational fluid dynamics. We show how "numerical" basins of attraction can complement the bifurcation diagrams in gaining more detailed global asymptotic behavior of time discretizations for nonlinear differential equations (DEs). We show how in the presence of spurious asymptotes the basins of the true stable steady states can be segmented by the basins of the spurious stable and unstable asymptotes. One major consequence of this phenomenon which is not commonly known is that this spurious behavior can result in a dramatic distortion and, in most cases, a dramatic shrinkage and segmentation of the basin of attraction of the true solution for finite time steps. Such distortion, shrinkage and segmentation of the numerical basins of attraction will occur regardless of the stability of the spurious asymptotes, and will occur for unconditionally stable implicit linear multistep methods. In other words, for the same (common) steady-state solution the associated basin of attraction of the DE might be very different from the discretized counterparts and the numerical basin of attraction can be very different from numerical method to numerical method. The results can be used as an explanation for possible causes of error, and slow convergence and nonconvergence of steady-state numerical solutions when using the time-dependent approach for nonlinear hyperbolic or parabolic PDEs.

KEY WORDS: Spurious steady-state numerical solutions, spurious asymptotes, global asymptotic behavior, nonlinear ODEs, numerical methods, time discretizations.

* Part of the material appeared in the Proceedings of the 9th GAMM Conference on Numerical Methods in Fluid Mechanics, Lausanne, Switzerland, Sept. 25-27, 1991. Full text appeared as a NAS Applied Research Technical Report RNR-92-008, March 1992, NASA Ames Research Center.

[†] Part of this work was performed as a visiting scientist at the NASA Ames Research Center.

1. INTRODUCTION

The tool that is utilized for the current study belongs to a multidisciplinary field of study in numerical analysis, sometimes referred to as “The Dynamics of Numerics¹”. Here the phrase “to study the dynamics of numerics” (dynamical behavior of a numerical scheme) is restricted to the study of local and global asymptotic behavior and bifurcation phenomena of the nonlinear difference equations resulting from finite discretizations of a nonlinear differential equation (DE) subject to the variation of discretized parameters such as the time step, grid spacing, numerical dissipation coefficient, etc. In this paper, standard terminologies of nonlinear dynamics, chaotic dynamics (Guckenheimer and Holmes, 1983; Hale and Kocak, 1991) and computational fluid dynamics (CFD) are assumed. For an introduction to the dynamics of numerics and its implications for algorithm development in CFD, see Yee *et al.* (1991) and Yee (1991) and references cited therein.

1.1 Background

The phenomenon that a nonlinear DE and its discretized counterpart can have different dynamical behavior (asymptotic behavior) was not uncovered fully until recently. Aside from truncation error and machine round-off error, a more fundamental distinction between the DE (continuum) and its discretized counterparts for genuinely nonlinear behavior is extra solutions in the form of spurious stable and unstable asymptotes that can be created by the numerical method. Here we use the term “discretized counterparts” to mean the finite difference equations (or discrete maps) resulting from finite discretizations of the underlying DE. Also we use the term “spurious asymptotic numerical solutions” to mean asymptotic solutions that satisfy the discretized counterparts but do not satisfy the underlying ordinary differential equations (ODEs) or partial differential equations (PDEs). Asymptotic solutions here include steady-state solutions (fixed points of period one for the discretized equations), periodic solutions, limit cycles, chaos and strange attractors. See Section III and Guckenheimer and Holmes (1983), Hale and Kocak (1991) and Yee *et al.* (1991) for definitions.

Iserles (1988) showed that while linear multistep methods (LMMs) for solving ODEs possess only the fixed points (fixed points of period one) of the original DEs, popular Runge-Kutta methods may exhibit additional, spurious fixed points. It has been demonstrated by the authors and collaborators (Yee *et al.*, 1991; Yee, 1991; Sweby *et al.*, 1990; Griffiths *et al.*, 1992; Yee and Sweby, 1993a, 1993b) for nonlinear ODEs, and Lafon and Yee (1991, 1992) for nonlinear reaction-convection model equations that such spurious fixed points as well as spurious fixed points of higher periods may be stable below the linearized stability limit of the scheme, depending on the initial data. Iserles *et al.* (1990), Hairer *et al.* (1989) and Humphries (1991) further advanced some theoretical understanding of the dynamics of numerics for initial value problems of ODEs. Iserles *et al.* and Hairer *et al.* classified and gave guidelines and theory on the types of Runge-Kutta methods that do not exhibit spurious period one or period two fixed points. Humphries (1991) showed that under appropriate assumptions if stable

¹ Named after the First IMA Conference on Dynamics of Numerics and Numerics of Dynamics, University of Bristol, England, July 31 August 2, 1990.

spurious fixed points exist as the time-step approaches zero, then they must either approach a true fixed point or become unbounded. However, convergence in practical calculations involves a finite time step Δt as the number of integrations $n \rightarrow \infty$ rather than $\Delta t \rightarrow 0$, as $n \rightarrow \infty$. There appear to be missing links between theoretical development and practical scientific computation. Our aim is to provide some of these missing links that were not addressed in Iserles (1988), Iserles *et al.* (1990), Hairer *et al.* (1989), Humphries (1991) and our earlier work. In particular, we want to show in more detail the global asymptotic behavior of time discretizations when finite but not extremely small Δt is used. Other aspects that were not addressed in Iserles (1988) for different iteration procedures in solving the resulting nonlinear algebraic equations are reported in greater depth in our companion papers (Yee and Sweby, 1993a, 1993b).

1.2 Relevance and Motivations

Although the understanding of the dynamics of numerics of systems of nonlinear ODEs and PDEs is important in its own right and has applications in the various nonlinear scientific fields, our main emphasis is CFD applications. Time-marching types of methods (time-dependent approach) are commonly used in CFD because the steady PDEs of higher than one dimension are usually of the mixed type. When a time-dependent approach is used to obtain steady-state numerical solutions of a fluid flow or a steady PDE, a boundary value problem (BVP) is transformed into an initial-boundary value problem (IBVP) with unknown initial data. If the steady PDE is strongly nonlinear and/or contains stiff nonlinear source terms, phenomena such as slow convergence, nonconvergence or spurious steady-state numerical solutions and limit cycles commonly occur even though the time step is well below the linearized stability limit and the initial data are physically relevant. One of our goals is to search for logical explanations for these phenomena via the study of the dynamics of numerics. Here the term "time-dependent approach" is used loosely to include some of the iteration procedures (due to implicit time discretizations), relaxation procedures, and preconditioners for convergence acceleration strategies used to numerically solve steady PDEs. This is due to the fact that most of these procedures can be viewed as approximations of time-dependent PDEs (but not necessarily the original PDE that was under consideration). If one is not careful, numerical solutions other than the desired one of the underlying PDE can be obtained (in addition to spurious asymptotes due to the numerics).

One consequence of the existence of stable and unstable spurious asymptotes below or above the linearized stability limit of the numerical schemes is that these spurious features may greatly affect the dynamical behavior of the numerical solution in practice due to the use of a finite time step. As discussed in details in later sections and also in Yee *et al.* (1991), Yee and Sweby (1993a, b), Lafon and Yee (1992), Sweby and Yee (1991), Yee *et al.* (1992), it is possible that for the same steady-state solution, the associated basin of attraction of the underlying DEs (which initial conditions lead to which asymptotic states) might be very different from that of the basin of attraction of the discretized counterparts due to the existence of spurious stable and unstable asymptotic numerical solutions. In other words, there is a separate dependence on initial data for the individual DEs and their discretized counterparts. Here the basin of attraction is a domain of a set of initial conditions whose solution curves (trajectories)

all approach the same asymptotic state. Also we use the term “exact” and “numerical” basins of attraction to distinguish “basins of attraction of the underlying DEs” and “basins of attraction of the discretized counterparts”.

In view of the spurious dynamics, it is possible that numerical computations may converge to an incorrect steady state or other asymptote which appears to be physically reasonable. One major implication is that what is expected to be physical initial data associated with the underlying steady state of the DE might lead to a wrong steady state, a spurious asymptote, or a divergence or nonconvergence of the numerical solution. In addition, the existence of spurious limit cycles may result in the type of nonconvergence of steady-state numerical solutions observed in time-dependent approaches to the steady states. It is our belief that the understanding of the symbiotic relationship between the strong dependence on initial data and permissibility of spurious stable and unstable asymptotic numerical solutions at the fundamental level can guide the tuning of the numerical parameters and the proper and/or efficient usage of numerical algorithms in a more systematic fashion. It can also explain why certain schemes behave nonlinearly in one way but not another. Here strong dependence on initial data means that for a finite time step Δt that is not sufficiently small, the asymptotic numerical solutions and the associated numerical basins of attraction depend continuously on the initial data. Unlike nonlinear problems, the associated numerical basins of attraction of linear problems are independent of Δt as long as Δt is below a certain upper bound.

Nonunique Steady-State Solutions of Nonlinear DEs vs. Spurious Asymptotes: The phenomenon of generating spurious steady-state numerical solutions (or other spurious asymptotes) by certain numerical schemes is often *confused* with the nonuniqueness (or *multiple steady states*) of the DE. In fact, the existence of nonunique steady-state solutions of the continuum can complicate the numerics tremendously (e.g., the basins of attraction) and is *independent* of the occurrence of spurious asymptotes of the associated scheme. But, of course, a solid background in the theory of nonlinear ODEs and PDEs and their dynamical behavior is a prerequisite in the study of the dynamics of numerics for nonlinear PDEs. See Yee *et al.*, 1991 for a discussion. It is noted that the approach and primary goal of our work is quite different from the work of e.g., Beam and Bailey (1988) and Jameson (1991). The main goal of Beam and Bailey (1988) and Jameson (1991) was to study the nonunique steady-state solutions admitted by the PDE as the physical parameter is varied. Our primary interest is to establish some working tools and guidelines to help delineate the true physics from numerical artifacts via the dynamics of numerics approach. The knowledge gained from our series of studies (Yee *et al.*, 1991; Lafon and Yee, 1991; Lafon and Yee, 1992) hopefully can shed some light on the controversy about the existence of multiple steady-state solutions through numerical experiments for certain flow types of the Euler and/or Navier Stokes equations.

1.3 Objectives and Outline

The primary goal of the series of papers (present and the companion papers Yee *et al.*, 1991; Yee and Sweby, 1993a, b; Lafon and Yee, 1991; Lafon and Yee, 1992) is to lay the foundation for the utilization of the dynamics of numerics in algorithm development for computational sciences in general and CFD in particular. This is part II of this series of papers on the same topic. Part I (Yee *et al.*, 1991) concentrated on the dynamical behavior

of time discretizations for scalar nonlinear ODEs. The intent of part I was to serve as an introduction to motivate this concept to researchers in the field of CFD and to present new results for the dynamics of numerics for first-order scalar autonomous ODEs.

The present paper, the second of this series, is devoted to the study of the dynamics of numerics for 2×2 systems of ODEs. Here we show how “numerical” basins of attraction can complement the bifurcation diagrams in gaining more detailed global asymptotic behavior of numerical methods for nonlinear DEs. We show how in the presence of spurious asymptotes the basins of the true stable steady states can be segmented by the basin of the spurious stable and unstable asymptotes. One major consequence of this phenomenon which is not commonly known is that this spurious behavior can result in a dramatic distortion and, in most cases, a dramatic shrinkage and segmentation of the basin of attraction of the true solution for finite time steps. Such distortion, shrinkage and segmentation of the numerical basins of attraction will occur regardless of the stability of the spurious asymptotes, and will occur for unconditionally stable implicit linear multistep methods. In other words, for the same steady-state solution, the associated basin of the DE might be very different from its discretized counterparts. The basins can also be very different from numerical method to numerical method. The present study reveals for the first time the detail interlocking relationship of numerical basins of attraction and the causes of error, and slow convergence and nonconvergence of steady-state numerical solutions when using the time-dependent approach.

The article of Lafon and Yee (1991), the third of this series, was devoted to the study of the dynamics of numerics of commonly used numerical schemes in CFD for a model reaction-convection equation. The article of Lafon and Yee (1992), the fourth of this series, was devoted to a more detailed study of the effect of numerical treatment of nonlinear source terms on nonlinear stability of steady-state numerical solution for the same model nonlinear reaction-convection BVP. In our companion papers (Sweby *et al.*, 1990; Griffiths *et al.*, 1991a, 1992b), a theoretical bifurcation analysis of a class of explicit Runge-Kutta methods and spurious discrete travelling wave phenomenon were presented. In yet another companion paper, Yee and Sweby (1993a), the global asymptotic nonlinear behavior of three standard iterative procedures in solving nonlinear systems of algebraic equations arising from four implicit LMMs is analyzed numerically.

1.4 Outline

The outline of this paper is as follows. Section II discusses the connection of the dynamics of numerics for systems of ODEs and numerical approximations of time-dependent PDEs. Section III reviews background material for nonlinear ODEs and their numerical methods. Section IV describes four 2×2 systems of nonlinear first-order autonomous model ODEs. Section V describes the 11 time discretizations and the associated bifurcation diagrams for the four model ODEs. Section VI discusses the combined basins of attraction and bifurcation diagrams for the underlying schemes. Comparison between a linearized implicit Euler and Newton method is briefly discussed in Section 6.5. The paper ends with some concluding remarks in Section VII.

2. THE DYNAMICS OF NUMERICS OF SYSTEMS OF ODEs AND NUMERICAL APPROXIMATIONS OF TIME-DEPENDENT PDEs

For finite discretizations of PDEs, spurious asymptotes and especially spatially-varying spurious steady states can be independently introduced by time and spatial discretizations (Yee *et al.*, 1991; Lafon and Yee, 1991; Lafon and Yee, 1992). The interaction between temporal and spatial dynamical behavior is more complicated when one is dealing with the nonseparable temporal and spatial finite-difference discretizations such as the Lax-Wendroff type. The analysis and the different features of the numerics due to temporal and spatial discretizations can become more apparent by separable temporal and spatial finite difference methods (FDM). A standard method for obtaining such a FDM is the method of lines (MOL) procedure where the time-dependent PDE is reduced to a system of ODEs (by replacing the spatial derivatives by finite difference approximations). The resulting approximation is called semi-discrete, since the time variable is left continuous. The semi-discrete system in turn can be solved by the desired time discretizations. Similar semi-discrete systems can be obtained by finite element methods except in this case an additional mass matrix is involved. Besides the MOL approach, coupled nonlinear ODEs can arise in many other ways when analyzing nonlinear PDEs. See for example Globus *et al.* (1991), Hung *et al.* (1991), Foias *et al.* (1985), Temam (1989), Kwak (1991), Schechter and Shearer (1990), and Shearer *et al.* (1987). Among these possibilities, the idea of inertial manifold (IM) and approximate inertial manifold (AIM) for incompressible Navier-Stokes (Foias *et al.*, 1985; Temam, 1989; Kwak, 1991), the relationship between shock waves, heteroclinic orbits of systems of ODEs (Schechter and Shearer, 1990; Shearer *et al.*, 1987), and flow visualization of numerical data (Globus *et al.*, 1991; Hung, 1991) are touched upon here.

2.1 *Asymptotic Analysis of the Method of Lines Approach*

When the ODEs are obtained from a semi-discrete approximations of PDEs, the resulting system of ODEs contains additional system parameters and discretized parameters as opposed to physical problems governed by ODEs. Depending on the number of grid points "J" used, the dimensions of the resulting system of semi-discrete approximations of ODEs can be very large. Also, depending on the differencing scheme the resulting discretized counterparts of a PDE can be nonlinear in Δt , the grid spacing Δx and the numerical dissipation parameters, even though the DEs consist of only one parameter or none. One major consideration is that one might be able to choose a "safe" numerical method to solve the resulting system of ODEs to avoid spurious stable steady states due to time discretizations. However, spurious steady states and especially spatially varying steady states introduced by spatial discretizations in nonlinear hyperbolic and parabolic PDEs for CFD applications appear to be more difficult to avoid. In the case of the MOL approach, if spurious steady states due to spatial discretizations exist, the resulting ODE system has already inherited this spurious feature as part of the exact solutions of the semi-discrete case. We remark that spurious stable and unstable asymptotes other than the steady states due to time discretizations are also more difficult to avoid than spurious steady states. See Sections V and VI for some illustrations. Taking for example the nonlinear ODE models that are

considered, it is relatively easy to avoid spurious steady states due to time discretizations since, if a numerical steady state U^* for the ODE $dU/dt = S(U)$ is spurious, then $S(U^*) \neq 0$. This is not the case for spurious asymptotes such as limit cycles.

In addition to the aforementioned considerations, it is well known from the theory of nonlinear dynamics for ODEs that much of the established theory and known behavior of nonlinear dynamics are restricted to lower dimensional first-order ODEs (or for problems that exhibit lower dimensional dynamical behavior). Moreover, if higher than two-time level numerical methods are used, the dynamics of these discretized counterparts usually are richer in structure and more complicated to analyze than their two-time level cousins. Therefore, in order to gain a first hand understanding of the subject we restrict our study to 2×2 systems of first-order autonomous ODEs and two-time level numerical methods with a fixed time step, even though the current study is far removed from the realistic setting. Studies of 3×3 systems and general $J \times J$ systems are in progress.

Due to the complexity of the subject matter, this paper concerns fixed time step (and fixed grid spacing) time-marching methods only. The fixed or local variable time step control method study can also shed some light on identifying whether certain flow patterns are steady or unsteady. See Yee *et al.* (1990) for some examples. Proper regulation of a variable time step to prevent the occurrence of spurious steady-state numerical solutions will be a subject of future research. In order to isolate the different causes and cures of slow convergence and nonconvergence of time-marching methods, our study concerns nonlinearity and stiffness that are introduced by DEs containing smooth solutions. Nonlinearity and stiffness that are introduced by the scheme, the coupling effect in the presence of a source term (terms) in coupled system of PDEs, the highly stretched nonuniform structured and unstructured grids, the discontinuities in grid interfaces and/or the discontinuities inherent in the solutions, and external flows that need special boundary condition treatment with a truncated finite computation domain are added factors and require additional treatment or different analysis. These are not considered at the moment. Generalization of our study to include grid adaption as one of the sources of nonlinearity and/or stiffness introduced by the numerics is reported in Sweby and Yee (1964) and Budd *et al.* (1994).

2.2 *Inertial Manifold (IM) and Approximate Inertial Manifold (AIM)*

The concept of IMs was introduced by Foias *et al.* (1985). See Foias *et al.* (1985), Temam (1989) and Kwak (1991) for details of the subject. The key idea of IMs and AIMs is to establish theories to aid in better understanding of nonlinear phenomena and turbulence via the study of the interaction of short and long wavelengths of dissipative systems. Basically, an IM is a finite-dimensional submanifold that contains all the attractors and invariant sets of an infinite-dimensional dynamical system described by some dissipative PDEs. It establishes the criterion for the reduction of long-term dynamics of certain infinite-dimensional problems to a finite system of ODEs. An attractive feature is that the reduction introduces no error in the problem. That is, the IM contains all pertinent information about the long-term dynamics of the original system. One of the main objectives of AIMs is to handle cases where the IMs are not known to exist. AIMs also can help in finding good algorithms for dealing with

the IMs that are known to exist. AIMs may also help reduce finite but extremely large systems of ODEs to lower-dimensional problems. In a nut shell, the derivation of IMs and AIMs is based on the decomposition of the unknown function into large-scale and small scale components. In the case of fluid dynamics, those structures can be identified as large and small eddies. Thus an IM or AIM corresponds to an exact or approximate interaction law between the short and long wavelengths. Kwak (1991) showed that the long-term dynamics of some two-dimensional incompressible Navier-Stokes equations can be completely described by a finite system of ODEs. Kwak does so by finding a nonlinear change of variable that embeds the incompressible Navier-Stokes equations in a system of reaction-diffusion equations that possess an IM. All of the theories of IMs and AIMs are very involved and interested readers are encouraged to read Foias *et al.* (1985), Temam (1989) and Kwak (1991) and the references cited therein.

2.3 Relationship Between Shock Waves and Heteroclinic Orbits of Systems of ODEs

Another example of the importance of understanding the “dynamics” and the “dynamics of numerics” of systems of ODEs is related to the study of shocks using equilibrium bifurcation diagrams of associated vector fields. This was introduced by Shearer *et al.* (1987). The authors find of great interest how one can reduce the study of admissible shock wave solutions of a 2×2 hyperbolic conservation laws to the study of heteroclinic orbits of a system of nonlinear ODEs. Further development in this area can help in constructing suitable approximate Riemann solvers in numerical computations. Schechter and Shearer (1990) studied undercompressive shocks for nonstrictly hyperbolic conservation laws by adding information to the equilibrium bifurcation diagrams (introduced by Shearer *et al.*) about heteroclinic orbits of the vector fields. The augmented equilibrium bifurcation diagrams are then used in the construction of solutions of Riemann problems.

2.4 Dynamics of Numerics and Flow Visualizations of Numerical Data

The use of flow visualization of numerical data (numerical solutions of finite discretizations of e.g., fluid flow problems) in an attempt to understand the true flow physics has become increasingly popular in the last decade. See, Globus *et al.* (1991) and Hung *et al.* (1991) and references cited therein. Many of the techniques rely on the extraction of the boundary surfaces by analyzing a set of appropriate vector fields. Approximations are then performed based on this set of vector fields. The study of the topological features of certain flow physics based on the numerical data is then related to the study of fixed points of the associated systems of ODEs. Fluid problems with known flow physics can be used to reveal how well the associated vector fields of the numerical data can mimic the true physics. It can also help to delineate spurious flow patterns that are solely due to the numerics. At the present time we are entering into the regime where CFD is extensively used to aid the understanding of complicated flow physics that is not amenable to analysis otherwise. In the situation where the numerical data indicate flow structures which are not easily understood, a good understanding of the spurious dynamics that can be introduced by the numerics is needed.

3. PRELIMINARIES

Consider a 2×2 system of first-order autonomous nonlinear ODEs of the form

$$\frac{dU}{dt} = S(U), \quad (3.1)$$

where U and S are vector functions of dimension 2, and $S(U)$ is nonlinear in U . A fixed point U_E of an autonomous system (3.1) is a constant solution of (3.1); that is

$$S(U_E) = 0, \quad (3.2)$$

where the subscript “E” stands for “exact” and U_E denotes the fixed points of the ODE as opposed to the additional fixed points of the discretized counterparts (spurious fixed points) due to the numerical methods which we will encounter later.

Let the eigenvalues of $J(U_E) = (\partial S / \partial U)|_{U_E}$ (the Jacobian matrix of $S(U)$ evaluated at U_E) be λ_1 and λ_2 . Here $J(U_E)$ is assumed to be nonzero. The fixed point U_E is hyperbolic if $\text{Re}(\lambda_i) \neq 0$, $i = 1, 2$. If both λ_i are real, U_E is a saddle if $\lambda_1 \lambda_2 < 0$ and a node if $\lambda_1 \lambda_2 > 0$. If exactly one $\lambda_i = 0$, then U_E is semihyperbolic. If the eigenvalues are complex, then U_E is a spiral. The “tightness” of the spiral is governed by the magnitude of the imaginary part of the eigenvalues. If the eigenvalues both have a zero real part, then U_E is non-hyperbolic. Such a fixed point is called a center. Under this situation, more analysis is needed to uncover the real behavior of (3.1) around a non-hyperbolic fixed point. The fixed point U_E is stable if both λ_1 and λ_2 have negative real parts. U_E is unstable if a λ_i has a positive real part. In the non-hyperbolic case the fixed point is neutral.

If due to a variation of a parameter of the ODE a fixed point becomes unstable, then, if at the point of instability the eigenvalues are distinct and real, the resulting bifurcation will be to another fixed point. Such bifurcation is called a steady bifurcation. If, however, the eigenvalues are complex, then the bifurcation will be of a Hopf type. This is a slightly simplified classification, since our main concern in this work is not on the variation of the ODE parameter. Detailed background information can be found in (Guckenheimer and Holmes, 1983; Hale and Kocak, 1991).

Consider a nonlinear discrete map from a finite discretization of (3.1)

$$U^{n+1} = U^n + D(U^n, r), \quad (3.3)$$

where $r = \Delta t$ and $D(U^n, r)$ is linear or nonlinear in r depending on the numerical method. A fixed point U_D of (3.3) is defined by $U^{n+1} = U^n$, or

$$U_D = U_D + D(U_D, r) \quad (3.4)$$

or $D(U_D, r) = 0$. A fixed point U_D of period $p > 0$ of (3.3) is defined by $U^{n+p} = U^n$ with $U^{n+k} \neq U^n$ of $k < p$. In the context of discrete systems, the term “fixed point” without indicating the period means “fixed point of period 1” or the steady-state solution of (3.3). Here we use the term asymptote to mean a fixed point of any period, a limit cycle (in the discrete sense – invariant set), chaos, or a strange attractor.

The type of finite discretization of (3.1) represented in (3.3) assumed the use of two-time level schemes. Otherwise the vector dimension of (3.3) would be $2(k-1)$ instead of 2 where k is the number of the time level of the scheme. Here the vector function D is assumed to be consistent with the ODE (3.1) in the sense that fixed points of the ODE are fixed points of the scheme; however, the reverse need not hold. It is this feature accompanied by other added dynamics, that the discretized counterparts of the underlying ODE possess a much richer dynamical behavior than the original ODE. Thus the fixed points U_D of $D(U_D, r) = 0$ may be true fixed points U_E of (3.1) or spurious fixed points U_S . The spurious fixed points U_S are not roots of $S(U) = 0$. That is $S(U_S) \neq 0$. Spurious asymptotes are asymptotic numerical solutions of (3.3) but not (3.1).

Letting $U^n = U_D + \delta^n$, then a perturbation analysis on (3.3) yields

$$\delta^{n+1} = \left(I + \frac{\partial D(U_D, r)}{\partial U} \right)^{n+1} \delta^0. \quad (3.5)$$

Assuming $\partial D(U_D, r)/\partial U \neq 0$, then the fixed point U_D is stable if the eigenvalues of $J_D = I + \partial D(U_D, r)/\partial U$ lie inside the unit circle. If both eigenvalues are real and both lie inside (outside) the unit circle, then the fixed point is a stable (unstable) node. If one is inside the unit circle and the other outside, then the fixed point is a saddle. If both eigenvalues are complex, then the fixed point is a spiral. If the eigenvalues lie on the unit circle, then the fixed point of (3.3) is indeterminate and additional analysis is required to determine the true behavior of (3.3) around this type of fixed point. For a more refined definition and the difference in fixed point definition between ODEs and discrete maps, see Panov *et al.* (1956), Perron (1929) and Hsu (1987) and references cited therein. The reader is referred to Guckenheimer and Holmes (1983), Hale and Kocak (1991), Langford and Iooss (1980), and Werner (1980) for full details on the subject of bifurcation theory.

An important feature which can arise (for both systems of ODEs (3.1) and their discretizations) as the result of a Hopf bifurcation is a limit cycle where the trajectory traverses a closed curve in phase space. In all but a few simple cases such limit cycles are beyond analysis.

4. MODEL 2×2 SYSTEMS OF NONLINEAR FIRST-ORDER AUTONOMOUS ODEs

Four 2×2 systems of nonlinear first-order autonomous model ODEs are considered. The systems considered with $U^T = (u, v)$ or $z = u + iv$ are a

1. Dissipative complex model:

$$\frac{dz}{dt} = z(i + \varepsilon - |z|^2) \quad (4.1)$$

2. **Damped Pendulum** model:

$$\frac{du}{dt} = v \quad (4.2a)$$

$$\frac{dv}{dt} = -\varepsilon v - \sin(u) \quad (4.2b)$$

3. **Predator-Prey** model:

$$\frac{du}{dt} = -3u + 4u^2 - 0.5uv - u^3 \quad (4.3a)$$

$$\frac{dv}{dt} = -2.1v + uv \quad (4.3b)$$

4. **Perturbed Hamiltonian System** model:

$$\frac{du}{dt} = \varepsilon(1 - 3u) + \frac{3}{4}[1 - 2u + u^2 - 2v(1 - u)] \quad (4.4a)$$

$$\frac{dv}{dt} = \varepsilon(1 - 3v) - \frac{3}{4}[1 - 2v + v^2 - 2v(1 - v)] \quad (4.4b)$$

Here ε is the system parameter for (4.1), (4.2) and (4.4).

The perturbed Hamiltonian model can be related to the numerical solution of the viscous Burgers' equation with no source term

$$\frac{\partial u}{\partial t} + \frac{1}{2} \frac{\partial(u^2)}{\partial x} = \beta \frac{\partial^2 u}{\partial x^2} \quad \beta > 0. \quad (4.5)$$

Let $u_j(t)$ represent an approximation to $u(x_j, t)$ of (4.5) where $x_j = j\Delta x$, $j = 1, \dots, J$, with Δx the uniform grid spacing. Consider the three-point central difference in space with periodic condition $u_{J+j} = u_j$, and assume $\sum_{j=1}^J u_j = \text{constant}$, which implies that $\sum_{j=1}^J du_j/dt = 0$. If we take $J = 3$ and $\Delta x = 1/3$ then, with $\varepsilon = 9\beta$, this system can be reduced to a 2×2 system of first-order nonlinear autonomous ODEs (4.4) with $U^T = (u_1, u_2) = (u, v)$. In this case, the nonlinear convection term is contributing to the nonlinearity of the ODE system (4.4).

These four equations were selected to bring out the dynamics of numerics for four different types of solution behavior of the ODEs. The dissipative complex system (4.1) possesses either a unique stable fixed point or limit cycle with an unstable fixed point depending on the value of ε . This is the rare situation where the analytical expression of a limit cycle can be found. The purpose of choosing (4.1) is to illustrate the numerical accuracy of computing a limit cycle and the spurious dynamics associated with this type of asymptote. The damped pendulum (4.2), arising from modelling of a physical process, exhibits a periodic structure of an infinite number of fixed points. The predator-prey model (4.3), arising from modelling of biological process, exhibits multiple stable fixed points without a periodic pattern as model (4.2). The perturbed Hamiltonian model (4.4), which arises as a gross simplification of finite discretization of

the viscous Burgers' equation, exhibits an unique stable fixed point. Following the classification of fixed points of (3.1) in Section III, one can easily obtain the following:

Fixed Point of (4.1): The dissipative complex model has a unique fixed point at $(u, v) = (0, 0)$ for $\varepsilon \leq 0$. The fixed point is a stable spiral if $\varepsilon < 0$. It is a center if $\varepsilon = 0$. For $\varepsilon > 0$, the fixed point $(0, 0)$ becomes unstable with the birth of a stable limit cycle with radius equal to $\sqrt{\varepsilon}$ centered at $(0, 0)$. Figure 4.1 shows the phase portrait $(u-v)$ plane of system (4.1) for $\varepsilon = -1$ and $\varepsilon = 1$ respectively. Here the entire (u, v) plane belongs to the basins of attraction of the stable fixed point $(0, 0)$ if $\varepsilon < 0$. On the other hand, if $\varepsilon > 0$, the entire (u, v) plane except the unstable fixed point $(0, 0)$ belongs to the basin of attraction of the stable limit cycle centered at $(0, 0)$.

Fixed Points of (4.2): The damped pendulum (4.2) has an infinite number of fixed points, namely $(k\pi, 0)$ for integer k . If k is odd, the eigenvalues of the Jacobian $J(U_\varepsilon)$ are of opposite sign and these fixed points are saddles. If k is even, however, two cases must be considered, depending on the value of ε . If $\varepsilon < 2$ and positive, the eigenvalues are complex with negative real part and the fixed points are stable spirals. If $\varepsilon \geq 2$, the eigenvalues are real and negative and the fixed points are nodes. If $\varepsilon = 0$, the spirals become centers. Figure 4.2 shows the phase portrait and their corresponding basins of attraction for system (4.2). The different shades of grey regions represent the various basins of attraction of the respective stable fixed points for $\varepsilon = 0.5$ and $\varepsilon = 2.5$.

Fixed Points of (4.3): The fixed points of the predator-prey equation are less regular than those for the damped pendulum equation. System (4.3) has four fixed points $(0, 0)$, $(0, 1)$, $(3, 0)$ and $(2.1, 1.98)$. By looking at the eigenvalues of the Jacobian of S , one finds that $(0, 0)$ is a stable node, $(2.1, 1.98)$ is a stable spiral, and $(1, 0)$ and $(3, 0)$ are saddles. Figure 4.3 shows the phase portrait and their corresponding basins of attraction for system (4.3). The different shades of grey regions represent the various basins of attraction of the respective stable fixed points. The white region represents the basin of

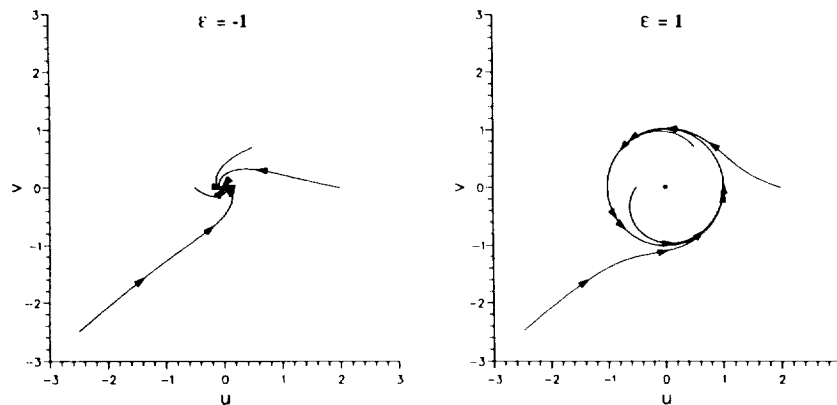


Figure 4.1 Phase Portraits and basins of Attraction Dissipative Complex Equation.

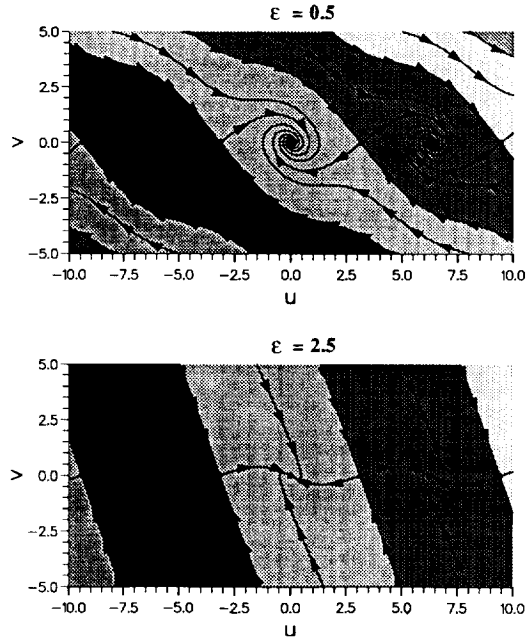


Figure 4.2 Phase Portraits and Basins of Attraction Damped Pendulum Equation.

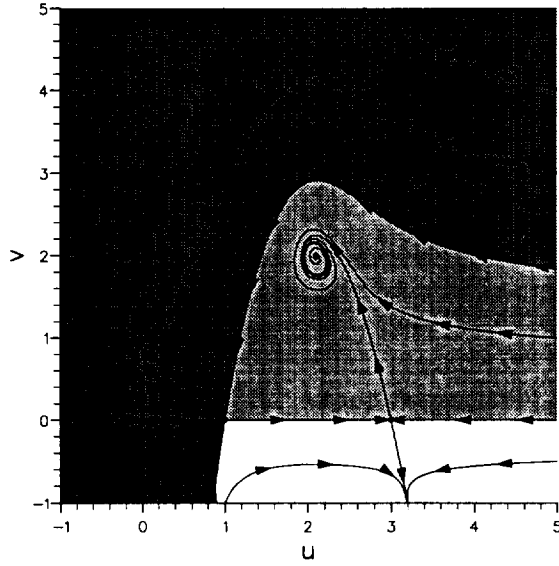


Figure 4.3 Phase Portraits and Basins of Attraction Predator-Prey Equation.

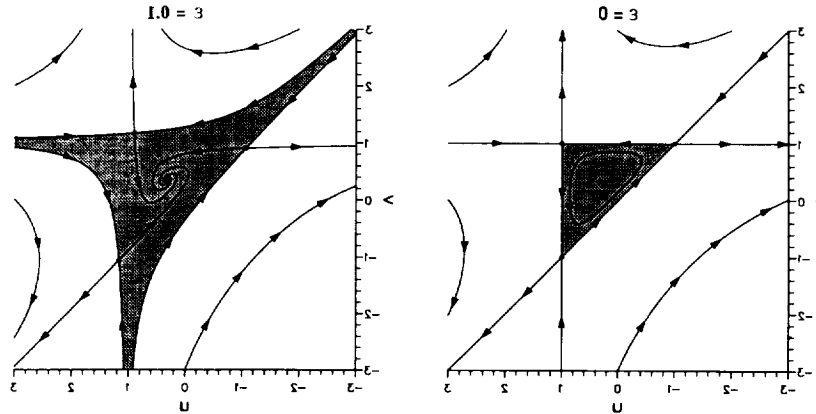


Figure 4.4 Phase Portraits and Basins of Attraction Viscous Burger's Equation (Central Difference in Space).

divergent solutions. Note that the trajectories near the unstable separatrices actually do not merge with the unstable branch of separatrices, but only appear to merge due to the thick drawings of the solution trajectories.

Fixed Points of (4.4): The perturbed Hamiltonian has four steady-state solutions of which three are saddles and one is a stable spiral at $(1/3, 1/3)$ for $\varepsilon \neq 0$. For $\varepsilon = 0$ the stable spiral becomes a center. Figure 4.4 shows the phase portrait and their corresponding basins of attraction for system (4.4). The shaded region represents the basins of attraction for the fixed point $(1/3, 1/3)$ for $\varepsilon = 0$ and $\varepsilon = 0.01$. The white region represents the basin of divergent solutions. From here on we refer to (4.4) also as a viscous Burgers' equation with central difference in space.

5. NUMERICAL METHODS AND BIFURCATION DIAGRAMS

This section describes the 11 time discretizations and their corresponding bifurcation diagrams for the four model ODEs (4.1)–(4.4). The 11 numerical methods are listed in Section 5.1. Section 5.2 discusses the stability of selected fixed points of the discretized counterparts of the model ODEs as functions of system parameters. Section 5.3 discusses the bifurcation diagrams as a function of the discretized parameter Δt with the system parameter held fixed.

5.1 Numerical Methods

The 9 explicit and two implicit methods considered are the explicit Euler, two second-order Runge-Kutta, namely, the modified Euler (R-K 2) and the improved Euler (R-K 2), two third-order Runge-Kutta (R-K 3), a fourth-order Runge-Kutta (R-K 4), the two and three-step predictor-corrector (Lambert, 1973), and noniterative linearized forms of the implicit Euler and the trapezoidal methods.

(1) **Explicit Euler (1st-order; R-K 1):**

$$U^{n+1} = U^n + rS^n; \quad S^n = S(U^n), \quad (5.1)$$

(2) **Modified Euler (R-K 2):**

$$U^{n+1} = U^n + rS\left(U^n + \frac{r}{2}S^n\right), \quad (5.2)$$

(3) **Improved Euler (R-K 2):**

$$U^{n+1} = U^n + \frac{r}{2}[S^n + S(U + rS^n)], \quad (5.3)$$

(4) **Heun (R-K 3):**

$$U^{n+1} = U^n + \frac{r}{4}(k_1 + 3k_3) \quad (5.4)$$

$$k_2 = S^n$$

$$k_2 = S\left(U^n + \frac{r}{3}k_1\right)$$

$$k_3 = S\left(U^n + \frac{2r}{3}k_2\right),$$

(5) **Kutta (R-K 3):**

$$U^{n+1} = U^n + \frac{r}{6}(k_1 + 4k_2 + k_3) \quad (5.5)$$

$$k_1 = S^n$$

$$k_2 = S\left(U^n + \frac{r}{2}k_1\right)$$

$$k_3 = S(U^n - rk_1 + 2rk_2),$$

(6) **R-K 4:**

$$U^{n+1} = U^n + \frac{r}{6}(k_1 + 2k_2 + 2k_3 + k_4) \quad (5.6)$$

$$k_1 = S^n$$

$$k_2 = S\left(U^n + \frac{r}{2}k_1\right)$$

$$k_3 = S\left(U^n + \frac{r}{2}k_2\right)$$

$$k_4 = S(U^n + rk_3),$$

(7, 8) **Predictor-corrector for m = 2, 3 (PC2, PC3):**

$$U^{(0)} = U^n + rS^n$$

$$U^{(k+1)} = U^n + \frac{r}{2}[S^n + S^{(k)}], \quad k = 0, 1, \dots, m-1$$

$$U^{n+1} = U^n + \frac{r}{2}[S^n + S^{(m-1)}], \quad (5.7)$$

(9) **Adam-Bashforth (2nd-order):**

$$U^{n+1} = U^n + \frac{r}{2}[3S(U^n) - S(U^{n-1})], \quad (5.8)$$

(10) **Linearized Implicit Euler:**

$$U^{n+1} = U^n + r(I - rJ^n)^{-1}S^n \quad (5.9)$$

$$J^n = \left(\frac{\partial S}{\partial U}\right)^n \quad \text{and} \quad \det(I - rJ^n) \neq 0,$$

(11) **Linearized Trapezoidal:**

$$U^{n+1} = U^n + r\left(I - \frac{r}{2}J^n\right)^{-1}S^n \quad (5.10)$$

$$J^n = \left(\frac{\partial S}{\partial U}\right)^n \quad \text{and} \quad \det\left(I - \frac{r}{2}J^n\right) \neq 0,$$

where the numeric identifier after the “**R-K**” indicates the order of accuracy of the scheme and $r = \Delta t$ and $\det(\)$ means the determinant of the quantity inside the (). Schemes (10) and (11) are unconditionally stable methods. See Beam and Warming (1976) and Yee (1989) for the versatility of the linearized implicit Euler and linearized trapezoidal methods in CFD applications. A comparison between Newton method in solving the steady part of the ODEs and the linearized implicit method (5.9) for model (4.4) is included in Section 6.5. Studies on Newton method in solving the steady state part of the PDE and some iteration procedures in solving the nonlinear algebraic

equation resulting from four implicit LMMs are reported in a separate paper (Yee and Sweby 1933a). Although the explicit Euler can be considered as an R-K 1, it is also a LMM. All of the R-K methods (higher than first order) and the predictor-corrector methods are nonlinear in the parameter space r , and all LMMs are linear in r . As discussed in Yee *et al.* (1991), a necessary condition for a scheme to produce spurious fixed points of period one is the introduction of nonlinearity in the parameter space r . It can be shown later that this property plays a major role on the shapes and sizes of the associated numerical basins of attraction of the scheme. For simplicity in referencing, hereafter we use “implicit Euler” and “trapezoidal” to mean the linearized forms (5.9) and (5.10), respectively, unless otherwise stated.

5.2 Stability of Fixed Points of Numerical Methods as a Function of System Parameters

In our later study, we assume a fixed system parameter so that only the discretized parameter comes into play. However, in order to get a feel for the numerical stability of these schemes around selected stable fixed points U_E as a function of the system parameter ε , Figures 5.1–5.3 show the stability regions of the schemes as a function of the

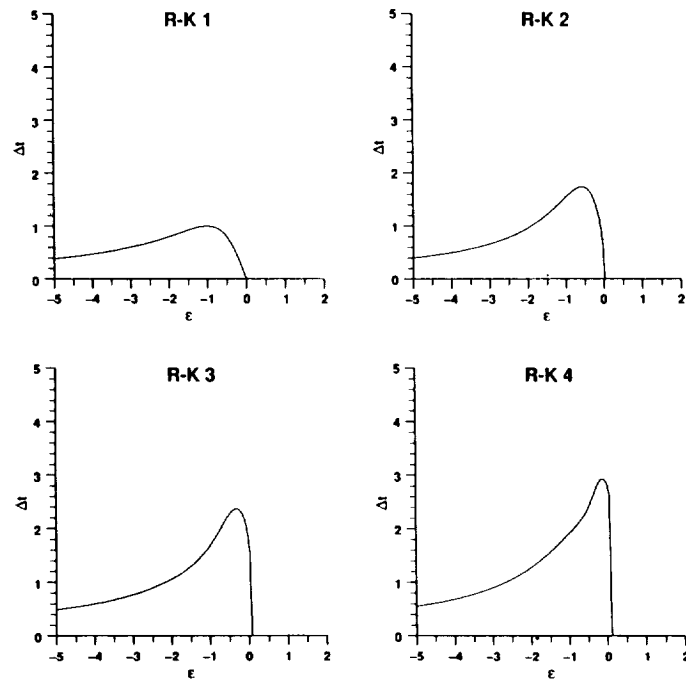


Figure 5.1 Stability Regions vs. System Parameters Dissipative Complex Equation.

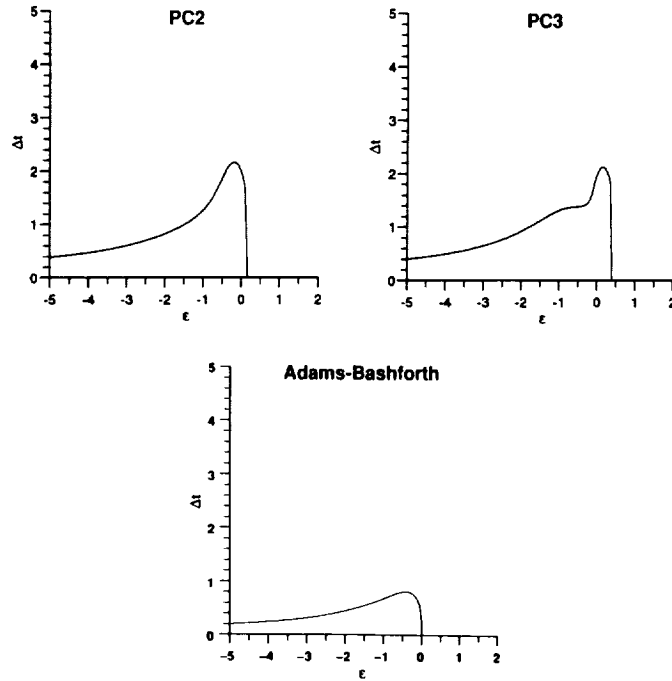


Figure 5.1 (Continued)

system parameter ε around a selected fixed point for each of the models. The linearized stability regions for the R-K methods of the same order behave in exactly the same manner, and the linearized stability regions around stable U_E of the linearized implicit methods are not interesting, since they have the same regions of stability as the ODEs.

The stability diagrams presented were obtained by numerically solving the absolute stability polynomials for the various methods, in most cases using Newton iteration. For the Runge-Kutta schemes (of order $p \leq 4$) the stability (Griffiths *et al.*, 1992; Lambert, 1973) condition is that

$$\left| 1 + \lambda r + \cdots + \frac{\lambda^p r^p}{p!} \right| < 1, \quad (5.11)$$

where λ are the eigenvalues of the Jacobian of $S(U)$. For the Predictor-Corrector of steps $p = 2, 3$ the stability condition is that

$$\left| 1 + \lambda r + \cdots + \frac{\lambda^p r^p}{2^p} \right| < 1, \quad (5.11)$$

and for the Adams-Bashforth method the roots μ of

$$\mu^2 - \left(1 + \frac{3\lambda r}{2}\right)\mu + \frac{\mu}{2} = 0 \tag{5.13}$$

satisfy $|\mu| < 1$. Note that all of these expressions only hold for the U_E fixed points of the system.

In all cases the boundary of the stability region is when unit modulus is attained. The linearized implicit Euler and trapezoidal methods are unconditionally stable for the stable exact fixed points U_E of the ODE systems we are considering.

These stability regions can be used to isolate the key regions of the ε parameter to be considered for the study of dynamics of numerics later. Due to the enormous number of possibilities, detailed study can only concentrate on one to two representative system parameters. Even with such a restriction, as can be seen later, computing the corresponding bifurcation diagrams and basins of attraction is very CPU intensive. Fortunately the computation can be made highly parallel. Figures 5.1–5.3 also can serve as a spot check on the numerical results presented in the next section.

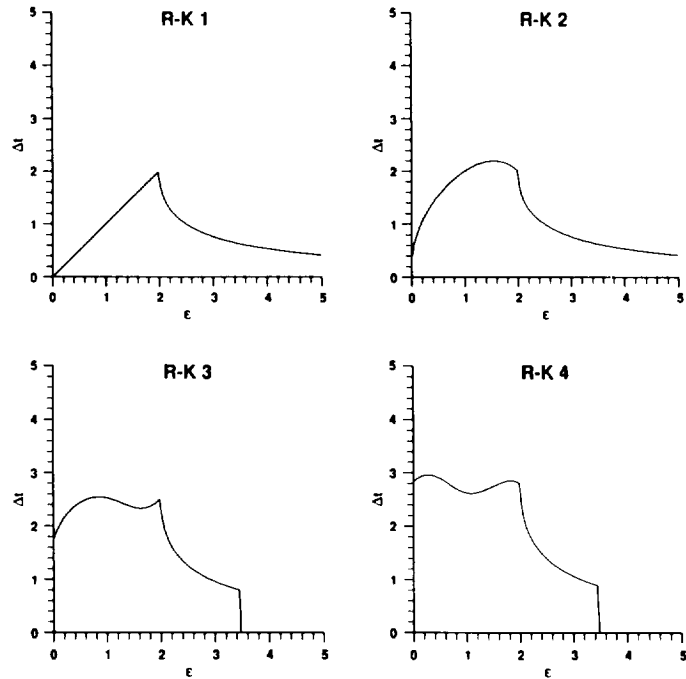


Figure 5.2 Stability Regions vs. System Parameters Damped Pendulum Equation.

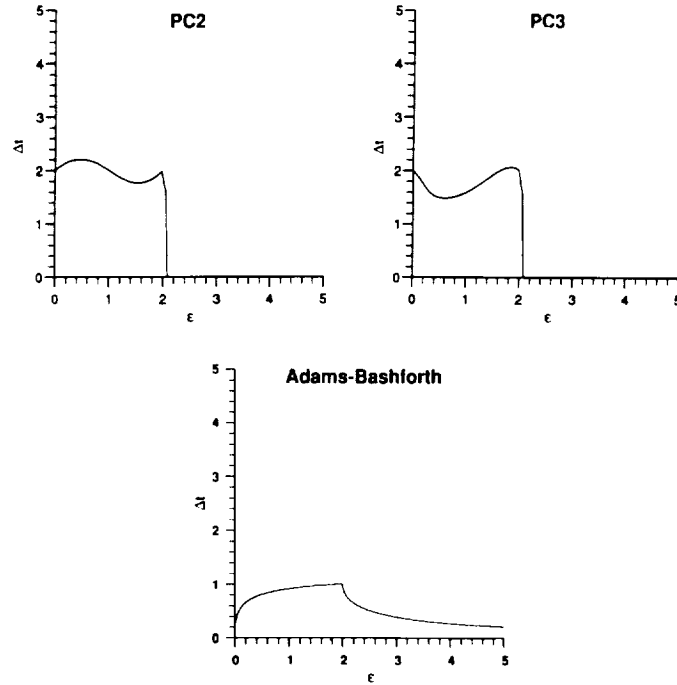


Figure 5.2 (Continued)

5.3 Bifurcation Diagrams

In this section, we show the bifurcation diagrams of selected R-K methods. It illustrates some of the many ways in which the dynamics of a numerical discretization of 2×2 first-order autonomous nonlinear system of ODEs can differ from the system itself. Note that there is no limit cycle or higher dimensional tori counterpart for the scalar first-order autonomous ODEs. Spurious limit cycles and higher dimensional tori can only be introduced by the numerics when solving nonlinear ODEs other than scalar first-order autonomous ODEs (if 2-time level schemes are used) and/or by using a scheme with higher than two-time level for the scalar first-order autonomous ODEs. In Section VI, we showed how numerical basins of attraction can complement the bifurcation diagrams in gaining more detailed global asymptotic behavior of numerical schemes. We purposely present our results in this order (not showing the basins of attraction) in order to bring out the importance of basins of attraction for the time-dependent approach in obtaining steady-state numerical solutions.

Even though the analytical solutions of these models are known, depending on the scheme, the dynamics of their discretized counterparts might be very difficult to analyze. In particular, some analytical linearized analysis (without numerical computations) of fixed points of periods one and two is possible for the predator-prey and the damped pendulum case. However, analytical analysis for the dissipative complex

model and the perturbed Hamiltonian is not practical. For a detailed analysis of these selected cases, readers are referred to Sweby and Yee (1991). *For the majority of the cases where rigorous analysis is impractical we study the dynamics of numerics using numerical experiments.*

Note that some global solution behavior of fixed points of the nonlinear discretized equations (5.1)–(5.10) for (4.1)–(4.4) can be obtained by the pseudo arclength continuation method devised by Keller (1977), a standard numerical method for obtaining bifurcation curves in bifurcation analysis. A major shortcoming of the pseudo arclength continuation method is that for problems with complicated bifurcation patterns, it cannot provide the complete bifurcation diagram without known start up solutions for each of the main bifurcation branches before one can continue the solution along a specific main branch. *For spurious asymptotes it is usually not easy to locate even just one solution on each of these branches.*

The nature of our calculations requires thousands of iterations of the same equation with different ranges of initial data on a preselected (u, v) domain and range of the discretized parameter space Δt . Since the NASA Ames CM-2 allows vast numbers (typically 65,536) of calculations to be performed in parallel, our problem is perfect for computation on the CM-2.

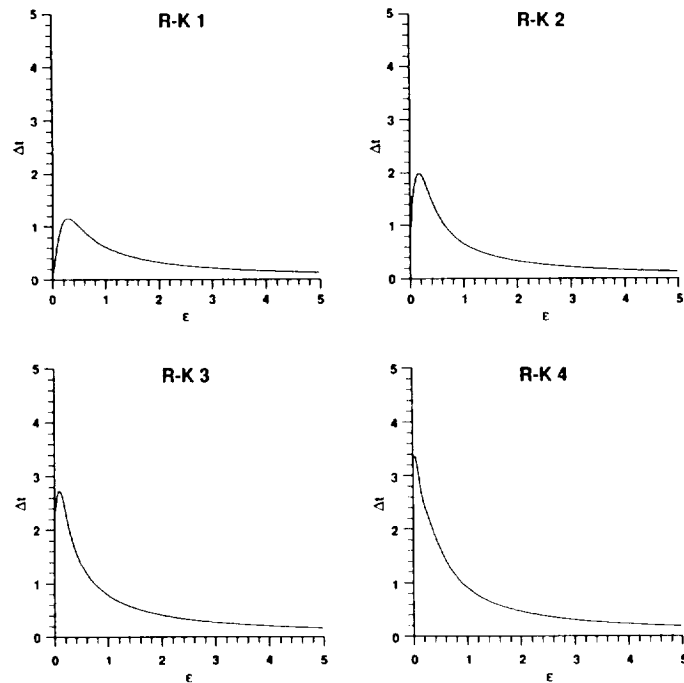


Figure 5.3 Stability Regions vs. System Parameters Viscous Burgers' Equation (Central Difference in Space).

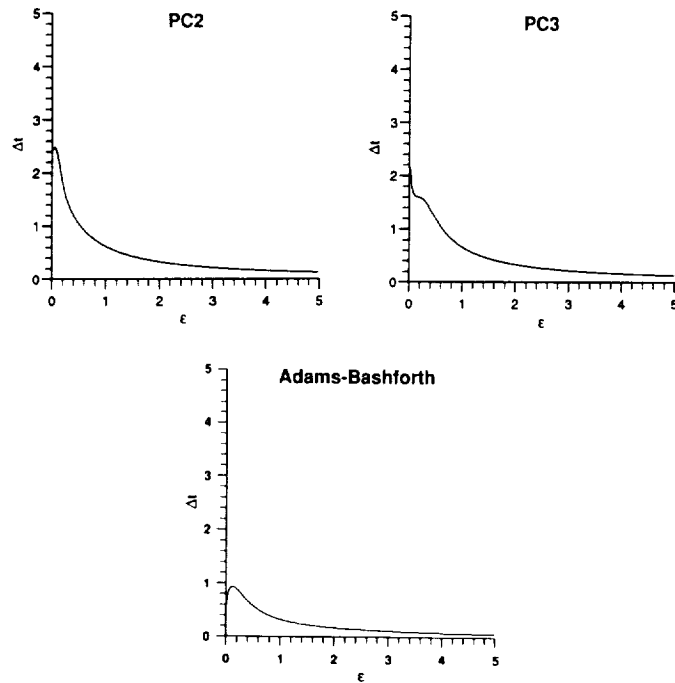


Figure 5.3 (Continued)

To obtain a “full” bifurcation diagram, the domain of initial data and the range of the Δt parameter are typically divided into 512 equal increments. For each initial datum and Δt , the discretized equations are preiterated 3,000–5,000 (more or less depending on the ODE and scheme) before the next 4,000–6,000 iterations are plotted. The preiterations are necessary in order for the trajectories to settle to their asymptotic value. The high number of iterations plotted (overlay on the same plot) is to detect periodic orbits or invariant sets. Since the results are a three dimensional graph $((\Delta t, u, v))$, we have taken slices in a given constant v - and u -plane in order to enhance viewing the decrease CPU computations. Note that with this method of computing the bifurcation diagrams, only the stable branches are plotted. Some of the bifurcation diagrams in a $v = \text{constant}$ plane for the four model ODEs and for the modified Euler, improved Euler, Kutta and R-K 4 methods are shown in Figures 5.4–5.8. Figure 5.4 shows a typical example of spurious stable fixed points (branches 3 and 4 on the diagram) occurring below the linearized stability by the modified Euler method. It also shows the existence of spurious asymptotes such as limit cycles, higher order periodic solutions and possibly numerical chaos (chaos introduced by numerics). See later sections and subsections for further details. Selected bifurcation diagrams for the rest of the numerical methods are illustrated in Section IV with basins of attraction superimposed (see Figures 6.3–6.5, 6.13, 6.14, and 6.19–6.20). See also the original NASA internal report RNR-92-008, March 1992 for additional illustrations. Due to the

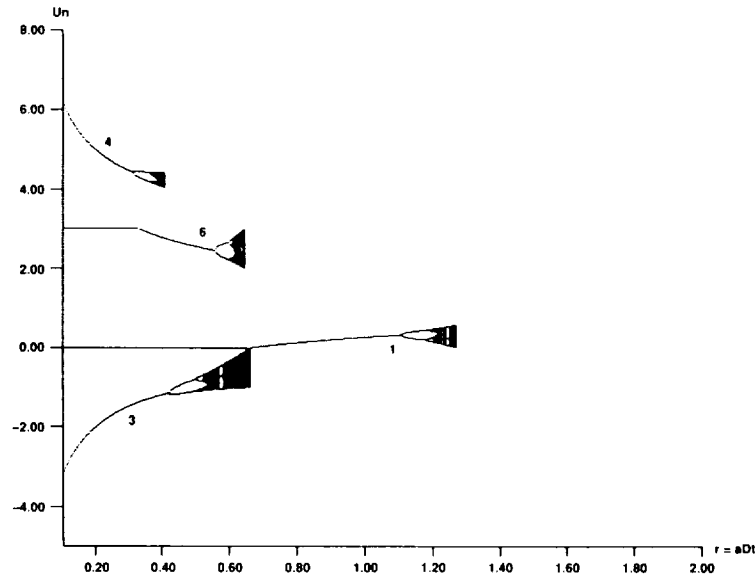


Figure 5.4 Bifurcation Diagram Predator-Prey Equation Modified Euler.

plotting package, the labels (u_n, v_n) on all of the figures are (u^n, v^n) . In the plots, $r = \Delta t$ unless stated.

The term “full bifurcation” as defined in Yee *et al.* (1991) is used to mean bifurcation diagrams that cover the essential lower-order periods in such a way as to closely resolve the “true” bifurcation diagram of the underlying discrete map for a selected range of initial data domains. This is necessary since solutions with different initial conditions will converge to different asymptotic limits. All of the computations shown are “full” bifurcation diagrams.

The following summarizes the spurious dynamical behavior of the 11 numerical methods based on selected domains of initial data and ranges of the discretized parameter r . Numerical results agree with the analytical linearized analysis reported in Sweby and Yee (1991).

Bifurcation Diagrams of Numerical Methods for Model (4.1): For $\varepsilon = 0$, (4.1) is nondissipative (or a Hamiltonian system), and all of the 11 numerical methods which are non-symplectic converge quite slowly to the fixed point $(0, 0)$. We conjecture that symplectic schemes (Sanz-Serna, 1990) would be more appropriate for $\varepsilon = 0$. For sufficiently small negative (positive) ε , all of the studied schemes converge extremely slowly to the stable spiral (limit cycle). This is a typical example of slow convergence of the numerical solution due to the stiffness of the system parameter. While the bifurcation diagrams for $\varepsilon \leq 0$ for the various numerical methods are not too interesting, the bifurcation diagrams for $\varepsilon > 0$ are very instructive. Figure 5.5 shows the bifurcation diagrams for the four R-K methods for $\varepsilon = 1$.

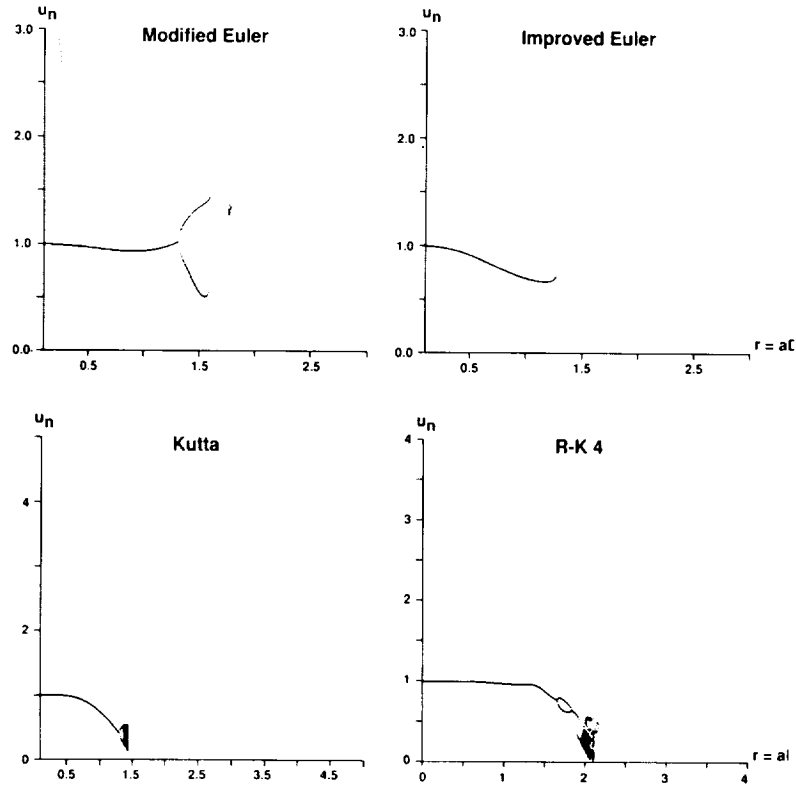


Figure 5.5 Bifurcation Diagrams Dissipative Complex Equation, $\varepsilon = 1$, $\nu = 0.0$.

Note also that R-K 4 method gives the most overall accurate numerical approximations of the true limit cycle with radius $\sqrt{\varepsilon}$ centered at $(0, 0)$. The Adam-Bashforth, PC2, PC3, implicit Euler and trapezoidal methods give the least accurate numerical approximation of the limit cycle for r closer to the linearized stability. The R-K 4 and Heun methods produced spurious higher-order limit cycles (invariant set of multiple circles on the diagrams). See Section IV and Figures 6.6 and 6.8 for more details. These diagrams illustrate the unreliability of trying to compute a true limit cycle with any sizable r . This should not be surprising since the scheme only gives an $O(r^p)$ approximation to the solution trajectories. In addition, since the limit cycle is not a fixed point, we would expect inaccuracies to be introduced. However, inaccuracies are not easy to detect in practice, especially when a numerical solution produces the qualitative features expected. See Section VI and Figures 6.3–6.9 for additional details. All of the studied explicit methods produce spurious asymptotes.

For $\varepsilon > 0$, the trapezoidal method produces no spurious steady states. However, the implicit Euler method in addition to maintaining an unconditionally stable feature of the exact limit cycle, also turns the unstable fixed point $U_E = (0, 0)$ of the ODE (4.1) into a stable fixed point for $r \geq 1$. See Figures 6.5, 6.8 and 6.9 for additional details.

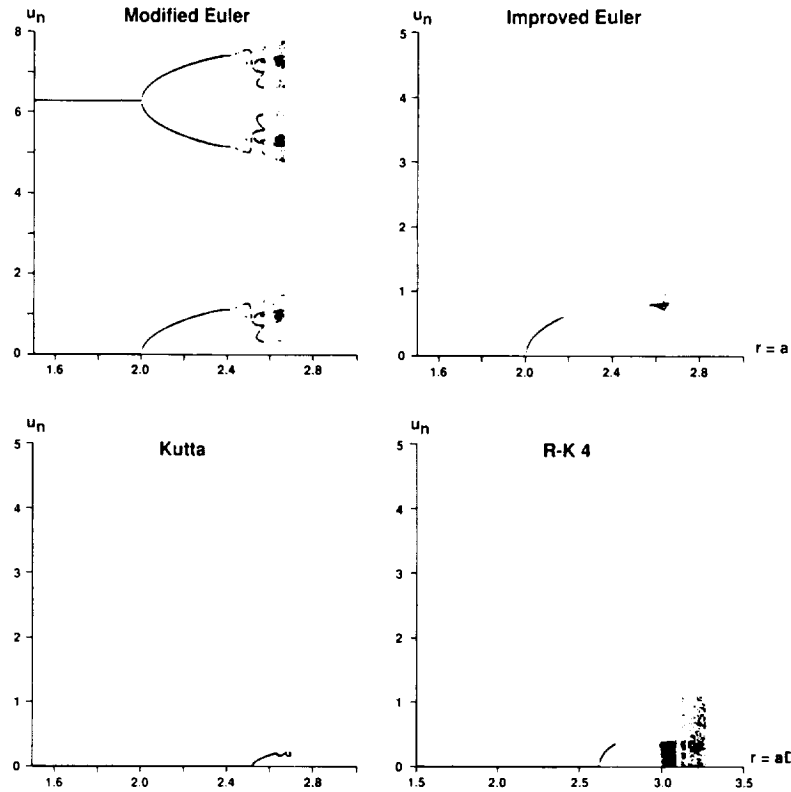


Figure 5.6 Bifurcation Diagrams Damped Pendulum Equation, $\varepsilon = 1$, $\nu = 0.0$.

Bifurcation Diagrams of Numerical Methods for Model (4.2): All of the studied explicit and implicit methods produce spurious asymptotes. In particular, some of the explicit methods (even explicit Euler) produce spurious limit cycles for certain ε values. For certain ranges of r and ε values the implicit Euler and trapezoidal methods turn the saddle points of (4.2) into an unstable fixed point of different type (see Figure 6.12). For the modified Euler method, spurious steady states occur below the linearized stability limit of the scheme. See Section VI and Figures 6.10–6.12 for additional details.

Bifurcation Diagrams of Numerical Methods for Model (4.3): Again, all of the studied explicit and implicit methods generate spurious asymptotes. Also, some of the explicit methods produce spurious limit cycles. For certain ranges of the r , the trapezoidal method turns the saddle points (exact fixed points of (4.3)) into unstable fixed points of different types, and the implicit Euler method turns the saddle points into stable fixed points of different type. The numerical results coincide with analytical analysis by examining the eigenvalues of the Jacobian of the resulting discrete map. Transcritical bifurcations introduced by the R-K 4 method resulted in the production of spurious steady state below (and very near) the linearized stability limit of the scheme. See, Section VI and Figures 6.13–6.18 for additional details.

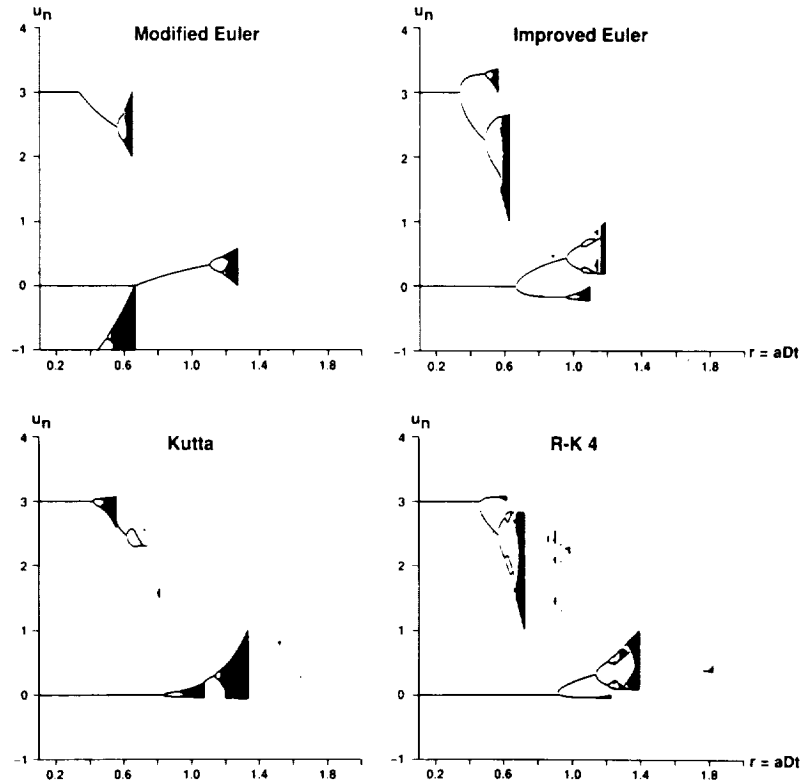


Figure 5.7 Bifurcation Diagrams Predator-Prey Equation, $v = 0.0$.

More than one spurious fixed point below the linearized stability of the scheme was introduced by the modified Euler method (see Fig. 5.4). From the form of the modified Euler scheme it is easily seen that as well as the exact fixed points U_E of the ODEs, any other value U_S satisfying

$$U_S + \frac{r}{2} S(U_S) = U_E \quad (5.14)$$

will also be a fixed point of the scheme. As mentioned earlier, we refer to these additional fixed points as spurious fixed points. Note that the U_E on the right-hand side of (5.14) encompasses both stable and unstable fixed points of the ODE and so, for the predator-prey equations (since S contains cubic terms in U), there are up to twelve (real) spurious steady states, three for each exact fixed point U_E . In fact there are six such spurious steady states which lie in the $v = 0$ plane. All of them occur below the linearized stability limits of the exact fixed points, although not all are stable there. Four (stable ones) of the six are shown in the bifurcation diagram of Figure 5.4, numbered 1, 3, 4, 6 of the bifurcation branch. The other two are unstable. Note also that the branch numbered 6 is in fact not stable but represents the stable eigen-direction (separatrix) in the $v = 0$ plane of a saddle point.

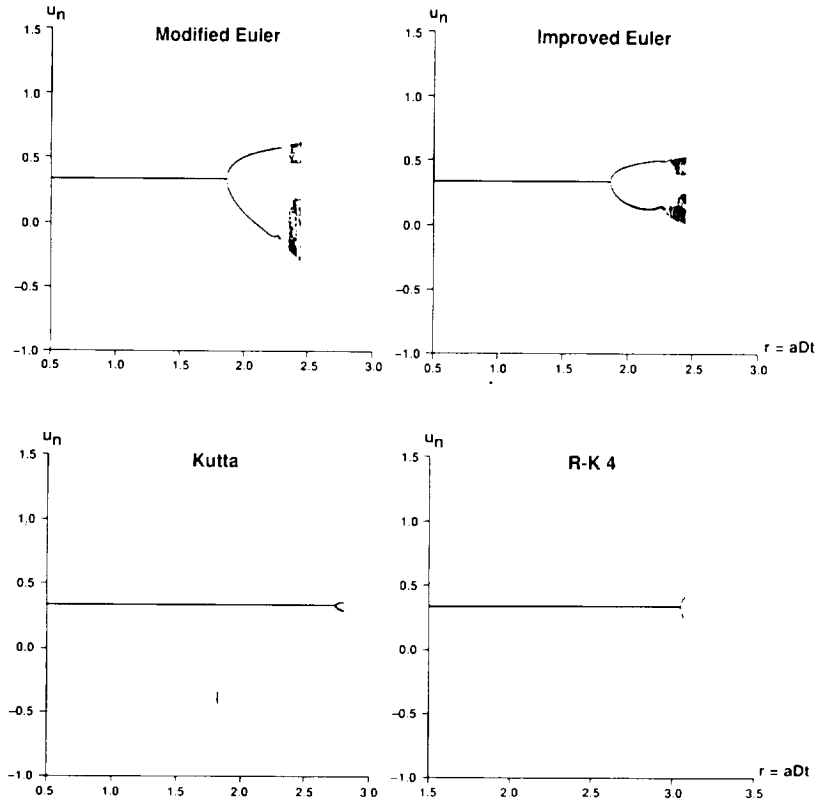


Figure 5.8 Bifurcation Diagrams Viscous Burgers' Equation, $\varepsilon = 0.1$, $\nu = 0.333$ (Central Difference in Space).

Bifurcation Diagrams of Numerical Methods for Model (4.4): For $\varepsilon = 0$, the ODE (4.4) is nondissipative and thus for small r , slow convergence was experienced. For r beyond the linearized limit and with $\varepsilon = 0$ all of the explicit methods produce spurious limit cycles. For $\varepsilon > 0$ (and not too large) all of the studied 11 explicit and implicit methods produce spurious asymptotes. Also, all of the explicit methods produce spurious limit cycles. For $\varepsilon = 0.1$, the Kutta and Heun methods introduce spurious asymptotes (higher than period one) that are below the linearized stability limit of the scheme. See Figures 6.19–6.25 for additional details.

6. BASINS OF ATTRACTION AND BIFURCATION DIAGRAM

This section illustrates how basins of attraction can complement the bifurcation diagrams in gaining more detailed global asymptotic behavior of time discretizations

for nonlinear DEs. Two different representations of the numerical basins of attraction were computed on the NASA Ames CM-2. One representation is bifurcation diagrams as a function of Δt with numerical basins of attraction superimposed on a constant v - or u -plane. The other representation is the numerical basins of attraction with stable asymptotes superimposed on the phase plane (u, v) . Before discussing numerical results for each of the model ODEs, the next subsection gives some preliminaries on how to compute and on how to interpret the basins of attraction diagrams for the CM-2.

6.1 Introduction

To obtain a bifurcation diagram with numerical basins of attraction superimposed on the CM-2, the preselected domain of initial data on a constant v - or u -plane and the preselected range of the Δt parameter are divided into 512 equal increments. Again, for the bifurcation part of the computations, with each initial datum and Δt , the discretized equations are preiterated 3,000–5,000 steps before the next 5,000 iterations (more or less depending on the problem and scheme) are plotted. The bifurcation curves appear on the figures as white curve, white dot and white dense dots. While computing the bifurcation diagrams it is possible to overlay basins of attraction for each value of Δt used. For the numerical basins of attraction part of the computation with each value of Δt used, we keep track of where each initial datum asymptotically approaches and color code them (appearing as a vertical strip) according to the individual asymptotes. While efforts were made to match color coding of adjacent strips on the bifurcation diagram, it was not always practical or possible. Care must therefore be taken when interpreting these overlays.

For the basins of attraction on the phase plane (u, v) with selected values of Δt and the stable asymptotes superimposed, the (u, v) domain is divided into 512×512 points of initial datum. With each initial datum and the selected Δt , we preiterate the respective discretized equation 3,000–5,000 steps and plot the next 5,000 steps to produce the asymptotes. Again, for the basins of attraction part of the computations, for each value of Δt used, we keep track of where each initial datum asymptotically approaches and color code them according to the individual asymptotes. All of the selected time steps Δt shown are based on the bifurcation diagram with the basins of attraction superimposed. The chosen time steps were selected to illustrate special features of the different bifurcation phenomena on the (u, v) plane. Details of the techniques used for detection of asymptotes and basins of attraction are given in the appendix of Sweby and Yee (1991). Note that in all of the plots, if color printing is not available, the different shades of grey represent different colors.

As a preliminary, and before discussing our major results, we discuss the numerical basins of attraction associated with modified Euler, improved Euler, Kutta and R-K 4 methods for the two scalar first-order autonomous nonlinear ODEs studied in part I of our companion paper (Yee *et al.*, 1991). The two scalar ODEs are:

$$\frac{du}{dt} = au(1 - u) \quad (6.1)$$

and

$$\frac{du}{dt} = au(1-u)(0.5-u). \quad (6.2)$$

The fixed points for (6.1) with $a > 0$ are $u = 0$ (unstable) and $u = 1$ (stable), and no additional higher order periodic fixed points or asymptotes exist. The basin of attraction for the stable fixed point $u = 1$ is the entire positive plane for all values of $a > 0$.

The fixed points for (6.2) with $a > 0$ are $u = 0$ (unstable), $u = 1$ (unstable) and $u = 0.5$ (stable) and no additional higher-order periodic solutions or asymptotes exist. The basin of attraction for the stable fixed point $u = 0.5$ is $0 < u < 1$ for all $a > 0$. The white curve, white dots and white dense dots of Figures 6.1 and 6.2 show the bifurcation diagrams for four of the R-K methods for (6.1) and (6.2). For more details of the dynamics of numerics for systems (6.1) and (6.2), see Yee *et al.* (1991). Intuitively, in the presence of spurious asymptotes the basins of the true stable steady states can be separated by the numerical basins of attraction of the stable and unstable spurious asymptotes.

Take, for example, the ODE (6.1) where the entire domain u is divided into two basins of attraction for the ODE independent of any real a . Now if one numerically integrates the ODE, depending on the scheme and r , extra stable and unstable fixed points of any order can be introduced by the scheme. The bifurcation part of Figures 6.1 and 6.2, cannot distinguish the types of bifurcation and the periodicity of the spurious fixed points of any order. With the numerical basins of attraction and their respective bifurcation diagrams superimposed on the same plot, the type of bifurcation and to which initial data asymptote to which stable asymptotes become apparent. Note that for Figures 6.1 and 6.2 $r = a\Delta t$.

For example, any initial data residing in the green region in Figure 6.1 for the modified Euler method belong to the numerical basin of attraction of the spurious (stable) branch emanating from $u = 3$ and $r = 1$. Thus, if the initial data is inside the green region, the solution can never converge to the exact steady state using even a small fixed but finite Δt (all below the linearized stability limit of the scheme). Note that the green region extends upward as r decreases below 1. Thus for certain ranges of r values, the domain is divided into four basins (instead of two for the ODE). But of course higher period spurious fixed points exist for other ranges of r and more basins are created within the same u domain.

A similar situation exists for the R-K 4 method (Fig. 6.1), except now the numerical basins of attraction of the spurious fixed points occur very near the linearized stability limit of the scheme, with a small portion occurring below the linearized stability limit. In contrast to the improved Euler method (Fig. 6.1), the green region represents the numerical basins of one of the spurious stable transcritical bifurcation branches of the fixed point. The bifurcation curve directly below it with the corresponding red portion is the basin of the other spurious branch. See Yee *et al.* (1991) or Hale and Kocak (1991) for a discussion of the different types of bifurcations. With this way of color coding the basins of attraction, one can readily see (from the plots) that for ODE (6.1), the modified Euler, improved Euler and R-K 4 methods, experience one steady bifurcation before a period doubling bifurcation occurs (Fig. (6.1)). Using the PC3 method to solve (6.1) (figure not shown; see Yee *et al.*, 1991), more than one consecutive steady bifurcation occurs before period doubling bifurcation. For ODE (6.2), the improved Euler experi-

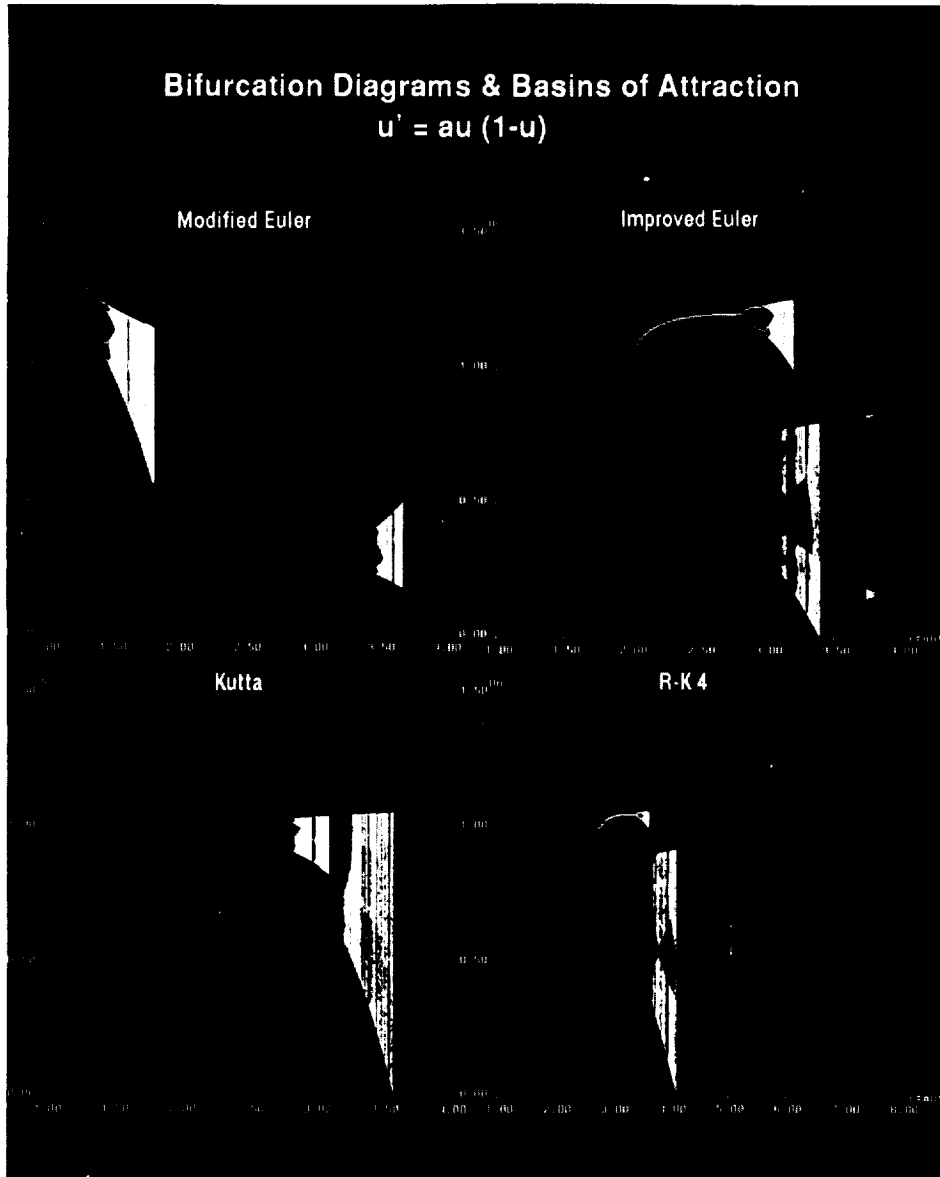


Figure 6.1 (See Color Plate I at the back of this issue.)

ences two consecutive steady bifurcations before a period doubling bifurcation occurs (Fig. (6.2)). Using the PC3 method to solve (6.2) (figure not shown; see Yee *et al.* 1991), four consecutive steady bifurcations occur before period doubling bifurcations. The modified Euler and R-K 4 methods, however, experience only one steady bifurcation before period doubling bifurcations occur.

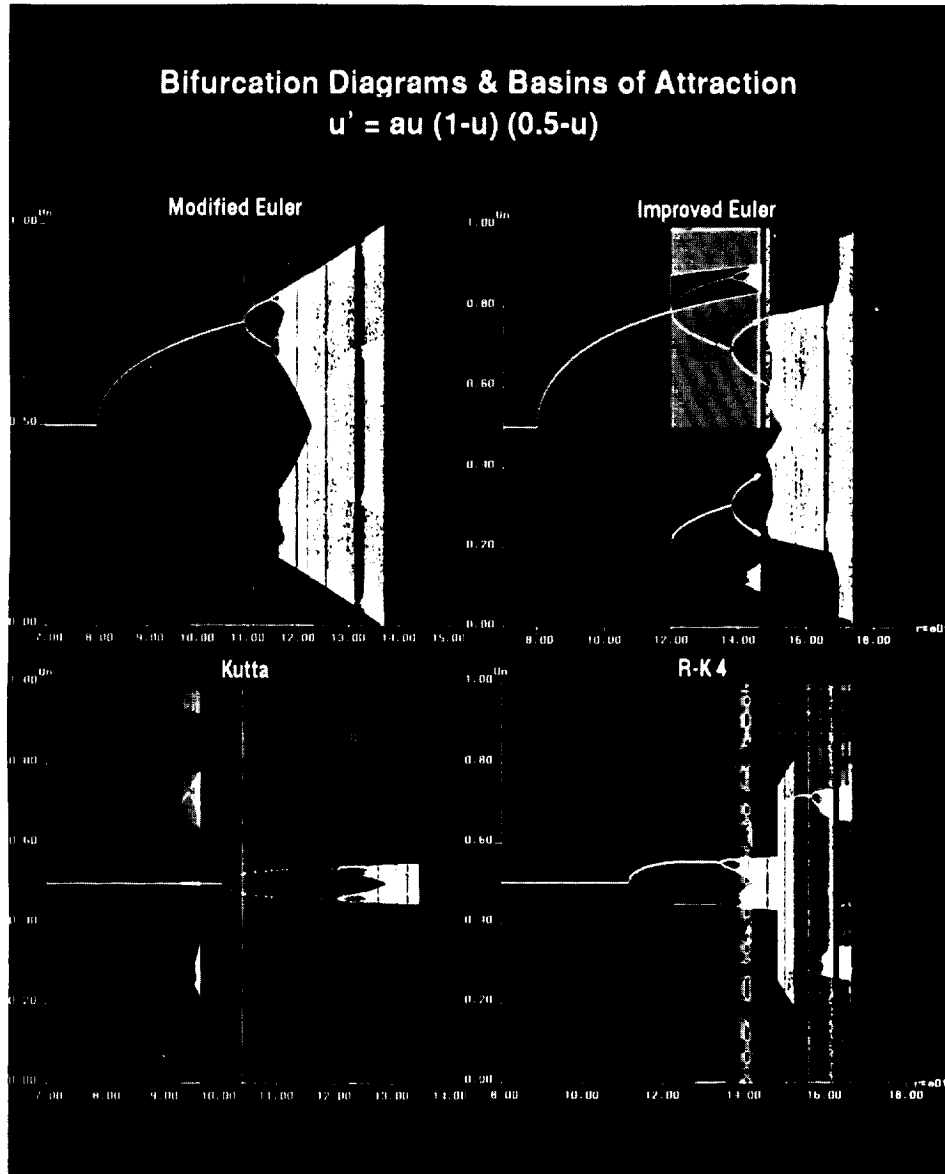


Figure 6.2 (See Color Plate II at the back of this issue.)

The next section presents similar diagrams for the 2×2 systems of model nonlinear ODEs (4.1)–(4.4). In this case, only basins of attraction with bifurcation diagrams superimposed on $v = \text{constant}$ planes are shown. Selected results for both representations of numerical basins of attraction are shown in Figures 6.3–6.5, 6.8–6.25 for the numerical methods. Section 6.6 summarizes similar results presented in Yee and

Sweby (1993a) for iterative procedures in solving nonlinear systems of algebraic equations arising from four implicit LMMs. In the plots $r = \Delta t$. White dots and white curves on the basins of attraction with bifurcation diagrams superimposed represent the bifurcation curves. White dots and white closed curves on the basins of attraction with the numerical asymptotes superimposed represent the stable fixed points, stable periodic solutions or stable limit cycles. The black regions represent divergent solutions.

Note that the streaks on some of plots are either due to the non-settling of the solutions within the prescribed number of preiterations or the existence of small isolated spurious asymptotes. Due to the high cost of computation, no further attempts were made to refine their detailed behavior since our purpose was to show how, in general, the different numerical methods behave in the context of nonlinear dynamics.

6.2 Numerical results for the Dissipative Complex Equation

Figures 6.3–6.5, 6.8, 6.9 show selected results for the two representations of numerical basins of attraction for model (4.1) for $\varepsilon = 1$. The exact solution for (4.1) with $\varepsilon = 1$ is a stable limit cycle with unit radius centered at $(0, 0)$. The basin of attraction for the limit cycle is the entire (u, v) plane except the unstable fixed point $(0, 0)$.

Comparing Figures 6.3–6.5 with Figure 5.5, one can appreciate the added information that the basin of attraction diagrams can provide. As Δt moves closer to the linearized stability limit of the limit cycle, the size (red) of the numerical basins of attraction decreases rapidly. This is due to the existence of spurious unstable asymptotes below as well as above the linearized stability limit. The green region, shown in Figure 6.5 using the implicit Euler method, is the numerical basin of attraction for the *stabilized* fixed point $(0, 0)$. Note how the implicit Euler method turns an unstable fixed point $(0, 0)$ of the ODE system into a stable one for $\Delta t \geq 1$.

Figures 6.6 and 6.7 show the phase trajectories and Figures 6.8 and 6.9 show the same figures with numerical basins of attraction superimposed for four different Δt by the R-K 4 and implicit Euler methods, respectively. Note how little information Figures 6.6 and 6.7 can provide as compared to Figures 6.8 and 6.9. Note also how rapidly the size of the basin (red) decreases as Δt increases for the R-K 4 method. This phenomenon can relate to practical computations where only a fraction of the allowable linearized stability limit of Δt is safe to use if the initial data is not known. For $\Delta t = 1.75$ and 2, spurious limit cycles of higher order period exist. (The multiple white circles with only one distinct basin of attraction). In this case, the red regions represent the basins of the spurious numerical solutions.

Figure 6.9 illustrates the situation where unconditionally stable LMM schemes can converge to a wrong solution if one picks the initial data inside the green region which are valid physical initial data for the ODE. Thus even though LMM preserved the same number of fixed points as the underlying ODE, these fixed points can change type and stability. This phenomenon is related to the “non-robustness” of implicit methods sometimes experienced in CFD computations. In this type of computation where the initial data are not known, the highest probability of avoiding spurious asymptotes is achieved when a fraction of the allowable linearized stability limit of Δt is employed.

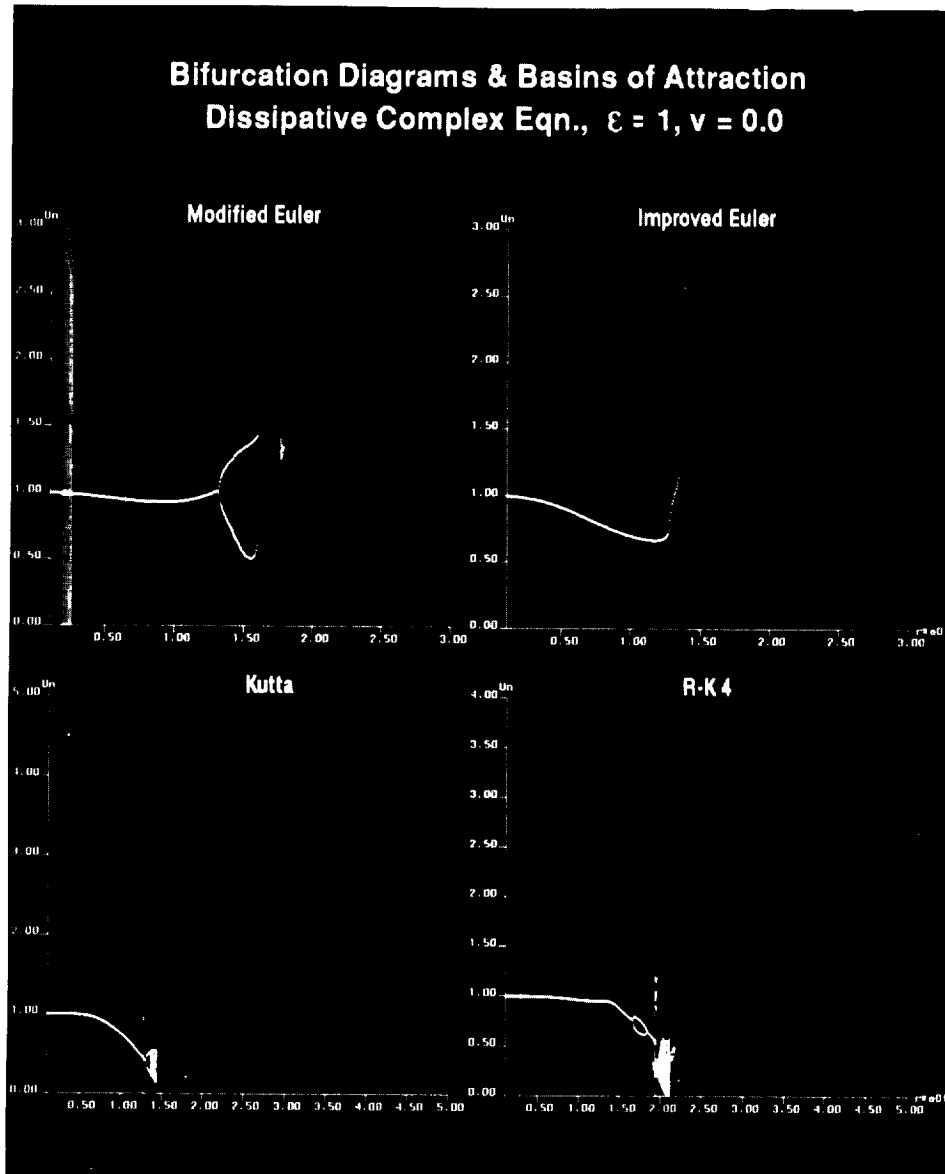


Figure 6.3 (See Color Plate III at the back of this issue.)

6.3 Numerical Results for the Damped Pendulum Equation

Selected results for the studied numerical methods for $\varepsilon = 1$ and $\varepsilon = 1.5$ are shown in Figures 6.10–6.12. Here, for each Δt value the different colors represent different numerical basins of attraction of the respective asymptotes. Observe the striking

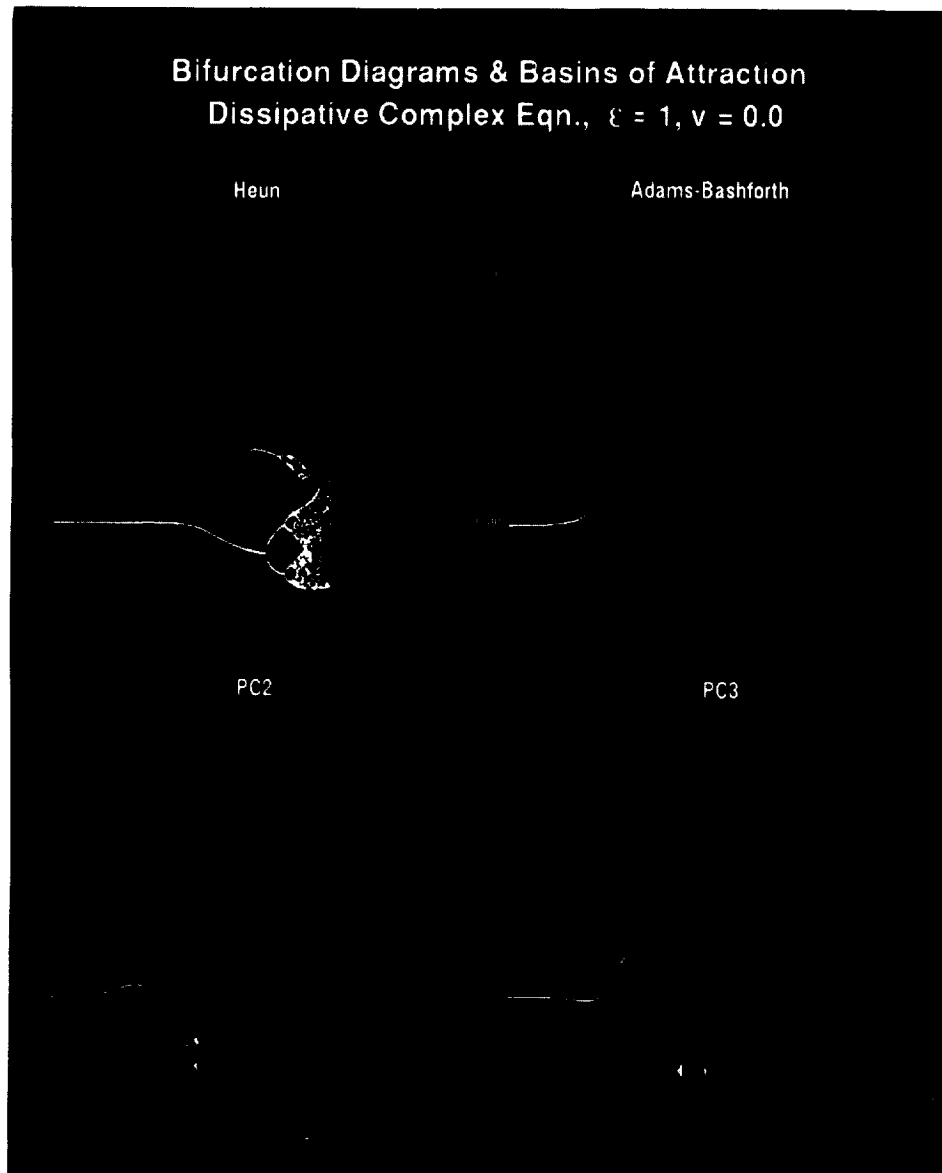


Figure 6.4 (See Color Plate IV at the back of this issue.)

difference in behavior between the explicit and implicit methods. The shapes and sizes of the numerical basins of attraction by the implicit Euler method for $\Delta t = 0.1$ shown in Figure 6.12 appear to be similar to the exact basins of attraction of the DE (4.2). From the different colors of the basins in Figure 6.10 one can readily identify that spurious higher than period one and spurious limit cycles exist for the different Δt values by the

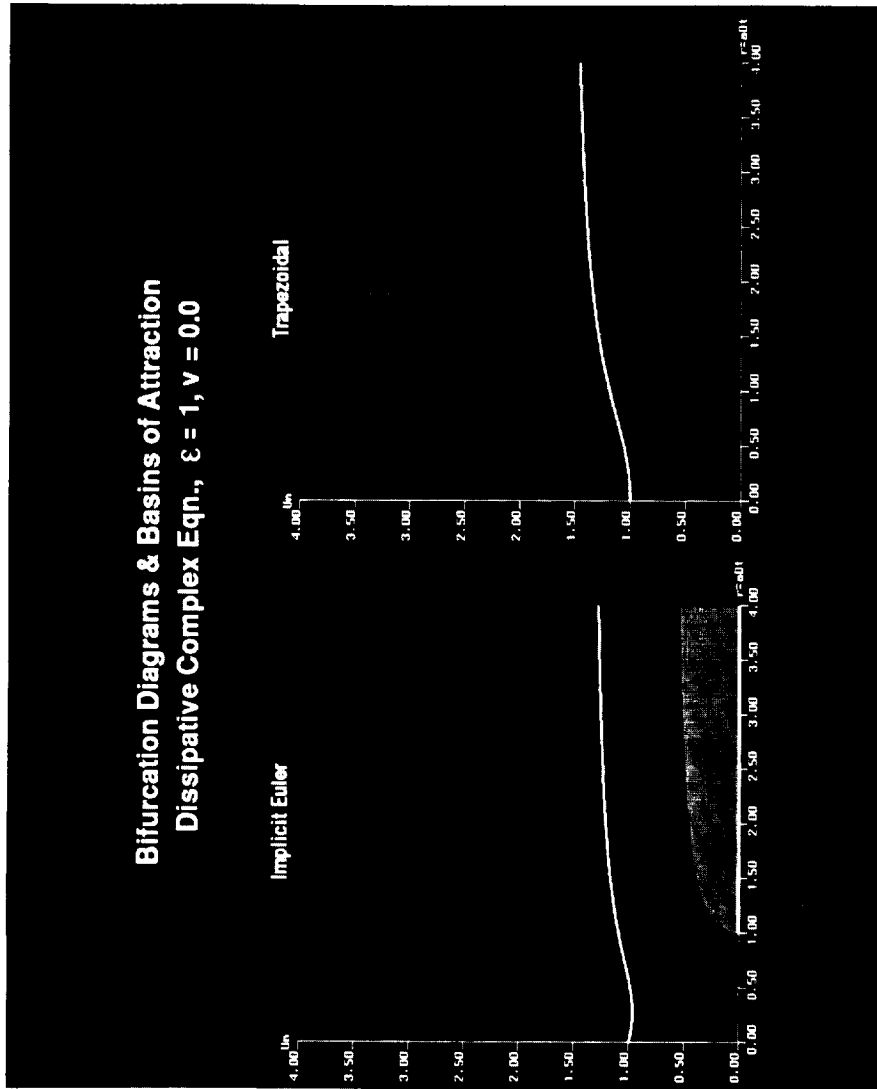


Figure 6.5 (See Color Plate V at the back of this issue.)

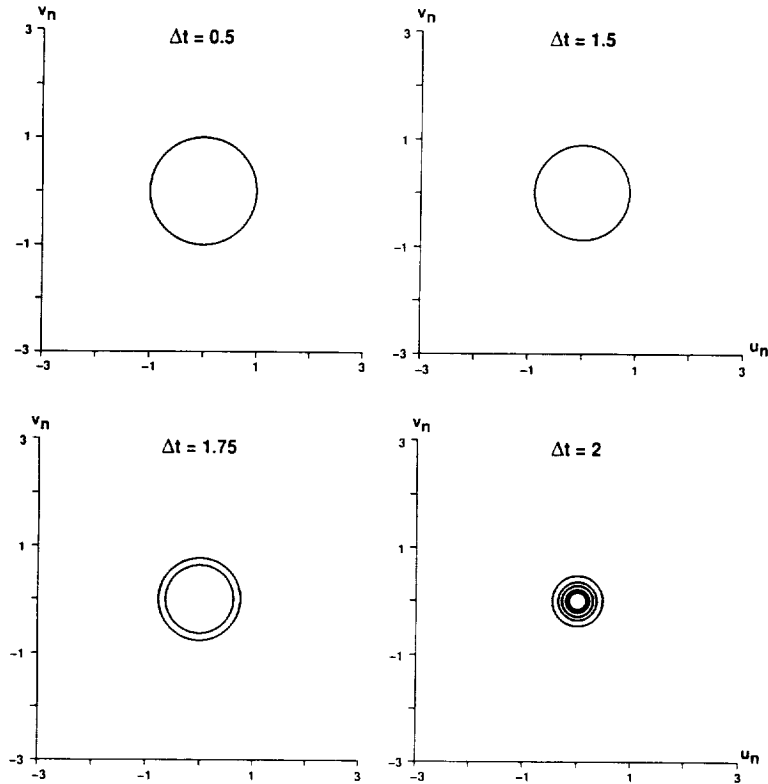


Figure 6.6 Phase Trajectories Dissipative Complex Equation, $\varepsilon = 1$, R-K 4.

explicit Euler method. For $\Delta t = 1.4$, the explicit Euler produces spurious period two fixed points. Figure 6.11 shows the existence of spurious fixed points below the linearized stability limit by the modified Euler method and spurious fixed points of period 4 (the four white dots one each basin) above the linearized stability limit by the R-K 4 method. Figure 6.12 shows the evolution (birth and death) of spurious fixed points of higher-order period for the implicit Euler method. This figure illustrates another situation where unconditionally stable schemes can converge to a wrong solution even though these schemes preserved the same number and type of fixed points as the underlying ODE. In this case it is the birth of spurious stable and unstable asymptotes or even numerical chaos that contributes to the size reduction of the true basins of attraction of the ODE.

6.4 Numerical Results for the Predator-Prey Equation

Selected results for the two representations of numerical basins of attraction are shown in Figures 6.13–6.18. Comparing Figures 6.13, 6.15, 6.16, with Figures 5.4 and 5.7, one can again appreciate the added information that the basin of attraction diagrams can

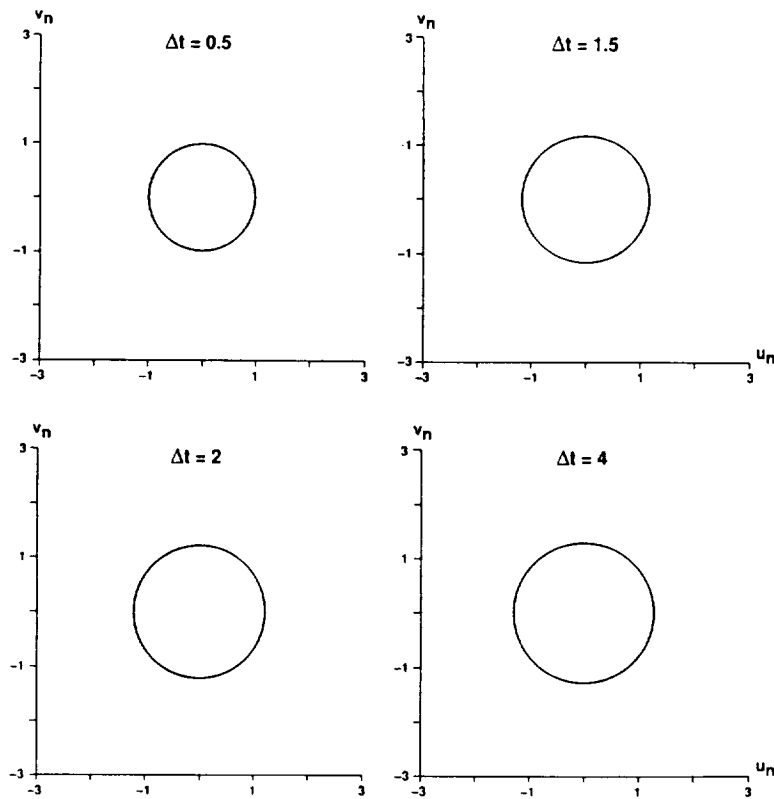


Figure 6.7 Phase Trajectories Dissipative Complex Equation, $\varepsilon = 1$ Linearized Implicit Euler.

provide. Here for all of these figures (except Fig. 6.15 for the last four Δt values), the green regions represent the numerical basins of attraction for the stable spiral (2.1, 1.98) and red regions represent the numerical basins of attraction for the stable node (0, 0).

The numerical basins of attraction in Figure 6.18 with $\Delta t = 0.1$ appear to be the same as the exact basins of attraction of the DE (4.3). The numerical basin of attraction by the implicit Euler for the fixed point (0, 0) with $\Delta t = 0.1$ is larger than the corresponding exact basin of attraction for the DE (4.3). In this case the numerical basin of attraction for the divergent solution (black region) is smaller than the true one. The dramatic difference in shapes and sizes of numerical basins of attraction for the different methods and solution procedure combinations compared with the exact basin of attraction is even more fascinating than for the previous two models.

Take, for example, one of the most interesting cases, the modified Euler method. Figure 6.15 shows how spurious stable fixed points can alter the numerical basins of attraction of the stable node and spiral of the ODE (4.3) for time steps that are below the linearized stability limit of both of these stable fixed points of the ODE (see Figs. 5.4

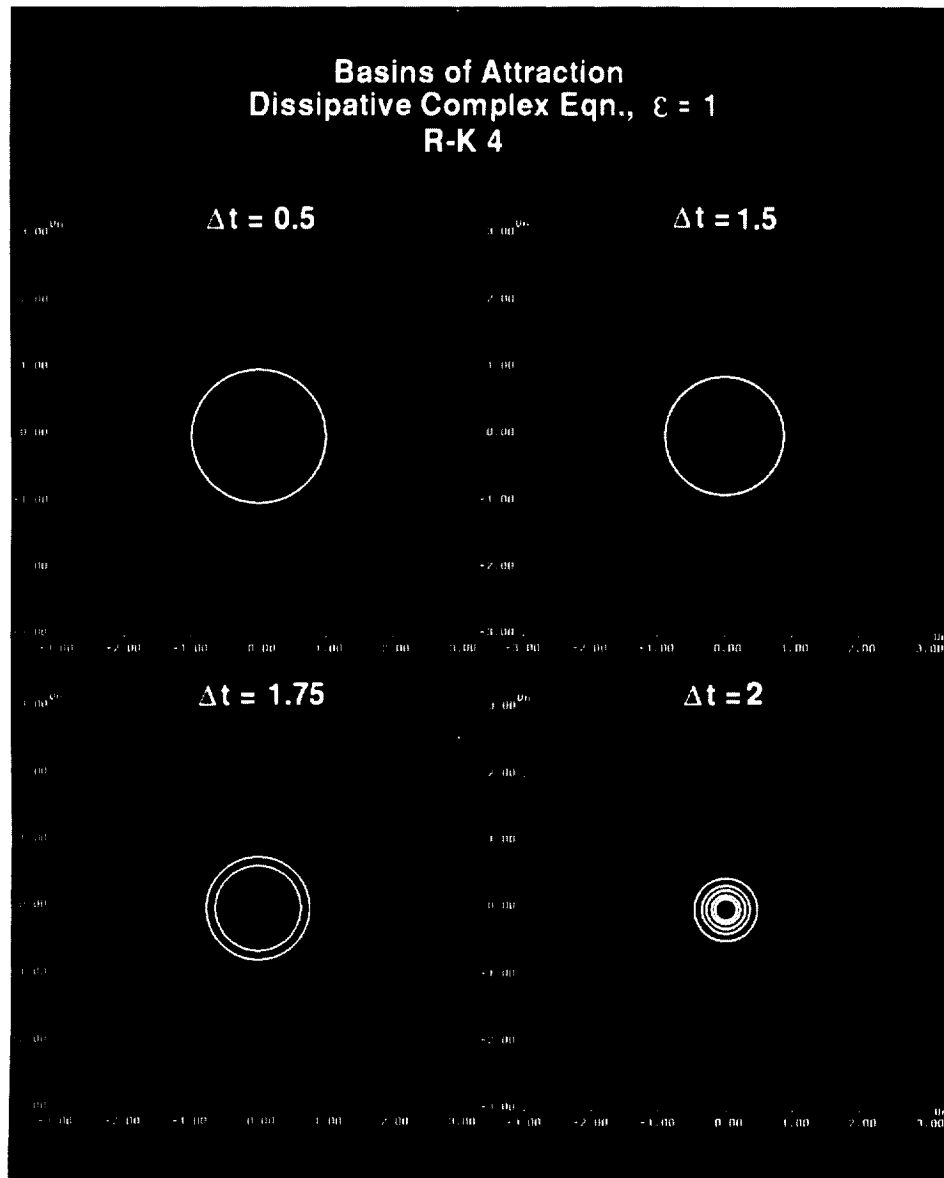


Figure 6.8 (See Color Plate VI at the back of this issue.)

and 6.13). For $\Delta t = 0.8$, the stable node bifurcates into a spurious fixed point. Without performing the bifurcation analysis one would not be able to detect this particular spurious fixed point, since the value of the spurious one is so close to the exact fixed point $U_E = (0, 0)$. For $\Delta t = 0.9524$, there is the birth of a spurious limit cycle (the white close curve). For $\Delta t = 1.2$, spurious higher-order periodic solutions exist. Note that for

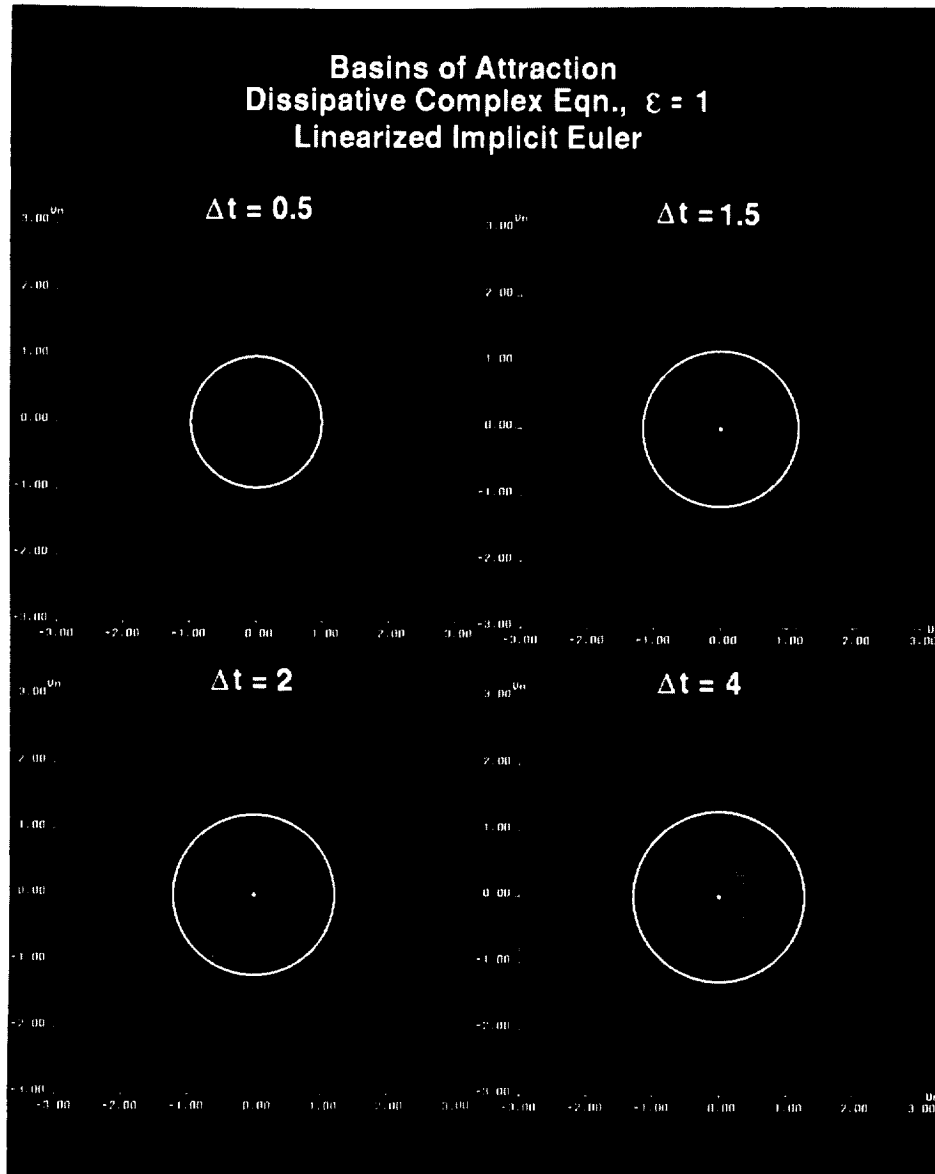


Figure 6.9 (See Color Plate VII at the back of this issue.)

the first four Δt values in Figure 6.15, the fixed points and asymptotic values are colored black instead of white due to the birth of additional numerical basins of attraction that are colored white.

The implicit methods change the two saddle points into stable or unstable fixed points of other types as illustrated in Figures 6.14, 6.17 and 6.18. For the implicit Euler,

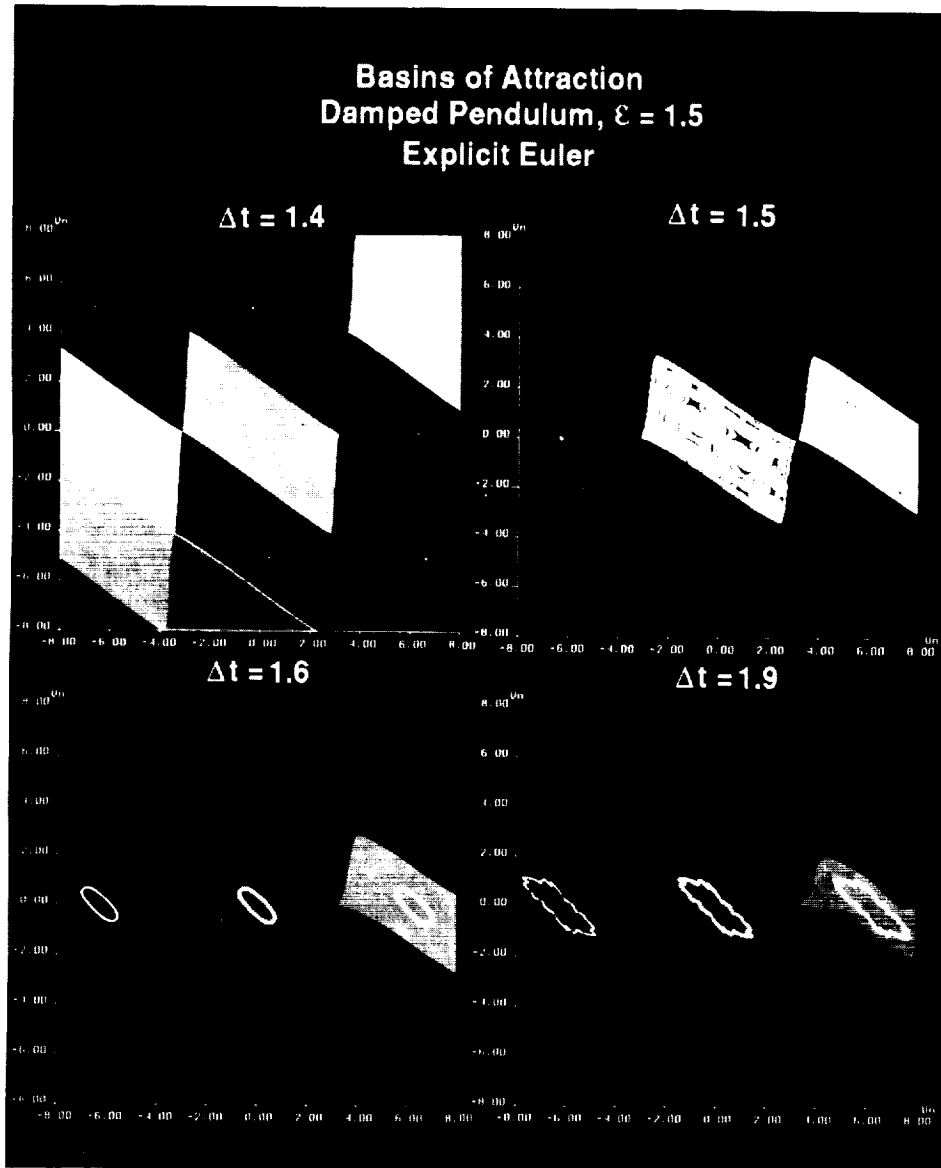


Figure 6.10 (See Color Plate VIII at the back of this issue.)

the two fixed points $(2.1, 1.98)$ and $(0, 0)$ are unconditionally stable and the *stabilized* fixed points $(1, 0)$ and $(3, 0)$ (saddles for the original ODE) are almost unconditionally stable except for small Δt . This is most interesting in the sense that the numerical basins of attraction for the stable exact fixed points U_E of the model (4.3) by the implicit Euler method were permanently altered for Δt near or larger than 3 as illustrated in

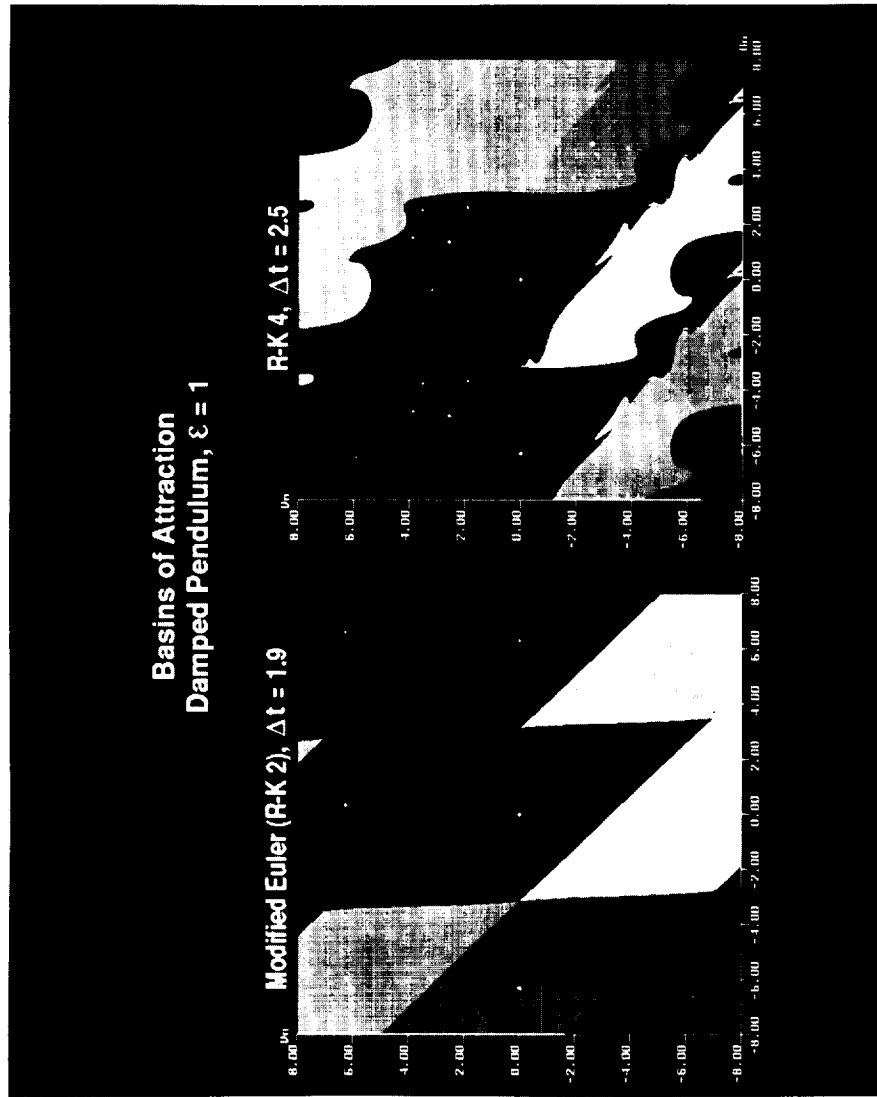


Figure 6.11 (See Color Plate IX at the back of this issue.)

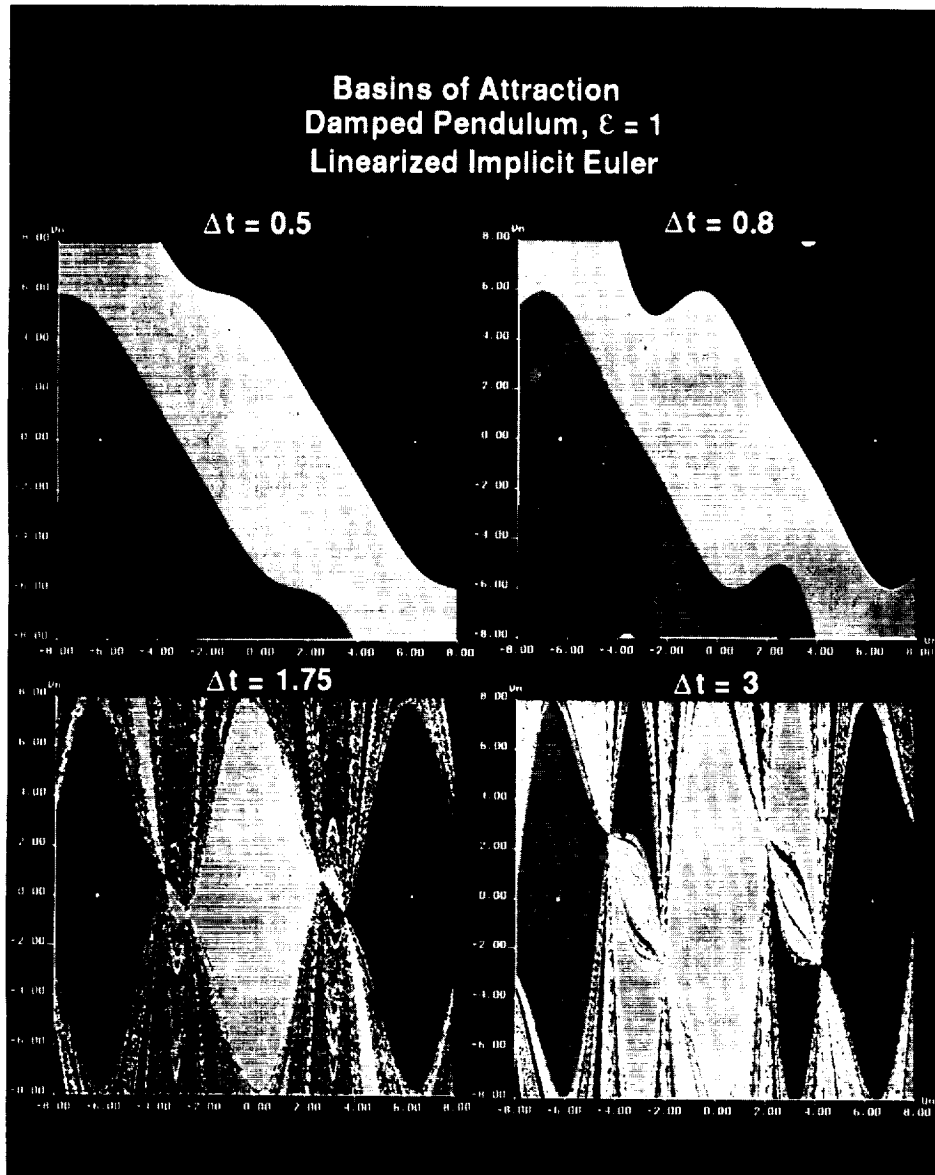


Figure 6.12 (See Color Plate X at the back of this issue.)

Figures 6.14, 6.17. It would be easier to interpret the results in Figure 6.14 if one interchanged the yellow and green colors for $\Delta t \geq 1$. Observe how the newly created numerical basins of attraction by the *stabilized* fixed points $(1, 0)$ and $(3, 0)$ resulted in the segmentation of the numerical basins of attraction of the stable node $(0, 0)$ and stable spiral $(2.1, 1.98)$. Although the trapezoidal method did not turn the two saddle

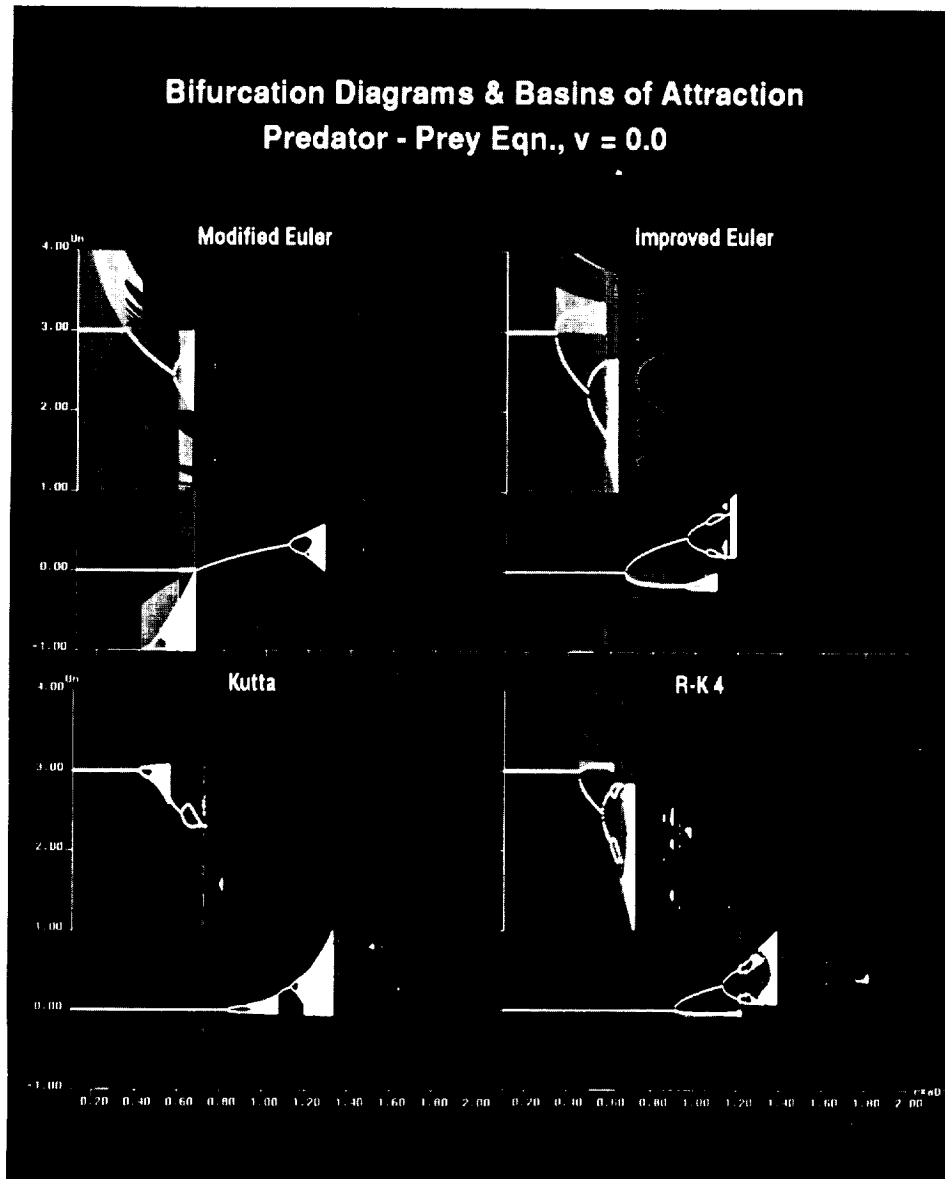


Figure 6.13 (See Color Plate XI at the back of this issue.)

points $(1,0)$ and $(3,0)$ into stable fixed points of different type, they did turn the two saddle points into *unstable* fixed points of different type.

The evolution of the numerical basin of attraction as Δt changes is very traumatic these implicit LMMs. The cause of nonconvergence of these implicit LMMs may due to the fact that their numerical basins of attraction are fragmented. Take for example the

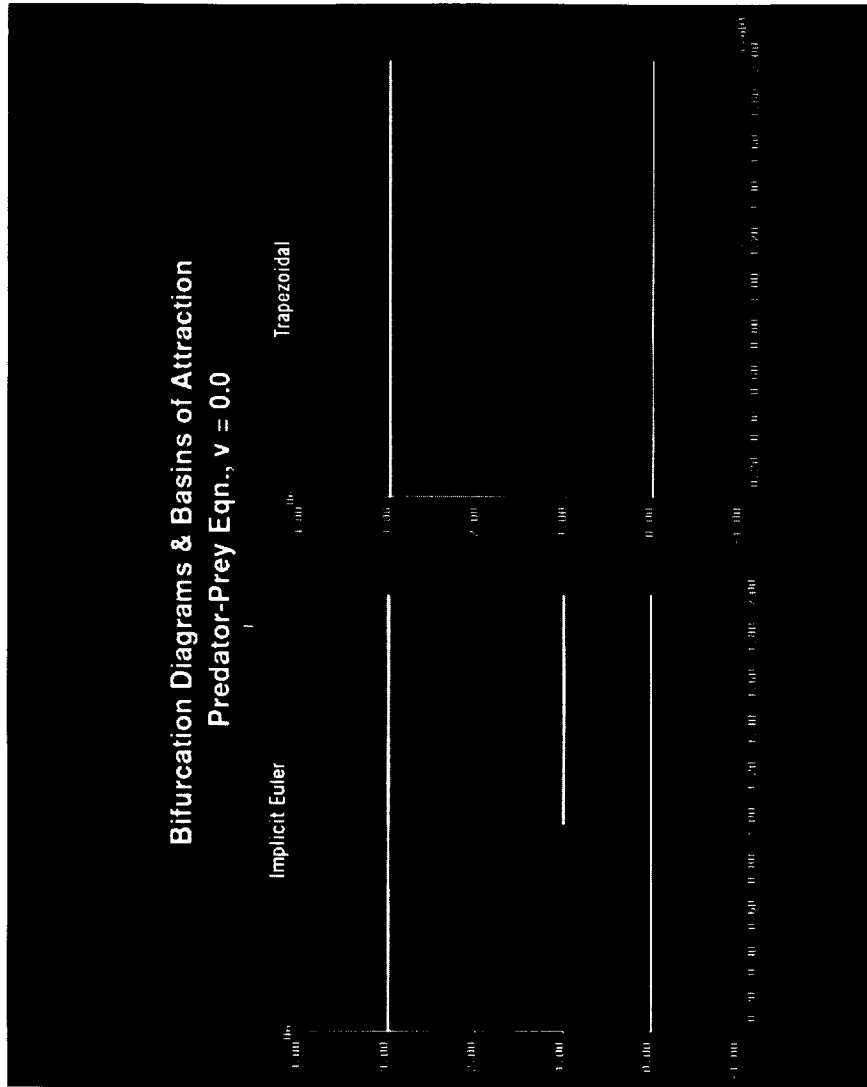


Figure 6.14 (See Color Plate XII at the back of this issue.)

trapezoidal method (Fig. 6.18) where the scheme becomes effectively unstable for large Δt . The size of the numerical basins of attraction for the stable fixed points U_E shrink to almost nonexistence. This phenomenon might be one of the contributing factor to the unpopularity of the trapezoidal method in CFD. The basins are so fragmented and small for large Δt that they are beyond the accuracy of the CM2 to resolve and no

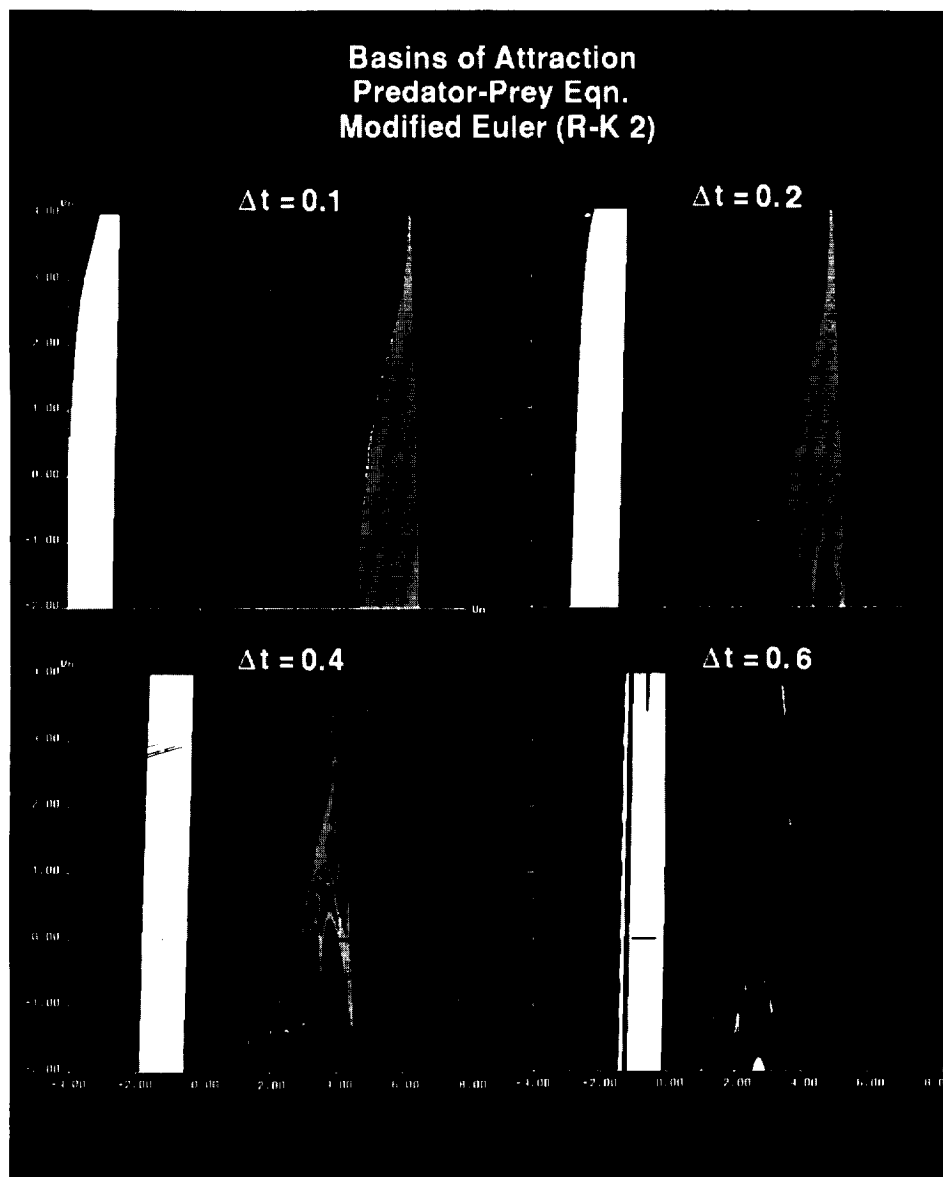


Figure 6.15 (See Color Plate XIII at the back of this issue.)

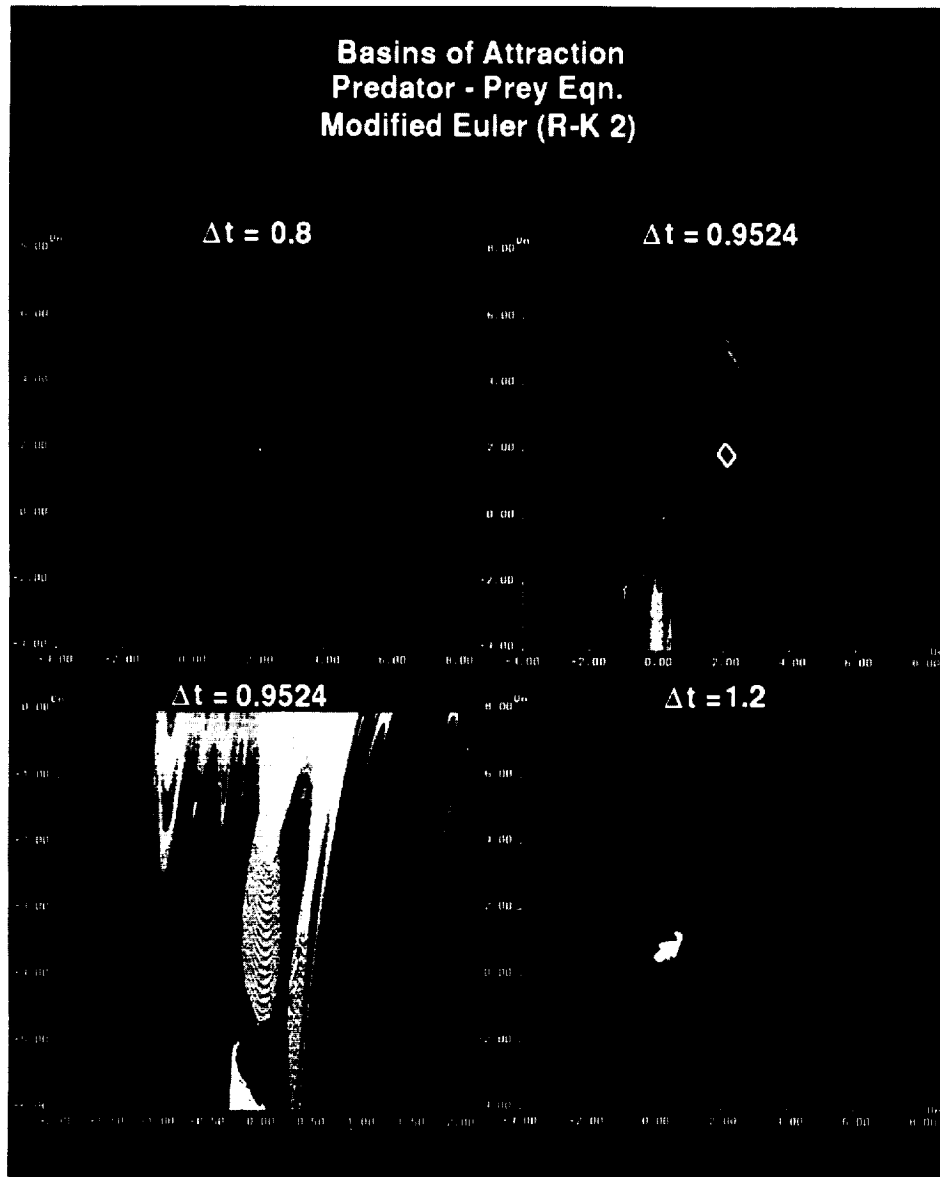


Figure 6.15 (Continued) (See Color Plate XIII at the back of this issue.)

further attempt was made. A better approach in computing these types of basins is to use interval arithmetic or the enclosure type method (Adams, 1990).

6.5 Numerical Results for the Perturbed Hamiltonian Equation

Selected results for the two representations of numerical basins of attraction of the various numerical methods for $\varepsilon = 0.1$ are shown in Figures 6.19–6.25. Our studies

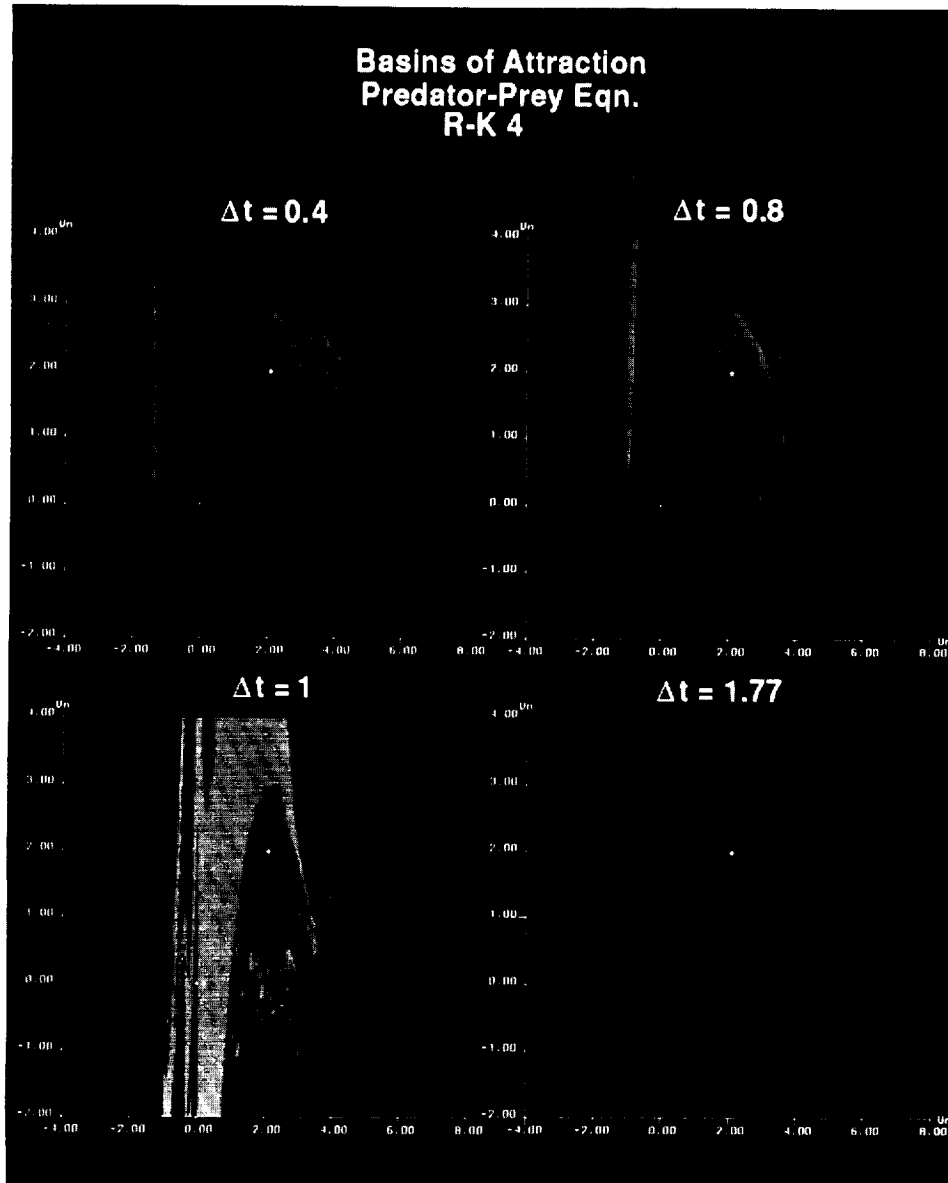


Figure 6.16 (See Color Plate XIV at the back of this issue.)

indicate that all of the studied Runge-Kutta methods exhibit spurious limit cycles and other spurious periodic solutions. For the Kutta and Heun methods, stable spurious asymptotes can occur below the linearized stability limit of the scheme. The implicit methods also exhibit spurious asymptotes. In particular, unstable spurious asymptotes were produced below the linearized stability limit by all of the studied schemes.

Although this example consists of an artificially small number of grid points, it can shed some light on the interplay between initial data, spurious stable and unstable asymptotes, basins of attraction and the time-dependent approach to the asymptotic numerical solutions. A solid understanding of this concept at the fundamental level can

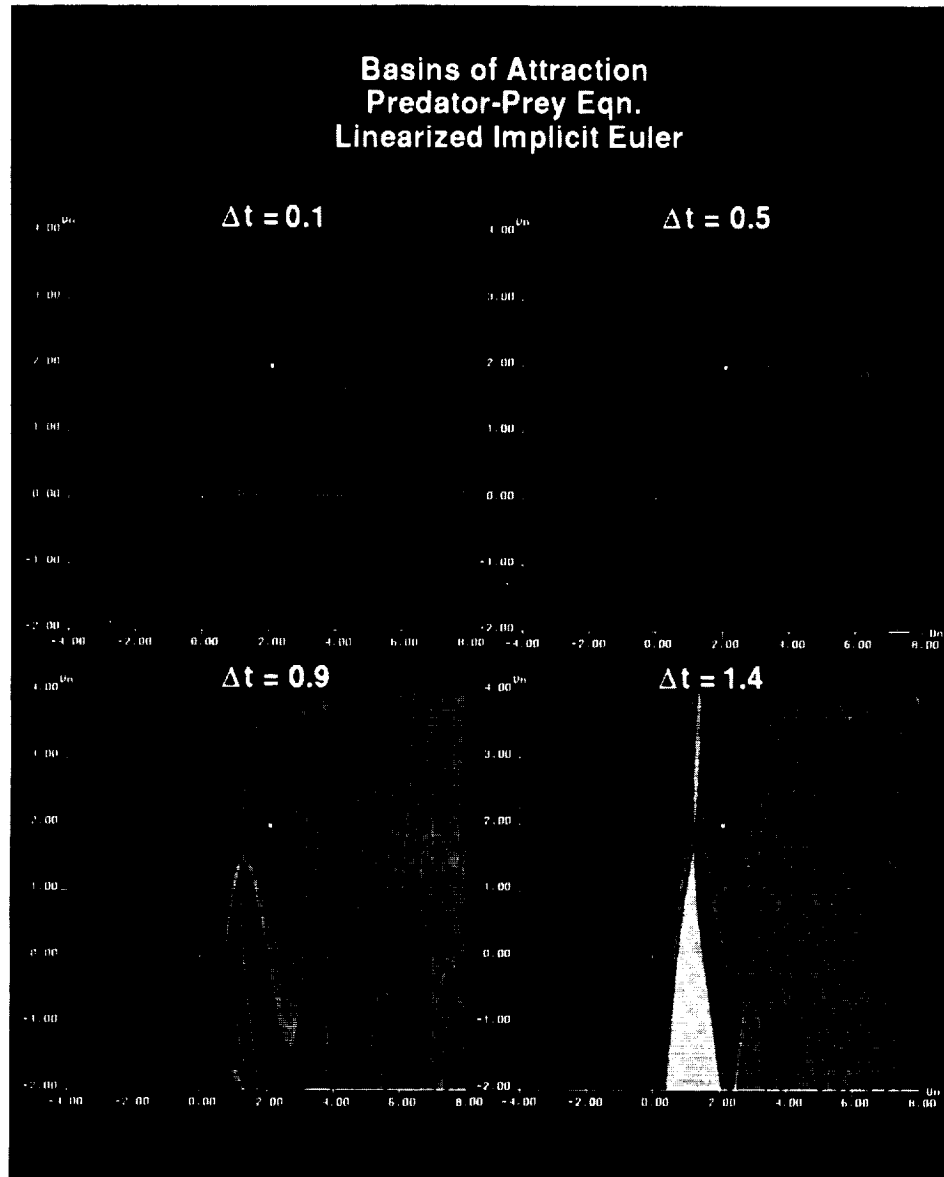


Figure 6.17 (See Color Plate XV at the back of this issue.)

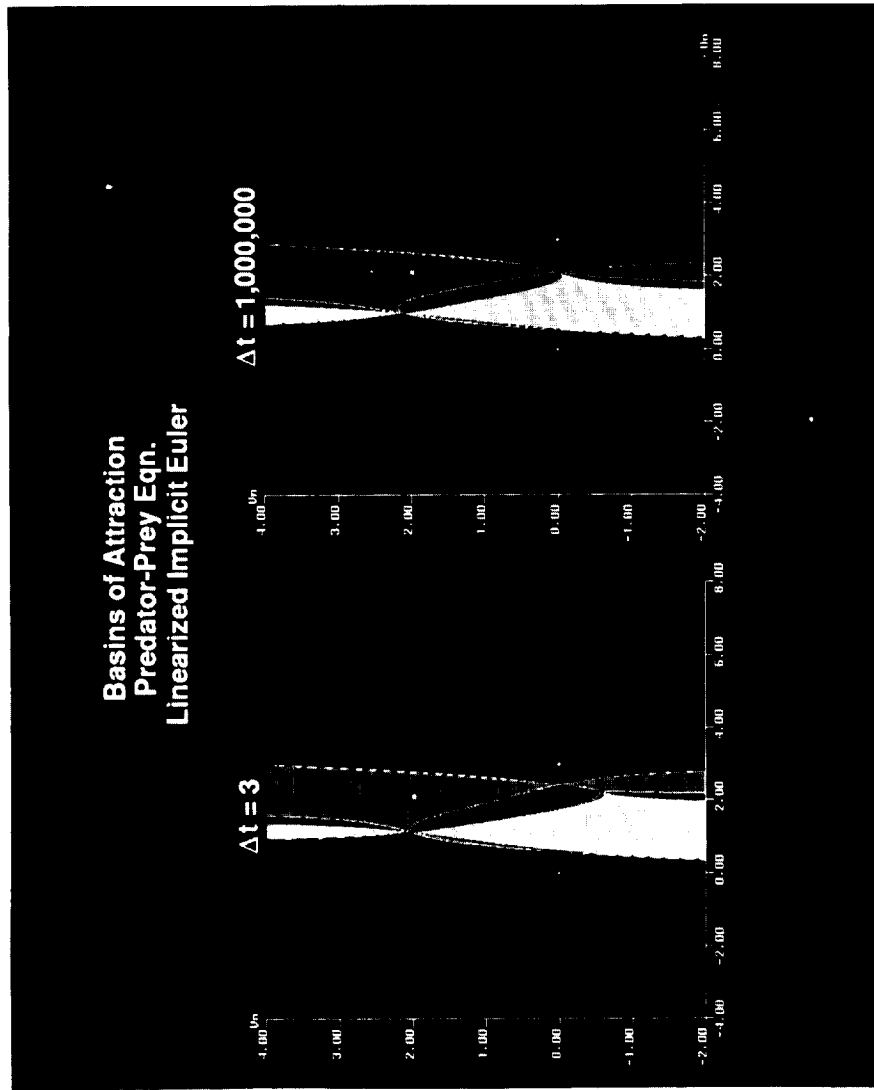


Figure 6.17 (Continued) (See Color Plate XV at the back of this issue.)

help to determine the reliability of the time-dependent approach to obtaining steady-state numerical solutions.

In all of Figures 6.19–6.25, red regions represent the numerical basins of attraction for the stable spiral $(1/3, 1/3)$ when Δt is below the linearized stability of the scheme. When Δt is above the linearized stability, some of the red regions represent the numerical basin of attraction of the stable spurious asymptotes. The numerical basins

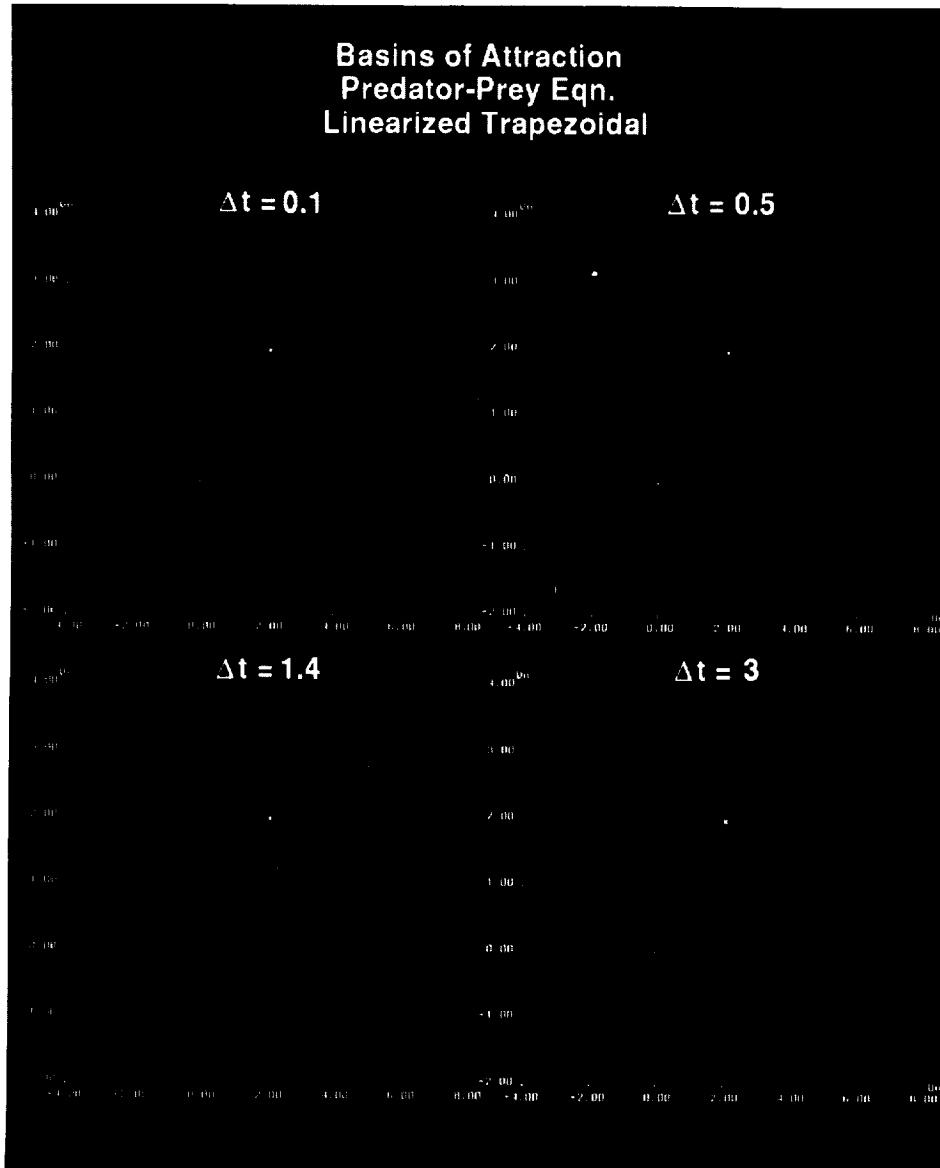


Figure 6.18 (See Color Plate XVI at the back of this issue.)

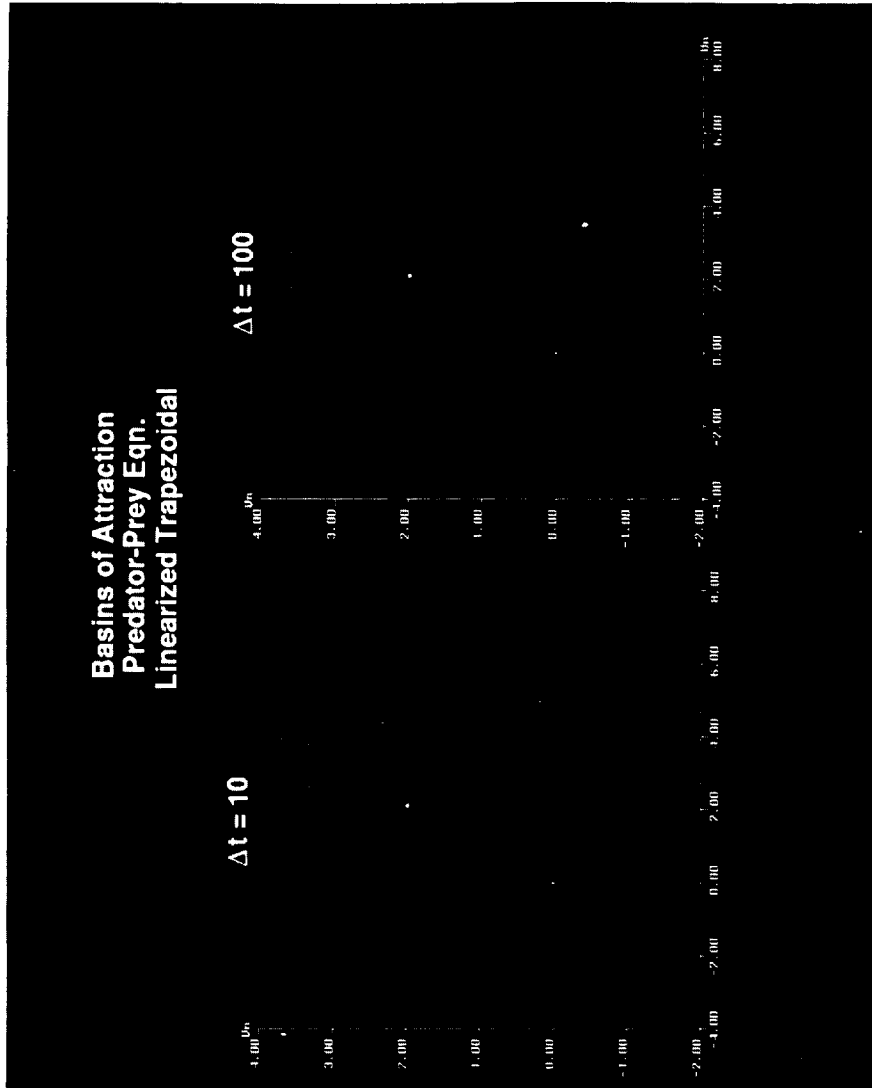


Figure 6.18 (Continued) (See Color Plate XVI at the back of this issue.)

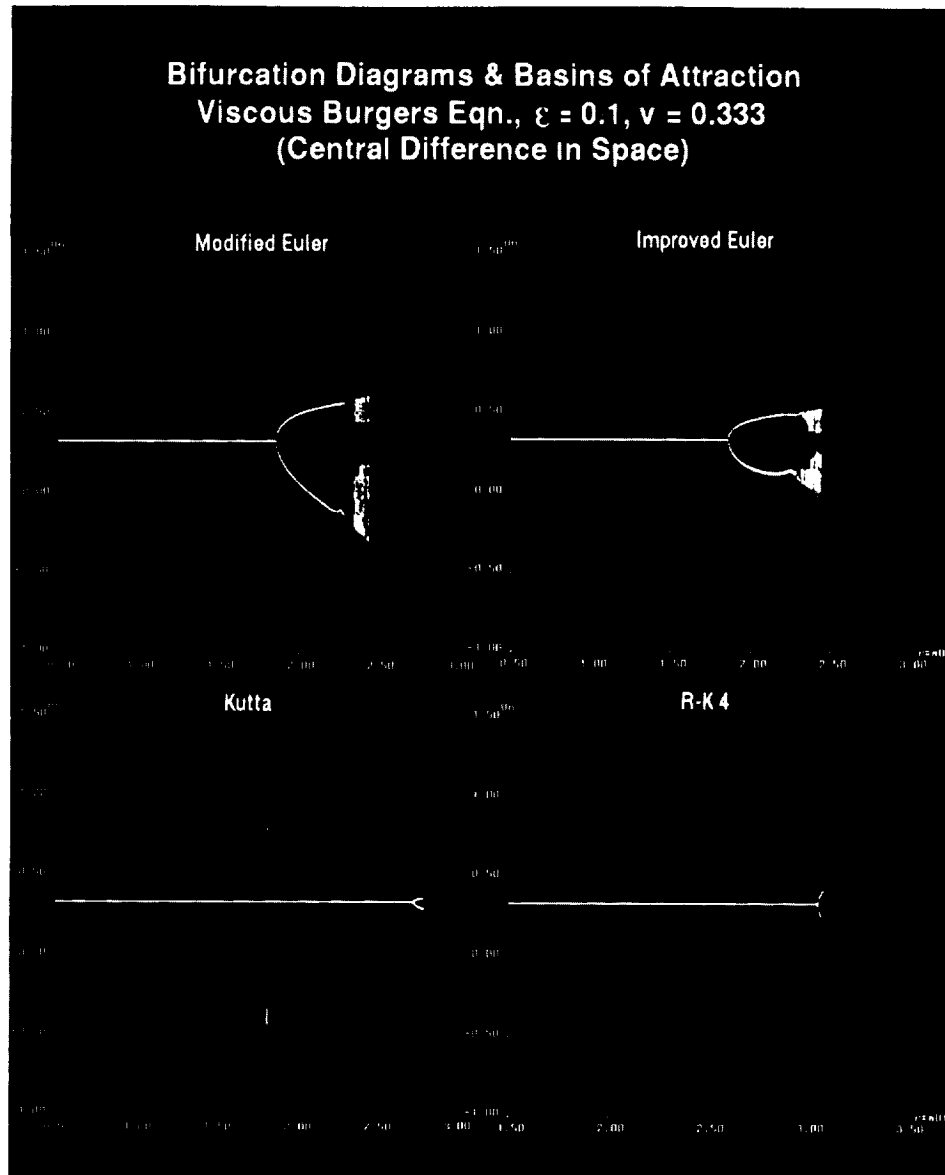


Figure 6.19 (See Color Plate XVII at the back of this issue.)

of attraction in Figures 6.21 with $\Delta t = 0.1$ appear to be the same as the exact basins of attraction. Note also that the possibility of the numerical basin of attraction being larger than the exact one does not always occur when the time step is the smallest. The numerical basin of attraction for $(1/3, 1/3)$ is larger than the corresponding exact basin of attraction for $\Delta t = 1$ by the improved Euler and Kutta methods and for $\Delta t = 0.1$ by

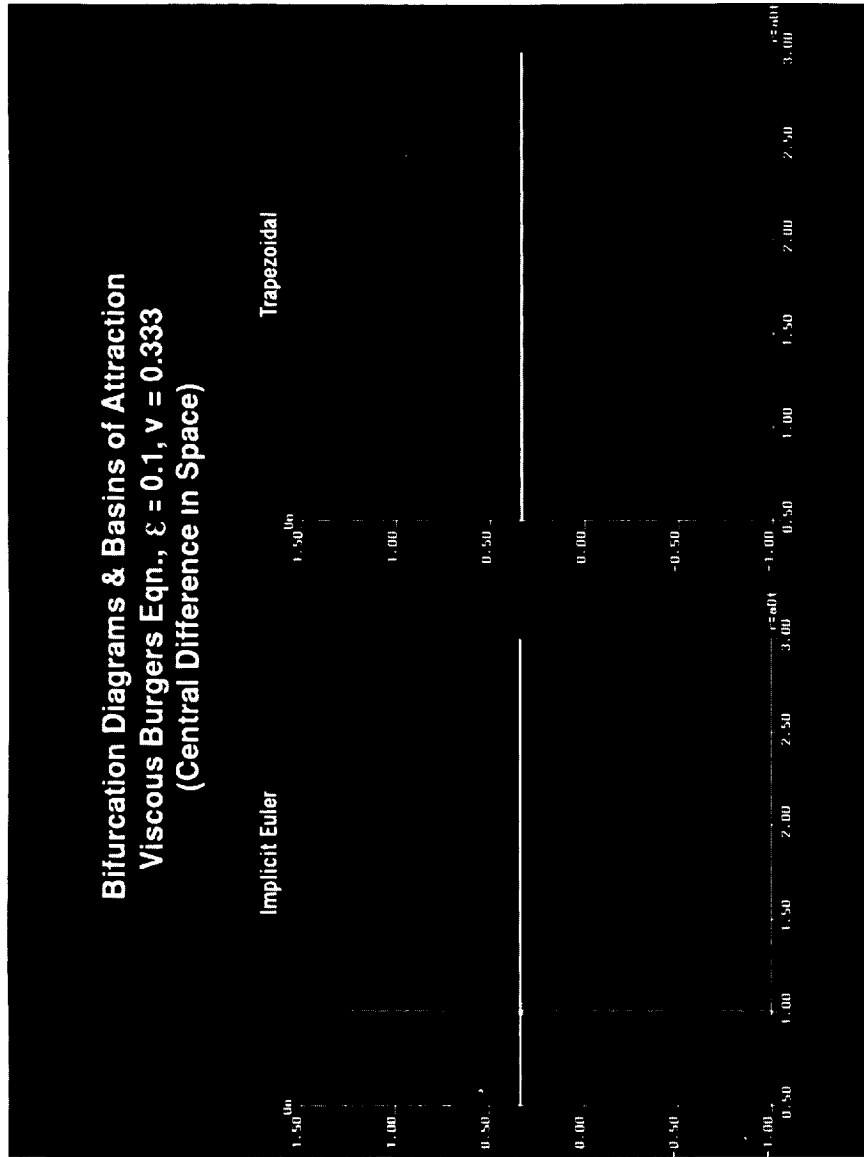


Figure 6.20 (See Color Plate XVIII at the back of this issue.)

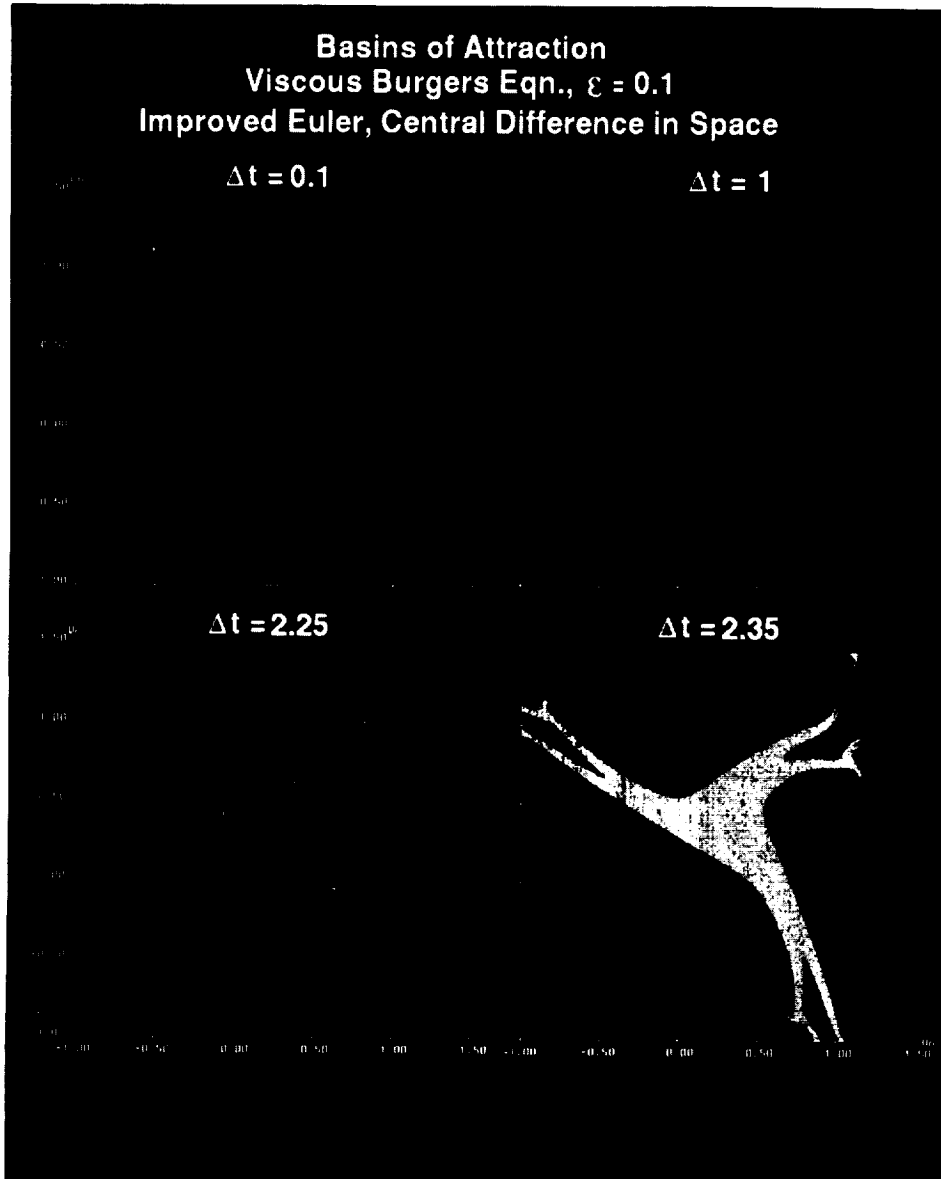


Figure 6.21 (See Color Plate XIX at the back of this issue.)

the implicit Euler and trapezoidal methods. See Figures 6.21–6.24. The following discusses results for the improved Euler, the Kutta, the implicit Euler and the trapezoidal methods.

Improved Euler Method: This example illustrates the existence of spurious limit cycles and its effect on the numerical basins of attraction for the exact steady state. Figure 6.21

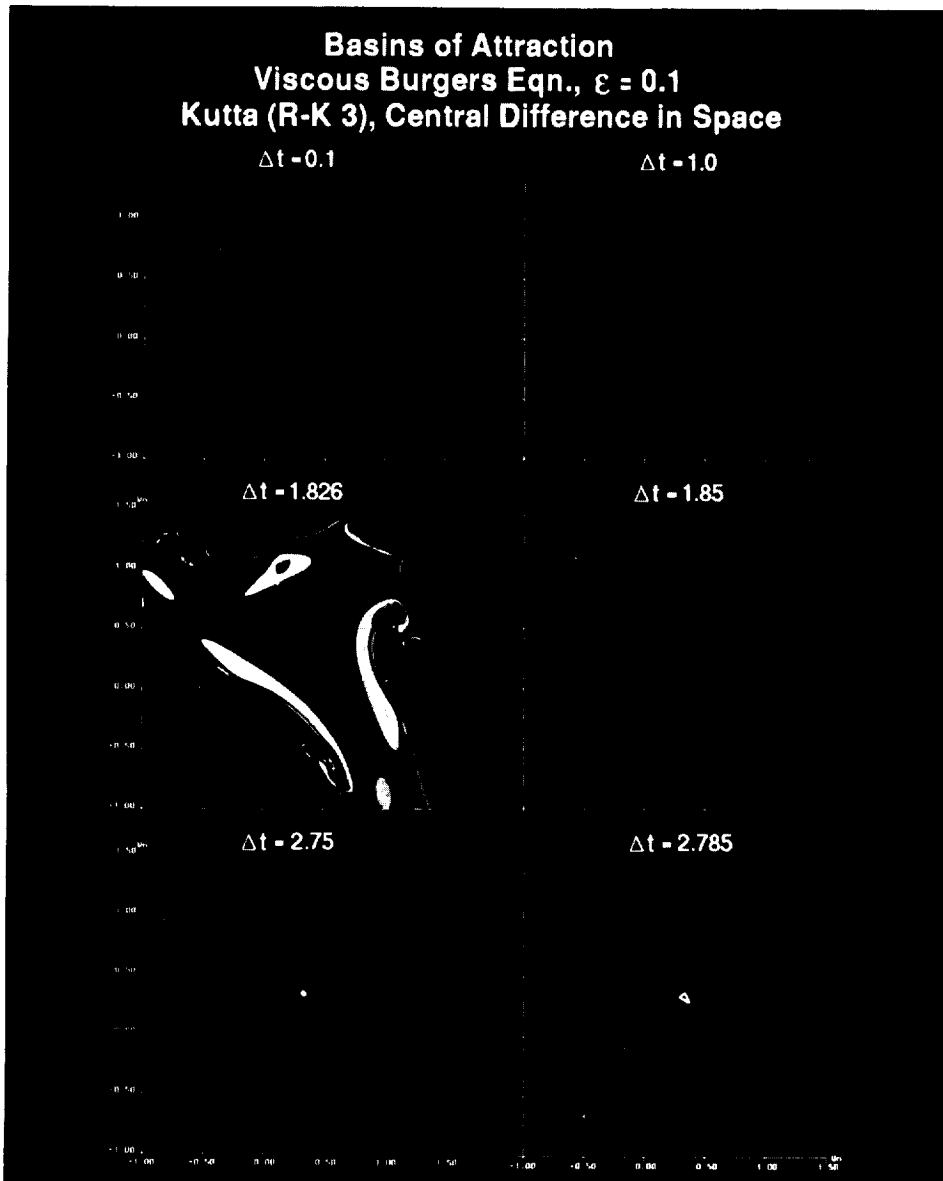


Figure 6.22 (See Color Plate XX at the back of this issue.)

shows the basins of attraction of the improved Euler method for 4 different $\Delta t = 0.1, 1, 2.25, 2.35$ with $\varepsilon = 0.1$. By a bifurcation computation shown in Figure 6.19, we found that the first two time steps are below the linearized stability limit around the exact stable steady state $(1/3, 1/3)$, and the last two time steps are above the limit.

Above the linearized stability limit spurious limit cycles and higher dimensional periodic solutions were observed. Further increasing Δt resulted in numerical chaos-type phenomena and eventually divergence (with additional increase in Δt). For $\Delta t = 2.25$ and 2.35 , the red or multicolor regions are the basins of the spurious limit cycle (the irregular white closed curve shown on Fig. 6.21) or other type of spurious

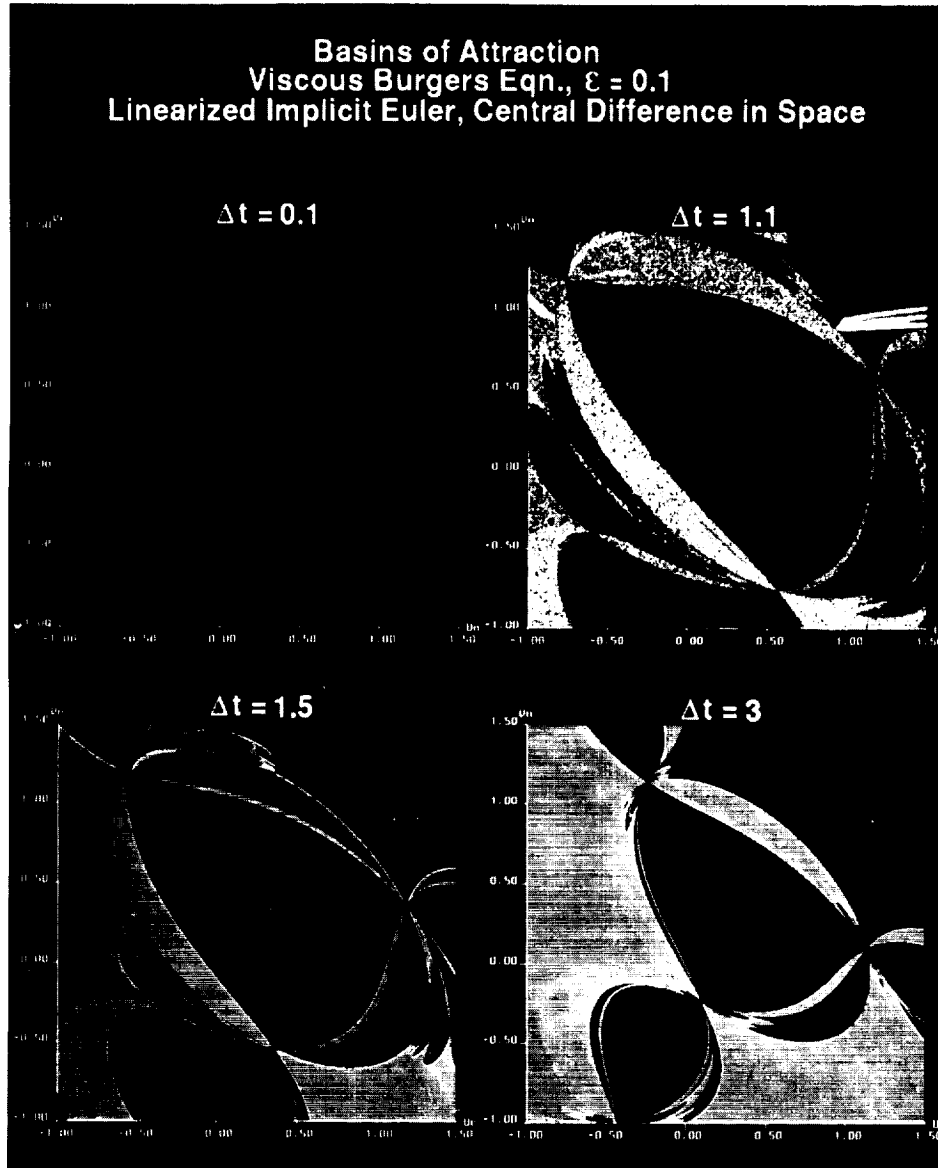


Figure 6.23 (See Color Plate XXI at the back of this issue.)

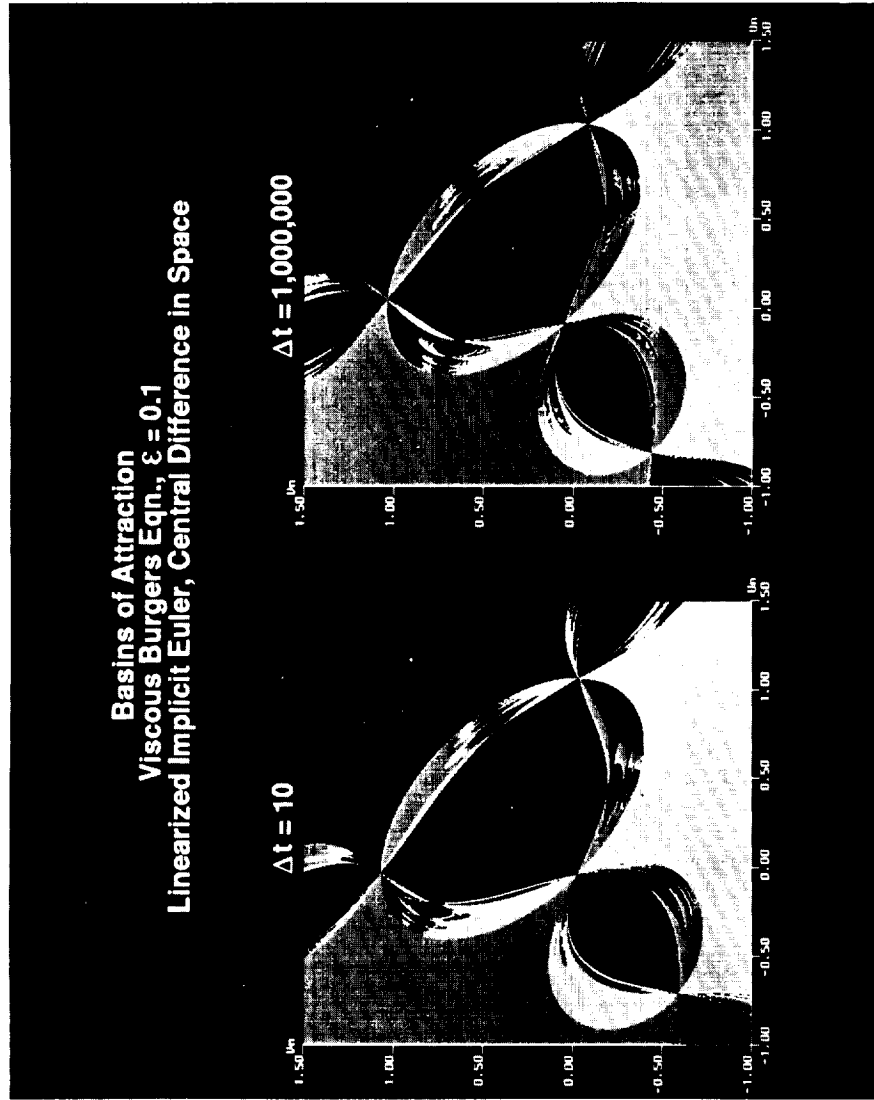


Figure 6.23 (Continued) (See Color Plate XXI at the back of this issue.)

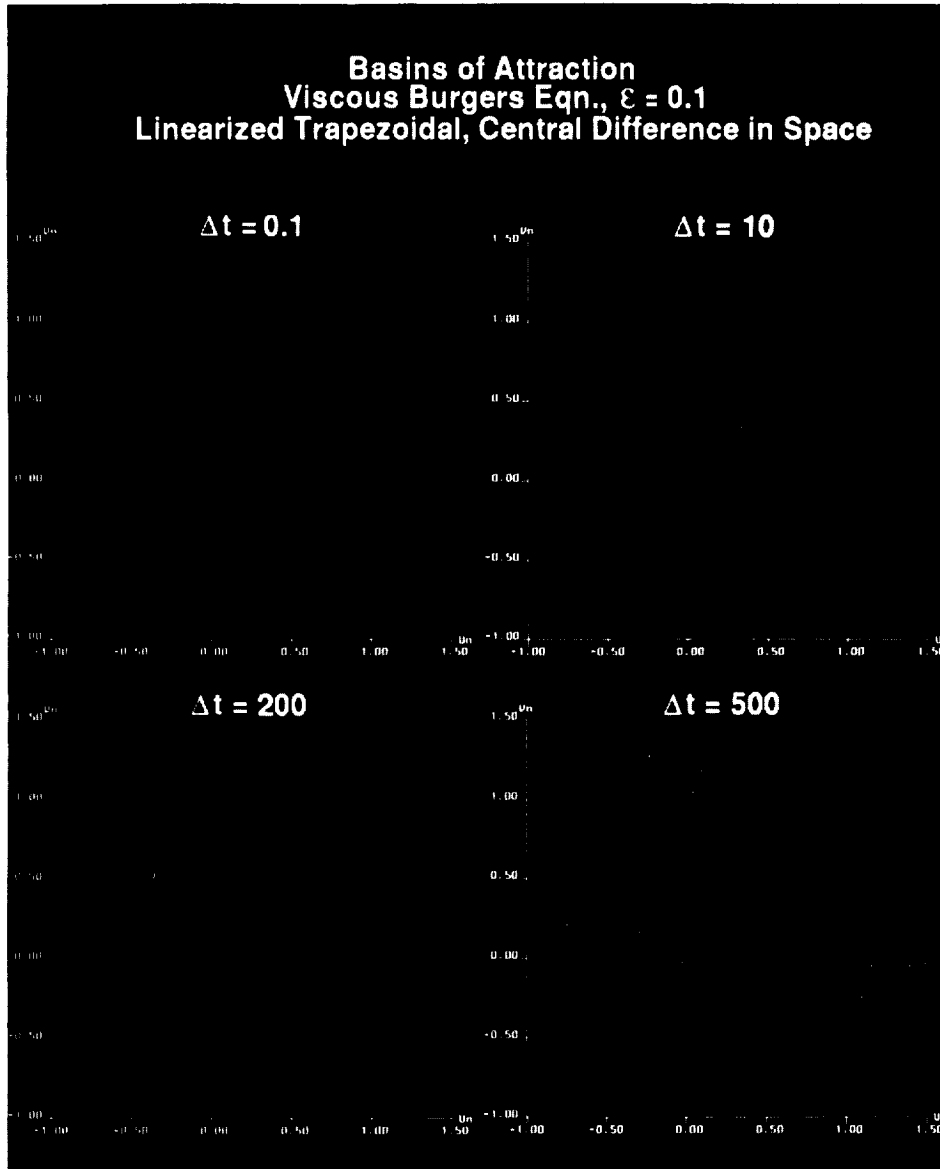


Figure 6.24 (See Color Plate XXII at the back of this issue.)

asymptote (white dots for Fig. 6.21). For these two time steps the numerical basins for the exact steady state $(1/3, 1/3)$ by the improved Euler method disappeared. However, if the initial data are in the red or multicolor region, one gets spurious solution instead of what the linearized stability predicts—divergent solution.

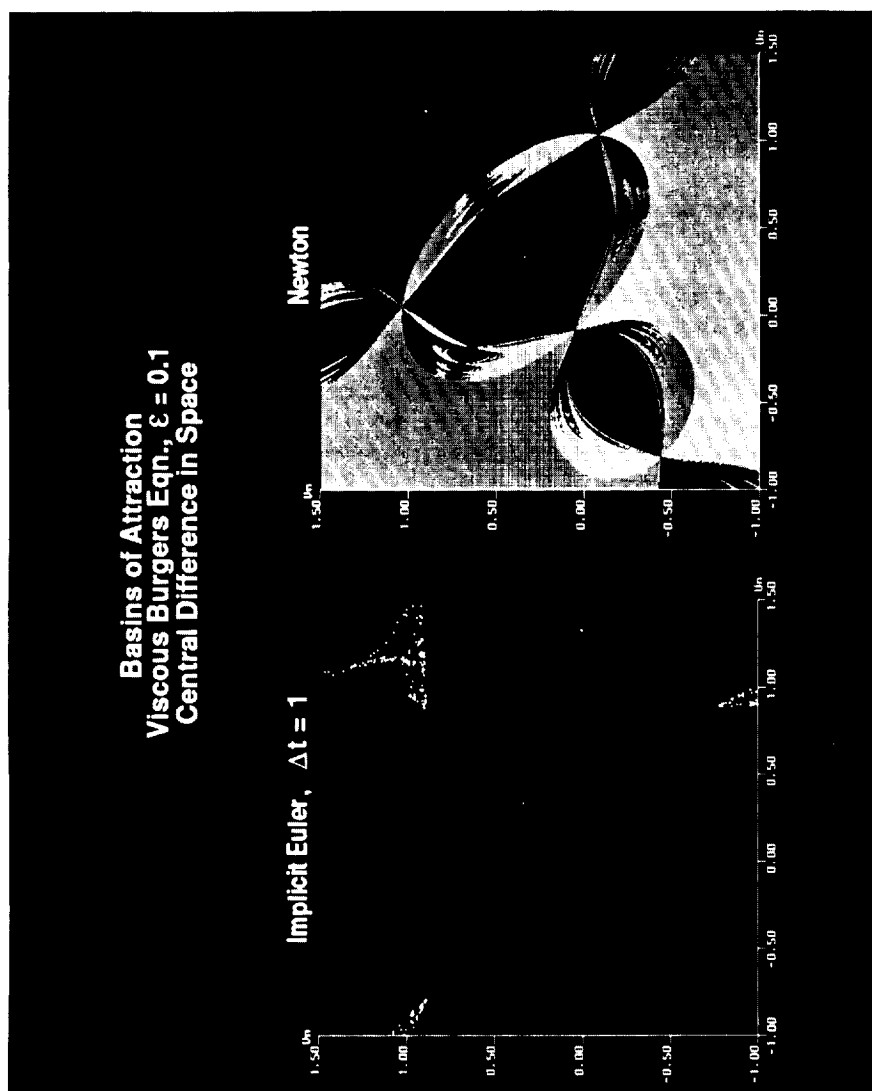


Figure 6.25 (See Color Plate XXIII at the back of this issue.)

Kutta Method: To give an example of the existence of spurious stable asymptotes below the linearized stability limit of the scheme, as well as the existence of spurious limit cycles above the linearized stability limit, Figure 6.22 shows the basins of attraction of the Kutta method for 6 different fixed time steps $\Delta t = 0.1, 1, 1.826, 1.85, 2.75$ and 2.785 (the first four below the linearized stability of the scheme) with $\varepsilon = 0.1$. For $\Delta t = 1.826$, the numerical basin for $(1/3, 1/3)$ has become fractal like with the birth of fragmented, isolated new basins of attraction due to the presence of spurious periodic solutions (the three white complicated closed curves with the associated purple, green and blue basins shown in Fig. 6.22). The last two time steps in Figure 6.22 show the disappearance of the numerical basin of attraction for the exact steady state with the birth of basins for the spurious limit cycle.

Implicit Euler Method: This is yet another interesting illustration of the use of an unconditionally stable implicit method where in practical computations, when the initial data are not known, the scheme has a higher chance of obtaining a physically correct solution if one uses a Δt restriction slightly higher than that for the stability limit of standard explicit methods (but with larger numerical basins of attraction than the explicit method counterparts). Figures 6.20 and 6.23 show the two representations of numerical basins of attraction using the implicit Euler method. These figures show the generation of stable spurious asymptotes for $\Delta t \geq 1$. As Δt increases further, the size of the same numerical basin decreases and becomes fractal like, and new numerical basins are generated. The behavior is similar to the predator-prey model (4.3) in a sense that the numerical basin of attraction for $(1/3, 1/3)$ was permanently altered for Δt near or larger than 10. Observe the fragmentation of the numerical basin of attraction for $(1/3, 1/3)$ by the basins of the spurious asymptotes.

Trapezoidal Method: Figures 6.20 and 6.24 show the two representations of numerical basins of attraction using the trapezoidal method. As in the implicit Euler case, this scheme has a higher probability of obtaining a physically correct solution if one uses a Δt similar to that of standard explicit methods (but with larger numerical basins of attraction than the explicit method counterparts). In a manner similar to the implicit Euler, the numerical basins of attraction for $(1/3, 1/3)$ are much larger than the corresponding exact basin of attraction for $\Delta t \leq 2$. Their sizes are bigger than the ones generated by the implicit Euler method with the same Δt values. The scheme becomes effectively unstable due to the fragmentation of the numerical basins of attraction. Again due to the high cost of double precision computations, no further attempts were made for Δt large. The computation of these basins requires an interval arithmetic or the enclosure-type (Adams, 1990) of mathematical operation before a more precise behavior can be revealed.

Straight Newton vs. Other Studied Methods: Figure 6.25 shows the basin of attraction using Newton method in solving the steady part of the ODE (hereafter referred to as straight Newton) compared with the implicit Euler at $\Delta t = 1$. One can see that straight Newton method has a smaller attracting basin for the stable spiral $(1/3, 1/3)$ than the implicit Euler method for small Δt . In fact its basin is the same as the implicit Euler using larger Δt . Figure 6.25 illustrates the situation where quadratic convergence by the Newton method can be achieved only if the initial data are in the red regions.

Figures 6.23 and 6.25 also illustrates the fact that using very large Δt by the (linearized) implicit Euler method has the same chance of obtaining the correct steady state as the Newton method if the initial data are not known. Comparison of Newton method with other iteration procedures for the implicit Euler and trapezoidal methods are reported in our companion paper (Yee and Sweby, 1993a).

Combining the current result with Yee and Sweby (1993a), we can conclude that contrary to popular belief, the initial data using the straight Newton method may *not* have to be close to the exact solution for convergence. Straight Newton also exhibits stable and unstable spurious asymptotes. Initial data can be reasonably removed from the asymptotic values and still be in the basin of attraction. However, the basins can be fragmented even though the corresponding exact basins of attraction are single closed domains. The cause of nonconvergence may just as readily be due to the fact that its numerical basins of attraction are fragmented.

6.6 *Global Asymptotic Behavior of Iterative Implicit Schemes*

The global asymptotic nonlinear behavior of some standard iterative procedures in solving nonlinear systems of algebraic equations arising from four implicit linear multistep methods (LMMs) in discretizing models (4.1), (4.3) and (4.4) is analyzed in our companion paper (Yee and Sweby, 1993a). The implicit LMMs include implicit Euler, trapezoidal, mid-point implicit and three-point backward differentiation methods. The iterative procedures include simple iteration and full and modified Newton iterations. The results are compared with standard Runge-Kutta explicit methods, a non-iterative implicit procedure, and straight Newton method. Here we give a summary of Yee and Sweby (1993a) so that the reader may get a bigger picture of implicit methods other than the ones studied in this paper.

Studies in Yee and Sweby (1993a) showed that all of the four implicit LMMs exhibit a drastic distortion but less shrinkage of the basin of attraction of the true solution than standard explicit methods studied in this paper. In some cases with smaller Δt , the implicit LMMs exhibit enlargement of the basins of attraction of the true solution. Overall, the numerical basins of attraction of a non-iterative implicit procedure mimic more closely the basins of attraction of the continuum than the studied iterative implicit procedures for the four implicit LMMs. In general the numerical basins of attraction bear no resemblance to the exact basins of attraction. The size can increase or decrease depending on the time step. Also the possible existence of the largest numerical basin of attraction that is larger than the exact one does not occur when the time step is the smallest. The dynamics of numerics of the implicit methods differ significantly from each other, and the different methods of solving the resulting non-linear algebraic equations are very different from each other since different numerical methods and solution procedures result in entirely different nonlinear discrete maps. Although unconditionally stable implicit methods allow a theoretically large time step Δt , the numerical basins of attraction (allowable initial data) for large Δt some-times are so fragmented and/or so small that the safe (or practical) choice of Δt is slightly larger or comparable to the stability limit of standard explicit methods (but with larger numerical basins of attraction than the explicit method counterparts). In general, if one uses a Δt that is a fraction of the stability limit,

one has a higher chance of convergence to the correct asymptote than the standard explicit methods.

Studies in Yee and Sweby (1993a) also showed that the variable time step control method can occasionally stabilize unstable fixed points, depending on the initial data, starting time step and the iterative tolerance value. One shortcoming is that the size of Δt needed to avoid spurious dynamics is impractical to use, especially for the explicit method.

7. CONCLUDING REMARKS

The global asymptotic nonlinear behavior and bifurcation phenomena for the explicit Euler method, five different multistage Runge-Kutta methods (modified Euler, improved Euler, Heun, Kutta and 4th-order methods), two and three-step predictor-corrector methods, Adams-Bashforth method, and implicit Euler and trapezoidal method with linearization are compared for different model nonlinear ODEs. The five multistage Runge-Kutta methods and the predictor-corrector methods are nonlinear in the discretized parameter space Δt and all LMMs are linear in Δt . With the aid of the CM-2, the complex behavior and sometimes fractal like structure of the associated numerical basins of attraction of these time discretizations are compared and revealed for the first time.

The numerical results indicate that with sufficiently small Δt and initial data close to the steady state (usually not known for the time-marching method), one can have the highest chance of convergence to the correct asymptote. In general, the initial data can be far removed from the exact steady state by the studied implicit methods provided that a fraction of the allowable time step restriction is used. Our study also indicates that bifurcation to a period two or lower order period solution is readily detectable in numerical calculations. However, bifurcation to a limit cycle will not be so obvious (without a phase portrait representation), especially in the vicinity of the bifurcation point. Indeed the phenomenon of an artificial time iteration to steady-state of a large system formed by spatial discretization which nears convergence before the residuals "plateaus out", could actually be the result of a stable spurious limit cycle around the Hopf bifurcation point. In addition, the bifurcation of spirals to limit cycles might account in part for the phenomenon of near (but lack of) convergence in large stiff systems.

For a given initial data and two finite but different Δt 's that are below the linearized stability limit of the scheme, their numerical solutions might converge to two different solutions even if no spurious *stable* steady-state numerical solution is introduced by the scheme and the initial data are physically relevant. The source of the behavior is due to the existence of *unstable* spurious asymptotes or stable asymptotes other than steady states which have the same detrimental (in terms of robustness) effect. However, in the case of occurrence of stable spurious steady states, they can be mistaken for the true steady state in practical computations. In other words depending on the initial data, for a given Δt below the linearized stability limit, the numerical solution can (a) converge to the correct steady state, (b) converge to a different steady state, (c) converge to a spurious periodic solution, (d) yield spurious asymptotes other than (a)-(c), or (e) diverge, even though the initial data are physically relevant.

Another important finding is that unlike the scalar first-order autonomous ODE discussed in part I (Yee *et al.*, 1991), the fixed points can change types as the time step is varied even for two-time-level unconditionally stable implicit LMMs. An unstable fixed point can become a stable fixed point and can e.g., change from a saddle to a stable or unstable node (for a fixed system parameter ε). Since these implicit methods can introduce spurious asymptotes as well, thus even though LMMs preserve the same number but not the same types of fixed points as the underlying DEs, the numerical basins of attraction of LMMs (explicit or implicit) do not always coincide with the exact basins of attraction of the underlying DEs. One major consequence of this behavior is that the flow pattern can change type as the discretized parameter is varied. Another consequence of these phenomena is the fragmentation of the numerical basin of attraction. In general, unconditionally stable implicit LMMs exhibit less shrinkage of the basin of attraction of the true solution than standard explicit methods. Another interesting result is that contrary to popular belief, the initial data using the straight Newton method may not have to be close to the exact steady state for convergence. However, we believe that one cause of nonconvergence in straight Newton or implicit LMMs with large time step may be due to the fact that the numerical basins of attraction are fragmented.

In conclusion, the present results can explain some of the roots of why one cannot achieve the theoretical linearized stability limit of the typical implicit Euler and trapezoidal time discretization in practice when solving strongly nonlinear DEs, e.g. in CFD. The results can also shed some light in bridging some of the gaps between theoretical convergence criterion ($\Delta t \rightarrow 0$, as $n \rightarrow \infty$) and practical scientific computation (finite Δt as $n \rightarrow \infty$).

Acknowledgements

The authors wish to thank A. M. Stuart and D. F. Griffiths for their valuable discussions during the course of this research and for suggesting the model equations (4.1) and (4.4). Special thanks to A. Lafon, M. Vinokur, T. Coakley and C. Y. McNeil for their critical review of the manuscript. Financial support from T. Lasinski for the second author as a visiting scientist at NASA Ames is gratefully acknowledged.

References

- Adams, E. (1990) "Periodic Solutions: Enclosure, Verification, and Applications", *Computer Arithmetic and Self-Validating Numerical Methods*, Academic Press, 199–245.
- Beam, R. M. and Bailey, H. E. (1988) "Direct Solver for Navier-Stokes Equations", Proceedings of International Conference on Computational Engineering Science, Atlanta, GA.
- Beam, R. M. and Warming, R. F. (1976) "An Implicit Finite-Difference Algorithm for Hyperbolic Systems in Conservation Law Form", *J. Comput. Phys.*, **22**, 87–110.
- Budd, C. J., Stuart, A. M., Koomullil, G. P. and Yee, H. C. (1994) "Numerical Solution Behavior of Model Convection-Diffusion BVP with Grid Adaptation", in preparation.
- Foias, C., Sell, G. and Temam, R. (1985) "Varieties Inertielles des Equations Differentielles Dissipatives", *C.R. Acad. Sci. Paris, Ser. I Math.*, **301**, 139–141.
- Globus, A., Levit, C. and Lasinski, T. (1991) "A Tool for Visualizing the Topology of Three-Dimensional Vector Fields", NAS Applied Research Branch Report RNR-91-017, NASA Ames Research Center.
- Griffiths, D. F., Sweby, P. K. and Yee, H. C. (1992a) "On Spurious Asymptotes Numerical Solutions of Explicit Runge-Kutta Schemes", *IMA J. Numer. Anal.*, **12**, 319–338.
- Griffiths, D. F., Stuart, A. M. and Yee, H. C. (1992b) "Numerical Wave Propagation in Hyperbolic Problems with Nonlinear Source Terms", *SIAM J. of Numer. Anal.*, **29**(5), 1244–1260.

- Guckenheimer, J. and Holmes, P. (1983) *Nonlinear Oscillations, Dynamical Systems, and Bifurcations of Vector Fields*, Springer-Verlag, New York.
- Hale, J. and Kocak, H. (1991) *Dynamics and Bifurcations*, Springer-Verlag, New York.
- Hairer, E., Iserles, A. and Sanz-Serna, J. M. (1989) "Equilibria of Runge-Kutta Methods", *Numer. Math.*
- Hsu, C. S. (1987) *Cell-to-Cell Mapping*, Springer-Verlag, New York.
- Hung, C. M., Sung, C. H. and Chen, C. L. (1991) "Computation of Saddle Point of Attachment", AIAA-91-1713, AIAA 22nd Fluid Dynamics, Plasma Dynamics and Lasers Conference, Honolulu, Hawaii.
- Humphries, A. R. (1992) "Spurious Solutions of Numerical Methods for Initial Value problems", *IMA J. Num. Anal.*
- Iserles, A. (1988) "Stability and Dynamics of Numerical Methods for Nonlinear Ordinary Differential Equations", DAMTP NA1, University of Cambridge, Cambridge, England.
- Iserles, A., Peplow, A. T. and Stuart, A. M. (1990) "A Unified Approach to Spurious Solutions Introduced by Time Discretisation", Part I: Basic Theory, DAMTP 1990/NA4, Numerical Analysis Reports, University of Cambridge.
- Jameson, A. (1991) "Airfoils Admitting Nonunique Solutions to the Euler Equations", AIAA-91-1625.
- Keller, H. B. (1977) "Numerical Solution of Bifurcation and Nonlinear Eigenvalue Problems", *Applications of Bifurcation Theory*, P. H. Rabinowitz, ed., Academic Press, 359-384.
- Kwak, M. (1991) "Finite Dimensional Inertial Forms for the 3D Navier-Stokes Equations," IMA preprint Series #828.
- Lafon, A. and Yee, H. C. (1991) "Dynamical Approach Study of Spurious Steady-State Numerical Solutions for Nonlinear Differential Equations", Part III: The Effects of Nonlinear Source Terms and Boundary Conditions in Reaction-Convection Equations, NASA TM-103877, to appear in *Intern. J. CFD*.
- Lafon, A. and Yee, H. C. (1992) "Dynamical Approach Study of Spurious Steady-State Numerical Solutions of Nonlinear Differential Equations", Part IV: Stability vs. Numerical Treatment of Nonlinear Source Terms, ONERA-CERT Technical Report DERAT 45/5005.38, to appear in *Intern. J. CFD*.
- Lambert, J. D. (1973) *Computational Methods in Ordinary Differential Equations*, John Wiley, New York.
- Langford, W. F. and Iooss, G. (1980) "Interactions of Hopf and Pitchfork Bifurcations", ISNM 54, *Bifurcation Problems and Their Numerical Solution*, Workshop on Bifurcation Problems and Their Numerical Solution, Dortmund, ed. H. D. Mittelman and H. Weber, Birkhauser Verlag, Basel, 103-134.
- Panov, A. M. (1956) "Behavior of the Trajectories of a System of Finite Difference Equations in the Neighbourhood of a Singular Point", *Uch. Zap. Ural. Gos. Univ. vyp.* **19**, 89-99.
- Perron, O. (1929) "Über Stabilität und Asymptotisches Überhalten de Lösungen eines Systems endlicher Differenzgleichungen", *J. Reine Angew. Math.*, **161**, 41-64.
- Richtmyer, R. D. and Morton, K. W. (1967) *Difference Methods for Initial-Value Problems*, Interscience-Wiley, New York.
- Sanz-Serna, J. M. (1990) "Numerical Ordinary Differential Equations vs. Dynamical Systems," Applied Math. Comput. Report 1990/3, Universidad de Valladolid.
- Schechter, S. and Shearer, M. (1990) "Undercompressive Shocks for Nonstrictly Hyperbolic Conservation Laws", IMA Preprint Series #619.
- Shearer, M., Schaeffer, D. G., Marchesin, D. and Paes-Leme, P. (1987) "Solution of the Riemann Problem for a Prototype 2×2 System of Non-Strictly Hyperbolic Conservation Laws", *Arch. Rat. Mech. Anal.*, **97**, 299-320.
- Strang, G. (1968) "On the Construction and Comparison of Difference Schemes", *SIAM J. Num. Anal.*, **5**, 506-517.
- Sweby, P. K., Yee, H. C. and Griffiths, D. F. (1990) "On Spurious Steady-State Solutions of Explicit Runge-Kutta Schemes", University of Reading, Department of Mathematics, Numerical Analysis Report 3/90, also NASA TM 102819, April 1990.
- Sweby, P. K. and Yee, H. C. (1991) "On Spurious Asymptotic Numerical Solutions of 2×2 Systems of ODEs", Numerical analysis Report 7/91, University of Reading, England.
- Sweby, P. K. and Yee, H. C. (1994) "On the Dynamics of Some Grid Adaptation Schemes", Proceedings of the 4th International Conference on Numerical Grid Generation in CFD and Related Fields," University College of Swansea, UK, also RIACS Technical Report 94.02, Feb. 1994.
- Temam, R. (1989) "Do Inertial Manifolds Apply to Turbulence?", *Physica D*, **37**, 146-152.
- Warner, B. (1980) "Turning Points of Branches of Positive Solutions", ISNM 54, *Bifurcation Problems and Their Numerical Solution*, Workshop on Bifurcation Problems and Their Numerical Solution, Dortmund, ed. H. D. Mittelman and H. Weber, Birkhauser Verlag, Basel, 211-226.
- Yee H. C. (1989) "A Class of High-Resolution Explicit and Implicit Shock-Capturing Methods", VKI Lecture Series 1989-04 March 6-10, 1989, also NASA TM-101088, Feb. 1989.
- Yee, H. C. (1991) "A Nonlinear Dynamical Approach to Algorithm Development in Hypersonic CFD", Proceedings of the 4th International symposium on Computational Fluid Dynamics, Davis, Calif.

- Yee, H. C., Klopfer, G. H. and Montagne, J.-L. (1990) "High-Resolution shock-capturing Schemes for Inviscid and Viscous Hypersonic Flows", *J. Comput. Phys.*, **88**, 31–61.
- Yee, H. C., Sweby, P. K. and Griffiths, D. F. (1991) "Dynamical Approach Study of Spurious Steady-State Numerical Solutions for Nonlinear Differential Equations", Part I: The Dynamics of Time Discretizations and Its Implications for algorithm Development in Computational Fluid Dynamics, NASA TM-102820, April 1990, also *J. Comput. Phys.*, **97**, 249–310.
- Yee, H. C., Sweby, P. K. and Lafon, A. (1992) "Basins of Attraction and the Time-Dependent Approach to Obtaining Steady-State Numerical Solutions", Proceedings of the ICFD Conference on Numerical Methods for Fluid Dynamics, Reading England.
- Yee, H. C. and Sweby, P. K. (1993a) "Global Asymptotic Behavior of Iterative Implicit Schemes", RIACS Technical Report 93.11, NASA Ames Research Center, to appear in *International J. of Bifurcation and Chaos*, Dec., 1994.
- Yee, H. C. and Sweby, P. K. (1993b) "On the Dynamics of Some Iterative Implicit schemes", Proceedings of the Chaotic Numerics Workshop, Deakin University, Geelong, Australia.

Bifurcation Diagrams & Basins of Attraction
 $u' = au(1-u)$

Modified Euler

Improved Euler



Kutta



R-K 4



Color Plate I

Figure 6.1 (See H.C. Yee and P. K. Sweby.)

Bifurcation Diagrams & Basins of Attraction
 $u' = au(1-u)(0.5-u)$

Modified Euler



Improved Euler



Kutta



R-K 4



Color Plate II **Figure 6.2** (See H.C. Yee and P. K. Sweby.)

Bifurcation Diagrams & Basins of Attraction
Dissipative Complex Eqn., $\varepsilon = 1, \nu = 0.0$

Modified Euler

Improved Euler

Modified Euler

Improved Euler

Kutta

R-K 4

Kutta

R-K 4

Color Plate III

Figure 6.3 (See H.C. Yee and P. K. Sweby.)

Bifurcation Diagrams & Basins of Attraction
Dissipative Complex Eqn. $\mu = 1, \nu = 0.0$

Heun

Adams-Bashforth



PC2

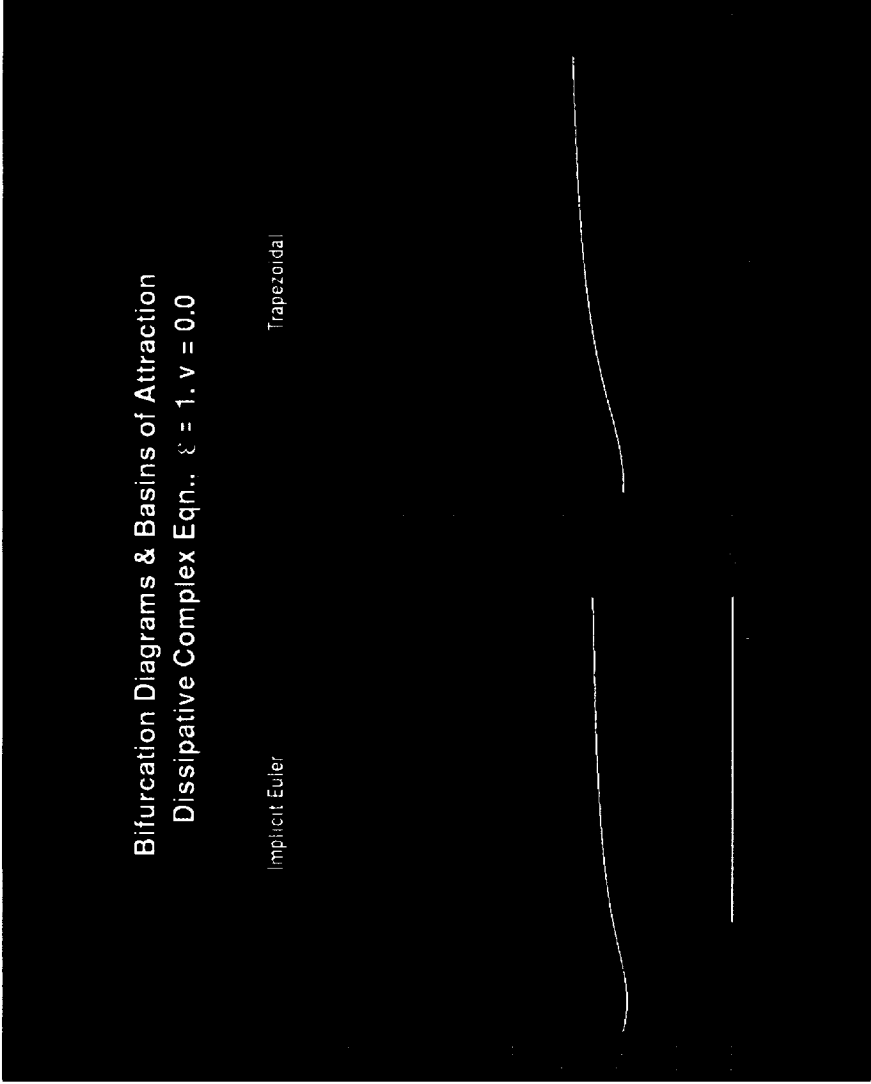
PC3

Color Plate IV **Figure 6.4** (See H.C. Yee and P. K. Sweby.)

Bifurcation Diagrams & Basins of Attraction
Dissipative Complex Eqn., $\epsilon = 1, \nu = 0.0$

Implicit Euler

Trapezoidal



Color Plate V Figure 6.5 (See H.C. Yee and P. K. Sweby.)

Basins of Attraction
Dissipative Complex Eqn., $\xi = 1$
R-K 4

$\sqrt{t} = 0.5$



$\sqrt{t} = 1.5$



$\sqrt{t} = 1.75$



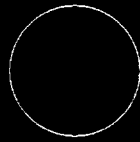
$\sqrt{t} = 2$



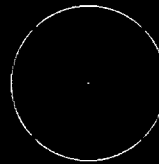
Color Plate VI **Figure 6.8** (See H.C. Yee and P. K. Sweby.)

Basins of Attraction
Dissipative Complex Eqn., $\xi = 1$
Linearized Implicit Euler

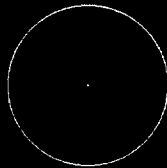
$\Delta t = 0.5$



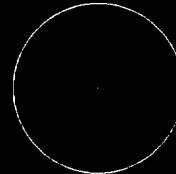
$\Delta t = 1.5$



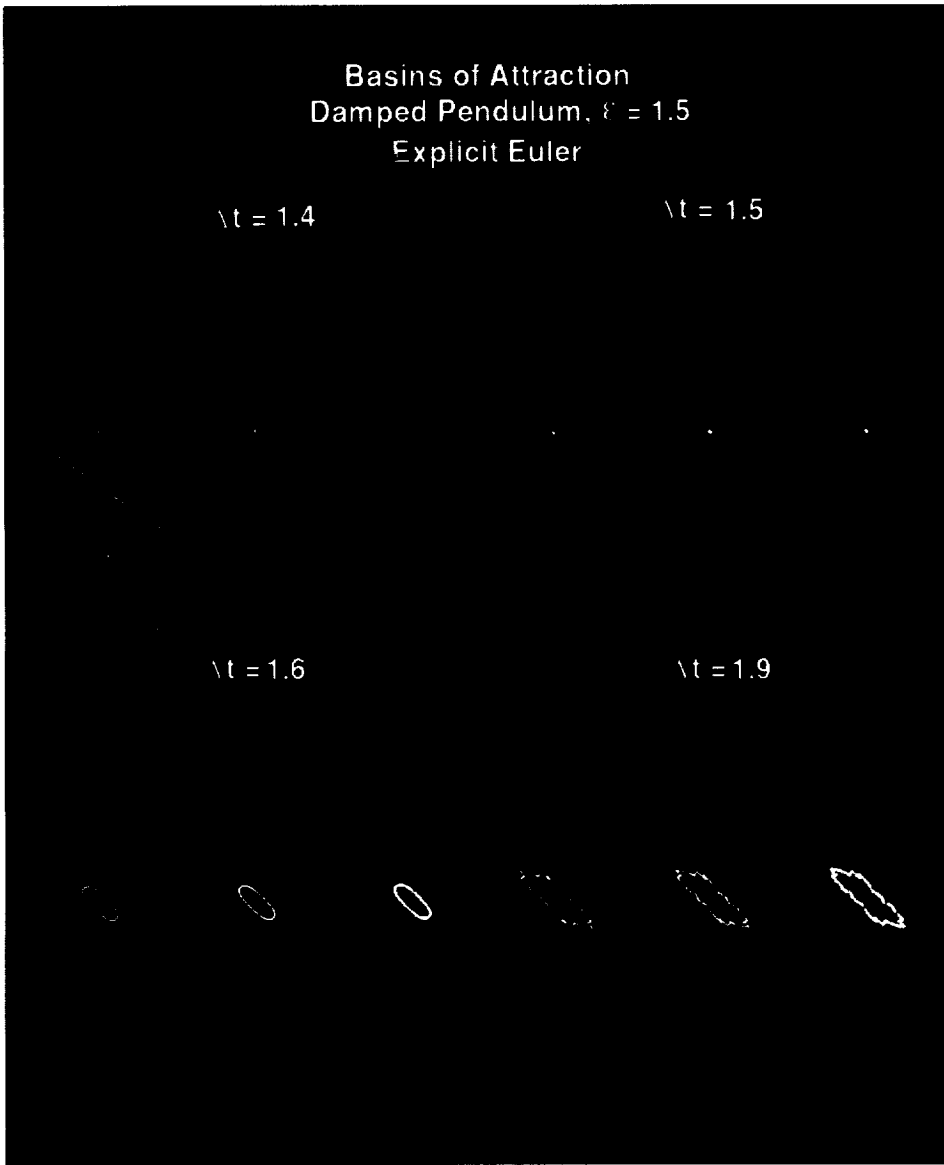
$\Delta t = 2$



$\Delta t = 4$



Color Plate VII Figure 6.9 (See H.C. Yee and P. K. Sweby.)

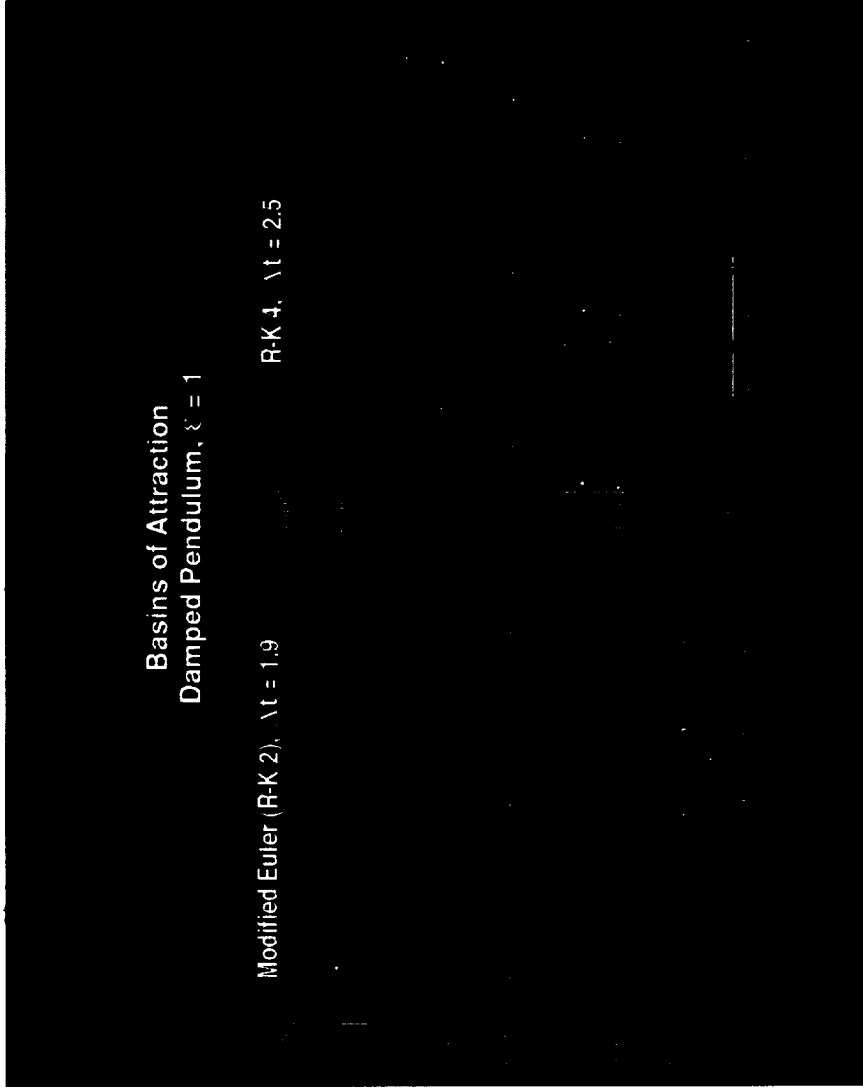


Color Plate VIII **Figure 6.10** (See H.C. Yee and P. K. Sweby.)

Basins of Attraction
Damped Pendulum, $\xi = 1$

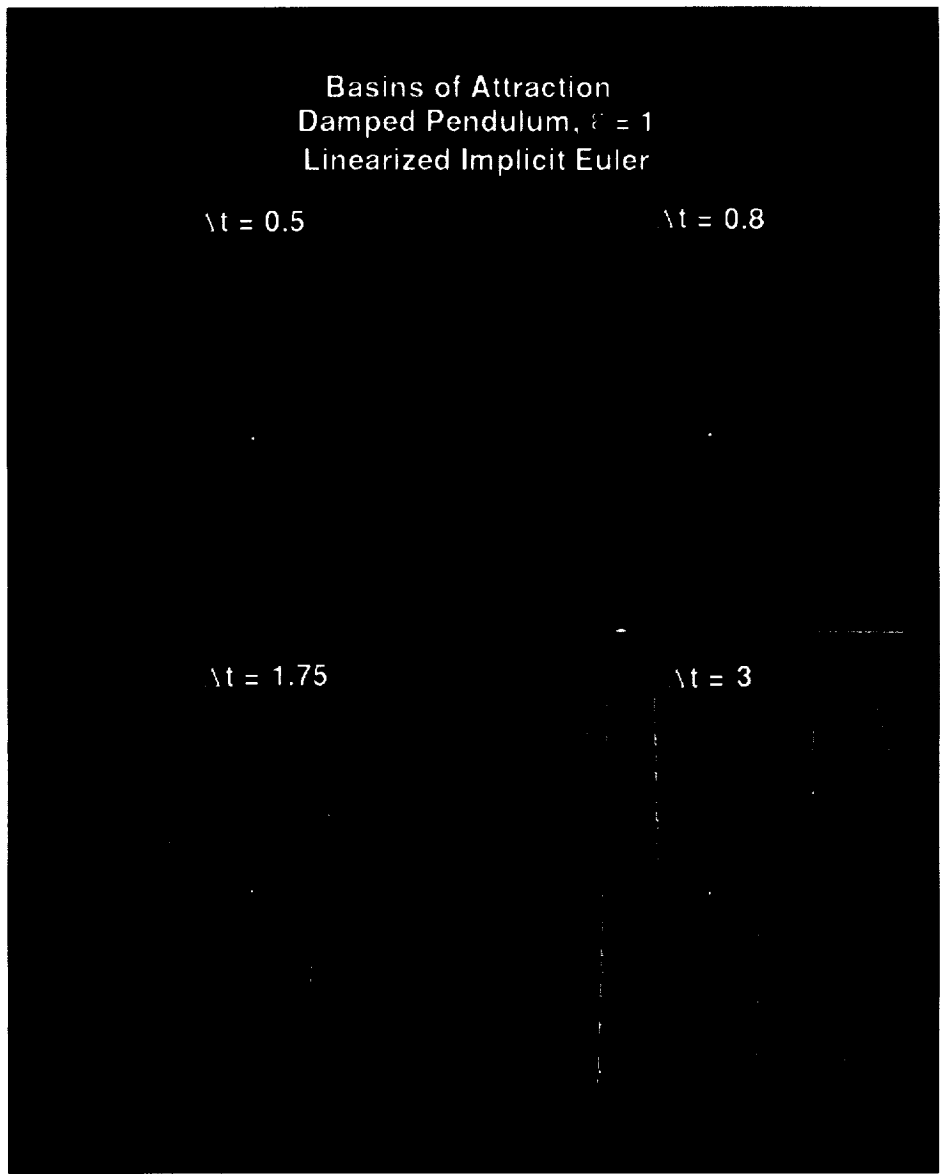
Modified Euler (R-K 2), $\Delta t = 1.9$

R-K 4, $\Delta t = 2.5$



Color Plate IX

Figure 6.11 (See H.C. Yee and P. K. Sweby.)



Color Plate X **Figure 6.12** (See H.C. Yee and P. K. Sweby.)

Bifurcation Diagrams & Basins of Attraction
Predator - Prey Eqn., $\nu = 0.0$

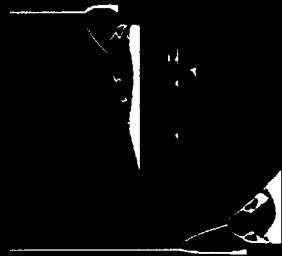
Modified Euler

Improved Euler



Kutta

R-K 4

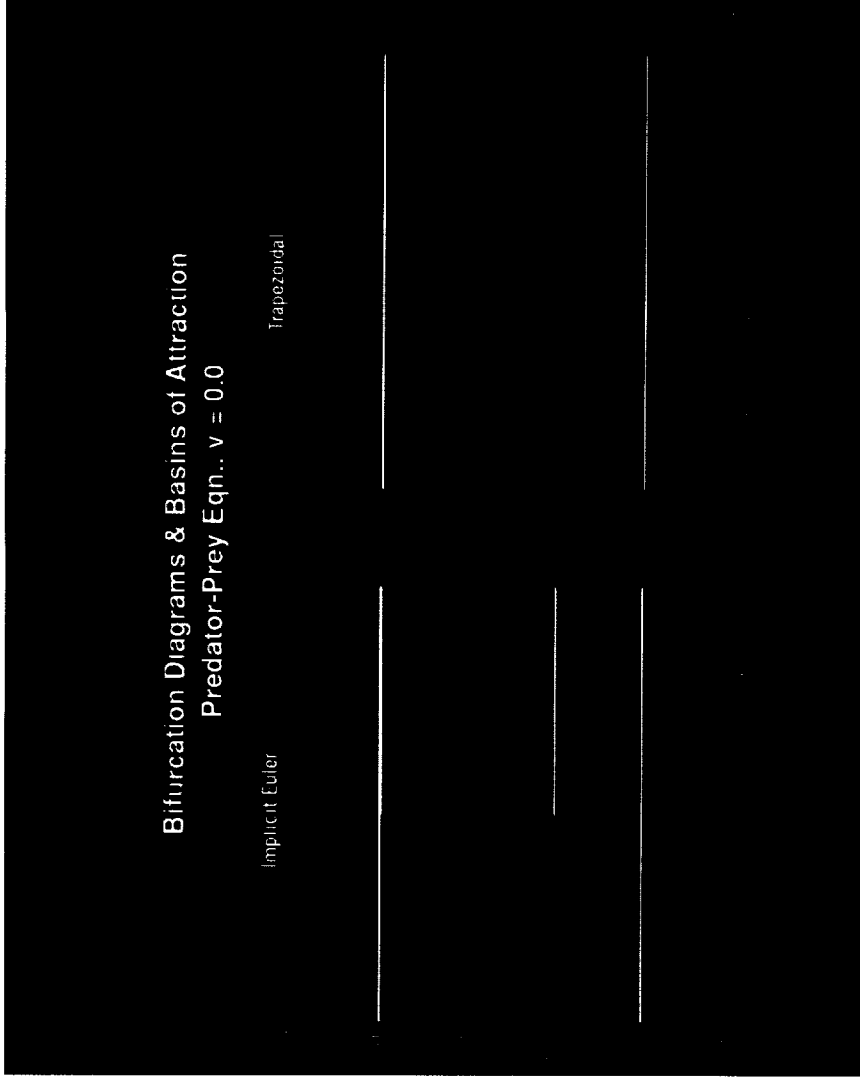


Color Plate XI Figure 6.13 (See H.C. Yee and P. K. Sweby.)

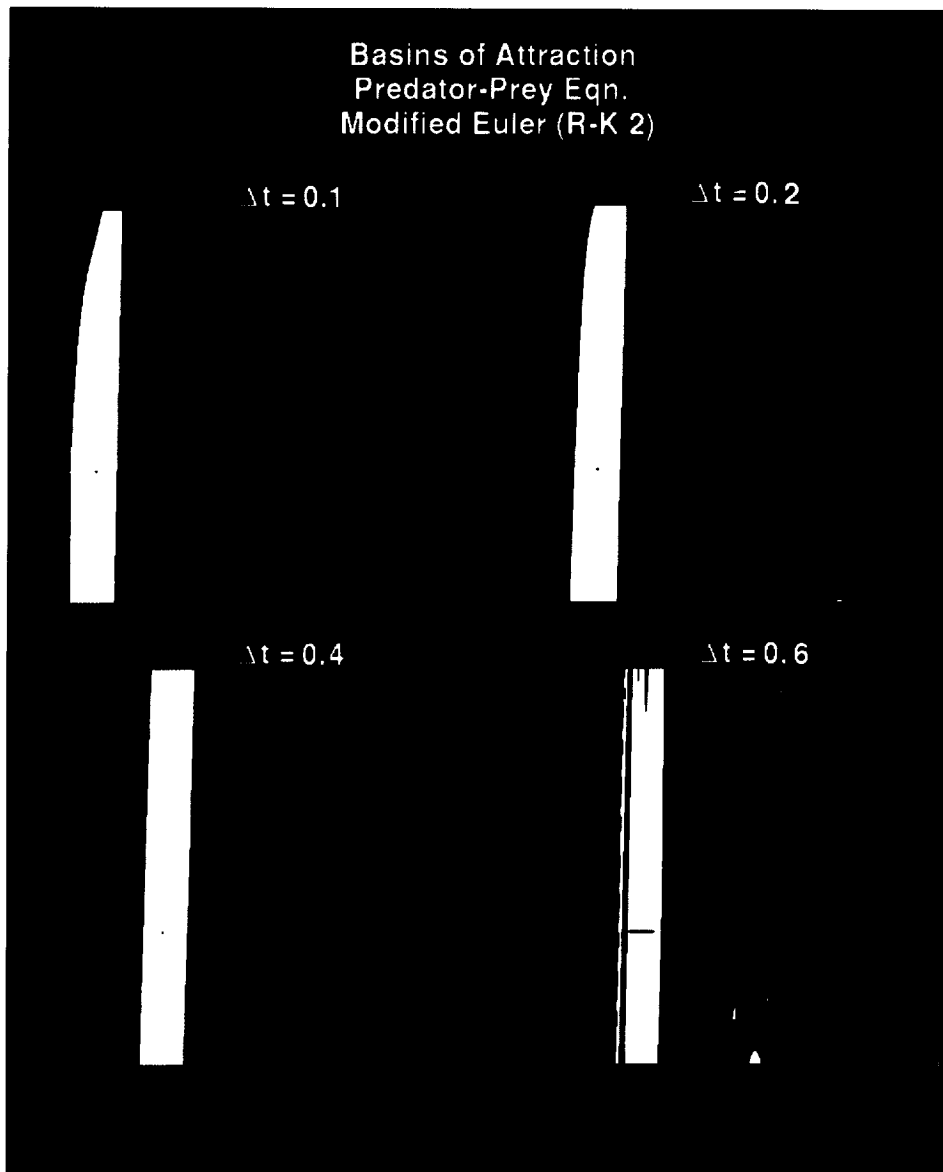
Bifurcation Diagrams & Basins of Attraction
Predator-Prey Eqn.. $v = 0.0$

Implicit Euler

Trapezoidal



Color Plate XII **Figure 6.14** (See H.C. Yee and P. K. Sweby.)



Color Plate XIII **Figure 6.15** (See H.C. Yee and P. K. Sweby.)

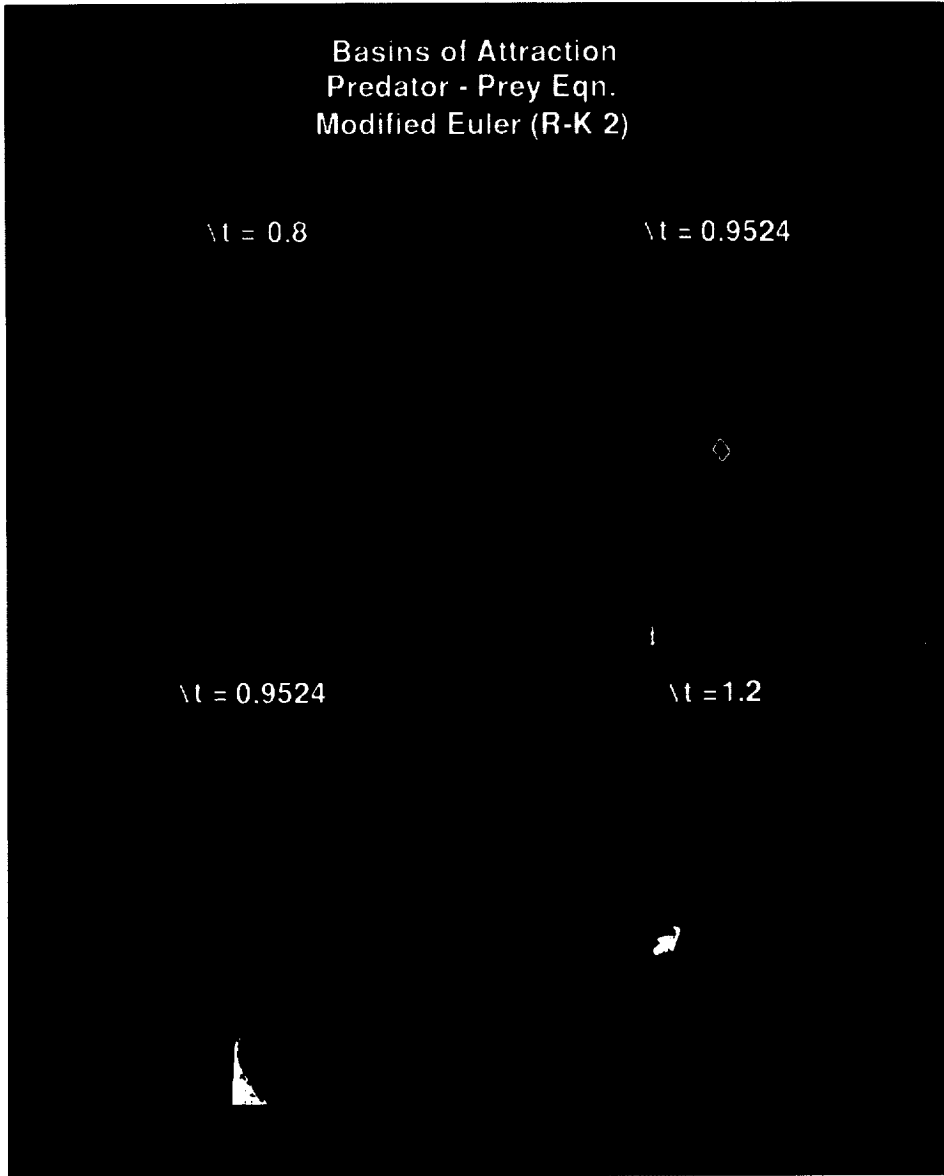
Basins of Attraction
Predator - Prey Eqn.
Modified Euler (R-K 2)

$\lambda t = 0.8$

$\lambda t = 0.9524$

$\lambda t = 0.9524$

$\lambda t = 1.2$



Color Plate XIII **Figure 6.15** (Continued) (See H.C. Yee and P. K. Sweby.)

Basins of Attraction
Predator-Prey Eqn.
R-K 4

$\Delta t = 0.4$

$\Delta t = 0.8$

$\Delta t = 1$

$\Delta t = 1.77$

Color Plate XIV Figure 6.16 (See H.C. Yee and P. K. Sweby.)

Basins of Attraction
Predator-Prey Eqn.
Linearized Implicit Euler

$\Delta t = 0.1$

$\Delta t = 0.5$

$\Delta t = 0.9$

$\Delta t = 1.4$

Color Plate XV **Figure 6.17** (See H.C. Yee and P. K. Sweby.)

Basins of Attraction
Predator-Prey Eqn.
Linearized Implicit Euler

$\Delta t = 3$

$\Delta t = 1,000,000$

Color Plate XV

Figure 6.17 (Continued) (See H.C. Yee and P. K. Sweby.)

Basins of Attraction
Predator-Prey Eqn.
Linearized Trapezoidal

$t = 0.1$

$t = 0.5$

$t = 1.4$

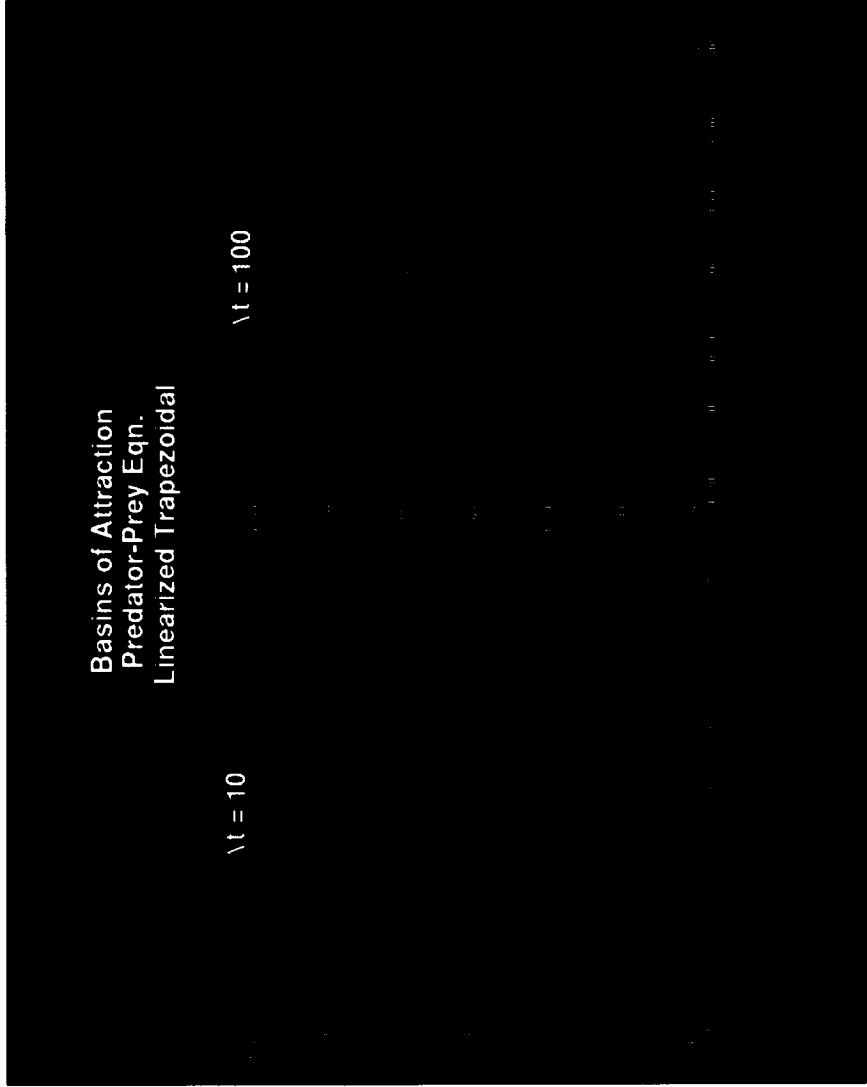
$t = 3$

Color Plate XVI **Figure 6.18** (See H.C. Yee and P. K. Sweby.)

Basins of Attraction
Predator-Prey Eqn.
Linearized Trapezoidal

$t = 10$

$t = 100$



Color Plate XVI Figure 6.18 (Continued) (See H.C. Yee and P. K. Sweby.)

Bifurcation Diagrams & Basins of Attraction
Viscous Burgers Eqn., $\epsilon = 0.1$, $\nu = 0.333$
(Central Difference in Space)

Modified Euler

Improved Euler



Kutta

R-K 4

Color Plate XVII **Figure 6.19** (See H.C. Yee and P. K. Sweby.)

Bifurcation Diagrams & Basins of Attraction
Viscous Burgers Eqn., $\xi = 0.1, \nu = 0.333$
(Central Difference in Space)

Trapezoidal

Implicit Euler



Color Plate XVIII **Figure 6.20** (See H.C. Yee and P. K. Sweby.)

Basins of Attraction
Viscous Burgers Eqn., $\epsilon = 0.1$
Improved Euler, Central Difference in Space

$\Delta t = 0.1$

$\Delta t = 1$

$\Delta t = 2.25$

$\Delta t = 2.35$

Color Plate XIX **Figure 6.21** (See H.C. Yee and P. K. Sweby.)

Basins of Attraction
Viscous Burgers Eqn., $\varepsilon = 0.1$
Kutta (R-K 3), Central Difference in Space

$Nt = 0.1$

$Nt = 1.0$

$Nt = 1.826$

$Nt = 1.85$

$Nt = 2.75$

$Nt = 2.785$

Color Plate XX Figure 6.22 (See H.C. Yee and P. K. Sweby.)

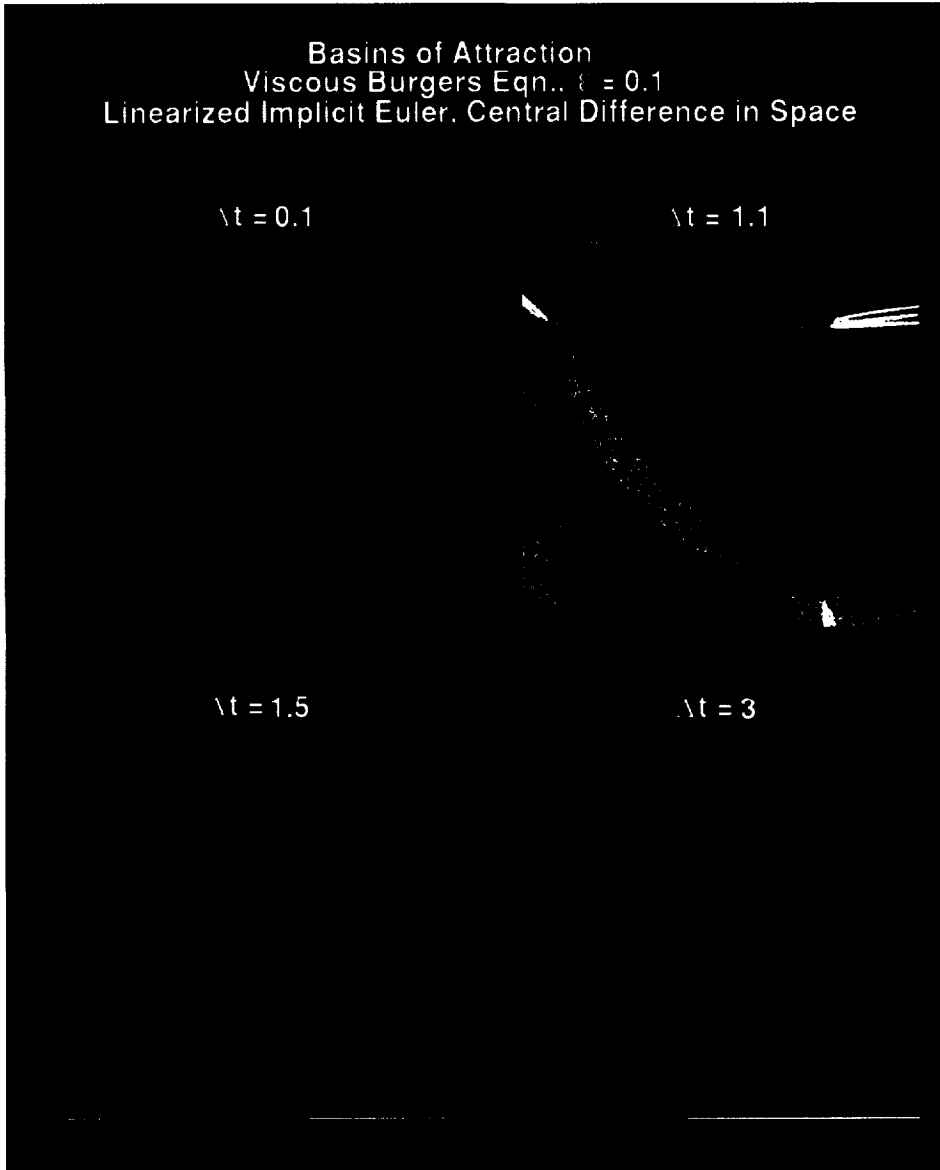
Basins of Attraction
Viscous Burgers Eqn., $\epsilon = 0.1$
Linearized Implicit Euler, Central Difference in Space

$\Delta t = 0.1$

$\Delta t = 1.1$

$\Delta t = 1.5$

$\Delta t = 3$



Color Plate XXI Figure 6.23 (See H.C. Yee and P. K. Sweby.)

Basins of Attraction
Viscous Burgers Eqn., $\epsilon = 0.1$
Linearized Implicit Euler, Central Difference in Space

$\Delta t = 10$

$\Delta t = 1,000,000$

Color Plate XXI Figure 6.23 (Continued) (See H.C. Yee and P. K. Sweby.)

Basins of Attraction
Viscous Burgers Eqn., $\epsilon = 0.1$
Linearized Trapezoidal, Central Difference in Space

$\Delta t = 0.1$

$\Delta t = 10$

$\Delta t = 200$

$\Delta t = 500$

Color Plate XXII

Figure 6.24 (See H.C. Yee and P. K. Sweby.)

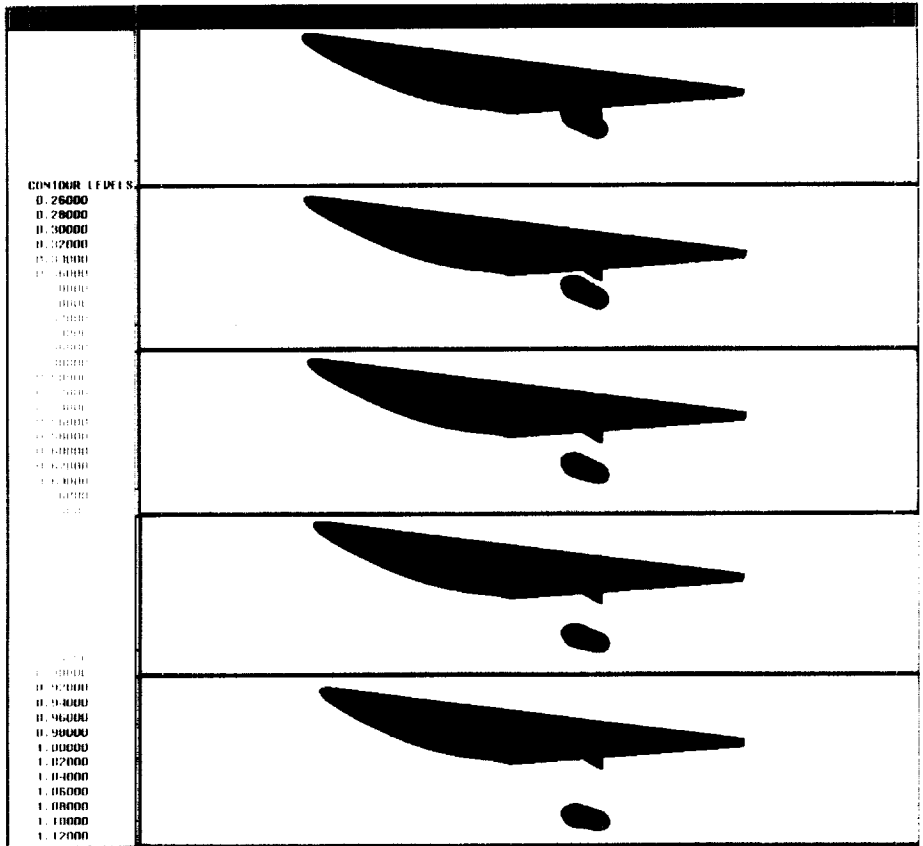
Basins of Attraction
Viscous Burgers Eqn., $\xi = 0.1$
Central Difference in Space

Implicit Euler, $\Delta t = 1$

Newton

Color Plate XXIII

Figure 6.25 (See H.C. Yee and P. K. Sweby.)



Color Plate XXIV

Figure 10 Computed surface pressure contours with store located in captive position and moving through 0.6, 1.0, 1.6, and 2.0 store diameters below the pylon. (See A. Arabshahi and D. L. Whitfield)